



January 23, 2017

## **Lambda global polarization in AuAu collisions at $\sqrt{s_{NN}} = 7.7, 11.5, 14.5, 19.6, 27, \text{ and } 39 \text{ GeV}$ from the STAR experiment**

5

Isaac Upsilon<sup>1</sup>

1. The Ohio State University, Columbus, USA

Email: [upsal.1@osu.edu](mailto:upsal.1@osu.edu)

### **Abstract**

Lambda global polarization results are shown for the BES energies



---

**10** **Contents**

<b>1</b>	<b>Introduction</b>	<b>10</b>
<b>2</b>	<b>Quality Assurance</b>	<b>18</b>
2.1	Event QA . . . . .	18
2.2	Event Plane determination . . . . .	29
15	2.2.1 Event plane resolution . . . . .	38
2.3	Track QA . . . . .	40
2.4	Lambda reconstruction . . . . .	43
25	2.4.1 Daughter PID . . . . .	43
	2.4.2 Lambda topological cuts . . . . .	53
<b>20</b>	<b>3 Data analysis</b>	<b>57</b>
3.1	Resolution Correction . . . . .	58
3.2	Mass background . . . . .	59
3.3	Detector acceptance correction . . . . .	64
25	3.3.1 Detector acceptance correction explanation . . . . .	64
	3.3.2 Detector acceptance correction results . . . . .	65
3.4	Helicity efficiency . . . . .	66
	3.4.1 Helicity efficiency description . . . . .	67
	3.4.2 Helicity efficiency effect . . . . .	76
30	3.5 Feed-down correction . . . . .	87
	3.5.1 Abstract for feeddown . . . . .	87
	3.5.2 Correction procedure and definitions . . . . .	87
	3.5.3 Which particles are included? . . . . .	87
	3.5.4 Feed-down matrices . . . . .	88
	3.5.5 Application to STAR data . . . . .	88
35	3.5.6 Acknowledgements . . . . .	91
	3.5.7 Extracting feed-down fractions from Bill Llope's THERMUS file . . . . .	91
	3.5.8 Communication with Jean Cleymans . . . . .	110
	3.5.9 Notes on Bill's THERMUS . . . . .	112
40	3.5.10 Sanity check . . . . .	114
	3.5.11 HIJING efficiency . . . . .	114
	3.5.12 Old feed-down correction using only $\Sigma^0$ s . . . . .	115

3.6 Discussion of statistical error . . . . .	116
---	-----

<b>4 Systematic errors</b>	<b>117</b>
----------------------------	------------

4.1 Topological cut dependencies . . . . .	117
--	-----

45      4.1.1 Covariance method idea . . . . .	117
--	-----

4.1.2 Mass purity . . . . .	119
-----------------------------	-----

4.1.3 Results . . . . .	124
-------------------------	-----

4.1.4 Simple cut variation . . . . .	129
--------------------------------------	-----

4.2 Residual effect . . . . .	131
-------------------------------	-----

50      4.3 Scaling errors . . . . .	134
--------------------------------------	-----

4.4 Conservation of momentum effects on event plane resolution . . . . .	135
--	-----

4.5 Feeddown . . . . .	140
------------------------	-----

<b>5 Systematic Dependencies</b>	<b>145</b>
----------------------------------	------------

5.1 Centrality . . . . .	145
--------------------------	-----

55      5.2 Energy . . . . .	167
------------------------------	-----

5.3 Rapidity . . . . .	173
------------------------	-----

5.4 Azimuthal angle . . . . .	182
-------------------------------	-----

<b>6 Signal falsification</b>	<b>185</b>
-------------------------------	------------

6.1 Simulation comparison . . . . .	185
-------------------------------------	-----

60      6.2 Rotated pions . . . . .	185
-------------------------------------	-----

<b>7 STAR 2007 results</b>	<b>188</b>
----------------------------	------------

## List of Figures

1	$P_H^{\Lambda,\bar{\Lambda}}$	11
2	schematic of collision	12
65	3 Lambda in event with black background schematic	13
4	overview of the STAR detector	13
5	Vorticity and magnetic field	14
6	Vorticity in $Hz$ ( $T = 160 MeV$ )	15
7	Vorticity in $fm^{-1}$ ( $T = 160 MeV$ )	16
70	8 Magnetic field in $T$ ( $T = 160 MeV$ )	17
9	Reference multiplicity	20
10	Z Vertex	20
11	ToF Multiplicity	21
12	BBC East ADC sum	21
75	13 BBC West ADC sum	22
14	7GeV R Vertex	23
15	11GeV R Vertex	24
16	15GeV R Vertex	25
17	19GeV R Vertex	26
80	18 27GeV R Vertex	27
19	39GeV R Vertex	28
20	BBC numbering scheme	29
21	STAR Coordinates	30
22	7GeV $\Psi_1$ distribution	32
85	23 11GeV $\Psi_1$ distribution	32
24	15GeV $\Psi_1$ distribution	33
25	19GeV $\Psi_1$ distribution	33
26	27GeV $\Psi_1$ distribution	34
27	39GeV $\Psi_1$ distribution	34
90	28 7GeV $\Psi_{1,W}$ vs. $\Psi_{1,E}$	35
29	11GeV $\Psi_{1,W}$ vs. $\Psi_{1,E}$	35
30	15GeV $\Psi_{1,W}$ vs. $\Psi_{1,E}$	36
31	19GeV $\Psi_{1,W}$ vs. $\Psi_{1,E}$	36
32	27GeV $\Psi_{1,W}$ vs. $\Psi_{1,E}$	37

95	33	39GeV $\Psi_{1,W}$ vs. $\Psi_{1,E}$ . . . . .	37
	34	Resolution Correction . . . . .	38
	35	Charged track $p_T$ . . . . .	40
	36	Charged track $\eta$ . . . . .	41
	37	Charged track N <sub>Hits Possible</sub> . . . . .	41
100	38	Charged track N <sub>Hits</sub> . . . . .	42
	39	Charged track Fit Ratio . . . . .	42
	40	7GeV dE/dx vs. p . . . . .	43
	41	7GeV 1/ $\beta$ vs. p . . . . .	44
	42	7GeV $m^2$ vs. p . . . . .	44
105	43	11GeV dE/dx vs. p . . . . .	45
	44	11GeV 1/ $\beta$ vs. p . . . . .	45
	45	11GeV $m^2$ vs. p . . . . .	46
	46	15GeV dE/dx vs. p . . . . .	46
	47	15GeV 1/ $\beta$ vs. p . . . . .	47
110	48	15GeV $m^2$ vs. p . . . . .	47
	49	19GeV dE/dx vs. p . . . . .	48
	50	19GeV 1/ $\beta$ vs. p . . . . .	48
	51	19GeV $m^2$ vs. p . . . . .	49
	52	27GeV dE/dx vs. p . . . . .	49
115	53	27GeV 1/ $\beta$ vs. p . . . . .	50
	54	27GeV $m^2$ vs. p . . . . .	50
	55	39GeV dE/dx vs. p . . . . .	51
	56	39GeV 1/ $\beta$ vs. p . . . . .	51
	57	39GeV $m^2$ vs. p . . . . .	52
120	58	Lambda reconstruction diagram . . . . .	53
	59	Proton DCA distribution . . . . .	54
	60	Pion DCA distribution . . . . .	54
	61	Daughter DCA distribution . . . . .	55
	62	Lambda DCA distribution . . . . .	55
125	63	Lambda decay length distribution . . . . .	56
	64	Lambda mass distribution . . . . .	56
	65	Resolution effect 0-80% . . . . .	58

66	Resolution effect 20-50% . . . . .	58
67	$\Lambda$ off mass distribution . . . . .	59
130	$\Lambda$ off mass comparison ( $m_{\text{inv}} > m_{\Lambda}$ ) . . . . .	60
69	$\Lambda$ off mass comparison ( $m_{\text{inv}} < m_{\Lambda}$ ) . . . . .	61
70	$\bar{\Lambda}$ off mass comparison ( $m_{\text{inv}} > m_{\Lambda}$ ) . . . . .	61
71	$\bar{\Lambda}$ off mass comparison ( $m_{\text{inv}} < m_{\Lambda}$ ) . . . . .	62
72	$\Lambda$ purity correction comparison . . . . .	63
135	$\bar{\Lambda}$ purity correction comparison . . . . .	63
74	Helicity efficiency diagram . . . . .	66
75	Helicity Efficiency Data . . . . .	67
76	Helicity Efficiency Simulation . . . . .	68
77	Helicity efficiency effect (39GeV $\Lambda$ ) . . . . .	69
140	Helicity efficiency effect (39GeV $\bar{\Lambda}$ ) . . . . .	70
79	Helicity efficiency effect (27GeV $\Lambda$ ) . . . . .	70
80	Helicity efficiency effect (27GeV $\bar{\Lambda}$ ) . . . . .	71
81	Helicity Efficiency Simulation . . . . .	72
82	$S_y$ asymmetry $\eta$ slices . . . . .	73
145	$S_y$ asymmetry with STAR $\eta$ cut . . . . .	74
84	$S_y$ asymmetry with helicity efficiency . . . . .	75
85	Helicity efficiency effect presentation p1 . . . . .	76
86	Helicity efficiency effect presentation p2 . . . . .	77
87	Helicity efficiency effect presentation p3 . . . . .	78
150	Helicity efficiency effect presentation p4 . . . . .	79
89	Helicity efficiency effect presentation p5 . . . . .	80
90	Helicity efficiency effect presentation p6 . . . . .	81
91	Helicity efficiency effect presentation p7 . . . . .	82
92	Helicity efficiency effect presentation p8 . . . . .	83
155	Helicity efficiency effect presentation p9 . . . . .	84
94	Helicity efficiency effect presentation p10 . . . . .	85
95	Helicity efficiency effect presentation p11 . . . . .	86
96	THERMUS input . . . . .	112
97	THERMUS output . . . . .	113
160	Invariant mass as a function of pion DCA . . . . .	119

99	Lambda invariant mass purity as a function of pion DCA . . . . .	120
100	Lambda invariant mass purity as a function of proton DCA . . . . .	120
101	Lambda invariant mass purity as a function of daughter DCA . . . . .	121
102	Lambda invariant mass purity as a function of Lambda DCA . . . . .	121
165	103 Lambda invariant mass purity as a function of Lambda decay length . . . . .	122
104	$\Lambda$ polarization covariance with cut quantities for each $\Lambda$ cut index . . . . .	124
105	$\Lambda$ polarization covariance with cut quantities for each $\Lambda$ cut index; zoomed in . . . . .	124
106	$\Lambda$ polarization “slope” from covariance with cut quantities for each $\Lambda$ cut index . . . . .	125
107	$\Lambda$ polarization “slope” from covariance with cut quantities for each $\Lambda$ cut index . . . . .	125
170	108 $\Lambda$ polarization “slope” from covariance with cut quantities for each $\Lambda$ cut index; zoomed in . . . . .	126
109	$\Lambda$ polarization “slope” from covariance with cut quantities for each $\Lambda$ cut index . . . . .	127
110	$\Lambda$ polarization “slope” from covariance with cut quantities for each $\Lambda$ cut index; zoomed in . . . . .	127
111	$\Lambda$ polarization “slope” from covariance with cut quantities for each $\Lambda$ cut index . . . . .	128
112	$\Lambda$ polarization “slope” from covariance with cut quantities for each $\Lambda$ cut index; zoomed in . . . . .	128
175	113 $\Lambda$ cut comparison . . . . .	129
114	$\bar{\Lambda}$ cut comparison . . . . .	129
115	Yadav’s study of MC effects on resolution p1 . . . . .	135
116	Yadav’s study of MC effects on resolution p2 . . . . .	135
117	Yadav’s study of MC effects on resolution p3 . . . . .	136
180	118 Yadav’s study of MC effects on resolution p4 . . . . .	136
119	Yadav’s study of MC effects on resolution p5 . . . . .	137
120	Yadav’s study of MC effects on resolution p6 . . . . .	137
121	Yadav’s study of MC effects on resolution p7 . . . . .	138
122	Yadav’s study of MC effects on resolution p8 . . . . .	138
185	123 Yadav’s study of MC effects on resolution p9 . . . . .	139
124	Yadav’s study of MC effects on resolution p10 . . . . .	139
125	Feed down variation away from THERMUS (low $\sqrt{s_{NN}}$ ) . . . . .	141
126	Feed down variation away from THERMUS (high $\sqrt{s_{NN}}$ ) . . . . .	142
127	Feed down variation fits (low $\sqrt{s_{NN}}$ ) . . . . .	143
190	128 Feed down variation fits (low $\sqrt{s_{NN}}$ ) . . . . .	144
129	$\Lambda$ more peripheral centrality . . . . .	145
130	$\Lambda$ more central centrality . . . . .	146
131	$\Lambda$ cut into halves of centrality . . . . .	146

---

132	$\Lambda$ cut into thirds of centrality . . . . .	147
195	$\Lambda$ for mid-centrality . . . . .	147
134	$\Lambda$ for bins of 20% centrality . . . . .	148
135	$\Lambda$ for 0-20% and 20-80% centrality . . . . .	148
136	$\Lambda$ right of mass peak ( $m_{\text{inv}} > m_{\Lambda}$ ) more peripheral centrality . . . . .	149
137	$\Lambda$ right of mass peak ( $m_{\text{inv}} > m_{\Lambda}$ ) more central centrality . . . . .	149
200	$\Lambda$ right of mass peak ( $m_{\text{inv}} > m_{\Lambda}$ ) cut into halves of centrality . . . . .	150
139	$\Lambda$ right of mass peak ( $m_{\text{inv}} > m_{\Lambda}$ ) cut into thirds of centrality . . . . .	150
140	$\Lambda$ right of mass peak ( $m_{\text{inv}} > m_{\Lambda}$ ) for mid-centrality . . . . .	151
141	$\Lambda$ right of mass peak ( $m_{\text{inv}} > m_{\Lambda}$ ) for bins of 20% centrality . . . . .	151
142	$\Lambda$ right of mass peak ( $m_{\text{inv}} > m_{\Lambda}$ ) for 0-20% and 20-80% centrality . . . . .	152
205	$\Lambda$ left of mass peak ( $m_{\text{inv}} < m_{\Lambda}$ ) more peripheral centrality . . . . .	152
144	$\Lambda$ left of mass peak ( $m_{\text{inv}} < m_{\Lambda}$ ) more central centrality . . . . .	153
145	$\Lambda$ left of mass peak ( $m_{\text{inv}} < m_{\Lambda}$ ) cut into halves of centrality . . . . .	153
146	$\Lambda$ left of mass peak ( $m_{\text{inv}} < m_{\Lambda}$ ) cut into thirds of centrality . . . . .	154
147	$\Lambda$ left of mass peak ( $m_{\text{inv}} < m_{\Lambda}$ ) for mid-centrality . . . . .	154
210	$\Lambda$ left of mass peak ( $m_{\text{inv}} < m_{\Lambda}$ ) for bins of 20% centrality . . . . .	155
149	$\Lambda$ left of mass peak ( $m_{\text{inv}} < m_{\Lambda}$ ) for 0-20% and 20-80% centrality . . . . .	155
150	$\bar{\Lambda}$ more peripheral centrality . . . . .	156
151	$\bar{\Lambda}$ more central centrality . . . . .	156
152	$\bar{\Lambda}$ cut into halves of centrality . . . . .	157
215	$\bar{\Lambda}$ cut into thirds of centrality . . . . .	157
154	$\bar{\Lambda}$ for mid-centrality . . . . .	158
155	$\bar{\Lambda}$ for bins of 20% centrality . . . . .	158
156	$\bar{\Lambda}$ for 0-20% and 20-80% centrality . . . . .	159
157	$\bar{\Lambda}$ right of mass peak ( $m_{\text{inv}} > m_{\Lambda}$ ) more peripheral centrality . . . . .	159
220	$\bar{\Lambda}$ right of mass peak ( $m_{\text{inv}} > m_{\Lambda}$ ) more central centrality . . . . .	160
159	$\bar{\Lambda}$ right of mass peak ( $m_{\text{inv}} > m_{\Lambda}$ ) cut into halves of centrality . . . . .	160
160	$\bar{\Lambda}$ right of mass peak ( $m_{\text{inv}} > m_{\Lambda}$ ) cut into thirds of centrality . . . . .	161
161	$\bar{\Lambda}$ right of mass peak ( $m_{\text{inv}} > m_{\Lambda}$ ) for mid-centrality . . . . .	161
162	$\bar{\Lambda}$ right of mass peak ( $m_{\text{inv}} > m_{\Lambda}$ ) for bins of 20% centrality . . . . .	162
225	$\bar{\Lambda}$ right of mass peak ( $m_{\text{inv}} > m_{\Lambda}$ ) for 0-20% and 20-80% centrality . . . . .	162
163	$\bar{\Lambda}$ left of mass peak ( $m_{\text{inv}} < m_{\Lambda}$ ) more peripheral centrality . . . . .	163
164	$\bar{\Lambda}$ left of mass peak ( $m_{\text{inv}} < m_{\Lambda}$ ) more central centrality . . . . .	163

165	$\bar{\Lambda}$ left of mass peak ( $m_{\text{inv}} < m_{\Lambda}$ ) more central centrality	163
166	$\bar{\Lambda}$ left of mass peak ( $m_{\text{inv}} < m_{\Lambda}$ ) cut into halves of centrality	164
167	$\bar{\Lambda}$ left of mass peak ( $m_{\text{inv}} < m_{\Lambda}$ ) cut into thirds of centrality	164
230	168 $\bar{\Lambda}$ left of mass peak ( $m_{\text{inv}} < m_{\Lambda}$ ) for mid-centrality	165
169	$\bar{\Lambda}$ left of mass peak ( $m_{\text{inv}} < m_{\Lambda}$ ) for bins of 20% centrality	165
170	$\bar{\Lambda}$ left of mass peak ( $m_{\text{inv}} < m_{\Lambda}$ ) for 0-20% and 20-80% centrality	166
171	$\Lambda$ polarization dependence on energy (2 bins)	167
172	$\Lambda$ polarization dependence on energy (3 bins)	167
235	173 $\Lambda$ right of mass peak ( $m_{\text{inv}} > m_{\Lambda}$ ) polarization dependence on energy (2 bins)	168
174	$\Lambda$ right of mass peak ( $m_{\text{inv}} > m_{\Lambda}$ ) polarization dependence on energy (3 bins)	168
175	$\Lambda$ left of mass peak ( $m_{\text{inv}} < m_{\Lambda}$ ) polarization dependence on energy (2 bins)	169
176	$\Lambda$ left of mass peak ( $m_{\text{inv}} < m_{\Lambda}$ ) polarization dependence on energy (3 bins)	169
177	$\bar{\Lambda}$ polarization dependence on energy (2 bins)	170
240	178 $\bar{\Lambda}$ polarization dependence on energy (3 bins)	170
179	$\bar{\Lambda}$ right of mass peak ( $m_{\text{inv}} > m_{\Lambda}$ ) polarization dependence on energy (2 bins)	171
180	$\bar{\Lambda}$ right of mass peak ( $m_{\text{inv}} > m_{\Lambda}$ ) polarization dependence on energy (3 bins)	171
181	$\bar{\Lambda}$ left of mass peak ( $m_{\text{inv}} < m_{\Lambda}$ ) polarization dependence on energy (2 bins)	172
182	$\bar{\Lambda}$ left of mass peak ( $m_{\text{inv}} < m_{\Lambda}$ ) polarization dependence on energy (3 bins)	172
245	183 $\Lambda$ polarization dependence on rapidity (2 bins)	173
184	$\Lambda$ polarization dependence on rapidity (3 bins)	173
185	$\Lambda$ polarization dependence on rapidity sign	174
186	$\Lambda$ right of mass peak ( $m_{\text{inv}} > m_{\Lambda}$ ) polarization dependence on rapidity (2 bins)	174
187	$\Lambda$ right of mass peak ( $m_{\text{inv}} > m_{\Lambda}$ ) polarization dependence on rapidity (3 bins)	175
250	188 $\Lambda$ right of mass peak ( $m_{\text{inv}} > m_{\Lambda}$ ) polarization dependence on rapidity sign	175
189	$\Lambda$ left of mass peak ( $m_{\text{inv}} < m_{\Lambda}$ ) polarization dependence on rapidity (2 bins)	176
190	$\Lambda$ left of mass peak ( $m_{\text{inv}} < m_{\Lambda}$ ) polarization dependence on rapidity (3 bins)	176
191	$\Lambda$ Left of mass peak ( $m_{\text{inv}} < m_{\Lambda}$ ) polarization dependence on rapidity sign	177
192	$\bar{\Lambda}$ polarization dependence on rapidity (2 bins)	177
255	193 $\bar{\Lambda}$ polarization dependence on rapidity (3 bins)	178
194	$\bar{\Lambda}$ polarization dependence on rapidity sign	178
195	$\bar{\Lambda}$ right of mass peak ( $m_{\text{inv}} > m_{\Lambda}$ ) polarization dependence on rapidity (2 bins)	179
196	$\bar{\Lambda}$ right of mass peak ( $m_{\text{inv}} > m_{\Lambda}$ ) polarization dependence on rapidity (3 bins)	179
197	$\bar{\Lambda}$ right of mass peak ( $m_{\text{inv}} > m_{\Lambda}$ ) polarization dependence on rapidity sign	180

260	198 $\bar{\Lambda}$ left of mass peak ( $m_{\text{inv}} < m_{\Lambda}$ ) polarization dependence on rapidity (2 bins) . . . . .	180
199	$\bar{\Lambda}$ left of mass peak ( $m_{\text{inv}} < m_{\Lambda}$ ) polarization dependence on rapidity (3 bins) . . . . .	181
200	$\bar{\Lambda}$ Left of mass peak ( $m_{\text{inv}} < m_{\Lambda}$ ) polarization dependence on rapidity sign . . . . .	181
201	$\Lambda$ polarization dependence on azimuthal angle . . . . .	182
202	$\Lambda$ right of mass peak ( $m_{\text{inv}} > m_{\Lambda}$ ) polarization dependence on azimuthal angle . . . . .	182
265	203 $\Lambda$ left of mass peak ( $m_{\text{inv}} < m_{\Lambda}$ ) polarization dependence on azimuthal angle . . . . .	183
204	$\bar{\Lambda}$ polarization dependence on azimuthal angle . . . . .	183
205	$\bar{\Lambda}$ right of mass peak ( $m_{\text{inv}} > m_{\Lambda}$ ) polarization dependence on azimuthal angle . . . . .	184
206	$\bar{\Lambda}$ left of mass peak ( $m_{\text{inv}} < m_{\Lambda}$ ) polarization dependence on azimuthal angle . . . . .	184
207	$\Lambda$ and $\bar{\Lambda}$ polarization with rotated pions . . . . .	186
270	208 $\Lambda$ off mass polarization with rotated pions . . . . .	186
209	$\bar{\Lambda}$ off mass polarization with rotated pions . . . . .	187

## 1 Introduction

The analysis is performed for the BES energies: 7.7, 11.5, 14.5, 19.6, 27, and 39 GeV.

275 Peripheral collisions have large angular momentum ( $\sim 10^4 - 10^5 \hbar$ ) which can be transferred, in part, to the fireball at mid-rapidity. In principle this could be related to baryon stopping. A partial thermalization of the angular degrees of freedom inside the fireball would lead to hadronic spin alignment with the angular momentum of the system. This spin alignment is the global polarization of the hadrons. The vorticity is the curl of a fluid's velocity field  $\vec{\omega} \equiv \nabla \times \vec{v}$ . In a hydrodynamic description the vorticity of the fluid is probed by the global polarization, which is largely unexplored in current transport models.

280 Lambda baryons are self analyzing which means that the daughter protons are preferentially emitted in the direction of the Lambda's spin (note that the proton is emitted opposite the spin for the antiparticle, the  $\bar{\Lambda}$ ). The distribution of emitted protons follows the following distribution

$$\frac{1}{N} \frac{dN}{d\Omega^*} = \frac{1}{4\pi} \left( 1 + \alpha \vec{S}_\Lambda^* \cdot \hat{p}_p^* \right), \quad (1)$$

where the \* denotes the rest frame of the  $\Lambda$ ,  $\vec{S}_\Lambda^*$  is the Lambda spin direction,  $\hat{p}_p^*$  is the daughter proton momentum direction.

285 The self analyzing nature of the  $\Lambda$ s allows us to make a measurement of the global  $\Lambda$  polarization. The global polarization is measured by looking to see if the spin of the  $\Lambda$  points preferentially in the direction of the angular momentum of the system  $\hat{L}$ .  $\hat{L}$  is found via the first order event plane,  $\Psi_1$ , which is found by using the BBC. Our measure of polarization is

$$\frac{8}{\pi\alpha} \langle \sin(\phi_p^* - \Psi_1) \rangle \quad (2)$$

where  $\phi_p^*$  is the proton's azimuthal angle.

290 Initially we planned on extracting the polarization due to the magnetic field and vorticity separately. We are no longer doing this now that we have switched from a PRL to a Nature paper. Plots and discussion from this are littered throughout. We plan on a followup PRC which will include this so I don't want to remove it.

The final plot for  $\Lambda$  and  $\bar{\Lambda}$  polarization

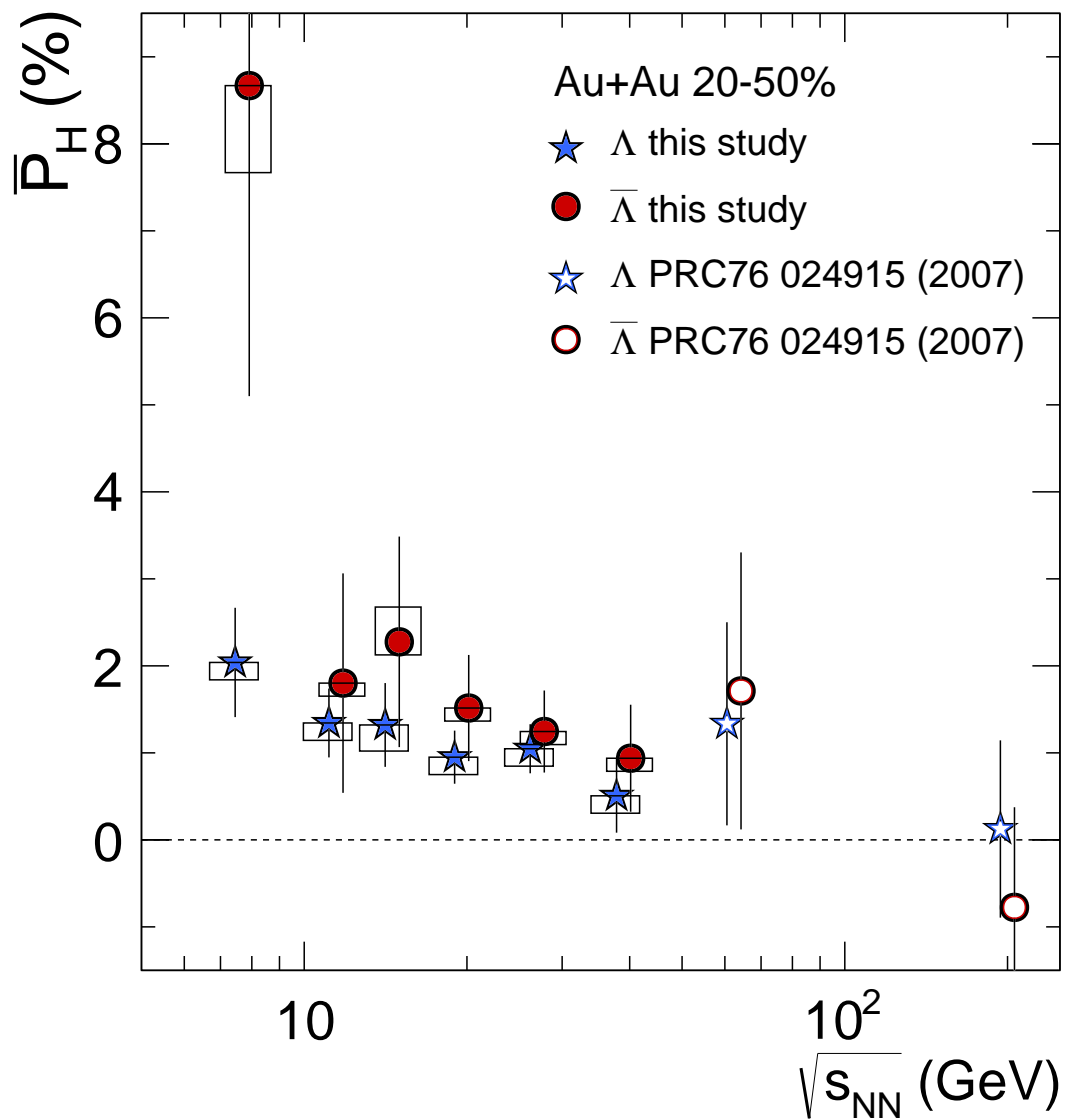


**Fig. 1:**  $\left\langle \frac{8}{\pi\alpha} \sin(\Psi_1 - \phi_{\Lambda,\bar{\Lambda}}^*) \right\rangle$  vs.  $\sqrt{s_{NN}}$  for 20-50% centrality

295 The supporting plots are

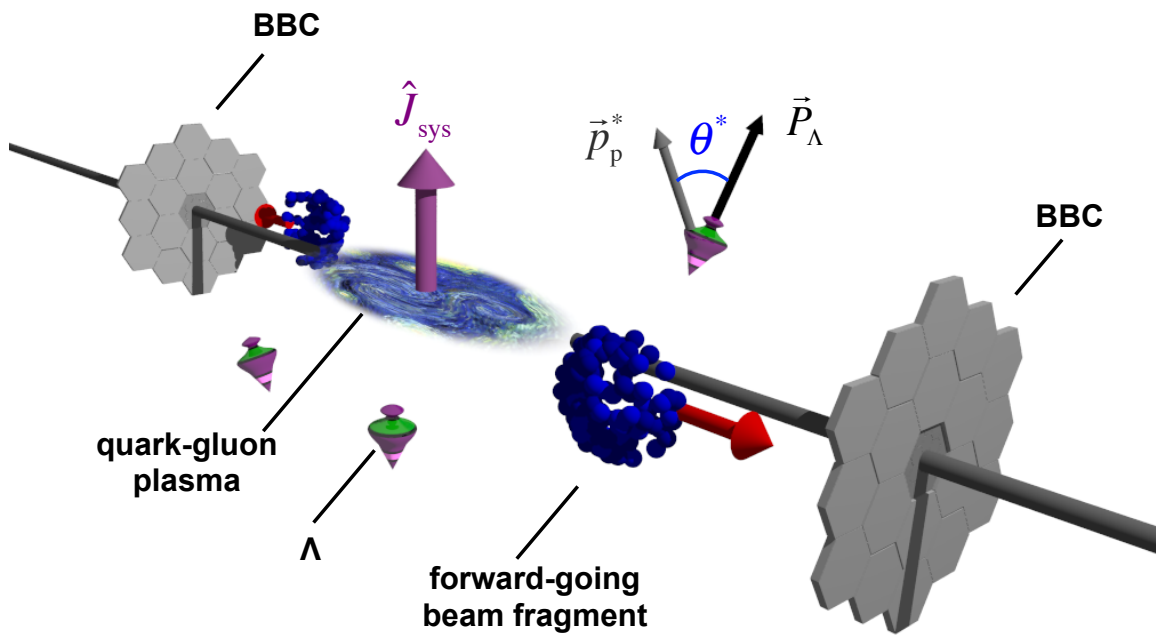


**Fig. 2:** schematic of collision.

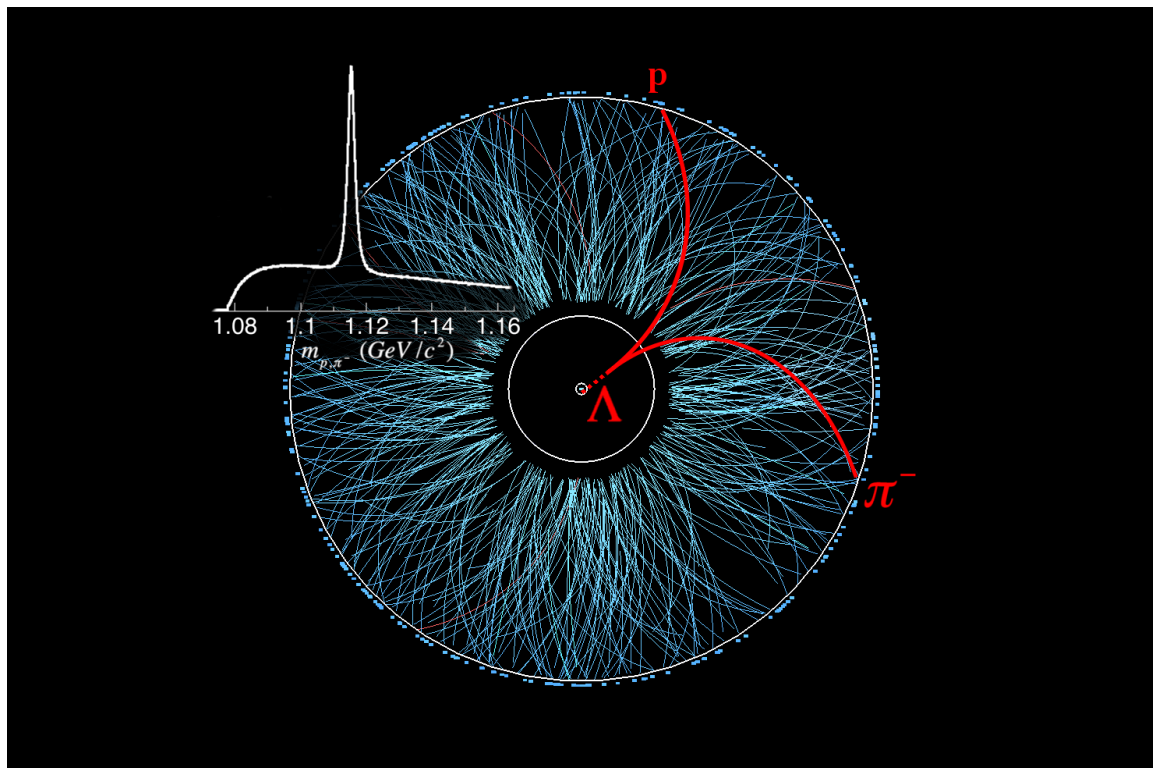


**Fig. 3:** Lambda in event with black background schematic.

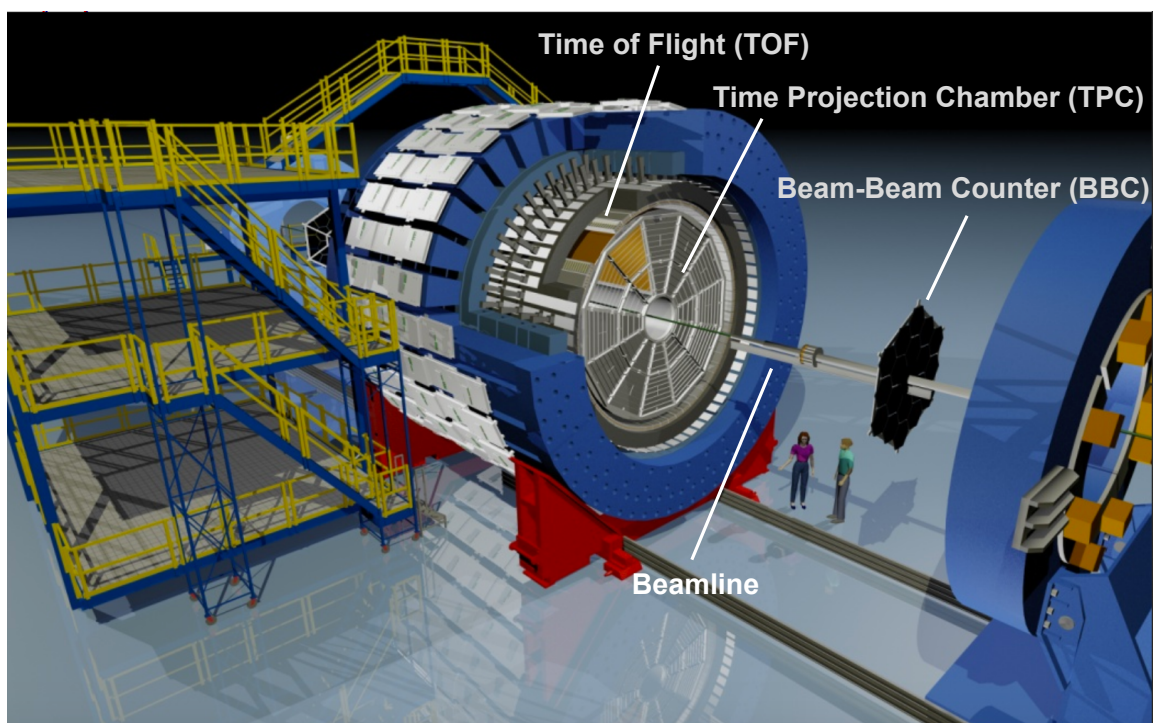


**Fig. 4:** overview of the STAR detector.

The following figures are not part of the Nature paper, but they are to be included in a PRC. These are found by the feed down correction described in sec. 3.5.

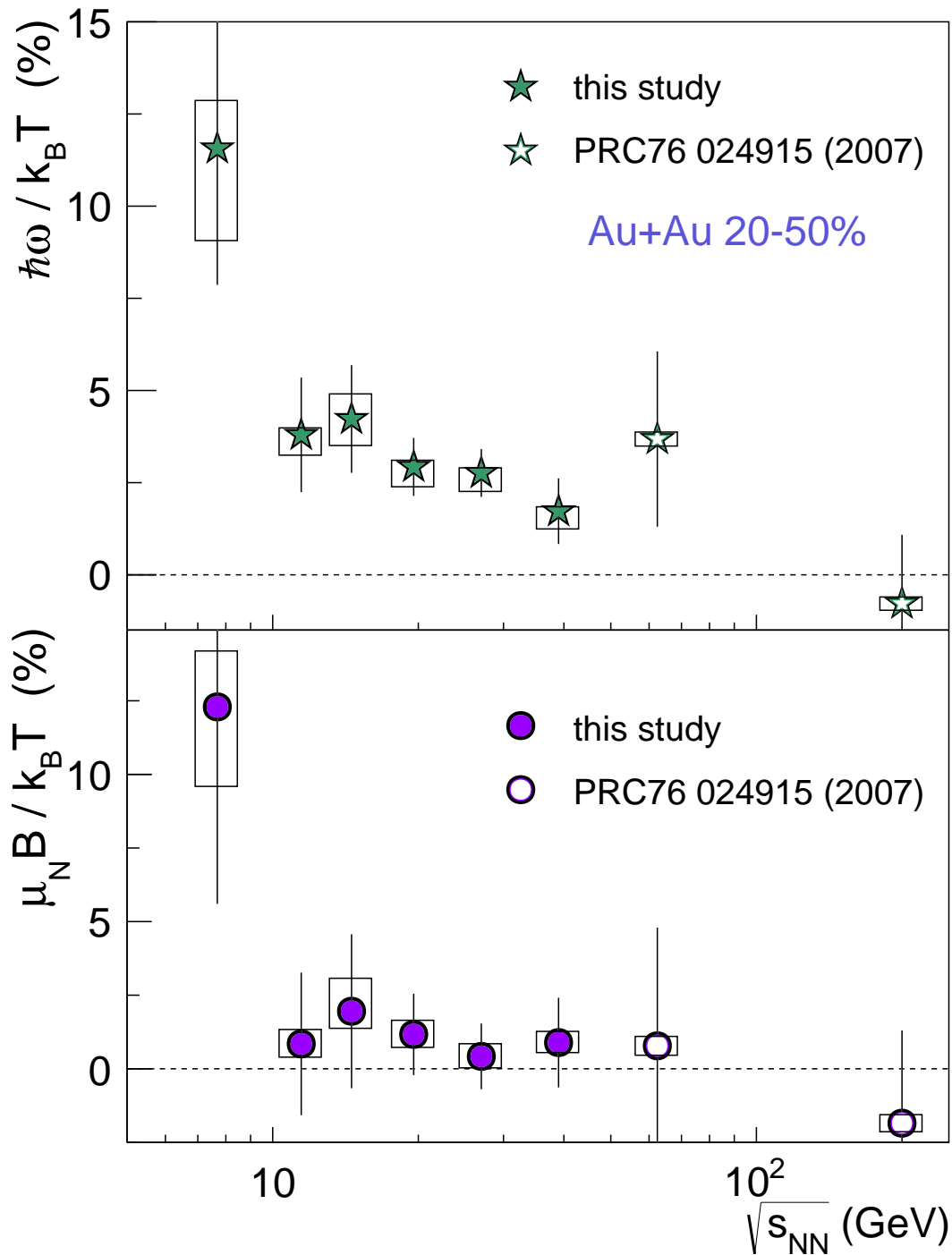


**Fig. 5:** Vorticity and magnetic field as a function of  $\sqrt{s_{NN}}$ .

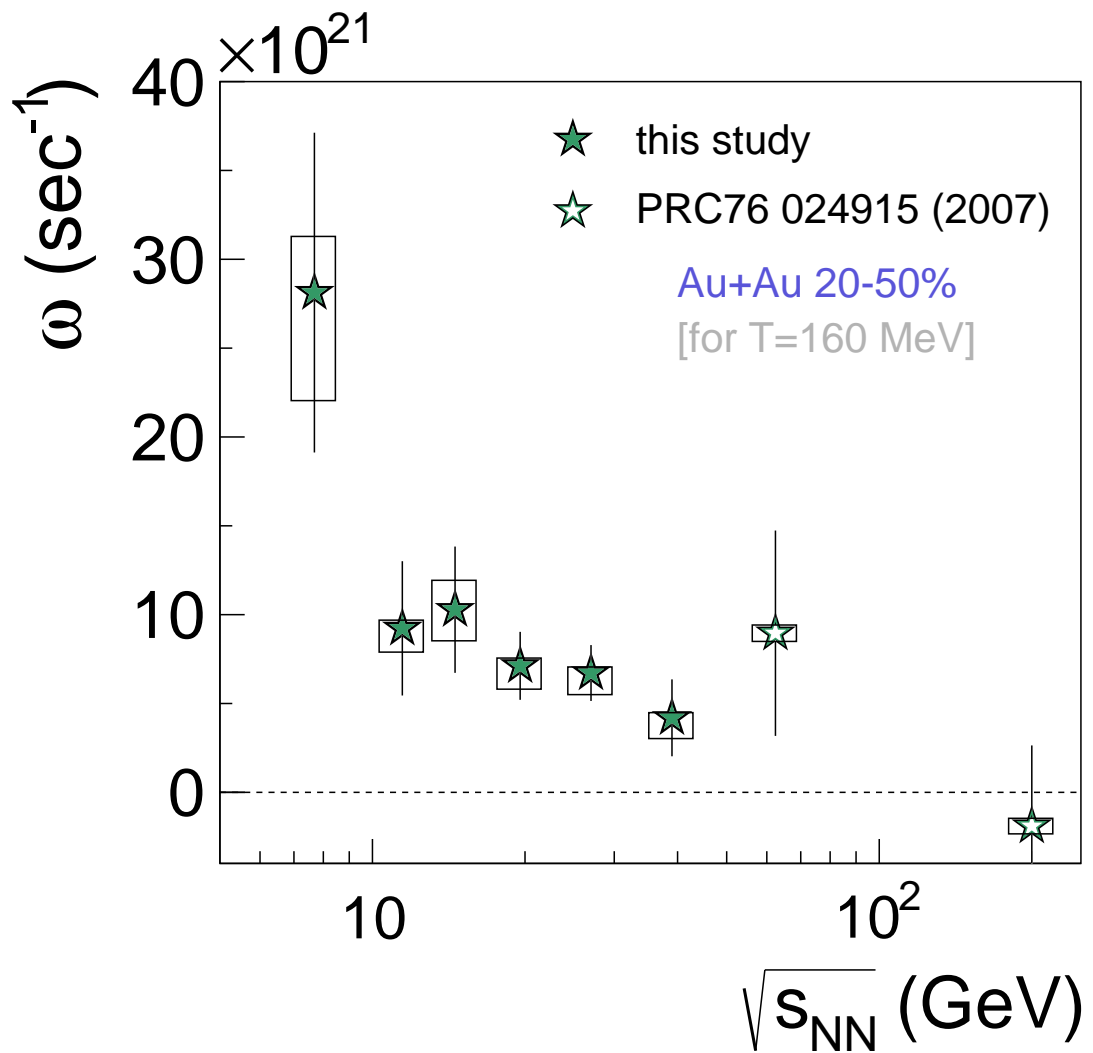


**Fig. 6:** Vorticity in  $H_z$  (assuming  $T = 160$  MeV) as a function of  $\sqrt{s_{NN}}$ .

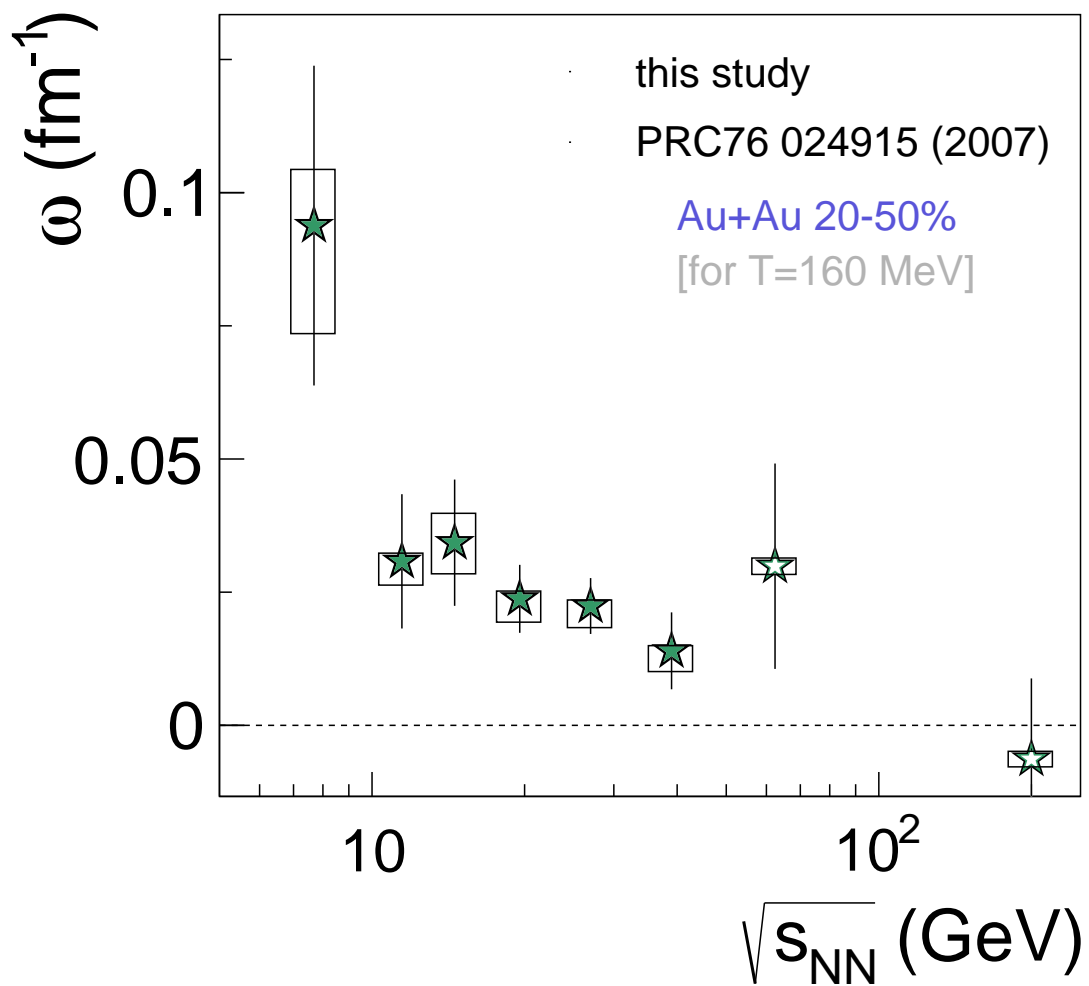


**Fig. 7:** Vorticity in  $fm^{-1}$  (assuming  $T = 160MeV$ ) as a function of  $\sqrt{s_{\text{NN}}}$ . This is just a scaling of 1.

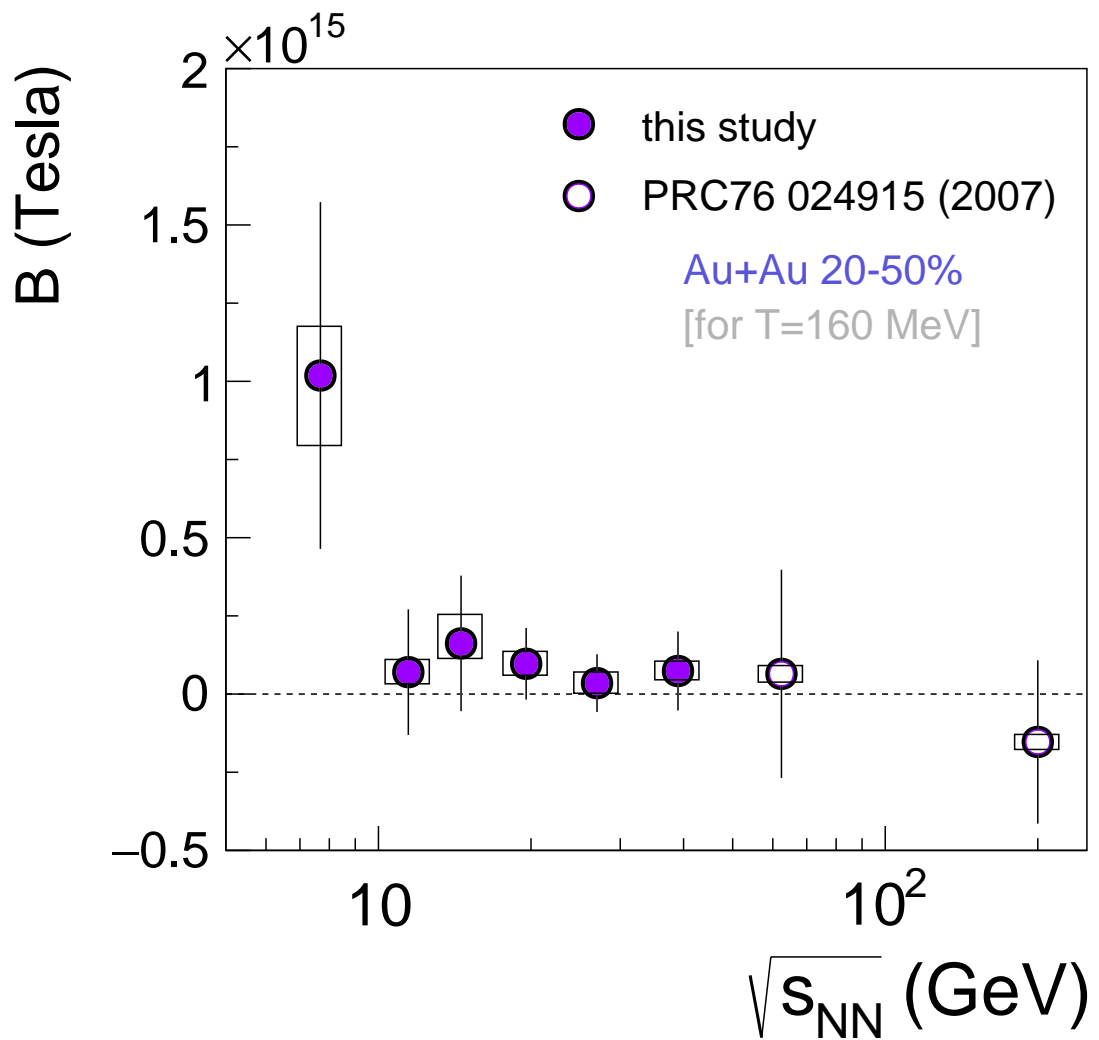


**Fig. 8:** Magnetic field in  $T$  (assuming  $T = 160\text{MeV}$ ) as a function of  $\sqrt{s_{NN}}$ .

## 2 Quality Assurance

### 300 2.1 Event QA

The events used in the analysis have the following cuts

- The magnitude of the z component of the primary vertex is  $\leq 70\text{cm}$ . At 39GeV this is a 40cm cut and at 11GeV this is 50cm cut.
- Tof multiplicity  $\geq 1$
- the R vertex component is required to be less than 2cm except in the case of 15GeV where it is less than 1cm and centered at (0, -0.89) cm.
- The adc sum for the East and West BBC are separately required to be  $\geq 75$
- Additionally there is an  $\eta$  symmetry cut so that  $|(N_{\eta>0} - N_{\eta<0}) / N_{\text{total}}| \leq 5$
- The centrality ID that we get from StRefMultCorr must be  $\geq 0$

310 The trigger list for each energy is

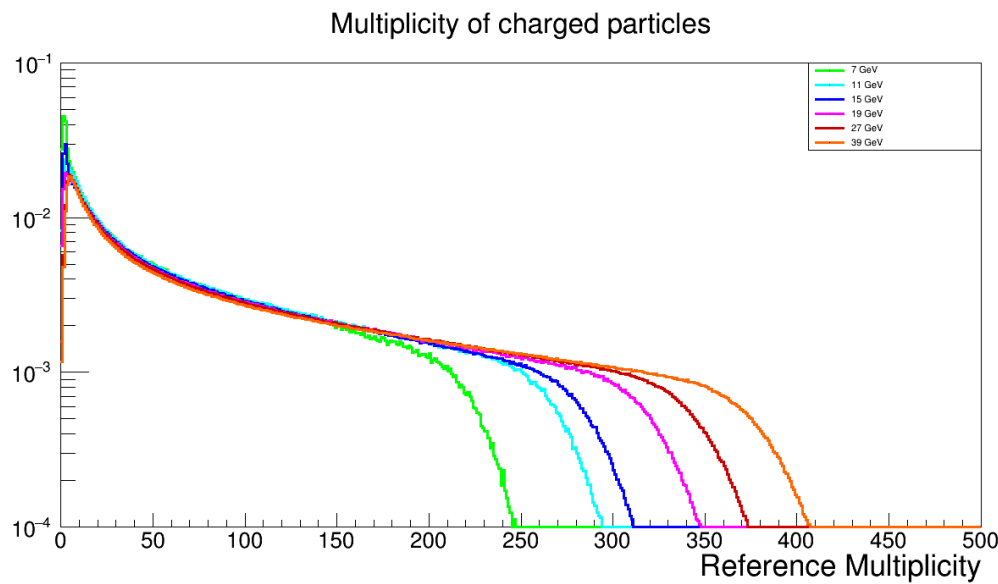
- 7.7GeV: 290001, 290004
- 11.5GeV: 310004, 310014
- 14.5GeV: 440005, 440015
- 19.6GeV: 340001, 340011, 340021
- 27GeV: 360001, 360002
- 39GeV: 280001, 280002

Additionally there is a list of rejected runs which is

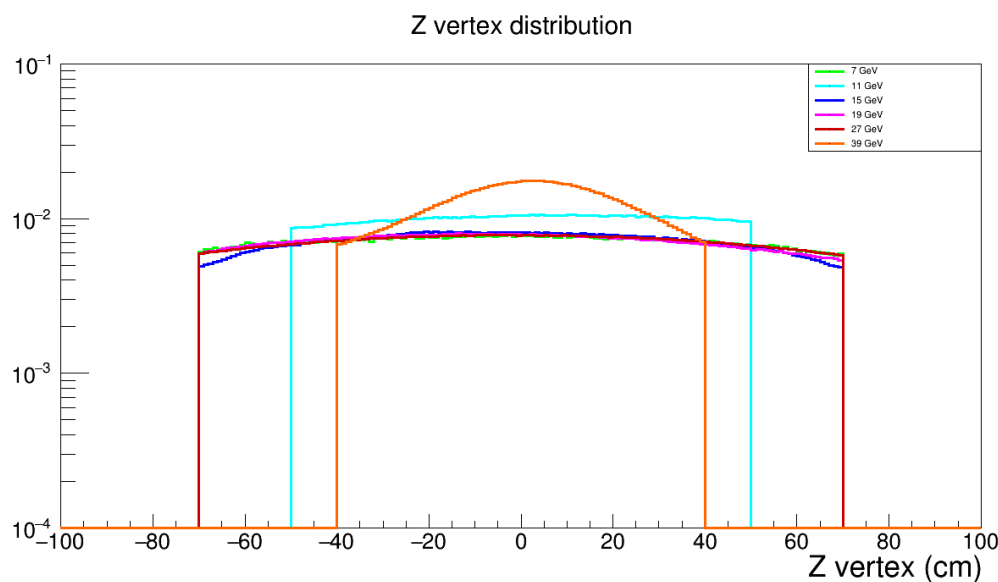
- 7.7GeV: 11199124, 11100002, 11100045, 11101046, 11102012, 11102051, 11102052, 11102053, 11102054, 11102055, 11102058, 11103035, 11103056, 11103058, 11103092, 11103093, 11105052, 11105053, 11105054, 11105055, 11107007, 11107042, 11107057, 11107061, 11107065, 11107074, 11108101, 11109013, 11109077, 11109088, 11109090, 11109127, 11110013, 11110034, 11110073, 11110076, 11111084, 11111085
- 11.5GeV: 11148039, 11148045, 11149001, 11149008, 11149010, 11149011, 11149015, 11149047, 11150016, 11150025, 11150028, 11151036, 11151040, 11151050, 11152016, 11152036, 11152078, 11153032, 11153042, 11155001, 11155009, 11156003, 11156009, 11157012, 11158006, 11158022, 11158024
- 14.5GeV: 15046073, 15046089, 15046094, 15046096, 15046102, 15046103, 15046104, 15046105, 15046106, 15046107, 15046108, 15046109, 15046110, 15046111, 15047004, 15047015, 15047016, 15047019, 15047021, 15047023, 15047024, 15047026, 15047027, 15047028, 15047029, 15047030, 15047039, 15047040, 15047041, 15047044, 15047047, 15047050, 15047052, 15047053, 15047056, 15047057, 15047061, 15047062, 15047063, 15047064, 15047065, 15047068, 15047069, 15047070, 15047071, 15047072, 15047074, 15047075, 15047082, 15047085, 15047086, 15047087, 15047093, 15047096, 15047097, 15047098, 15047100, 15047102, 15047104, 15047106, 15048003, 15048004,

- 15048012, 15048013, 15048014, 15048016, 15048017, 15048018, 15048019, 15048020, 15048021,  
 335 15048023, 15048024, 15048025, 15048026, 15048028, 15048029, 15048030, 15048031, 15048033,  
 15048034, 15048074, 15048075, 15048076, 15048077, 15048078, 15048079, 15048080, 15048081,  
 15048082, 15048083, 15048084, 15048085, 15048086, 15048087, 15048088, 15048089, 15048091,  
 15048092, 15048093, 15048094, 15048095, 15048096, 15048097, 15048098, 15049002, 15049003,  
 340 15049009, 15049013, 15049014, 15049015, 15049016, 15049017, 15049018, 15049019, 15049020,  
 15049021, 15049022, 15049023, 15049025, 15049026, 15049027, 15049028, 15049030, 15049031,  
 15049032, 15049033, 15049037, 15049038, 15049039, 15049040, 15049041, 15049074, 15049077,  
 15049083, 15049084, 15049085, 15049086, 15049087, 15049088, 15049089, 15049090, 15049091,  
 15049092, 15049093, 15049094, 15049096, 15049097, 15049098, 15049099, 15050001, 15050002,  
 345 15050003, 15050004, 15050005, 15050006, 15050010, 15050011, 15050012, 15050013, 15050014,  
 15050015, 15050016, 15051131, 15051132, 15051133, 15051134, 15051137, 15051141, 15051144,  
 15051146, 15051147, 15051148, 15051149, 15051156, 15051157, 15051159, 15051160, 15052001,  
 15052004, 15052005, 15052006, 15052007, 15052008, 15052009, 15052010, 15052011, 15052014,  
 15052015, 15052016, 15052017, 15052018, 15052019, 15052020, 15052021, 15052022, 15052023,  
 15052024, 15052025, 15052026, 15052040, 15052041, 15052042, 15052043, 15052060, 15052061,  
 350 15052062, 15052063, 15052064, 15052065, 15052066, 15052067, 15052068, 15052069, 15052070,  
 15052073, 15052074, 15052075, 15053027, 15053028, 15053029, 15053034, 15053035, 15053052,  
 15053054, 15053055, 15054053, 15054054, 15055018, 15055137, 15056117, 15057055, 15057059,  
 15058006, 15058011, 15058021, 15059057, 15059058, 15061001, 15061009, 15062006, 15062069,  
 15065012, 15065014, 15066070, 15068013, 15068014, 15068016, 15068018, 15069036, 15070008,  
 355 15070009, 15070010
- 19.6GeV: 12113091, 12114007, 12114035, 12114078, 12114092, 12114116, 12115009, 12115014,  
 12115015, 12115016, 12115018, 12115019, 12115020, 12115022, 12115023, 12115062, 12115073,  
 12115093, 12115094, 12116012, 12116054, 12117010, 12117016, 12117020, 12117065, 12119040,  
 12119042, 12120017, 12120026, 12121017, 12121022, 12121034, 12121050, 12121067, 12122019
  - 27GeV: 12172050, 12172051, 12172055, 12173030, 12173031, 12173032, 12173033, 12173034,  
 360 12174067, 12174085, 12175062, 12175087, 12175113, 12175114, 12175115, 12176001, 12176044,  
 12176054, 12176071, 12177015, 12177061, 12177092, 12177099, 12177101, 12177106, 12177107,  
 12177108, 12178003, 12178004, 12178005, 12178006, 12178013, 12178099, 12178120
  - 39GeV: 11199124, 11100002, 11100045, 11101046, 11102012, 11102051, 11102052, 11102053,  
 365 11102054, 11102055, 11102058, 11103035, 11103056, 11103058, 11103092, 11103093, 11105052,  
 11105053, 11105054, 11105055, 11107007, 11107042, 11107057, 11107061, 11107065, 11107074,  
 11108101, 11109013, 11109077, 11109088, 11109090, 11109127, 11110013, 11110034, 11110073,  
 11110076, 11111084, 11111085

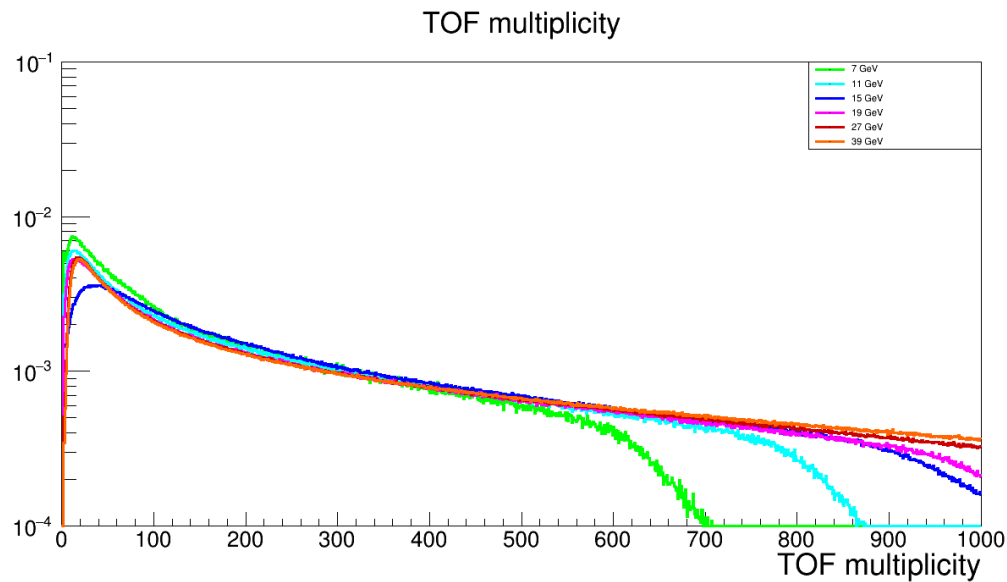
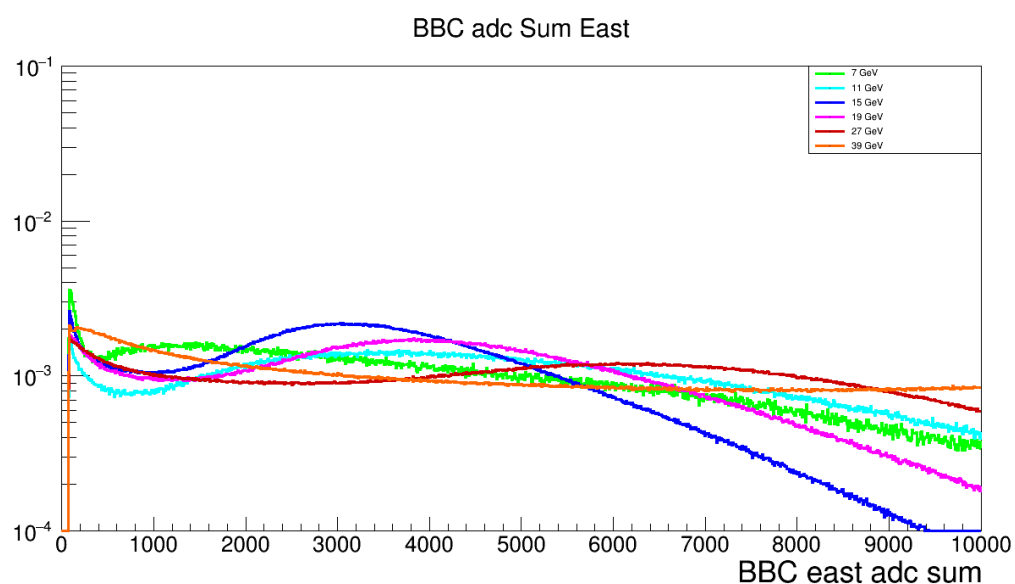
In addition to the bad runs list 15GeV events are taken only from running days 53-70.



**Fig. 9:** Multiplicity of charged tracks (normalized)



**Fig. 10:** Z component of event vertex (normalized)

**Fig. 11:** TofMultiplicity (normalized)**Fig. 12:** BBC East ADC sum (normalized)

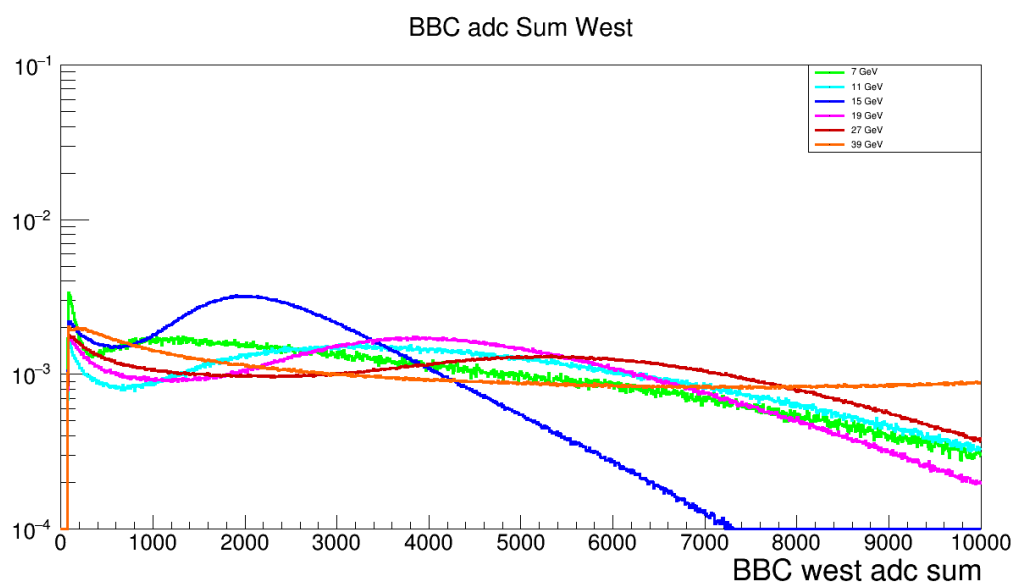


**Fig. 13:** BBC West ADC sum (normalized)

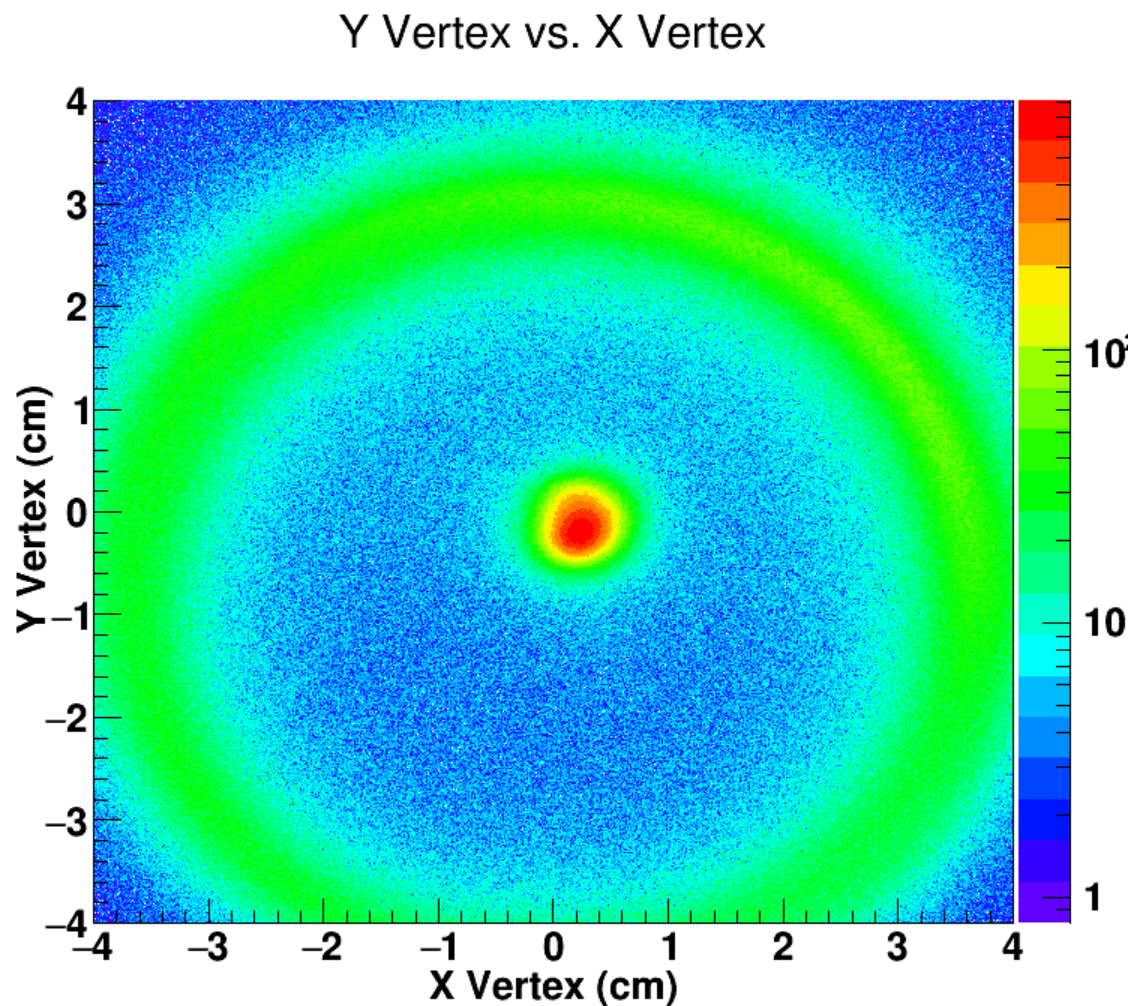


**Fig. 14:**  $y$  component of primary vertex vs.  $x$  component of primary vertex for 7GeV

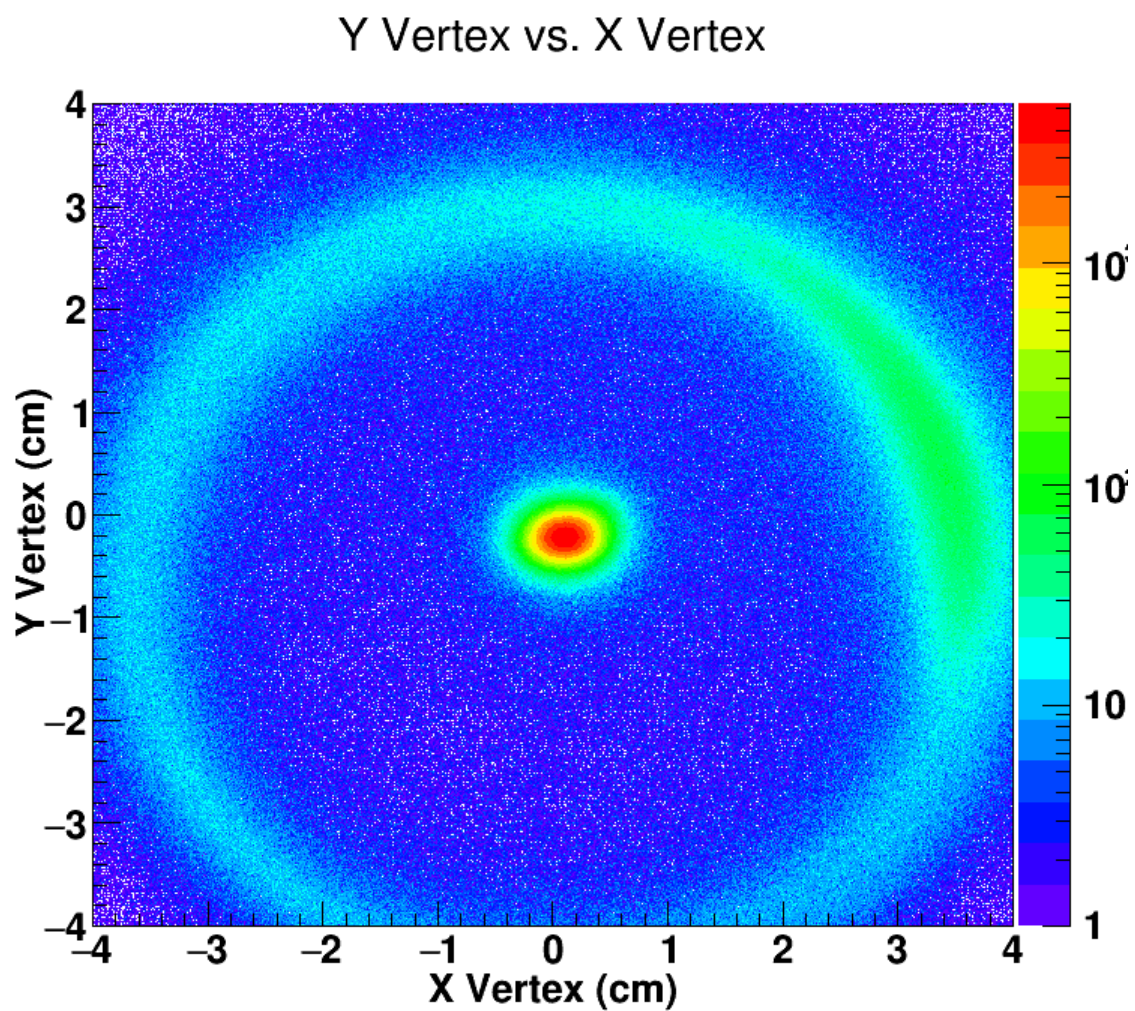


**Fig. 15:**  $y$  component of primary vertex vs.  $x$  component of primary vertex for 11GeV

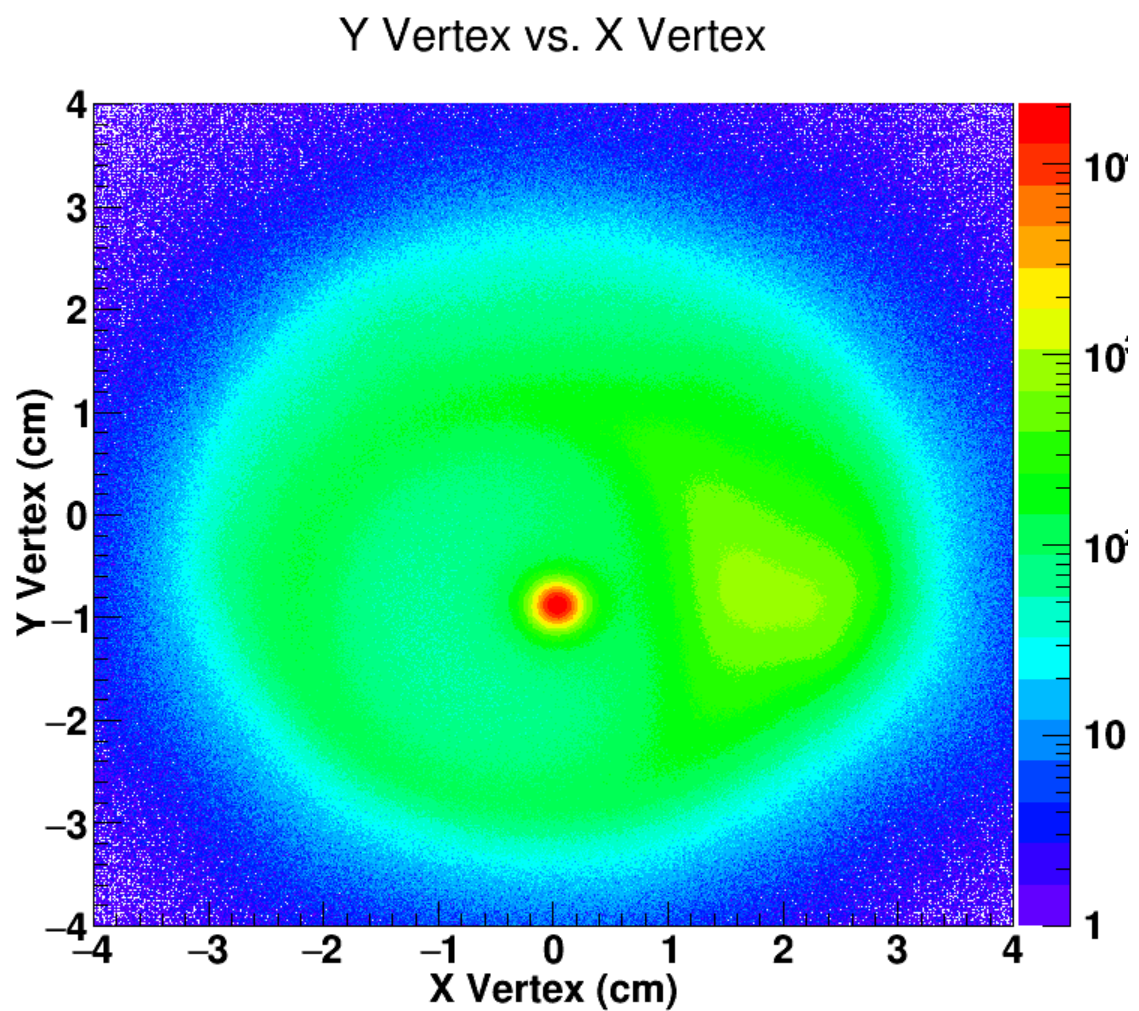


**Fig. 16:**  $y$  component of primary vertex vs.  $x$  component of primary vertex for 15GeV

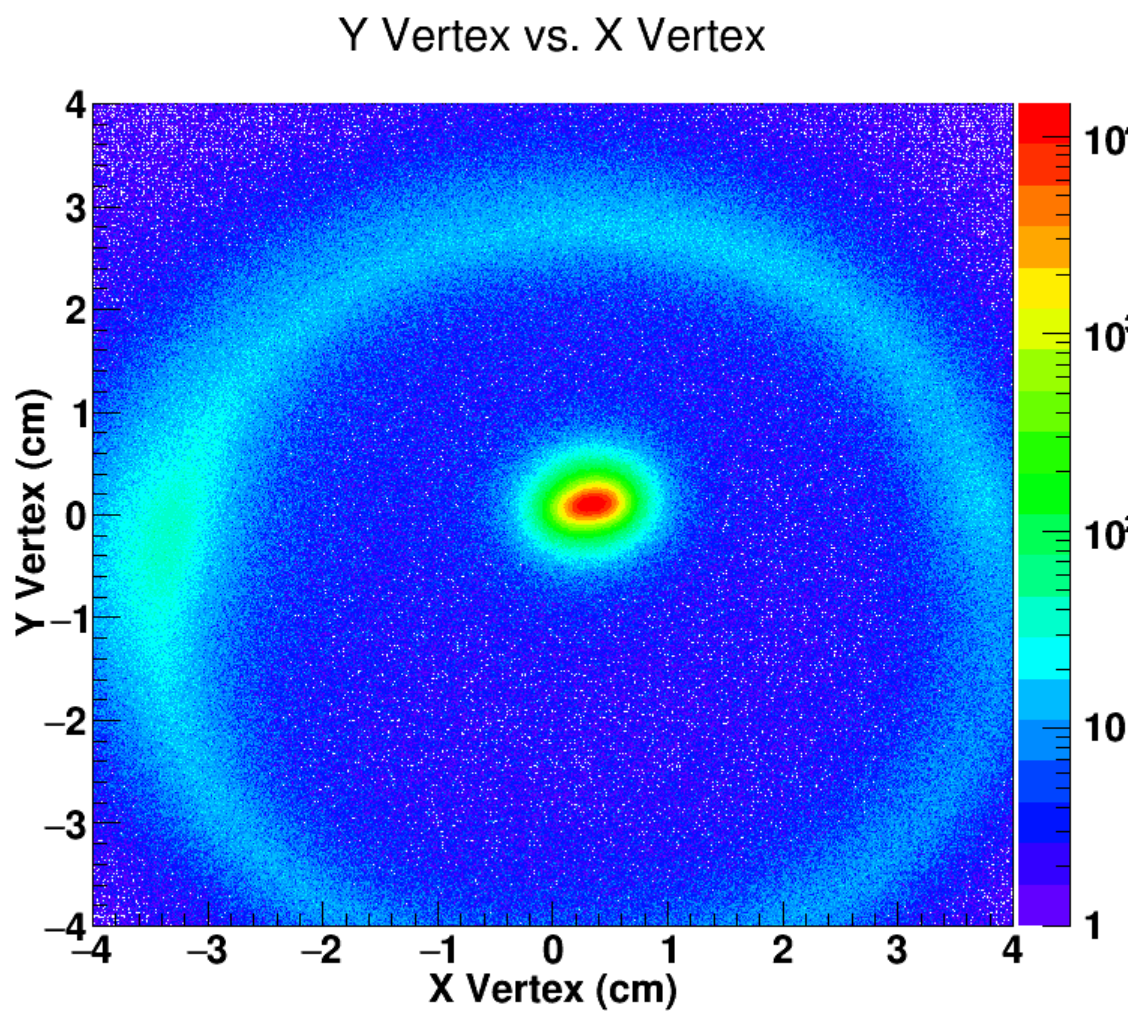


**Fig. 17:**  $y$  component of primary vertex vs.  $x$  component of primary vertex for 19GeV

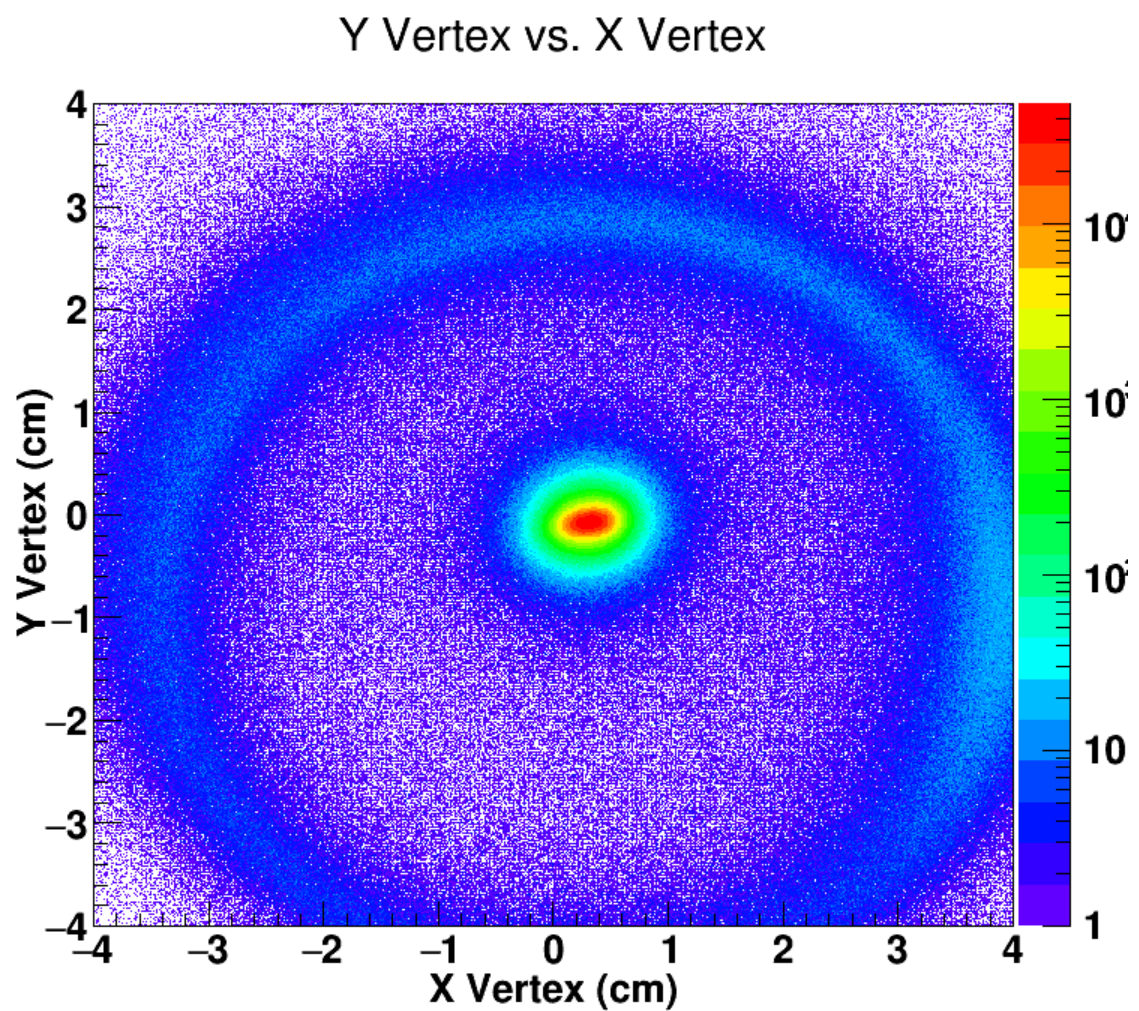


**Fig. 18:**  $y$  component of primary vertex vs.  $x$  component of primary vertex for 27GeV

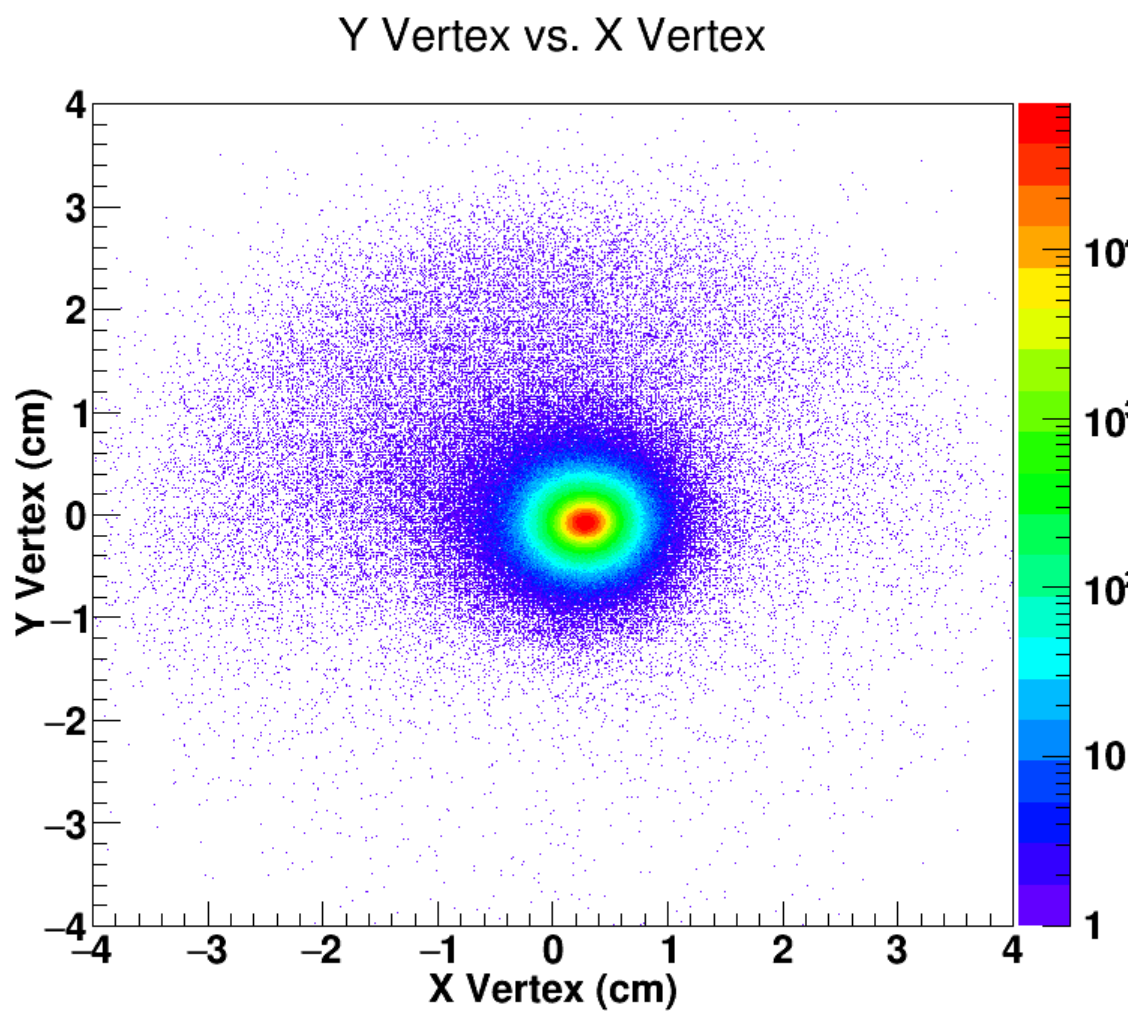


**Fig. 19:**  $y$  component of primary vertex vs.  $x$  component of primary vertex for 39GeV

370 **2.2 Event Plane determination**

The analysis uses the first order event plane,  $\Psi_1$ , determined by the east and west BBCs (beam beam counters). Generally the event plane is found by weighting the tile geometry by the ADC value for that given tile. The numbering scheme for the inner tiles of the detector (only the inner tiles are used) is shown below for one looking a very large  $|z|$

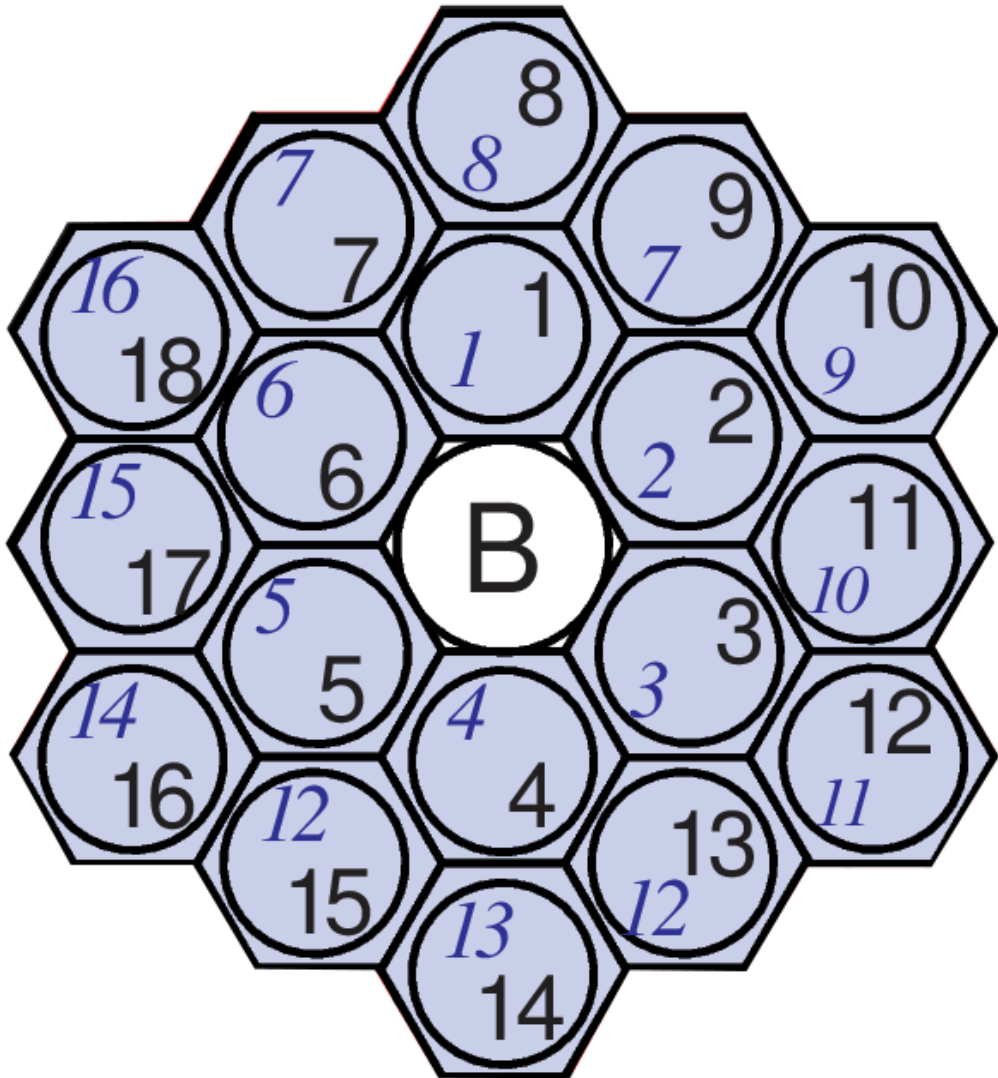


**Fig. 20:** BBC numbering scheme looking at very large  $|z|$ . Black numbers represent tile number while blue numbers represent PMT number.

375 Tiles 7 and 9 (13 and 15) share PMTs which means it is impossible to tell whether one was hit or the other. Many analyses deal with this by randomly ambiguity by assigning the ADC value in its entirety to tile 7 (13) XOR tile 9 (15). I prefer to count the tile pair's contribution as being between them so  $\pi/2$  ( $3\pi/2$ ). I think that this scheme makes more sense and certainly makes comparisons with ones own code or the code of others much easier. In practice I have not seen a noticeable difference between the 380 two methods. Note that either way the tiles are mirrored about the  $x$  axis but not the  $y$  axis so that a line parallel to the  $z$  axis might go through tile 11 on the West BBC and tile 17 on the East BBC while such a line could go through both tile 8s.

$v_1 * y > 0$  by conventions most reasonable to the STAR event plane. Therefore the west BBC reconstructs the "right" event plane. Spectators on the east side BBC hit a position which is  $180^\circ$  in  $x - y$  from those that hit the west. This means that there is a negative sign for the east BBC event plane. More simply  
 $Psi_E = 0 \implies Q_{x,West} = x_{STAR}$  which would mean  $Psi_E = \pi \implies Q_{x,East} = -x_{STAR}$ . A particularly nice picture of the STAR coordinate system (<https://drupal.star.bnl.gov/STAR/public/img/SketchUpSTAR>) is

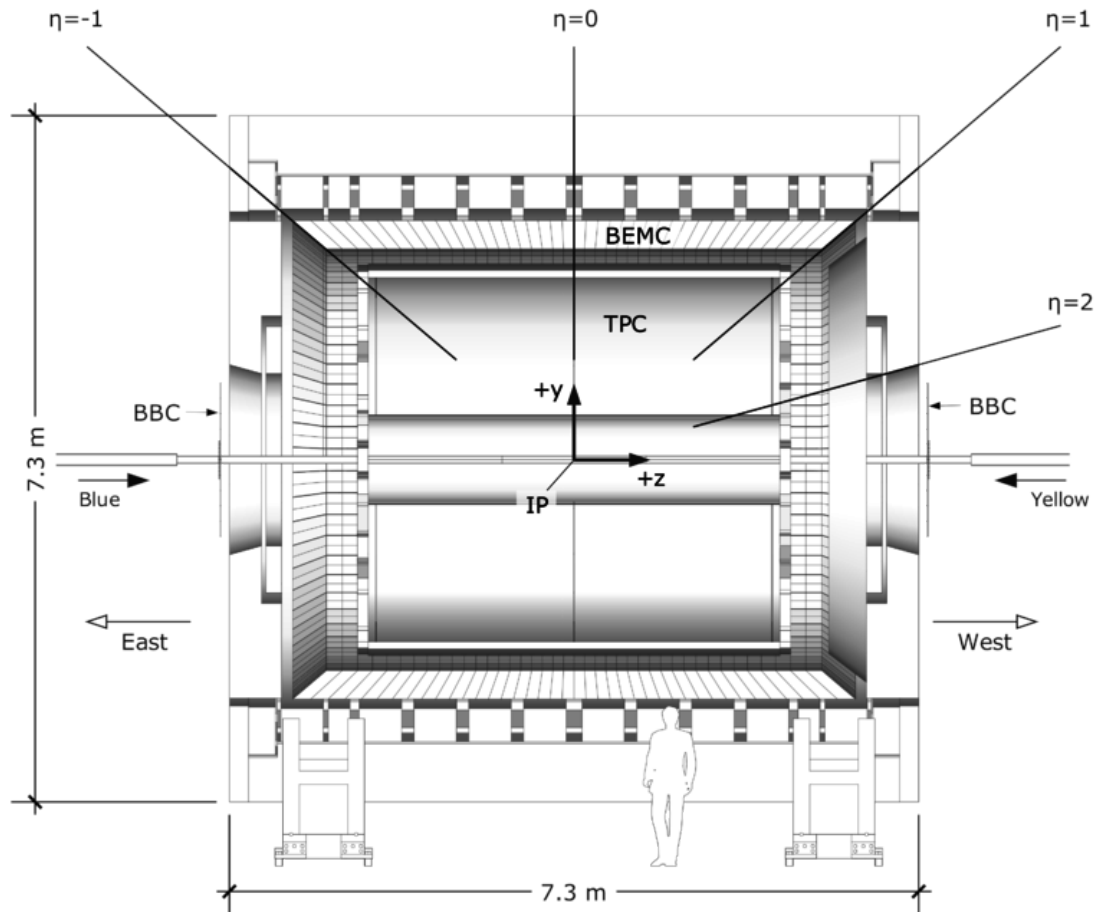


**Fig. 21:** STAR coordinate system

The "raw" (uncorrected) event plane is found by weighting tile geometry by the ADC for the relevant tile. This sum over the ADC channels creates a standard flow Q vector,  $Q_1 = (\sum_{i=1}^{16} ADC_i * \cos(\phi_i), \sum_{i=1}^{16} ADC_i * \sin(\phi_i))$ . We make (and correct) Q vectors for east and west separately which allows us to get a resolution correction later. The Q vector for the full event plane is basically made by taking  $Q_{1,W} - Q_{1,E}$ . After this raw event plane is found we do a series of corrections to the event plane. The corrections are done in the following order:

- Gain correction: The idea of the gain correction is that not all BBC tiles may output the same adc value for the same hit, some can be hot/cold. To correct for this we normalize the number of hits in each tile by the amount that tile fired relative to the other tiles making sure that the bank of "other tiles" is equally likely to be hit. So, innermost tiles 1-6 are normalized together while, separately tiles 7-18 are normalized together. This normalization should be done over enough time to get reasonable statistics and a small enough time that the normalization is relevant. I do this normalization for each new run number.
- Recentering correction: The Q vector averaged over all events has to be zero since, of course, there is no preferred impact parameter. Even with the gain correction it is possible that the Q vector doesn't average to zero since adcs can saturate and it is possible that a particular adc is more likely to saturate than the others. In principal the recentering correction well motivated, in practice this correction tends to be minimally impactful
- $\Psi$  shift correction: This is the least well motivated of the corrections. In principal the event plane distributions should all be flat since there is no preferred event plane, this correction takes each Psi distribution (full/east/west) and applies a flattening method which flattens in harmonics of the distribution (decomposed into sines and cosines). The harmonics of the distribution are then subtracted off. Typically only the first few harmonics are non-zero. This is a steamroller that runs over the distribution. The best justification for why the shift correction is okay is the  $\Psi_E$  vs  $\Psi_W$  plot where the  $\Psi_E$  vs  $\Psi_W$  are separately corrected. In such a plot the correlation is seen to be better after the shifting. We have done nothing, in such a case, to require that to happen. The correction is done to 20th order, this is overkill but it isn't expensive to do.

415 The following plots show the event plane distributions as they are corrected for all relevant energies

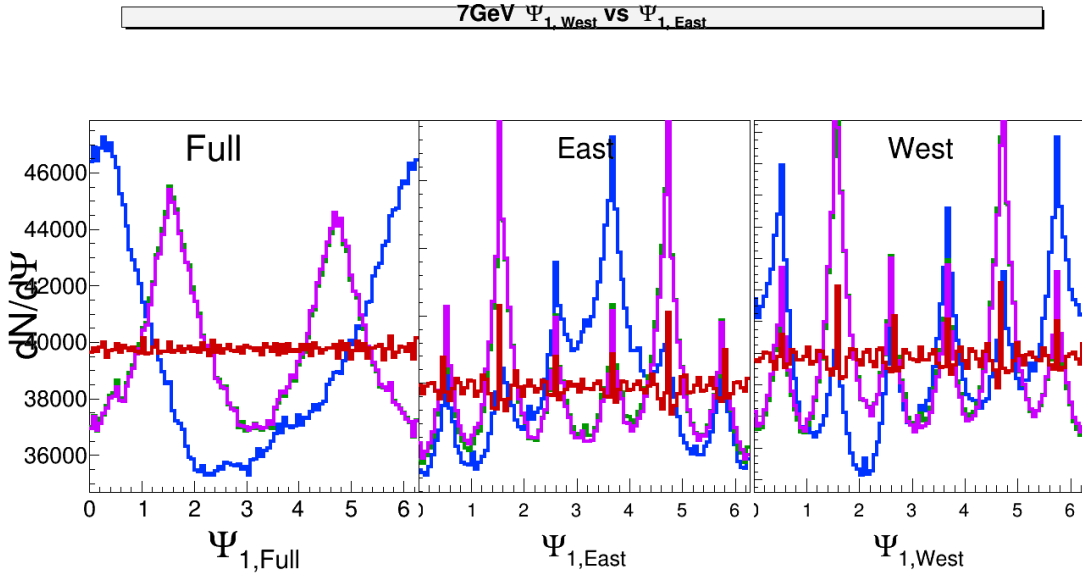


**Fig. 22:** 7GeV  $\Psi_1$  distribution as corrections are applied. Blue - Raw, Green - Gain corrected, Violet - Recentered, Red - Shifted.

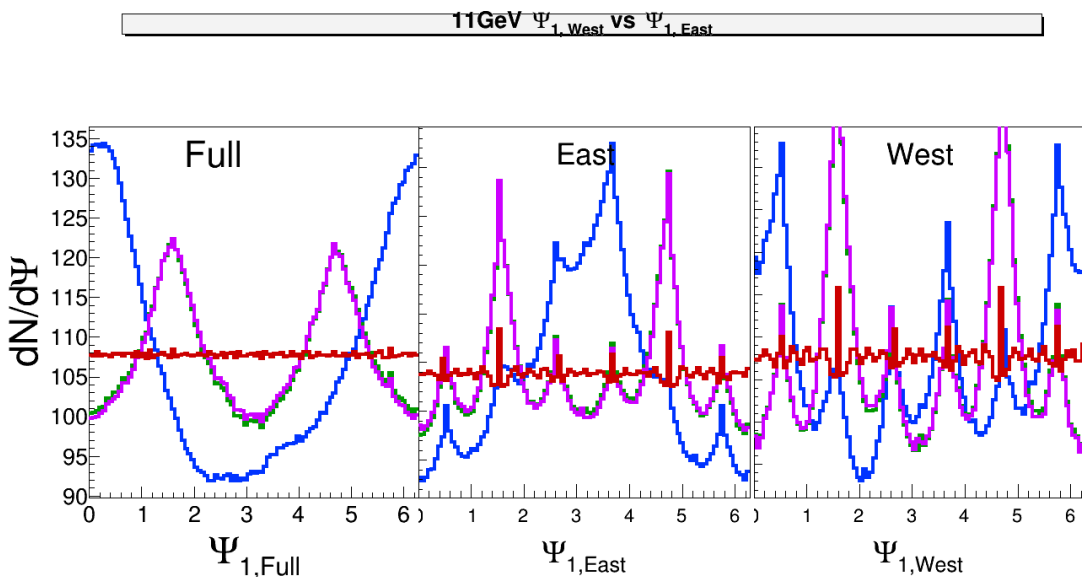


**Fig. 23:** 11GeV  $\Psi_1$  distribution as corrections are applied. Blue - Raw, Green - Gain corrected, Violet - Recentered, Red - Shifted.

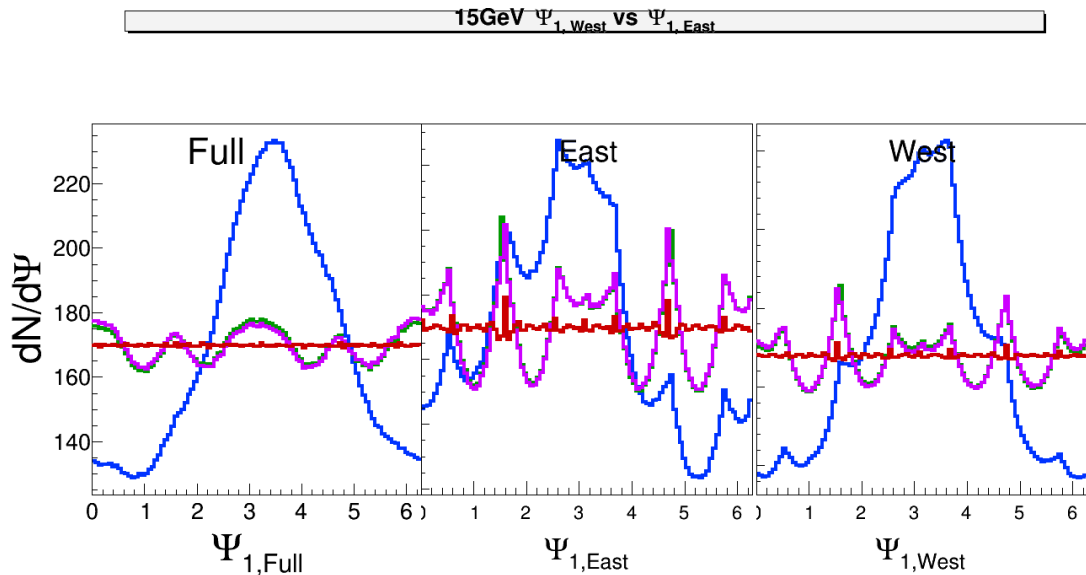


**Fig. 24:** 15GeV  $\Psi_1$  distribution as corrections are applied. Blue - Raw, Green - Gain corrected, Violet - Recentered, Red - Shifted.

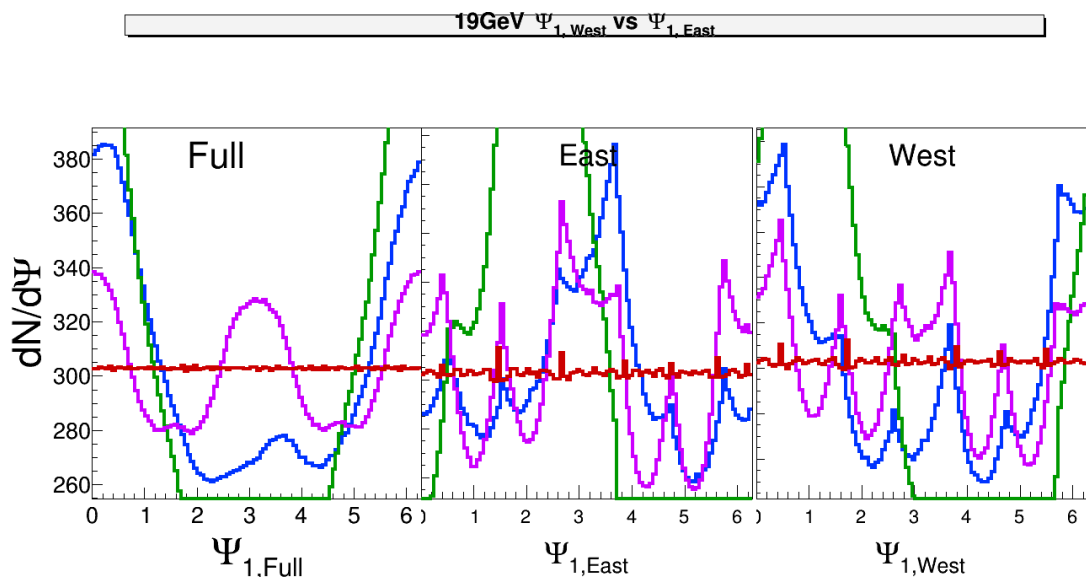


**Fig. 25:** 19GeV  $\Psi_1$  distribution as corrections are applied. Blue - Raw, Green - Gain corrected, Violet - Recentered, Red - Shifted.

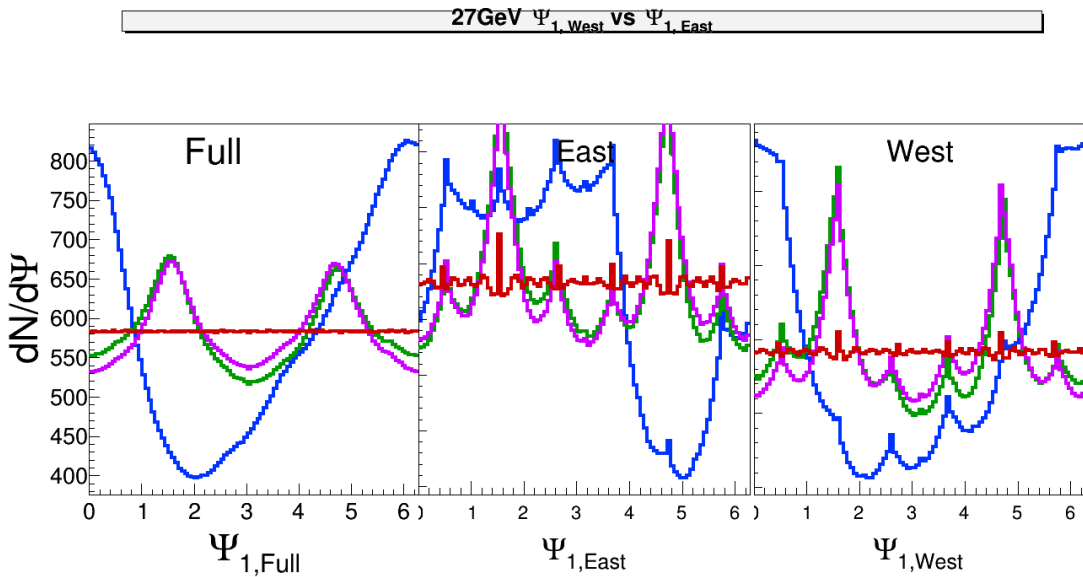


**Fig. 26:** 27GeV  $\Psi_1$  distribution as corrections are applied. Blue - Raw, Green - Gain corrected, Violet - Recentered, Red - Shifted.

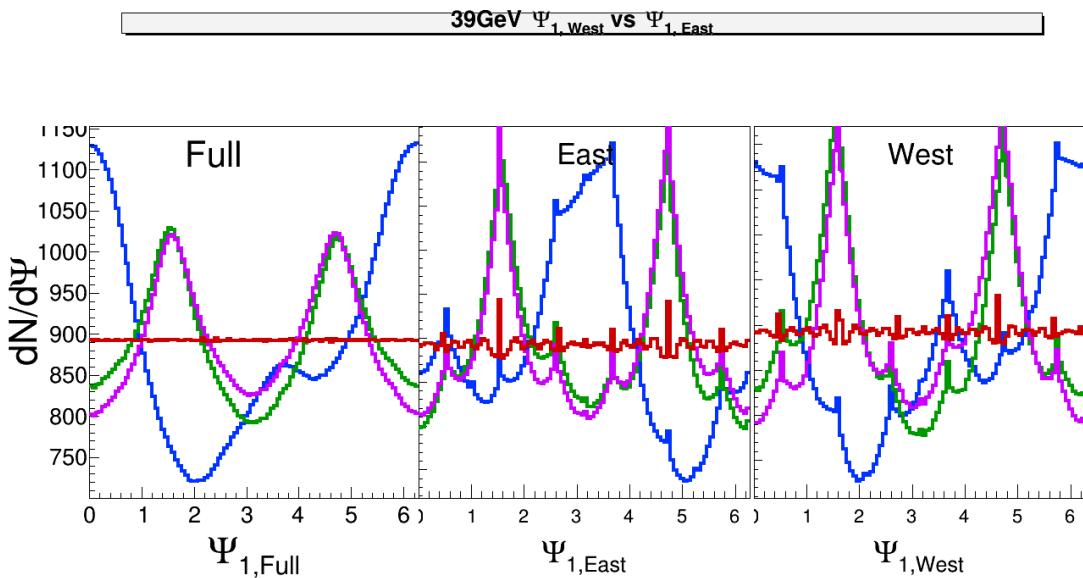


**Fig. 27:** 39GeV  $\Psi_1$  distribution as corrections are applied. Blue - Raw, Green - Gain corrected, Violet - Recentered, Red - Shifted.

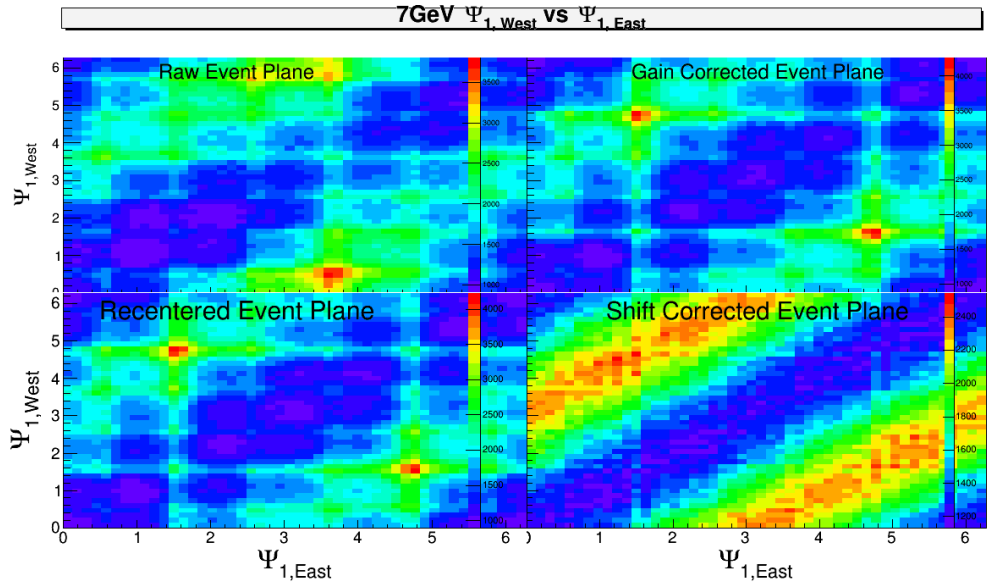


**Fig. 28:** BBC West  $\Psi_1$  vs. BBC East  $\Psi_1$  for 7GeV as corrections are applied

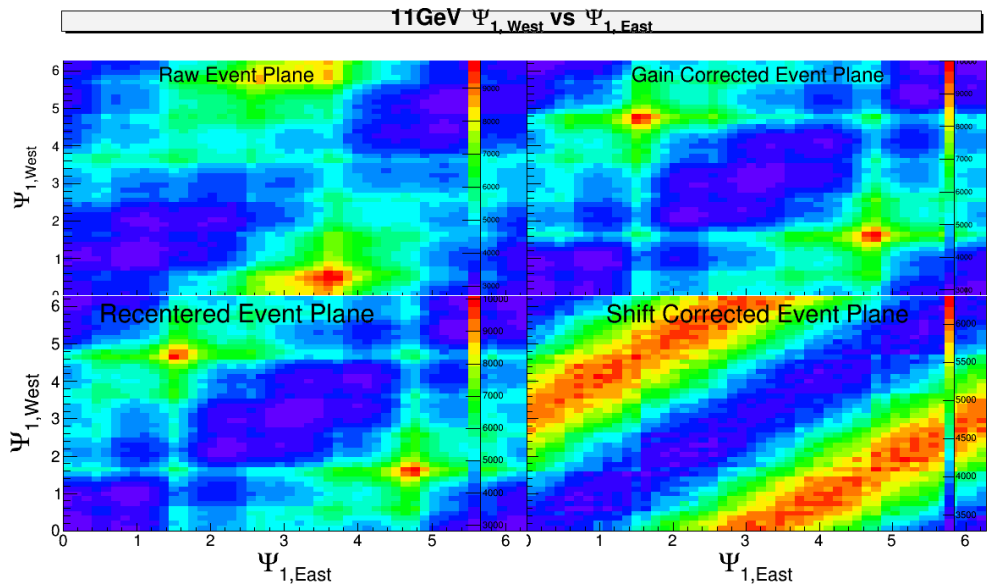


**Fig. 29:** BBC West  $\Psi_1$  vs. BBC East  $\Psi_1$  for 11GeV as corrections are applied

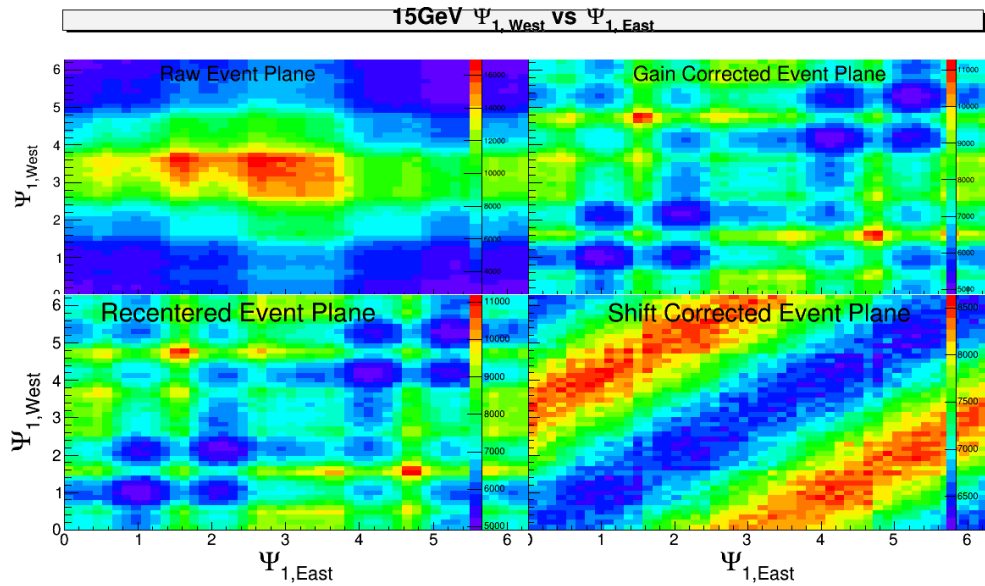


**Fig. 30:** BBC West  $\Psi_1$  vs. BBC East  $\Psi_1$  for 15GeV as corrections are applied

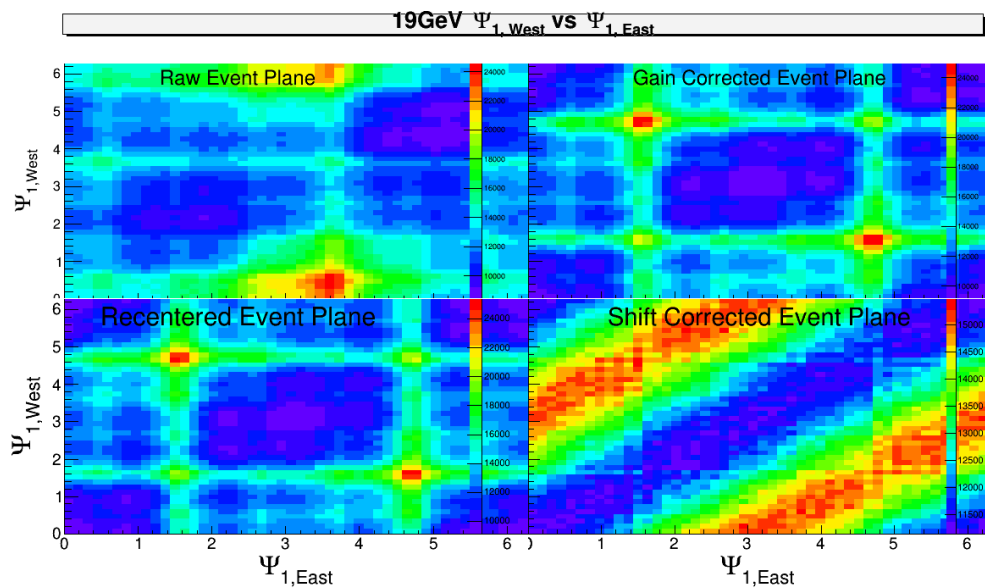


**Fig. 31:** BBC West  $\Psi_1$  vs. BBC East  $\Psi_1$  for 19GeV as corrections are applied

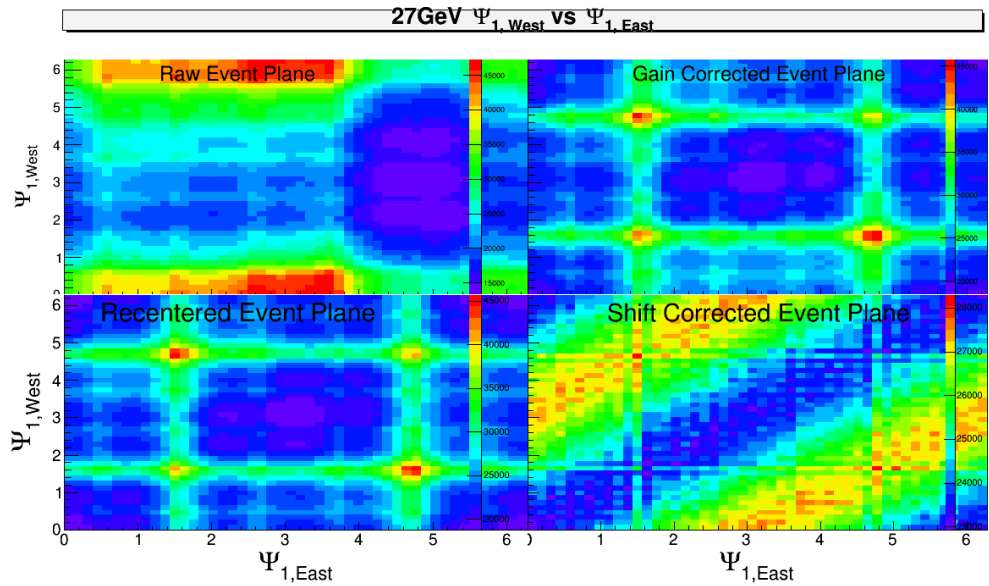


**Fig. 32:** BBC West  $\Psi_1$  vs. BBC East  $\Psi_1$  for 27GeV as corrections are applied

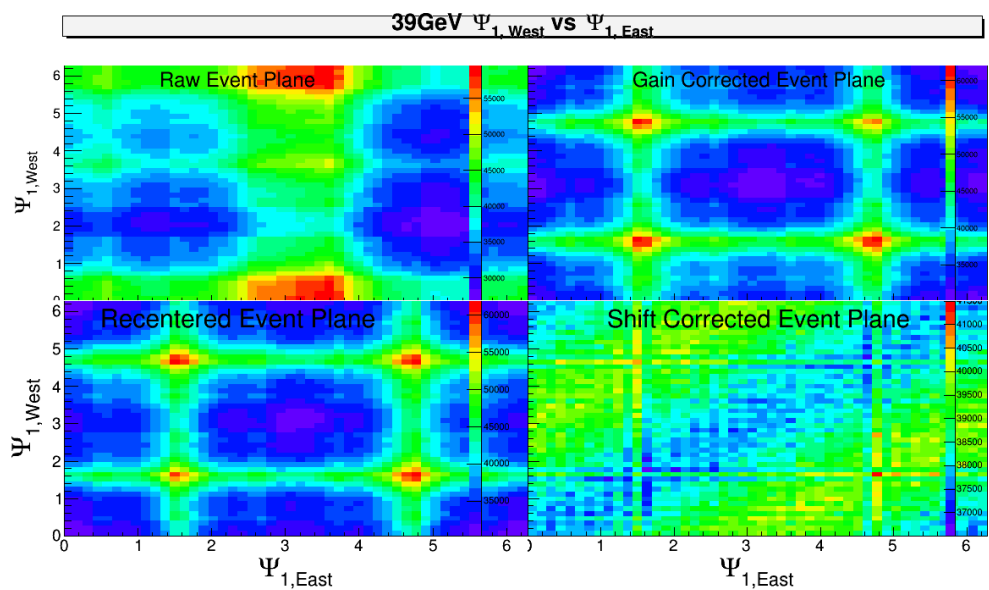


**Fig. 33:** BBC West  $\Psi_1$  vs. BBC East  $\Psi_1$  for 39GeV as corrections are applied

### 2.2.1 Event plane resolution

Finally we have a resolution correction factor which is found in the typical way outlined here (<http://arxiv.org/abs/0809.2949v1>). The relative magnitude of the corrections is the correlator of the east and west planes:  $\cos(\Psi_{1,W} - \Psi_{1,E})$ , the actual values are found by inverting Bessel equations (eq. 10 of this paper) using the sub event plane resolution. This resolution is solved for each central value of the sub event plane resolution as well as the statistical error bars. Of course the statistical error bars of the sub-event plane resolution are symmetric, but this is not guaranteed when they are put through the root finding algorithm. If the sizes of the up and down error bars differed by less than a percent I just defined the error bar to be the average of them. In fact the difference was less than 1% every time (it could have been smaller but I don't remember the factor) so I never had to consider what to do in case of asymmetry. The values are

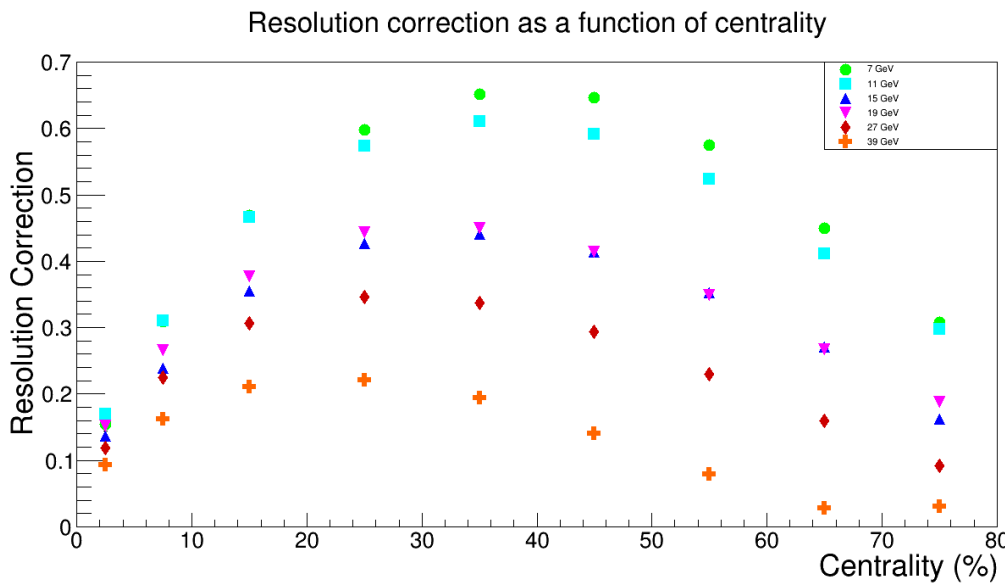


**Fig. 34:** Resolution correction as a function of centrality

I started putting all of this information in a table but that is both very time consuming and not as useful as arrays. The “values” below are resolution and the “errors” are the errors on the resolution

//resolution as a function of centrality in order 70-80, 60-70, 50-60, 40-50, 30-40, 20-30, 10-20, 5-10, 0-5:

```

430 float Value7[9] = {0.307486, 0.449667, 0.574805, 0.646084, 0.651441, 0.597433, 0.468886, 0.309121,
0.154215};

float Error7[9] = {0.00350804, 0.0018571, 0.00128989, 0.00101399, 0.000984015, 0.00120613, 0.00178403,
0.00439411, 0.00936414};

float Value11[9] = {0.297083, 0.41103, 0.523299, 0.591951, 0.610235, 0.573203, 0.466745, 0.310846,
0.170367};

float Error11[9] = {0.00216346, 0.0013164, 0.000902906, 0.000735164, 0.000702311, 0.000788124,
0.00108837, 0.0026144, 0.00496451};

float Value15[9] = {0.162577, 0.270896, 0.352444, 0.41449, 0.440722, 0.426715, 0.35558, 0.238906,
0.136717};

float Error15[9] = {0.00319226, 0.00177016, 0.00119992, 0.000993054, 0.000897895, 0.000969794,
0.00125653, 0.00294766, 0.00530565};

float Value19[9] = {0.187944, 0.266781, 0.348138, 0.414074, 0.449791, 0.443808, 0.377452, 0.265421,
0.136717};

```

0.151509};

float Error19[9] = {0.00208176, 0.00127301, 0.000934693, 0.000738721, 0.00067166, 0.000690424,  
445 0.000881327, 0.00196368, 0.00349595};

float Value27[9] = {0.0915621, 0.159324, 0.230443, 0.294388, 0.337777, 0.346737, 0.306512, 0.225316,  
0.118245};

float Error27[9] = {0.00294643, 0.00154611, 0.00108434, 0.000810682, 0.00070117, 0.000693721,  
0.000825761, 0.00167731, 0.00329719};

450 float Value39[9] = {0.0304321, 0.0277353, 0.0795904, 0.140791, 0.193922, 0.220535, 0.211103, 0.162255,  
0.093857};

float Error39[9] = {0.00737913, 0.0081295, 0.00258267, 0.00147021, 0.00104289, 0.000912287, 0.000975987,  
0.0018576, 0.00328591};

### 2.3 Track QA

455 The cuts I use to select tracks

- Track flag  $\geq 0$
- $0.15\text{GeV} < p_T < 10\text{GeV}$
- $|\eta| < 1$
- NHitsPossible  $\geq 5$
- $15 < \text{Number of hits} < 100$
- NHitsFit/NHitsPossible  $\geq 0.52$

460

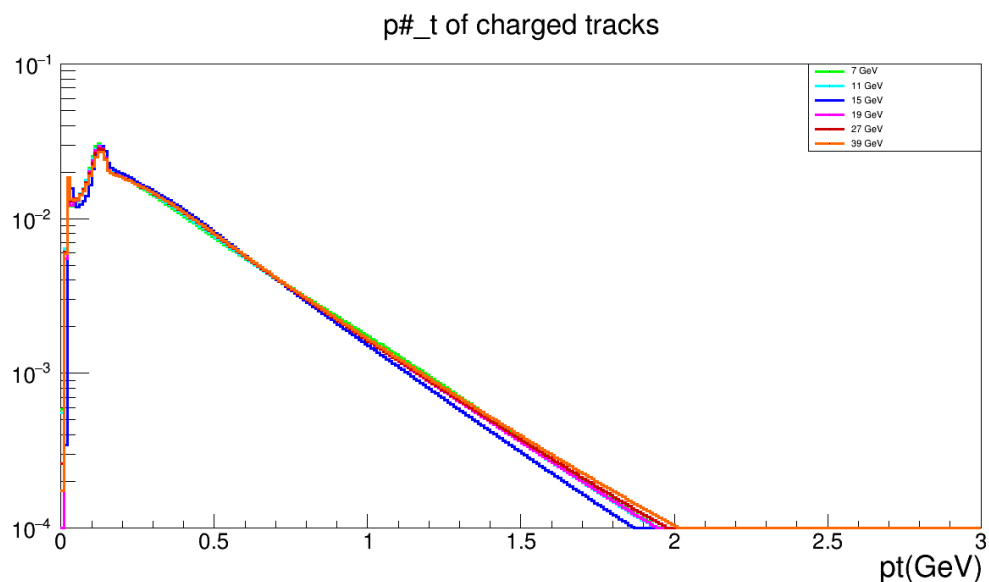


**Fig. 35:**  $\frac{dN}{d(pt)}$  vs  $p_T$

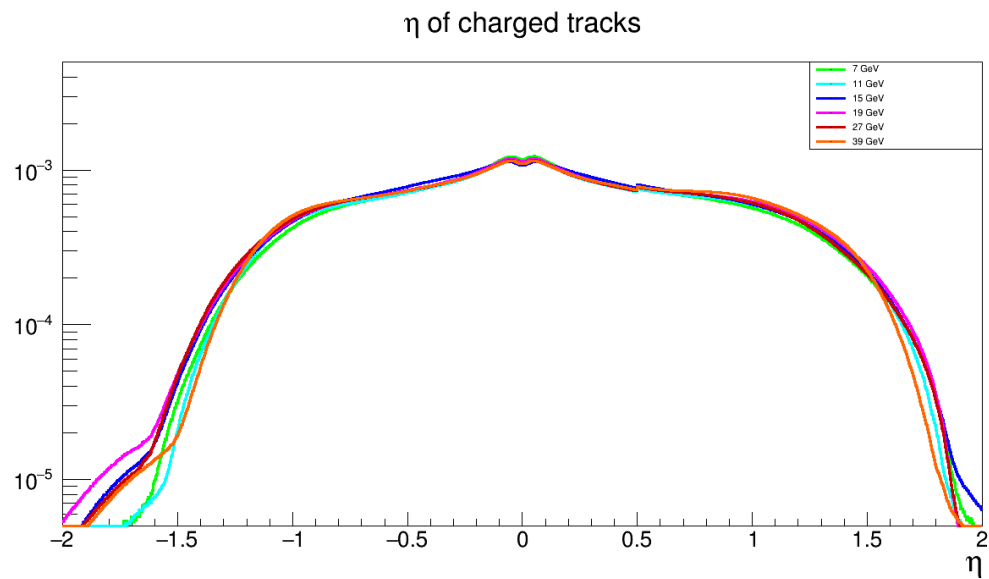


**Fig. 36:**  $\frac{dN}{d\eta}$  vs  $\eta$

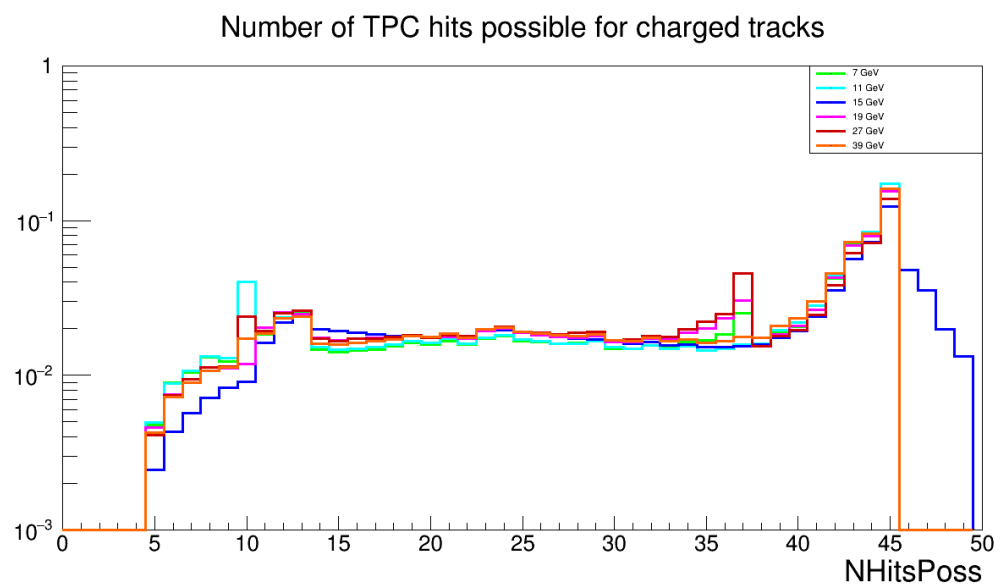


**Fig. 37:**  $\frac{dN}{dN_{\text{Hits Possible}}}$  vs  $N_{\text{Hits Possible}}$

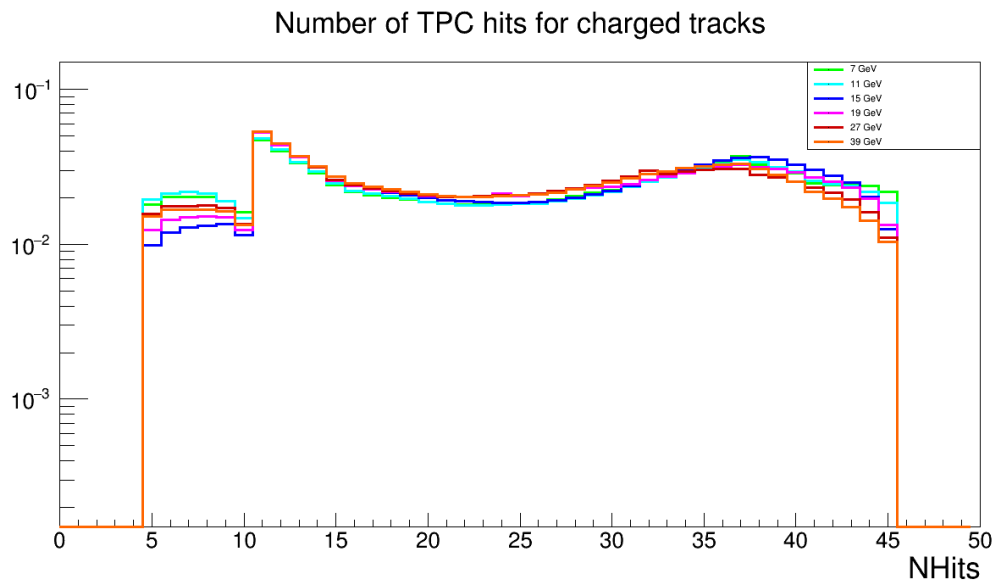


**Fig. 38:**  $\frac{dN}{dN_{\text{Hits}}}$  vs N<sub>Hits</sub>

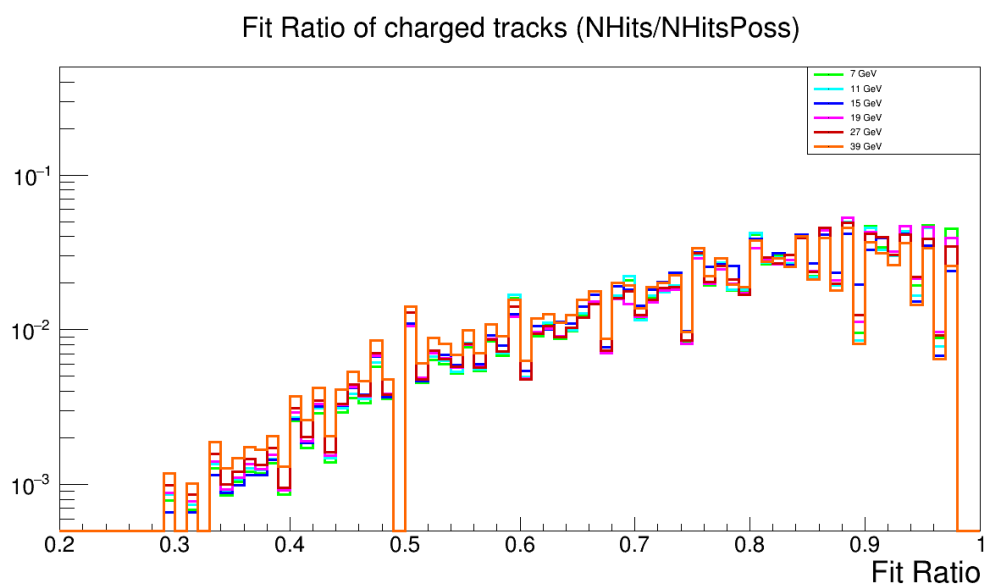


**Fig. 39:**  $\frac{dN}{d(\text{Fit Ratio})}$  vs Fit Ratio

## 2.4 Lambda reconstruction

### 2.4.1 Daughter PID

Of course Lambdas are reconstructed from proton and pion tracks, so the first step in the reconstruction  
465 is the proton and pion track particle identification. This analysis uses TPC dE/dx and the ToF  $1/\beta$  for PID. ToF information is not required so the ToF mass cuts are only used if the information exists. The cuts are as follows

- Proton:  $|N_{\sigma, \text{proton}}| < 3$
- Proton:  $0.5\text{GeV}^2 < m_{\text{ToF}}^2 < 1.5\text{GeV}^2$
- 470 – Pion:  $|N_{\sigma, \text{pion}}| < 3$
- Pion:  $0.017\text{GeV}^2 - 0.013\text{GeV}^2 * p < m_{\text{ToF}}^2 < 0.04\text{GeV}$

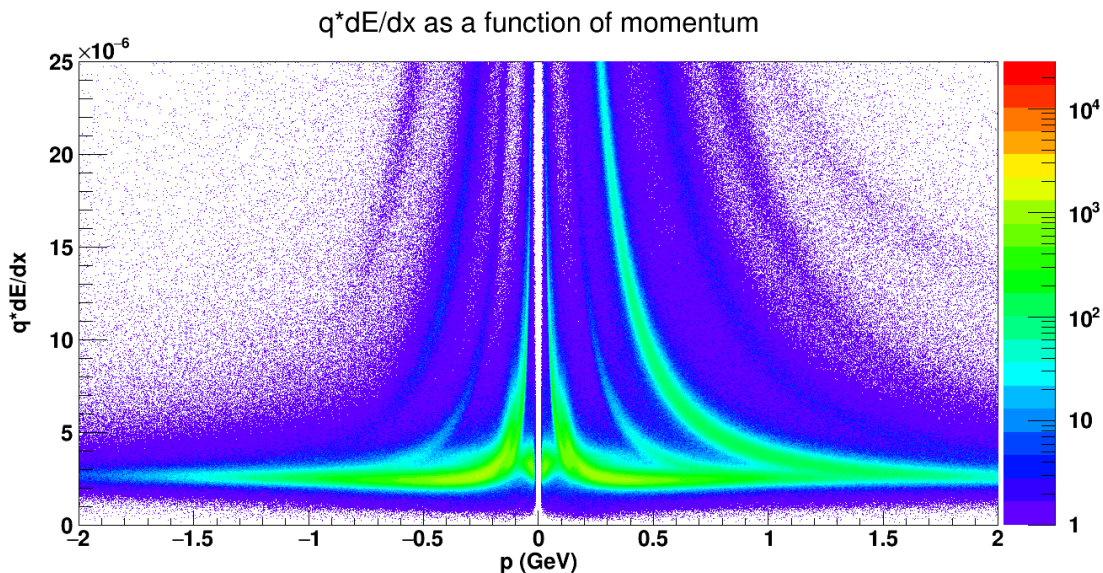


**Fig. 40:** 7GeV charged track dE/dx vs. p from the TPC

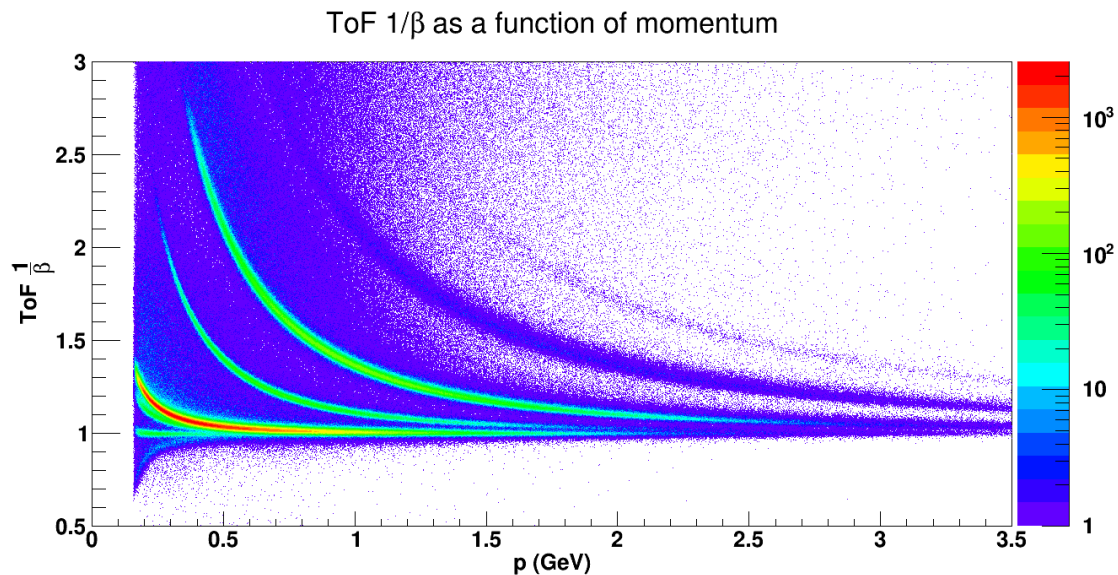


**Fig. 41:** 7GeV charged track  $1/\beta$  vs.  $p$  from the ToF

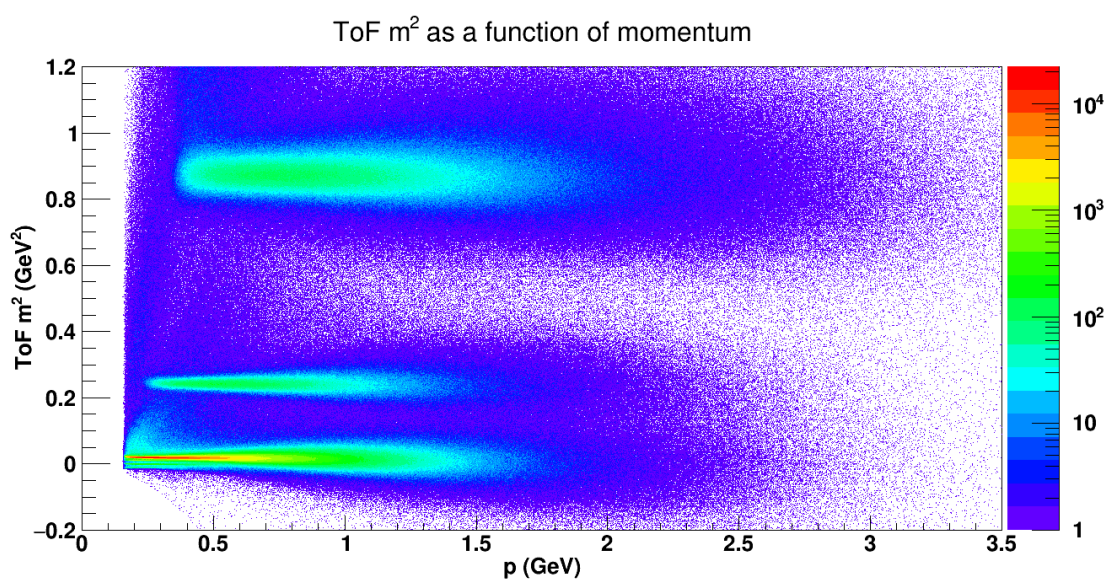


**Fig. 42:** 7GeV charged track  $m^2$  vs  $p$  from the ToF

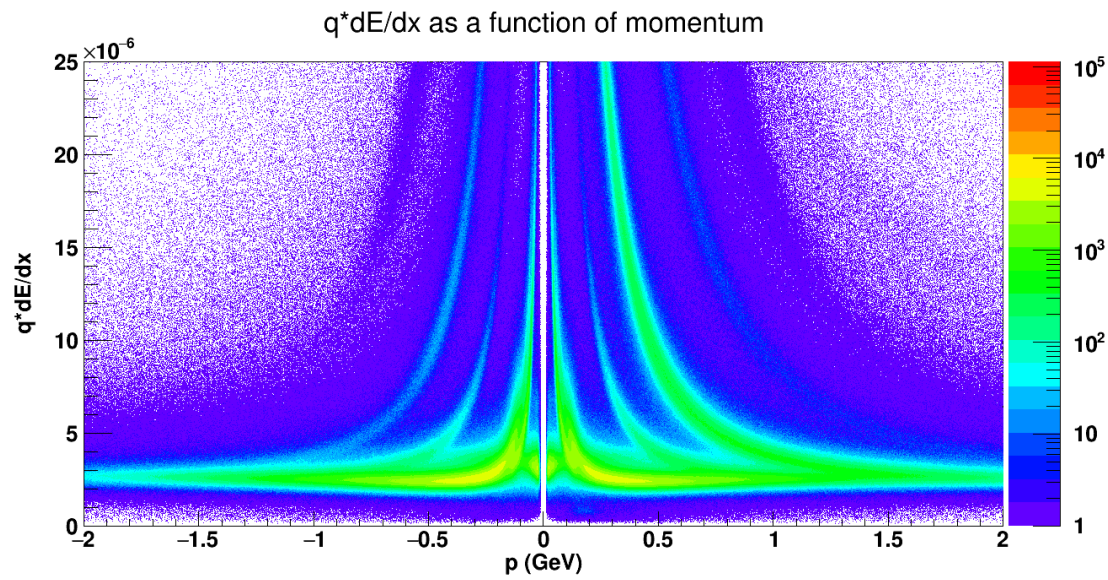


**Fig. 43:** 11GeV charged track  $dE/dx$  vs.  $p$  from the TPC

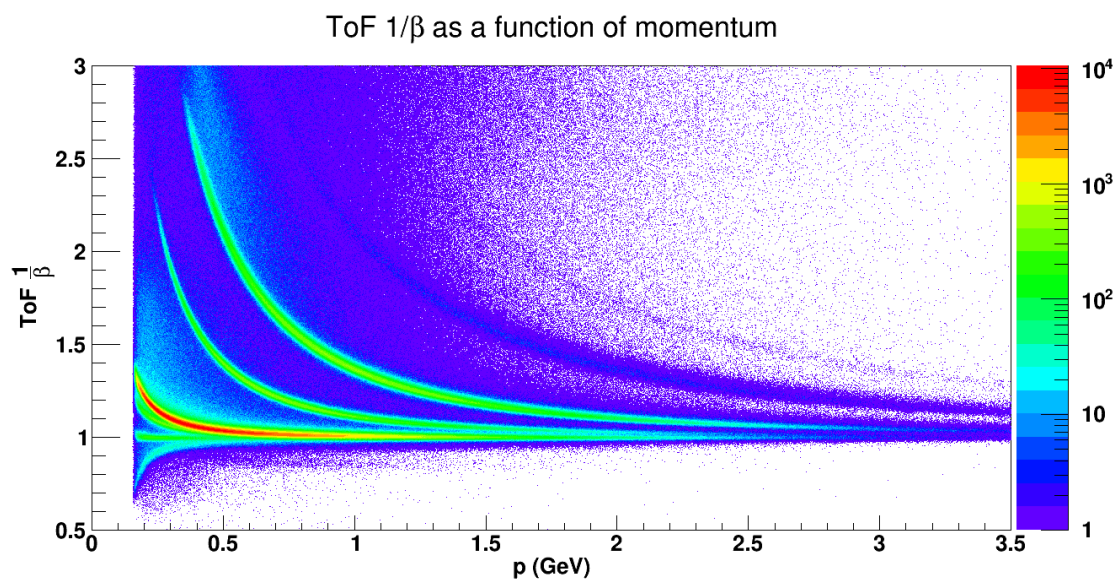


**Fig. 44:** 11GeV charged track  $1/\beta$  vs.  $p$  from the ToF

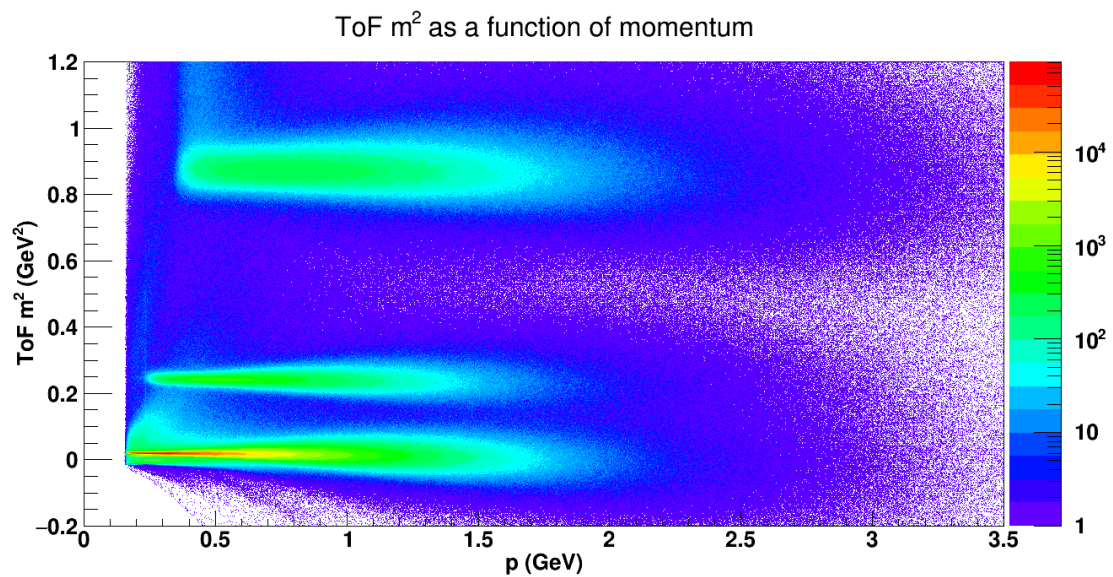


**Fig. 45:** 11GeV charged track  $m^2$  vs  $p$  from the ToF

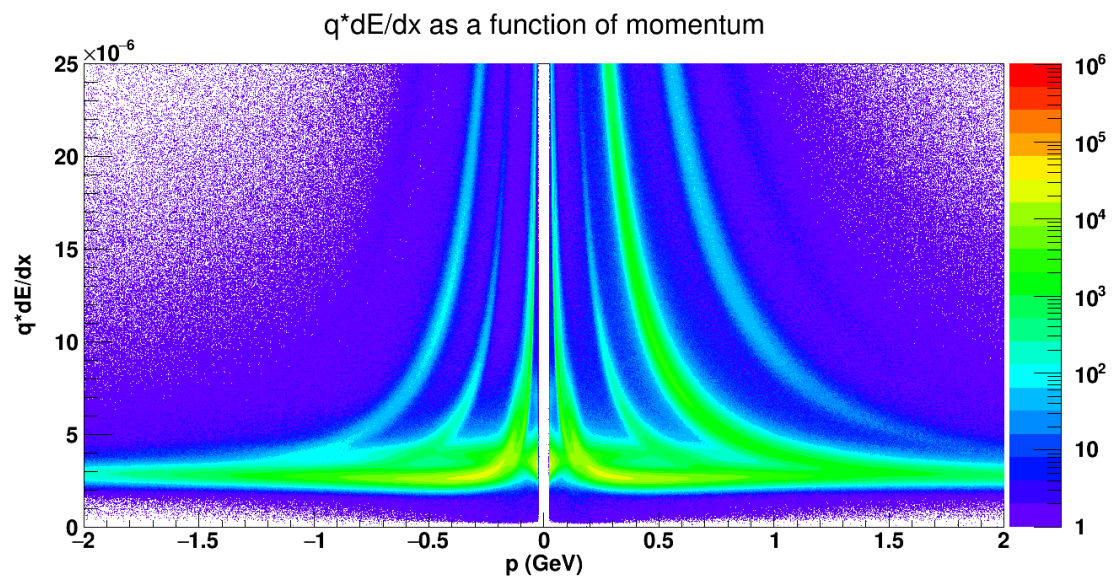


**Fig. 46:** 15GeV charged track  $dE/dx$  vs.  $p$  from the TPC

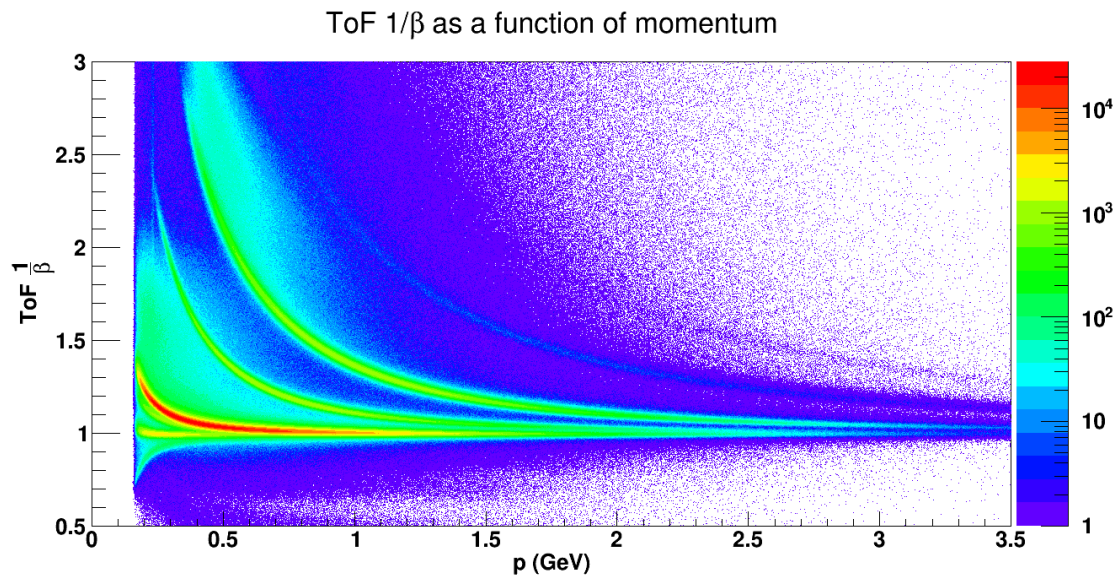


**Fig. 47:** 15GeV charged track  $1/\beta$  vs.  $p$  from the ToF

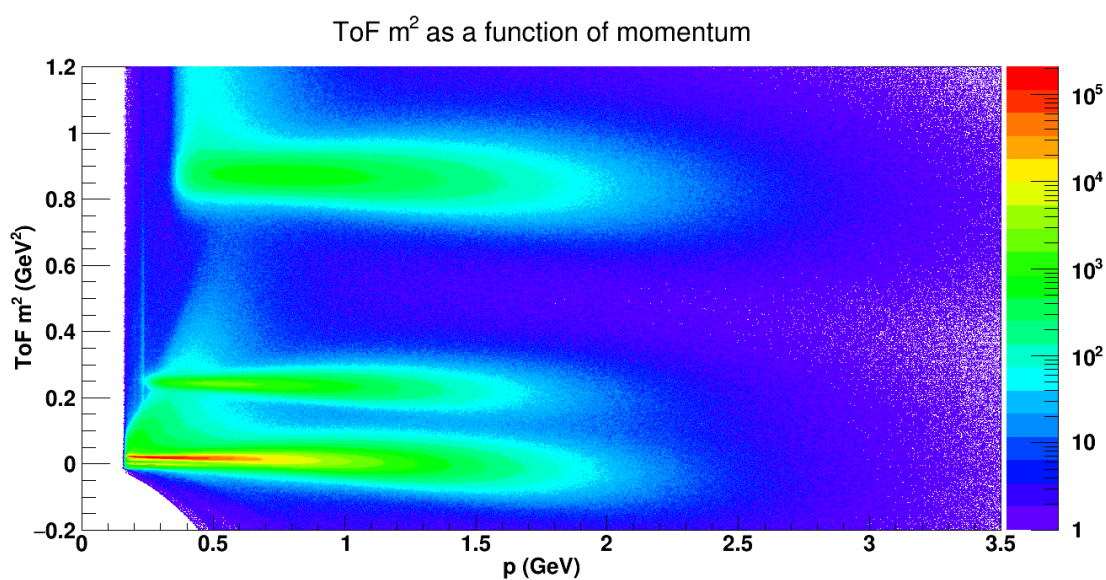


**Fig. 48:** 15GeV charged track  $m^2$  vs  $p$  from the ToF

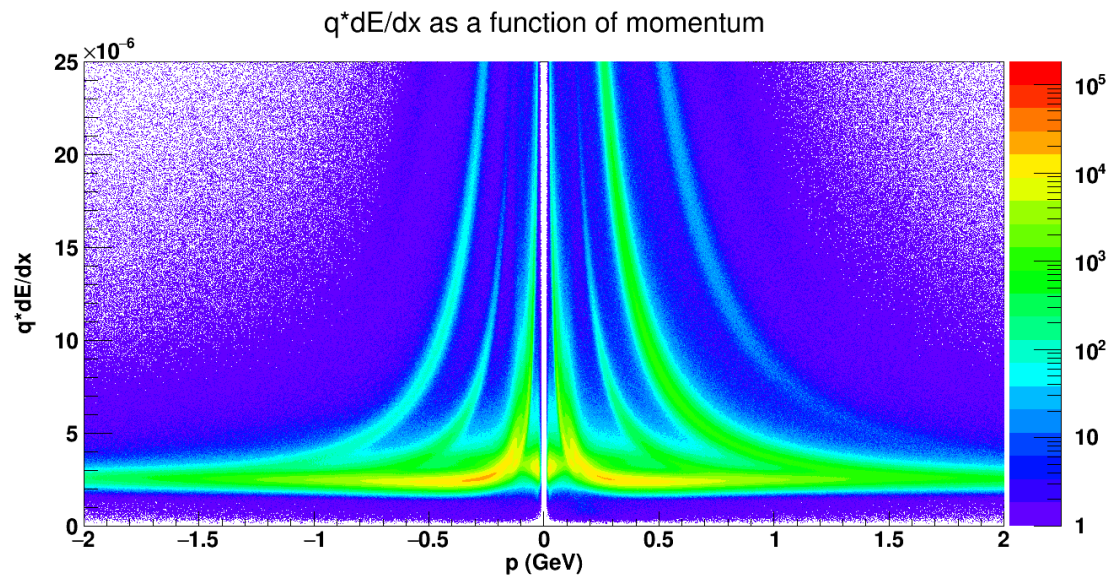


**Fig. 49:** 19GeV charged track dE/dx vs. p from the TPC

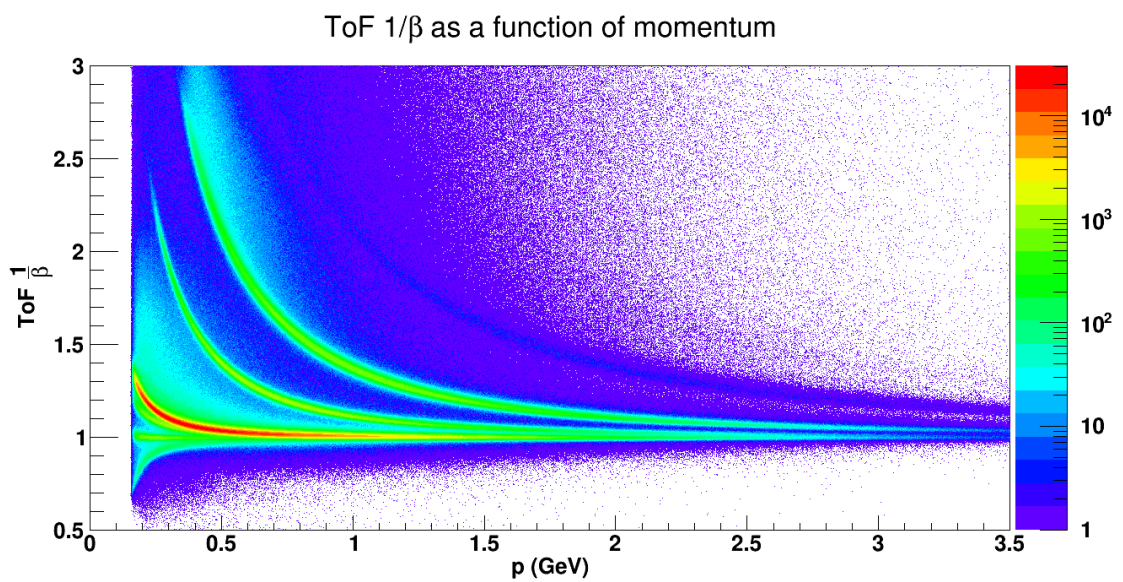


**Fig. 50:** 19GeV charged track 1/β vs. p from the ToF

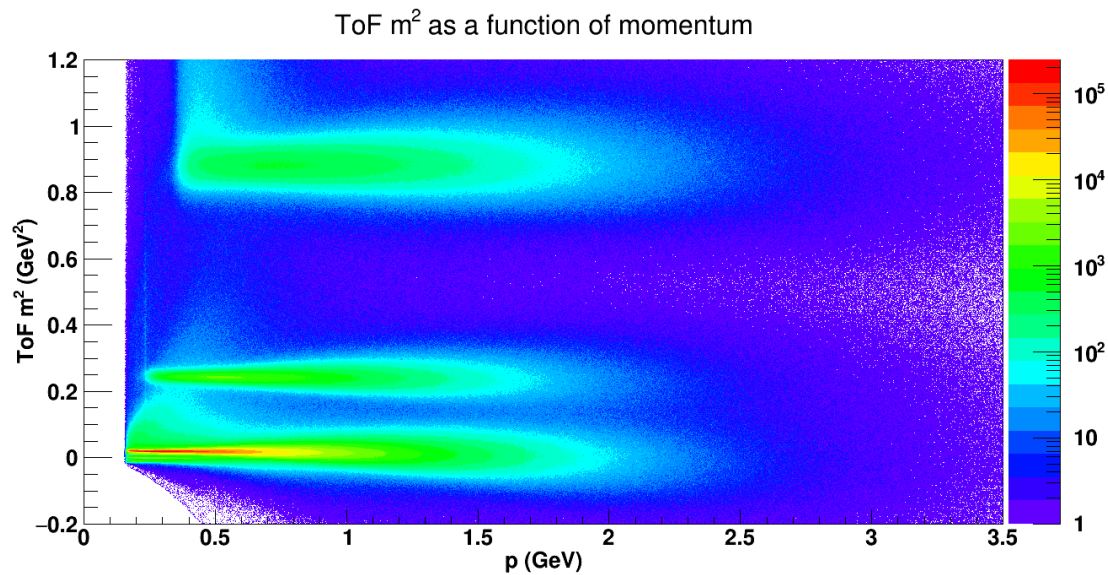


**Fig. 51:** 19GeV charged track  $m^2$  vs  $p$  from the ToF

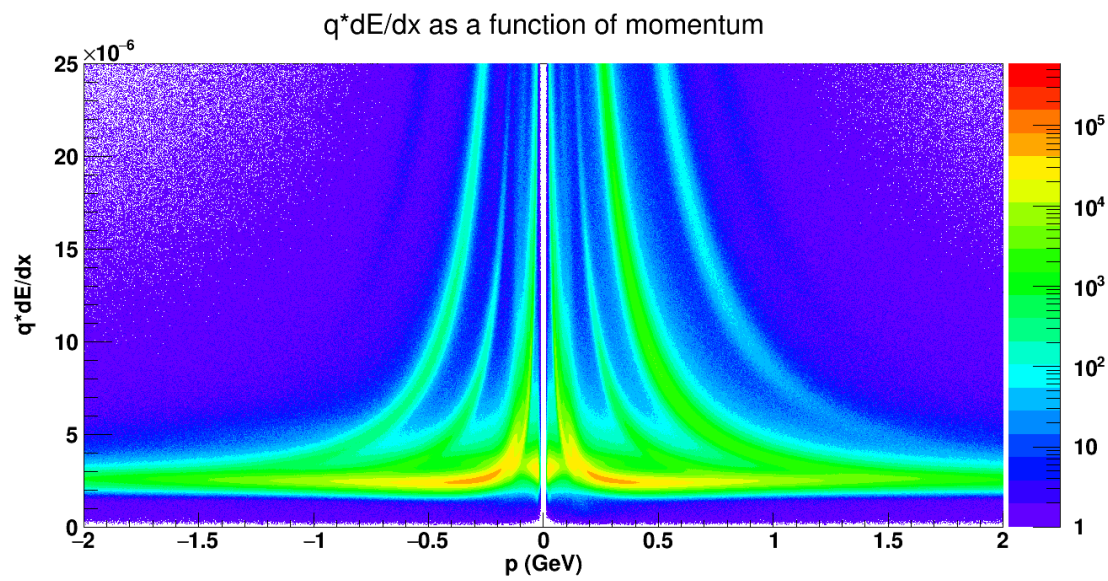


**Fig. 52:** 27GeV charged track  $dE/dx$  vs.  $p$  from the TPC

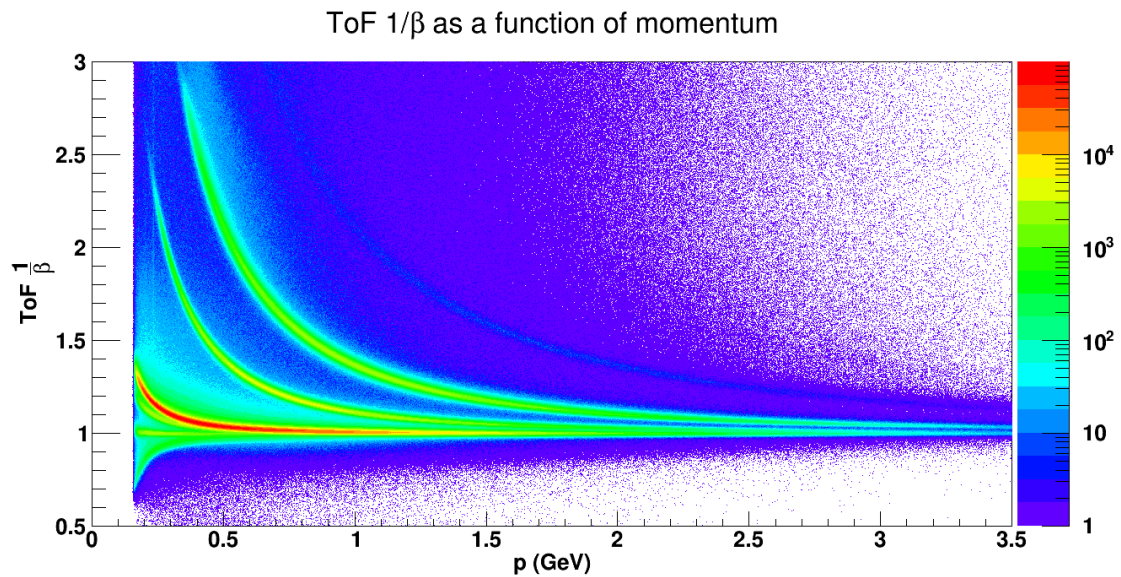


**Fig. 53:** 27GeV charged track  $1/\beta$  vs.  $p$  from the ToF

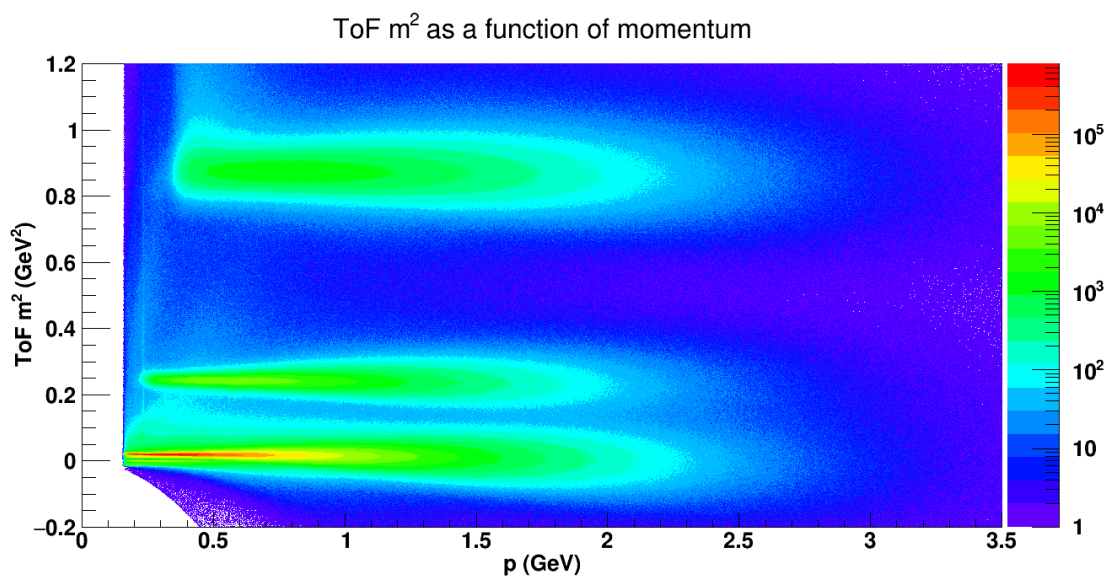


**Fig. 54:** 27GeV charged track  $m^2$  vs  $p$  from the ToF

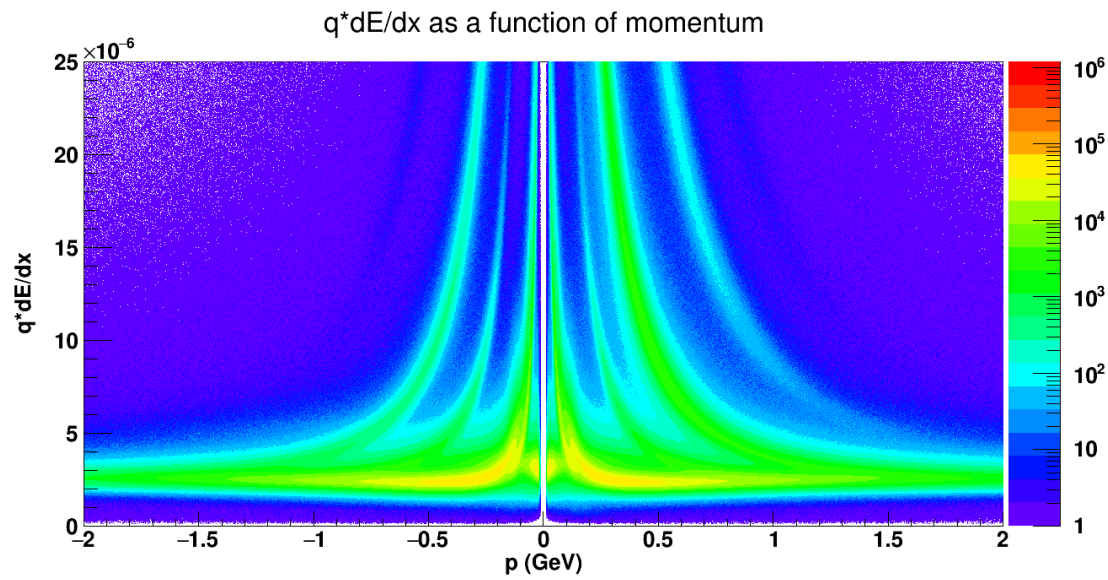


**Fig. 55:** 39GeV charged track  $dE/dx$  vs.  $p$  from the TPC

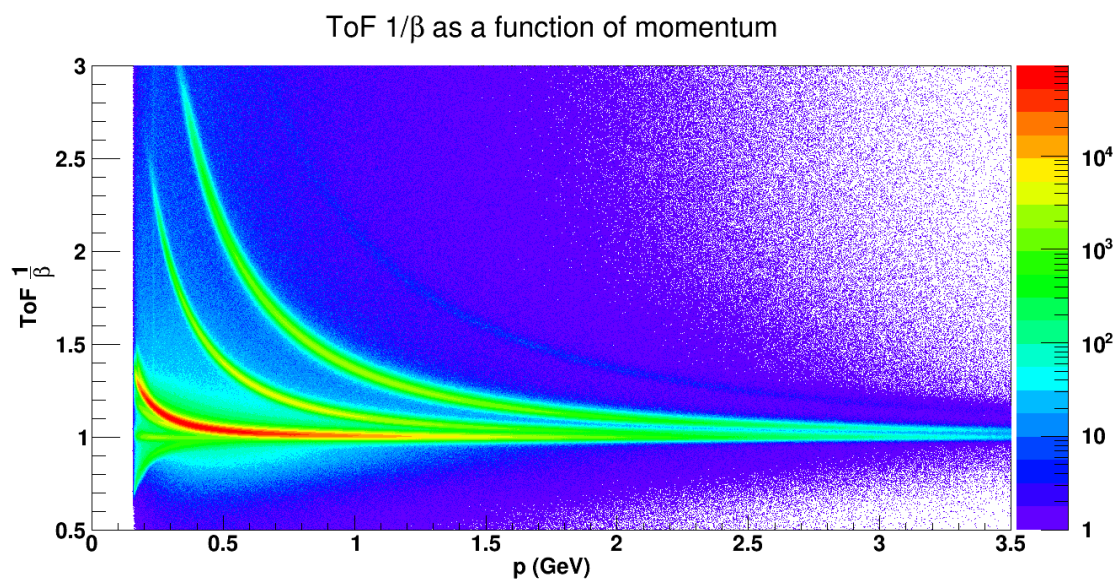


**Fig. 56:** 39GeV charged track  $1/\beta$  vs.  $p$  from the ToF

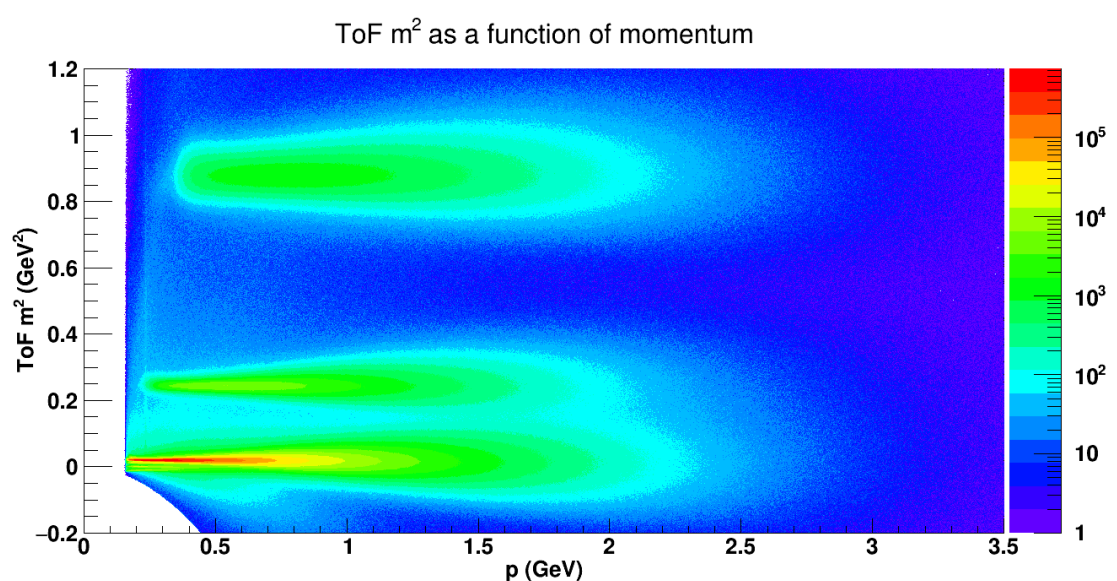


**Fig. 57:** 39GeV charged track  $m^2$  vs  $p$  from the ToF

### 2.4.2 Lambda topological cuts

Lambdas are reconstructed from the protons and pions using a series of topological cuts. The scheme for the cuts is rather complicated as the cut values themselves depend on whether or not the candidate proton and pion separately have ToF information.

- (Proton ToF and Pion ToF, Proton ToF and !Pion ToF, !Proton ToF and Pion ToF, !Proton ToF and !Pion ToF)
- Proton DCA to PV  $\geq (0.1, 0.15, 0.5, 0.6)$  cm
- Pion DCA to PV  $\geq (0.7, 0.8, 1.5, 1.7)$  cm
- Lambda DCA to PV  $\leq (1.3, 1.2, 0.75, 0.75)$  cm
- Lambda decay length  $\geq (2, 2.5, 3.5, 4)$  cm
- Proton to Pion DCA to each other  $\leq 1$  cm
- Finally there is a cut ensuring that the Lambda is moving away from the primary vertex.
- Lambdas are taken in the mass window  $(1.115683 \pm 0.005)\text{GeV}$
- As described in section 4.1 for systematic error reasons we actually do not include Lambdas for which the pion has ToF data and the proton does not

- Proton DCA is a cut on a minimum ( $\text{DCA} > x$ )
- Pion DCA is a cut on a minimum
- Proton to Pion DCA is a cut on a maximum
- $\Lambda$  DCA is a cut on a maximum
- $\Lambda$  Decay Length is a cut on a minimum

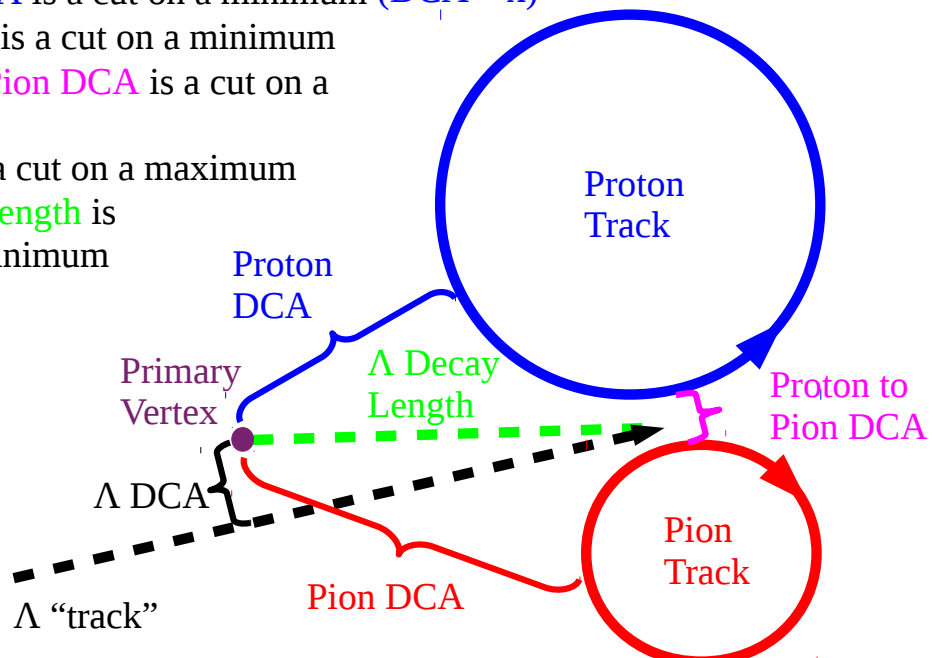


**Fig. 58:** Diagram of how cuts are applied to reconstruct lambdas

It should be mentioned here that the quantities I am plotting below are made by greatly loosening, though not eradicating, the cuts. Therefore all such plots display quantities after all of the cuts, in some form, have been applied to them. This means that there will be some non-trivial structure. I will come back  
<sup>490</sup> with plots for this later.

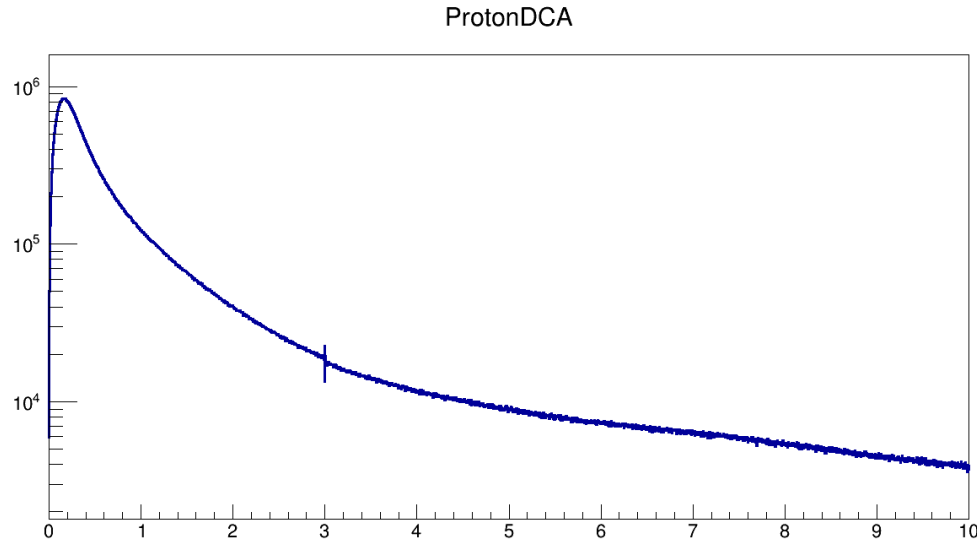


**Fig. 59:** Counts vs. proton DCA to the primary vertex (cm)

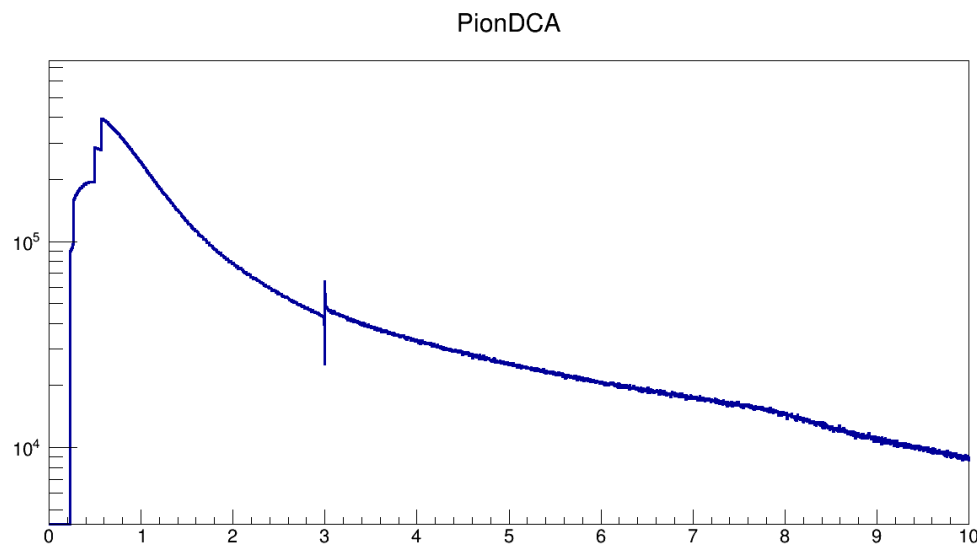


**Fig. 60:** Counts vs. pion DCA to the primary vertex (cm)

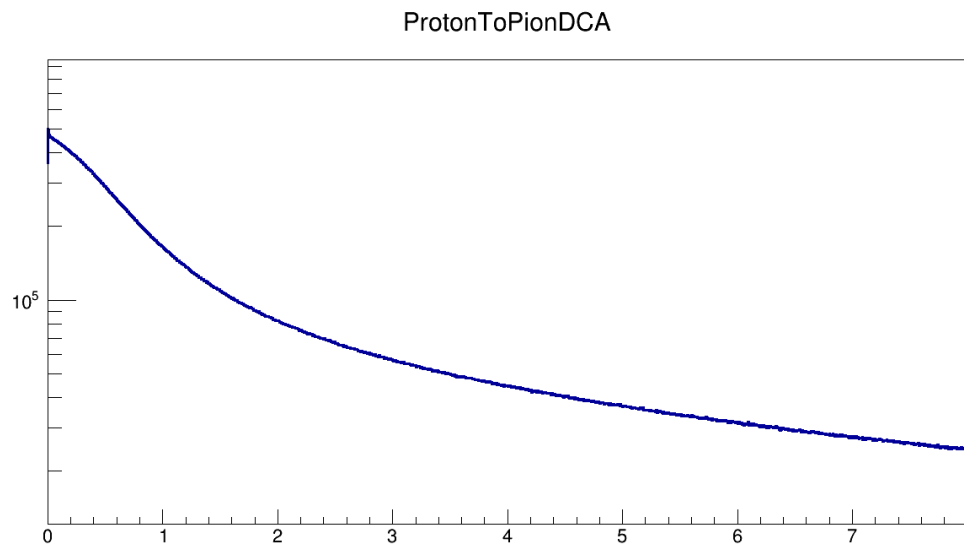


**Fig. 61:** DCA of one daughter track to another (cm)

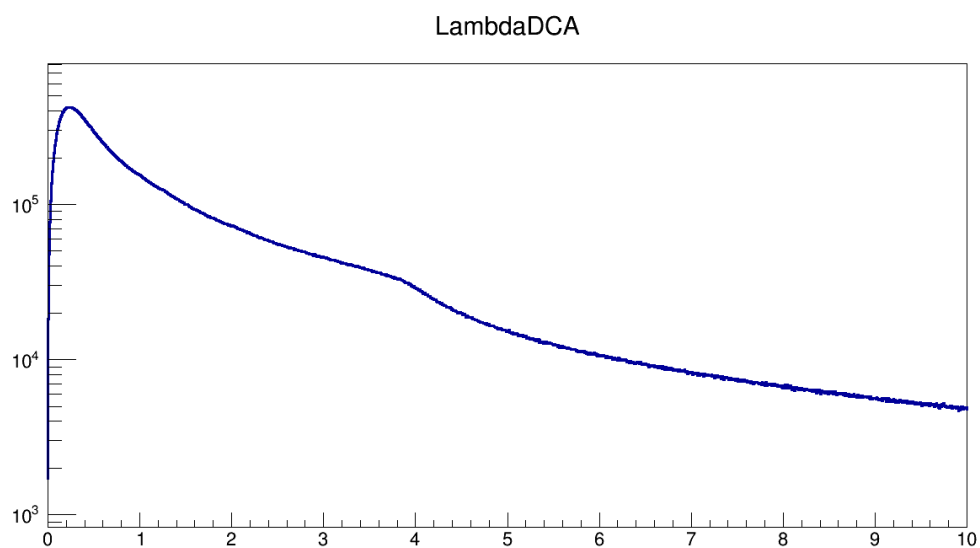


**Fig. 62:** Counts vs. Lambda DCA to the primary vertex (cm)

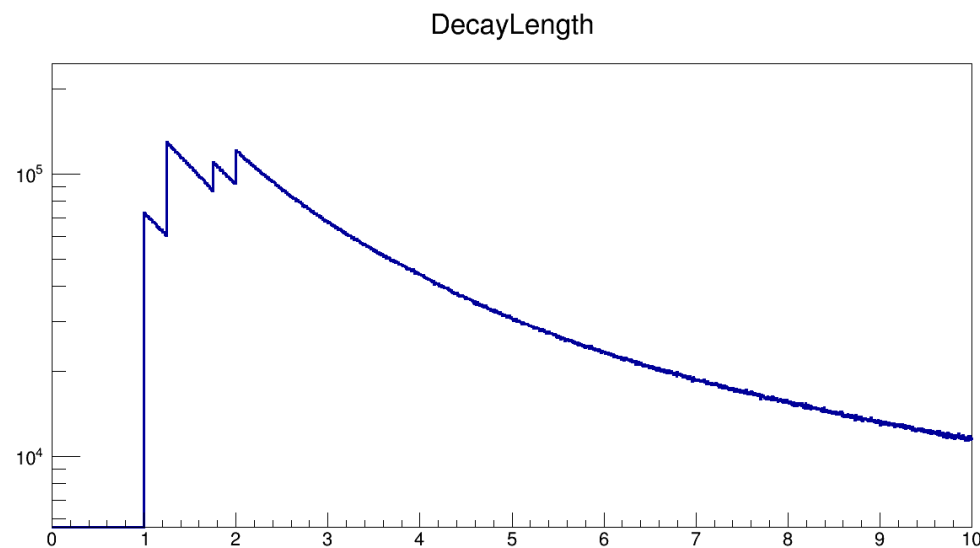


**Fig. 63:** Counts vs. Lambda decay length (cm)

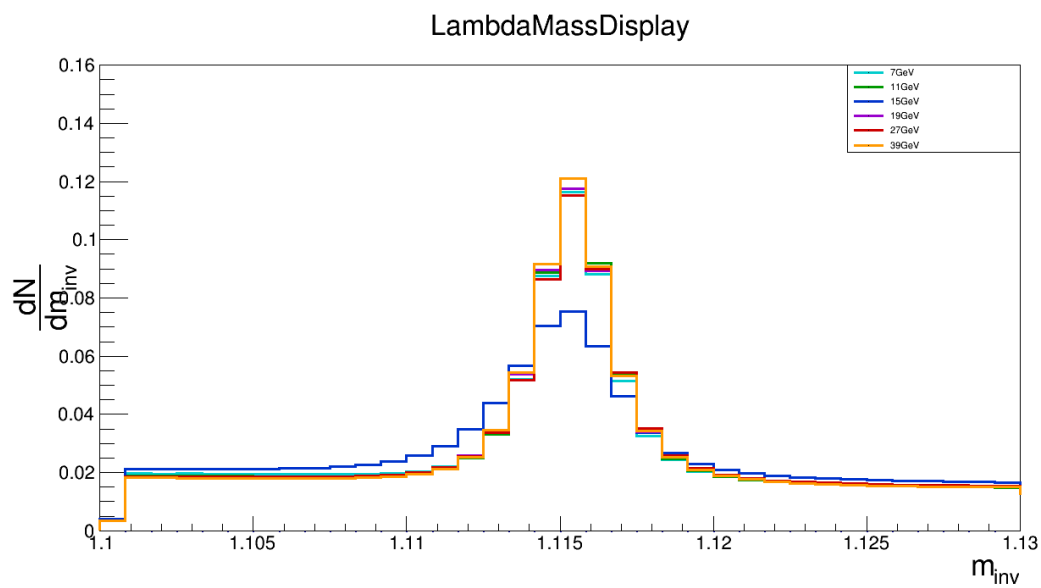


**Fig. 64:**  $\frac{dN}{dm_{\Lambda}}$  vs.  $m_{\Lambda}(\text{GeV})$ . Note the strange mass distribution at 15GeV, probably from the HFT

### 3 Data analysis

The idea of the measurement is described in the introduction. In this section I'll include some final and corrected results, explain what corrections are made, and talk about some efficiency and reconstruction issues that occur in the measurement. Aside from the final result and unless otherwise mentioned most plots depict  $\langle \sin(\Psi_1 - \phi_{\Lambda}^*) \rangle$  with a resolution correction, which neglects the constant factor  $\frac{8}{\pi\alpha}$ . The general idea of this section is to provide both the steps to doing this analysis and to explain issues that are deemed fundamentally important to the QA of the analysis. In order what is done is

- Apply event cuts (sec. 2.1)
- Determine the event plane (sec. 2.2)
- Make arrays of tracks which pass track cuts (sec. 2.3)
- Loop over track arrays and apply Lambda topological cuts to find Lambda candidates (sec. 2.4.2)
- Fill TProfiles with  $\sin(\Psi_1 - \phi_{\Lambda}^*)$  (that is average) for each centrality
- Divide by resolution correction,  $R$  and multiply by  $\frac{8}{\pi\alpha}$  (sec. 2.2.1)
- Apply mass purity correction (sec. 3.2)
- Apply acceptance correction (sec. 3.3)
- Apply helicity efficiency correction (sec. 3.4.2) – these are the final  $P_H$  values
- Separate into vortical and magnetic components with feed-down correction (3.5)

See sec. 3.6 for a brief discussion of the statistical errors and sec 4 for a discussion of the systematic errors. Note that in the above table the decay parameter  $\alpha_H$  is taken to be  $0.647 \pm 0.013$  for both the  $\Lambda$  and  $\bar{\Lambda}$  results. This is the decay parameter of the  $\Lambda$ . This may seem an odd choice as  $\alpha_{\bar{\Lambda}}$  has been measured independently. It is of fundamental interest whether these values differ but measured values have consistently found to be the same within statistical errors and it is largely assumed that they are, in fact, identical. Using different values would be confusing in as far as we are looking for differences in the data between  $\Lambda$  and  $\bar{\Lambda}$  polarization and would be endorsing the more unlikely scenario that they are different. At any rate it is evident that the difference is small and the errors in the  $\alpha_H$  are nearly negligible compared to the relatively large statistical uncertainty in the measure.

### 3.1 Resolution Correction

Since  $\langle \sin(\Psi_1 - \phi_\Lambda^*) \rangle$  is a culant it has the same resolution correction as any flow parameter  $v_n$  which is to say it is divided, centrality bin by centrality bin, by the values in Fig. 2.2.1 ( $\langle \sin(\Psi_1 - \phi_\Lambda^*) \rangle / R$ ).  
520 On the centrality bin by centrality bin basis this is a constant scale so the significance of the result is preserved. However, since the resolution is not uniform over all centrality ranges, the significance of the result may be changed. A comparison to illustrate this is below.

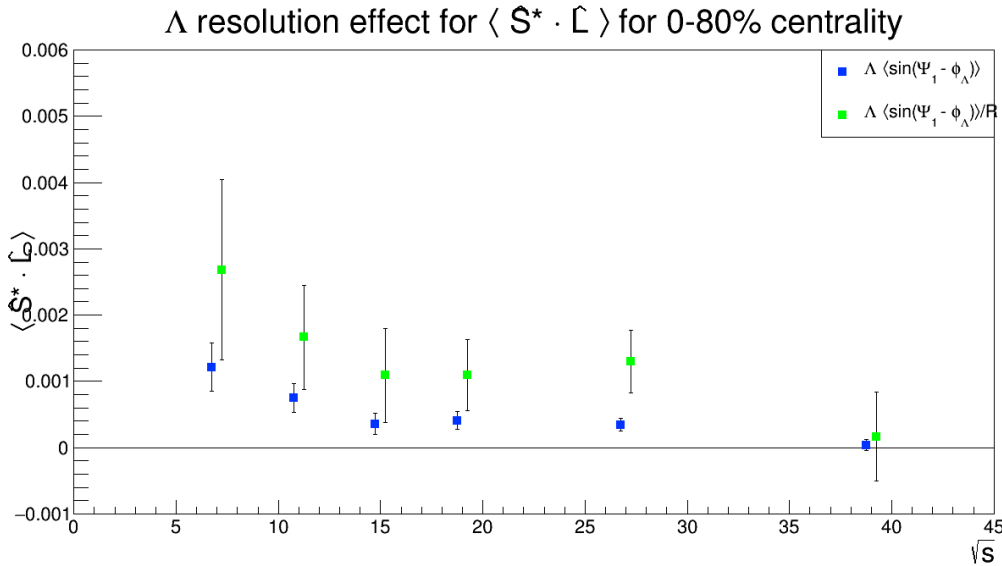


Fig. 65: Effect of resolution correction at effect 0-80% this is really  $\langle \sin(\Psi_1 - \phi_\Lambda^*) \rangle / R$ , not what the axis claims.

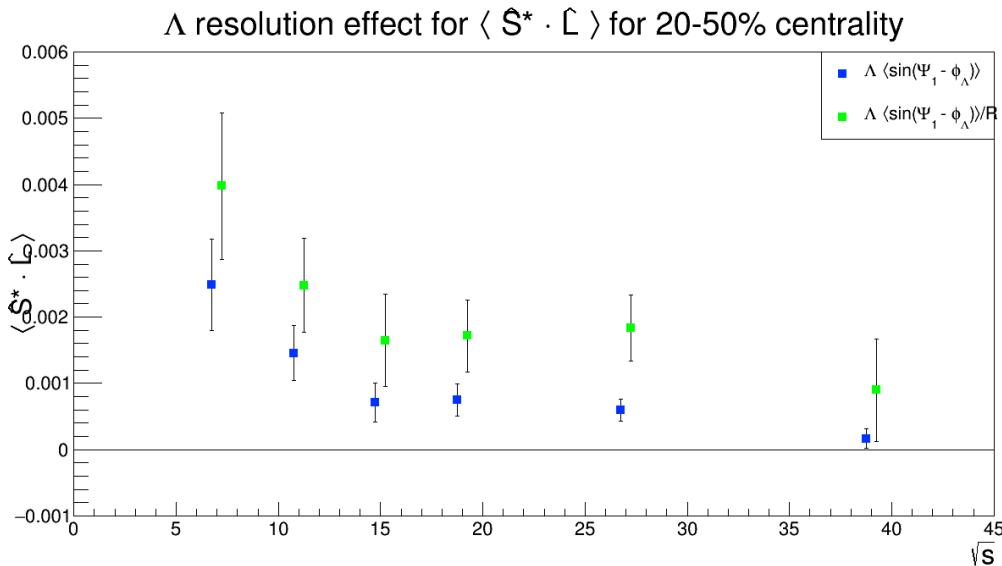
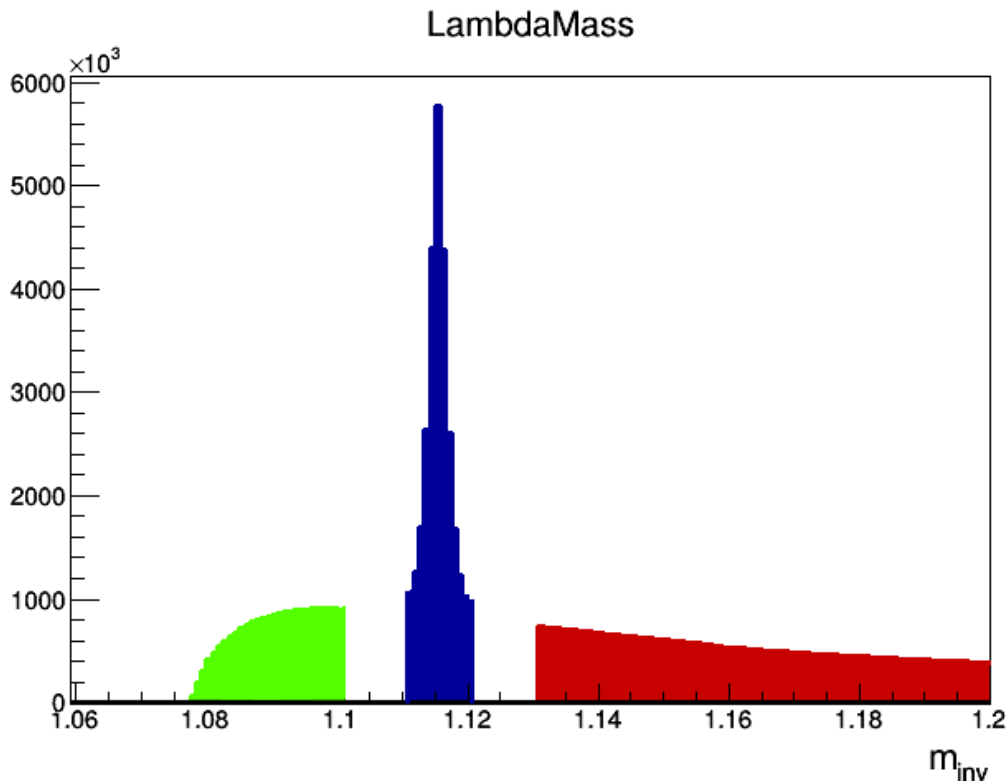


Fig. 66: Effect of resolution correction at effect 20-50% this is really  $\langle \sin(\Psi_1 - \phi_\Lambda^*) \rangle / R$ , not what the axis claims.

### 3.2 Mass background

A natural place to look for signal falsification is the wings of the Lambda mass distribution. In principle proton and pion pairs sufficiently away from the mass peak are not daughters of real Lambdas and thus should have no preference for the proton's momentum in the pair rest frame. We split our Lambda candidates into three categories: on mass peak, left of the mass peak ( $m_{\text{inv}} < m_{\Lambda}$ ), pairs with invariant mass right of the mass peak ( $m_{\text{inv}} > m_{\Lambda}$ ). The purity of the on peak Lambda candidates is estimated from the mass distribution by simply assuming a linear trend of the background between the points  $1.108\text{GeV}$  and  $1.125\text{GeV}$  and getting the counts. Obviously this is problematic for the  $15\text{GeV}$  data, but changing procedure will complicate things. We leave a gap between the distributions so that the mass distribution used looks like this



**Fig. 67:** Lambda mass distribution showing the regions right and left of the mass peak that are used in the analysis.

The signal for the Lambda polarization could leak into the mass wings via protons which are real Lambda daughters being paired with pions which are not their siblings. This effect is difficult to quantify but it isn't as incredible as it might sound. Proton DCA cuts are designed to pick only non-primary protons, the majority of which should come from Lambdas. The off mass signals we see have turned out not to be anomalies, as they persist through systematic checks of signal dependencies (as in different regions of  $E_\Lambda$ ,  $y_\Lambda$ , centrality,  $\phi_\Lambda$ , and the suit of topology cuts). If the height of the signal of the mass distribution is S and the height of the background is B we can do a similar subtraction of the off mass component as a flow measurement would do. In the final analysis we do not take this scaling into account (we assume zero background) but this calculation is important for the systematic errors. The off mass component is averaged from the  $m_{\text{inv}} > m_\Lambda$  and the  $m_{\text{inv}} > m_\Lambda$  component. Looking at the on mass peak Lambdas we measure

$$\langle \sin(\Psi_1 - \phi_\Lambda^*) \rangle_{\text{On Peak}} = \frac{S \langle \sin(\Psi_1 - \phi_\Lambda^*) \rangle_\Lambda + B \langle \sin(\Psi_1 - \phi_\Lambda^*) \rangle_{\text{Off Peak}}}{S + B} \quad (3)$$

Of course we want to know the  $\Lambda$  portion of the above equation so the mass corrected value takes the form (note that  $(S+B)/S \sim 1.2$ )

$$\langle \sin(\Psi_1 - \phi_\Lambda^*) \rangle_\Lambda = \frac{S+B}{S} \langle \sin(\Psi_1 - \phi_\Lambda^*) \rangle_{\text{On Peak}} - \frac{B}{S} \langle \sin(\Psi_1 - \phi_\Lambda^*) \rangle_{\text{Off Peak}} \quad (4)$$

The on peak results compared to the off peak results can be seen below

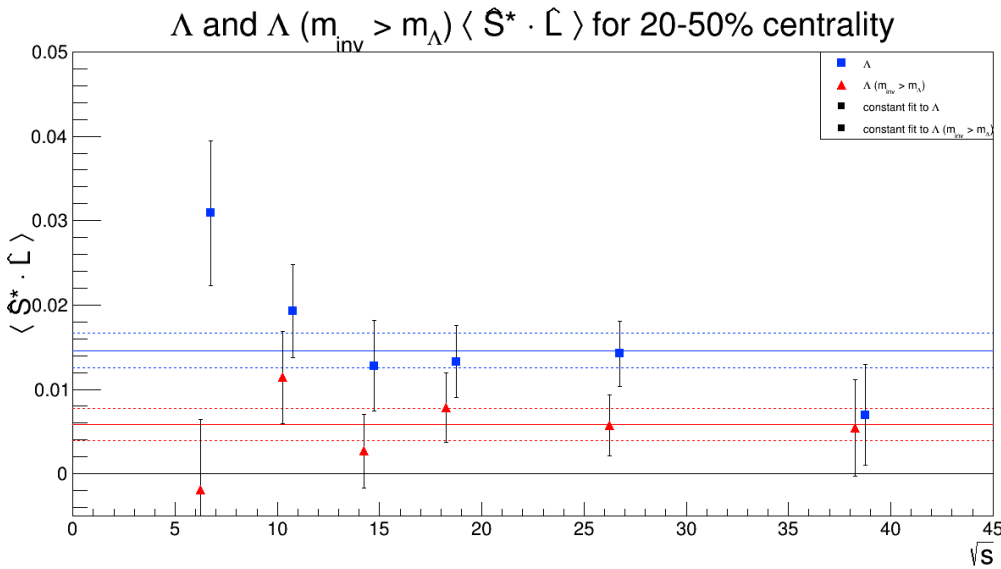


**Fig. 68:**  $\Lambda$  on peak result compared to this result  $m_{\text{inv}} > m_\Lambda$ . In order to show that the off mass results are significantly lower than the on peak results the two sets of data have been fit with a constant function, with error bars in dashed lines.

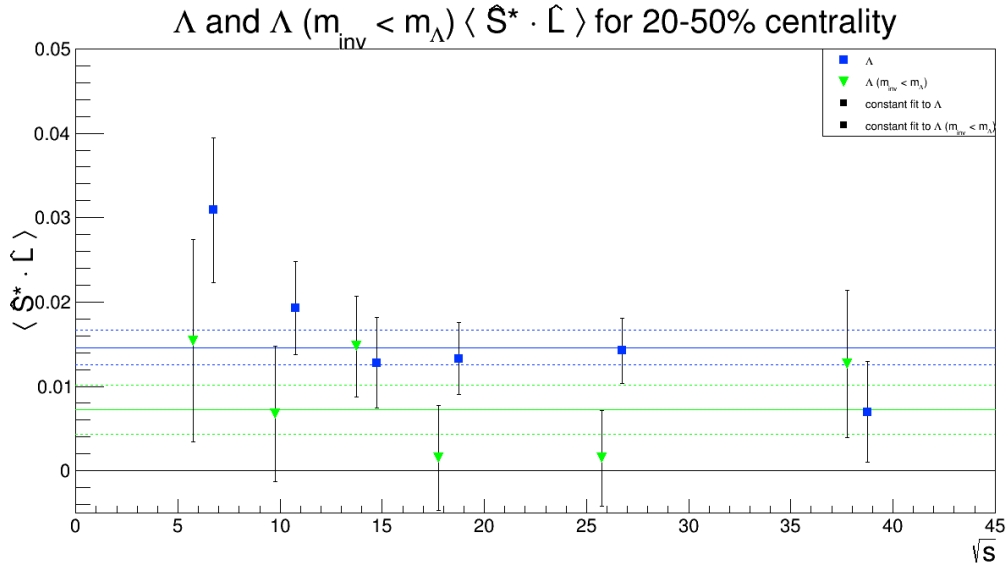


**Fig. 69:**  $\Lambda$  on peak result compared to this result  $m_{inv} < m_\Lambda$ . In order to show that the off mass results are significantly lower than the on peak results the two sets of data have been fit with a constant function, with error bars in dashed lines.

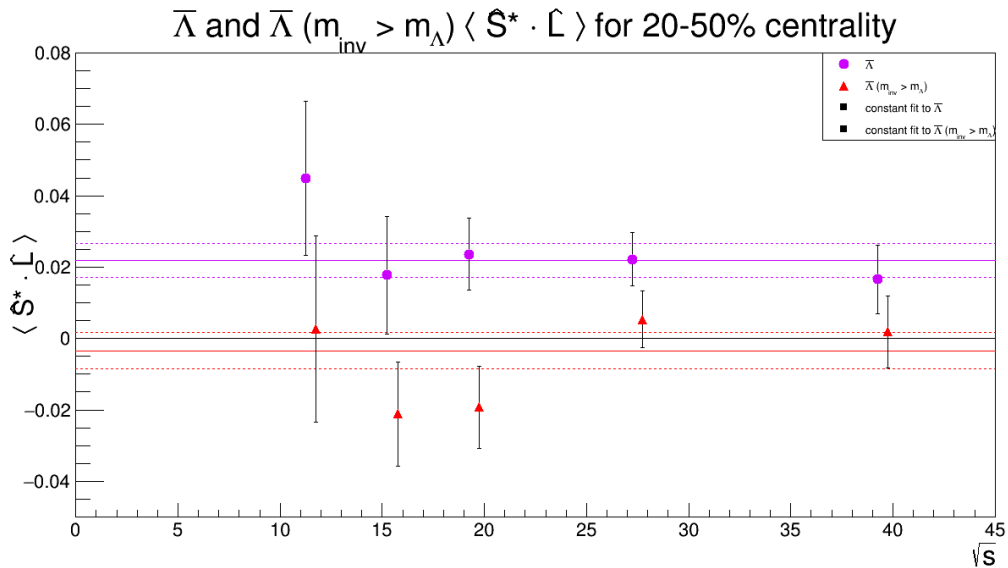


**Fig. 70:**  $\bar{\Lambda}$  on peak result compared to this result  $m_{inv} > m_\Lambda$ . In order to show that the off mass results are significantly lower than the on peak results the two sets of data have been fit with a constant function, with error bars in dashed lines.

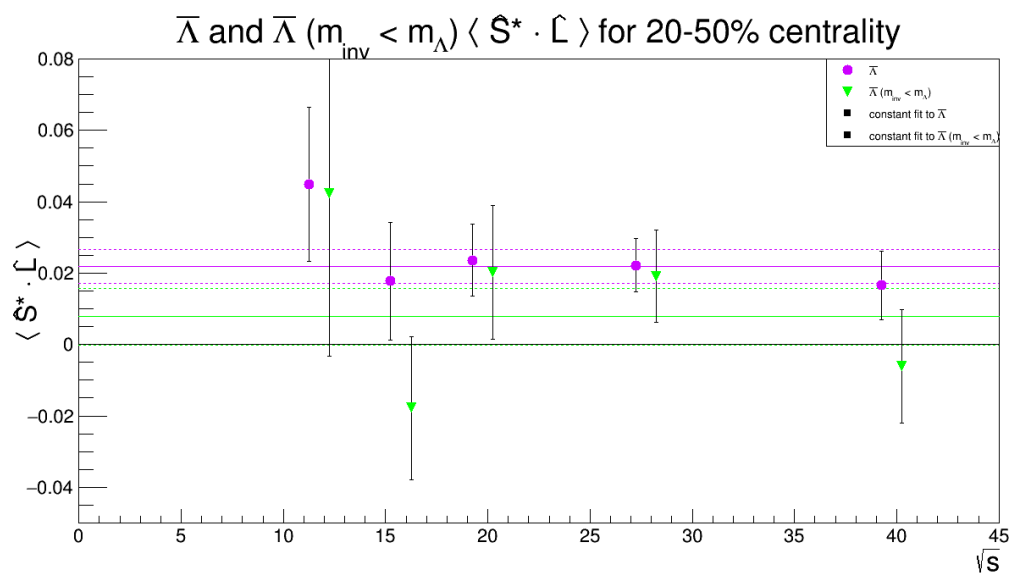


**Fig. 71:**  $\bar{\Lambda}$  on peak result compared to this result  $m_{inv} < m_\Lambda$ . In order to show that the off mass results are significantly lower than the on peak results the two sets of data have been fit with a constant function, with error bars in dashed lines.

We can do the corrections described in equation 4 including this off-mass term and not including the off mass term (that is taking zero for the second term) and compare them. In the further analysis we assume the off-mass contribution is zero. This difference is a source of systematic errors in the analysis.

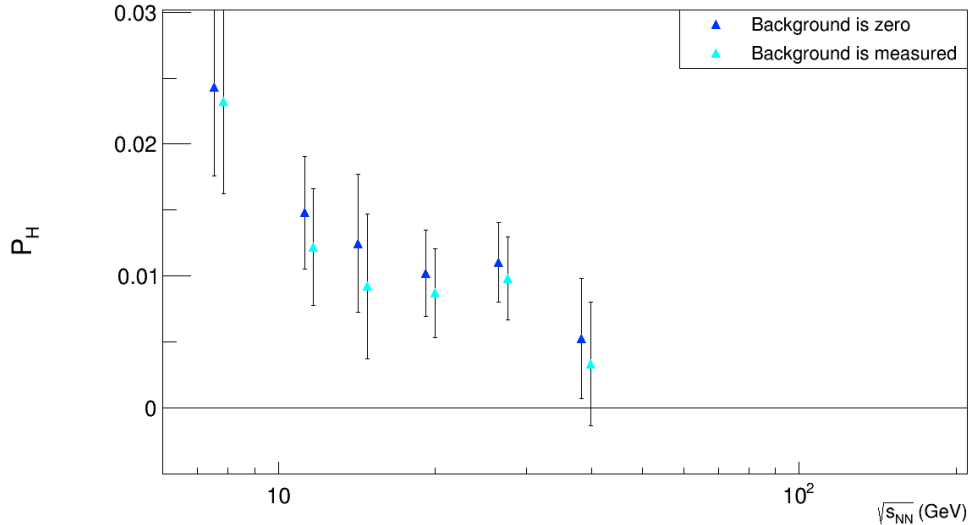


**Fig. 72:**  $\Lambda$  polarization results corrected for purity in the mass background. Results are corrected assuming the second term of eq. 4 is zero and by taking that second term from the data (measured).

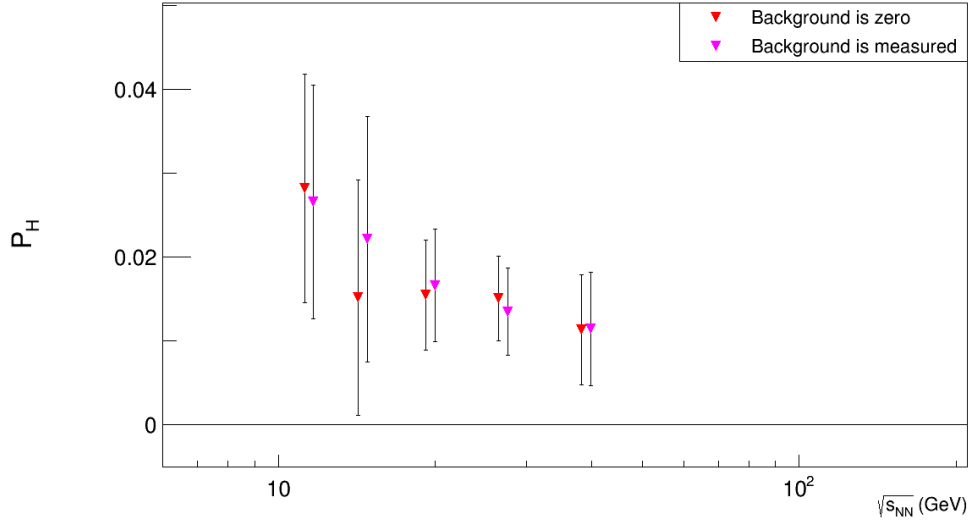


**Fig. 73:**  $\bar{\Lambda}$  polarization results corrected for purity in the mass background. Results are corrected assuming the second term of eq. 4 is zero and by taking that second term from the data (measured).

550 **3.3 Detector acceptance correction**

Much of this section is the same as section C in the 2007 global polarization paper by STAR. Keep in mind that the negative sign error in that paper is propagated here as a substitution  $\phi_p^* - \Psi_{RP} \longrightarrow \Psi_{RP} - \phi_p^*$ .

**3.3.1 Detector acceptance correction explanation**

The polarization as  $\langle \sin(\Psi_{RP} - \phi_p^*) \rangle$  assumes a perfect detector. To correctly take into account the detector acceptance we note that the integral over the solid angle (for the proton boosted into the Lambda's rest frame)  $d\Omega_p^* = d\phi_p^* \sin(\theta_p^*) d\theta_p^*$ . What we actually get when we consider detector acceptance is

$$\langle \sin(\Psi_{RP} - \phi_p^*) \rangle = \int \frac{d\Omega_p^*}{4\pi} \frac{d\phi_H^*}{2\pi} A(\mathbf{p}_H, \mathbf{p}_p^*) \int_0^{2\pi} \frac{d\Psi_{RP}}{2\pi} \sin(\Psi_{RP} - \phi_p^*) [1 + \alpha_H P_H(\mathbf{p}_H; \Psi_{RP}) \sin \theta_p^* \cdot \sin(\Psi_{RP} - \phi_p^*)] \quad (5)$$

where  $\mathbf{p}_H$  is the hyperon 3-momentum and  $A(\mathbf{p}_H, \mathbf{p}_p^*)$  is a function to account for the acceptance; the integral of which is unity. Since the polarization can, in principle, depend on the Lambda's azimuthal angle and the detector is even with respect to  $\phi$  we can expand the polarization into a sum over even harmonics:

$$P_H(\Psi_{RP} - \phi_p^*, p_T^H, \eta^H) = \sum_{n=0}^{\infty} P_H^{(2n)}(p_T^H, \eta^H) \cos \{2n[\Psi_{RP} - \phi_p^*]\}. \quad (6)$$

In this paper the we are not quoting any such azimuthal dependence of the signal so we quote the polarization averaged over all possible values of  $\phi_H - \Psi_{RP}$ :

$$P_H(p_T^H, \eta^H) \equiv \overline{P_H(\Psi_{RP} - \phi_p^*, p_T^H, \eta^H)} = P_H^{(0)}(p_T^H, \eta^H) \quad (7)$$

By substituting eq.6 into eq.5 and integrating over the reaction plane we get

$$\langle \sin(\Psi_{RP} - \phi_p^*) \rangle = \frac{\alpha_H}{2} \int \frac{d\Omega_p^*}{4\pi} \frac{d\phi_H^*}{2\pi} A(\mathbf{p}_H, \mathbf{p}_p^*) \sin \theta_p^* \left[ P_H(p_T^H, \eta^H) - \frac{1}{2} \cos[2(\phi_H - \phi_p^*)] P_H^{(2)}(p_T^H, \eta^H) \right]. \quad (8)$$

From here the observable  $P_H = \frac{8}{\pi \alpha_H} \langle \sin(\Psi_{RP} - \phi_p^*) \rangle$  can be written

$$\begin{aligned} \frac{8}{\pi \alpha_H} \langle \sin(\Psi_{RP} - \phi_p^*) \rangle &= \frac{4}{\pi} \overline{\sin \theta_p^*} P_H(p_T^H, \eta^H) - \frac{2}{\pi} \overline{\sin \theta_p^* \cos[2(\phi_H - \phi_p^*)]} P_H^{(2)}(p_T^H, \eta^H) \\ &= A_0(p_T^H, \eta^H) P_H(p_T^H, \eta^H) - A_2(p_T^H, \eta^H) P_H^{(2)}(p_T^H, \eta^H), \end{aligned} \quad (9)$$

565 where the functions  $A_0(p_T^H, \eta^H)$  and  $A_2(p_T^H, \eta^H)$  are defined by the average of  $\sin \theta_p^*$  and  $\sin \theta_p^* \cos[2(\phi_H - \phi_p^*)]$  over the detector acceptance according to

$$A_0(p_T^H, \eta^H) = \frac{4}{\pi} \overline{\sin \theta_p^*} \equiv \frac{4}{\pi} \int \frac{d\Omega_p^*}{4\pi} \frac{d\phi_H^*}{2\pi} A(\mathbf{p}_H, \mathbf{p}_p^*) \sin \theta_p^* \quad (10)$$

$$A_2(p_T^H, \eta^H) = \frac{2}{\pi} \overline{\sin \theta_p^* \cos[2(\phi_H - \phi_p^*)]} \equiv \frac{2}{\pi} \int \frac{d\Omega_p^*}{4\pi} \frac{d\phi_H^*}{2\pi} A(\mathbf{p}_H, \mathbf{p}_p^*) \sin \theta_p^* \cos[2(\phi_H - \phi_p^*)]. \quad (11)$$

$\sqrt{s_{NN}}$	$A_0$	$A_0$ error
7.7GeV	1.034	2.56e-4
11.5GeV	1.032	1.59e-4
14.5GeV	1.026	1.23e-4
19.6GeV	1.027	9.26e-5
27GeV	1.026	6.45e-5
39GeV	1.022	5.75e-5

**Table 1:**  $A_0$  averaged over  $p_T^H$  and  $\eta^H$

### 3.3.2 Detector acceptance correction results

Here are the numerical results for  $A_0$  averaged over  $p_T^H$  and  $\eta^H$ . We do not look at the dependencies for this measurement since the quoted values for the measurement itself already are integrated over  $p_T^H$  and  $\eta^H$ . The polarization is divided by these numbers to arrive at the acceptance corrected values.

### 3.4 Helicity efficiency

An efficiency issue which is important for this analysis has to do with the direction the Lambda daughters are emitted in the rest frame of the Lambda with respect to the momentum of the Lambda in the lab frame. If we end up with a Lambda daughter pion with very low momentum it is unlikely to be measured in the detector. Since protons are much more massive even protons with low momentum (relative, of course, to other protons) are likely to be measured. Since the proton is emitted preferentially in the direction of (opposite to) the  $\Lambda$ 's ( $\bar{\Lambda}$ 's) spin in its rest frame,  $\hat{S}^*$ , we measure more positive (negative) than negative (positive) helicity  $\Lambda$ s ( $\bar{\Lambda}$ s). A schematic is shown below.

- Serious efficiency issue for decays where the pion points backwards in  $\Lambda$  rest frame

Low Efficiency:

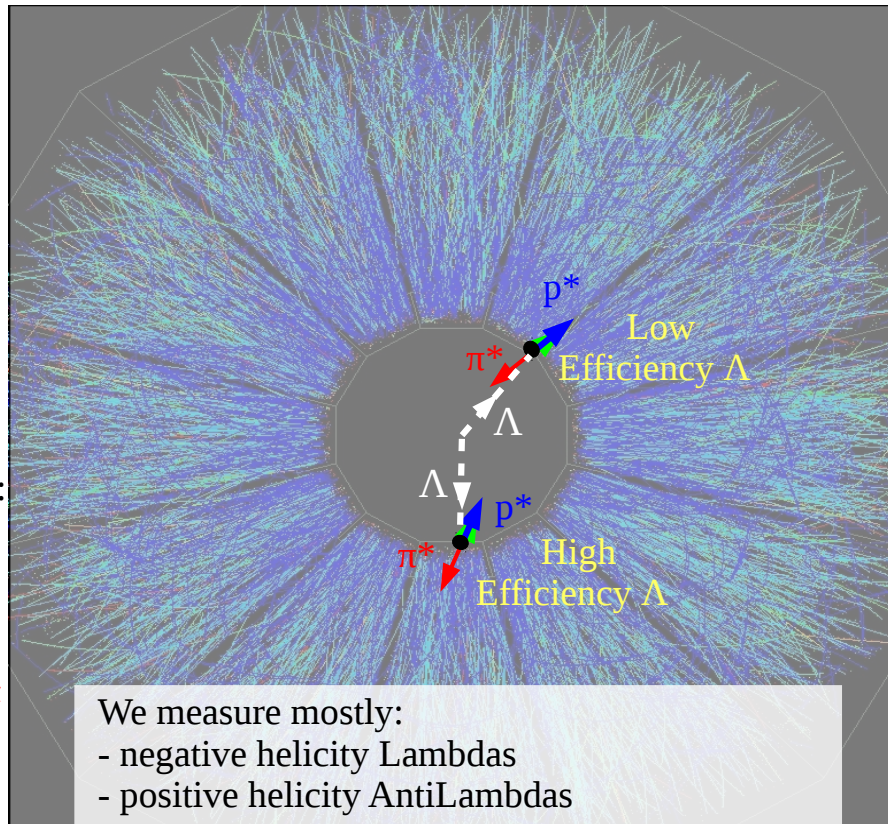
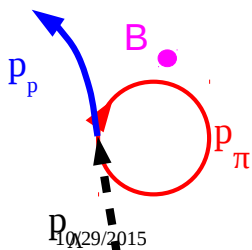


**Fig. 74:** Diagram to show the poor efficiency of Lambdas with low momentum pion daughters as compared to Lambdas with low momentum proton daughters.

Primarily this effect will not effect the data analysis and will be discussed in more detail in sec. 3.4.1.  
 580 However a real polarization signal can, in fact, receive a small modification due to this efficiency. This modification is discussed in 3.4.2

### 3.4.1 Helicity efficiency description

This effect can be seen in data as well as simulation. If the measurement of  $\sin(\Psi_1 - \phi_{\Lambda, \bar{\Lambda}}^*)$  is conducted azimuthally insensitively then this effect averages out but if one wants to take the measurement that is azimuthally dependent it is essential that the effect is known. To look at this effect and its cause I'll plot  
 585  $\hat{p}_{\text{proton}}^* \cdot \hat{p}_\Lambda$  for data and HIJING.

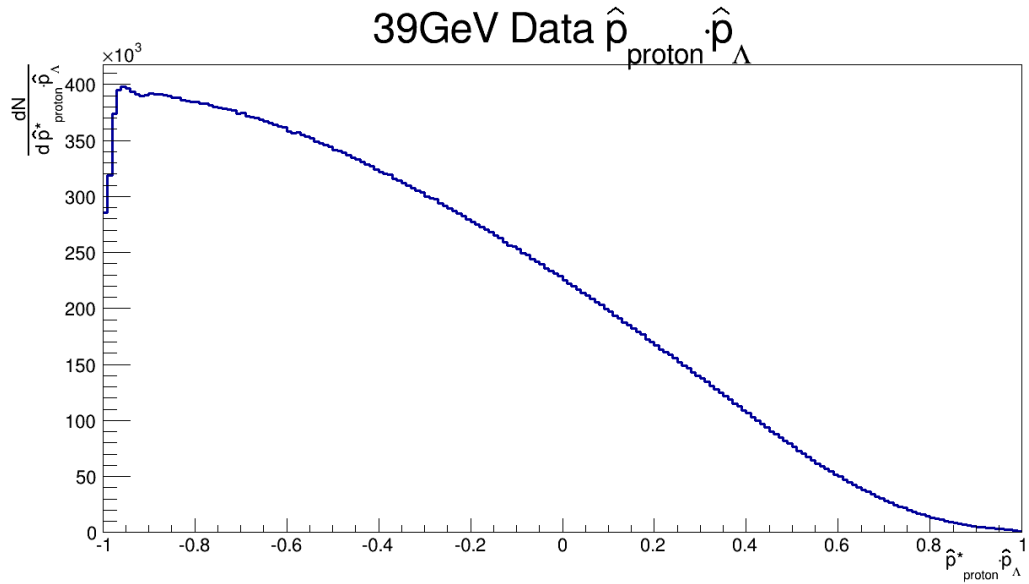


**Fig. 75:** Despite some of the axes this is  $\hat{p}_{\text{proton}}^* \cdot \hat{p}_\Lambda$  for 39GeV. This is essentially the same for all  $\sqrt{s_{NN}}$ . Naturally, physically, this plot should be totally flat since there should be no preffered direction for proton momentum (ignoring some sort of coupling of polarization with emission angle and Lambda yields - which we can basically ignore).

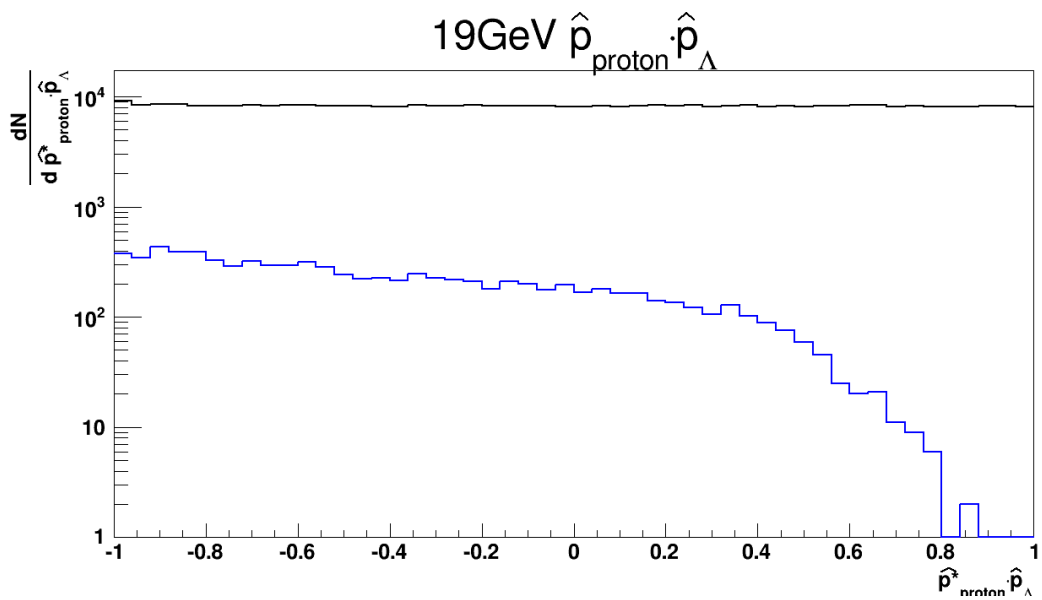


**Fig. 76:** This is the same as Fig. 3.4.1, but made using HIJING data. The black curve is from pure simulation  $\Lambda$ s. The blue curve is made from requiring basic reconstruction cuts (those which are possible: proton  $p_T$ , pion  $p_T$ , proton DCA, pion DCA, and Lambda decay length) of these simulated  $\Lambda$ s. By far the most (actually only!) important cut to this plot is the minimum pion  $p_T$  which causes this shape.

To see how this effects the data one can look at  $\sin(\Psi_1 - \phi_{\Lambda, \bar{\Lambda}}^*)$  vs.  $\Psi_1 - \phi_{\Lambda, \bar{\Lambda}}$ . In the following plots the label of “Polarization” means  $-\sin(\Psi_1 - \phi_{\Lambda, \bar{\Lambda}}^*)$ . At the time of making these plots there were a few negative signs that I had not correctly accounted for. Much like the previous STAR paper on this 590 polarization I had a negative sign in my definition of  $\hat{L}$  which is where the negative sign above comes out. Additionally there is a negative sign in how I determined  $\Psi_1$ , this and the previous mistake cancel out. Finally I also had a sign error in the  $\bar{\Lambda}$  result since the antiproton is emitted opposite the  $\bar{\Lambda}$  spin, which I did not af first realize. The summary of the previous points on sign errors is that in the following two 595 plots the  $\Lambda$  results are okay but the results for  $\bar{\Lambda}$ s should be flipped about the y axis. Due to an incorrect definition early in the analysis (the same as in the 2007 STAR paper) there is a sign error in the  $\Lambda$  results. There are two sign errors in the  $\bar{\Lambda}$  results that cancel. Therefore the  $\Lambda$  plots should simply be flipped about the y axis. Remember that the angular momentum points in negative y and that the efficiency is such that we are more likely to reconstruct (Anti)Lambdas with negative (positive) helicity!!

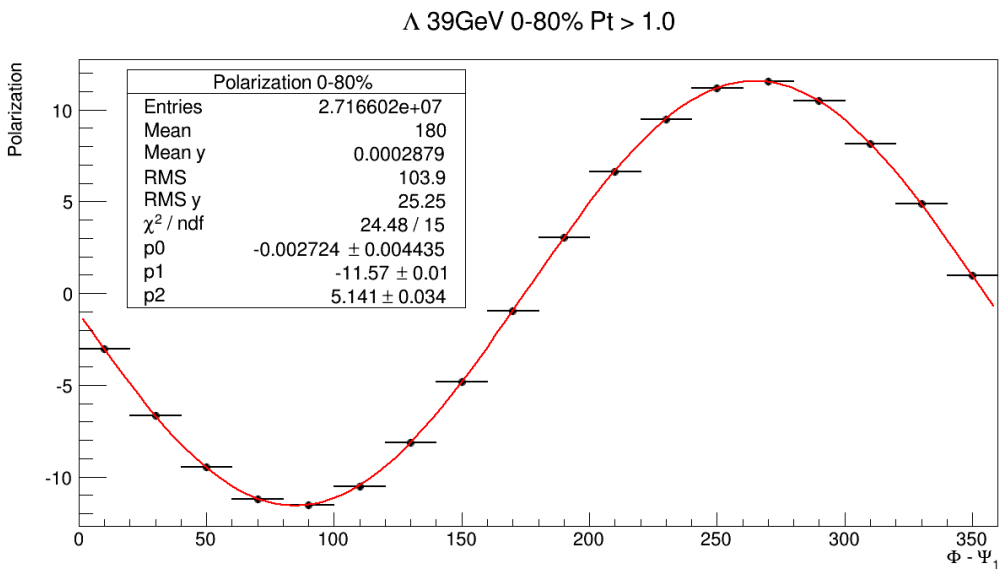


**Fig. 77:**  $\sin(\Psi_1 - \phi_{\Lambda}^*)$  vs.  $\Psi_1 - \phi_{\Lambda}$  for 39GeV  $\Lambda$ s with  $p_T > 1\text{GeV}$ . The data have been fit by the function  $p0 + p1 * \sin(x + p2)$ . The overall sinusoidal shape comes from the effect mentioned above and seen in Fig. 3.4.1. The specific phase shift comes from the STAR magnetic field which increases with  $p_T$ . 39GeV data has a RFF field alignment. There is a sign error in the  $\Lambda$  results.

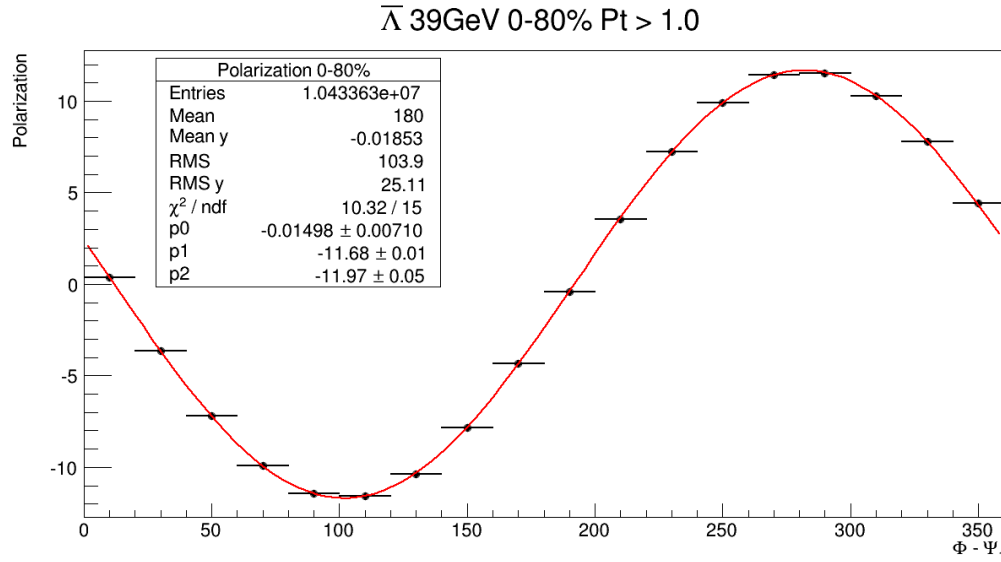


**Fig. 78:**  $\sin(\Psi_1 - \phi_{\bar{\Lambda}}^*)$  vs.  $\Psi_1 - \phi_{\bar{\Lambda}}$  for 39GeV  $\Lambda$ s with  $p_T > 1$ GeV. The data have been fit by the function  $p0 + p1 * \sin(x + p2)$ . The overall sinusoidal shape comes from the effect mentioned above and seen in Fig. 3.4.1. The specific phase shift comes from the STAR magnetic field which increases with  $p_T$ . 39GeV data has a RFF field alignment. Note that the phase is opposite in sign to what is seen in Fig. 3.4.1.

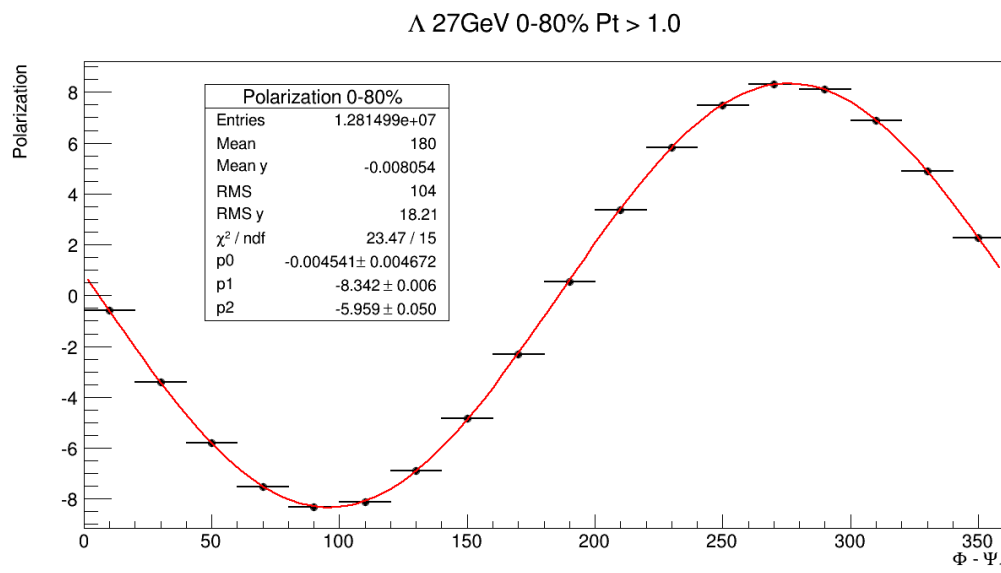


**Fig. 79:**  $\sin(\Psi_1 - \phi_{\bar{\Lambda}}^*)$  vs.  $\Psi_1 - \phi_{\bar{\Lambda}}$  for 27GeV  $\Lambda$ s with  $p_T > 1$ GeV. The data have been fit by the function  $p0 + p1 * \sin(x + p2)$ . The overall sinusoidal shape comes from the effect mentioned above and seen in Fig. 3.4.1. The specific phase shift comes from the STAR magnetic field which increases with  $p_T$ . 27GeV data has a FF field alignment. Note that the phase is opposite in sign to what is seen in Fig. 3.4.1. **There is a sign error in the  $\Lambda$  results.**

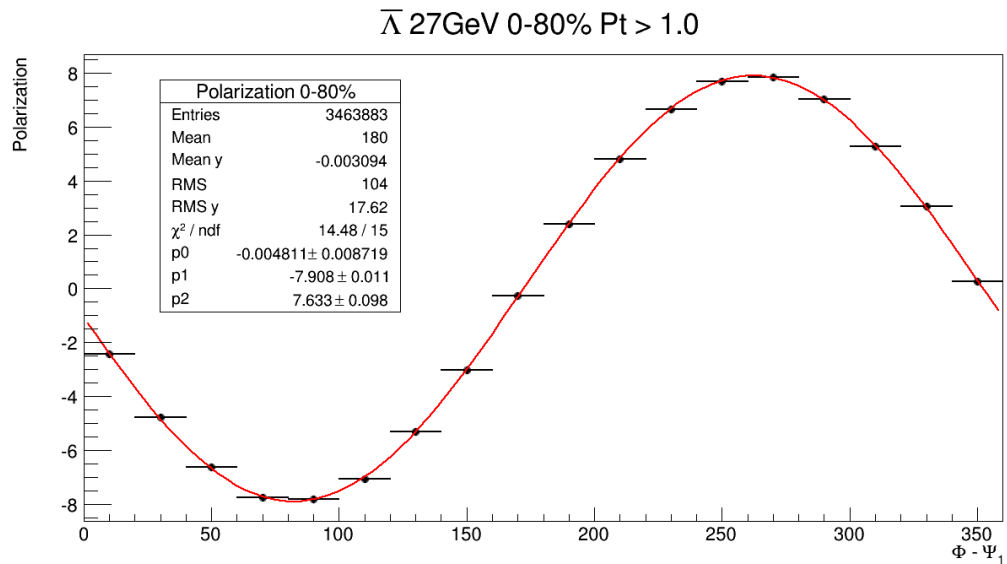


**Fig. 80:**  $\sin(\Psi_1 - \phi_{\bar{\Lambda}}^*)$  vs.  $\Psi_1 - \phi_{\bar{\Lambda}}$  for 27GeV  $\bar{\Lambda}$ s with  $p_T > 1\text{GeV}$ . The data have been fit by the function  $p0 + p1 * \sin(x + p2)$ . The overall sinusoidal shape comes from the effect mentioned above and seen in Fig. 3.4.1. The specific phase shift comes from the STAR magnetic field which increases with  $p_T$ . 27GeV data has a RFF field alignment. Note that the phase is opposite in sign to what is seen in Fig. 3.4.1.

Knowing that we tend to see the Lambdas with backwards going protons means that we will see this sinusoidal behavoir. Ignore, for now, the phase shift and focus just on the overall sine shape seen above. Also, in the following discussion, assume that there is no global polarization so that an azimuthally integrated measure would give a null result. Finally take  $\hat{L}$  to be pointing in  $\pi/2$  with respect to the event plane. For a  $\Lambda(\bar{\Lambda})$  with  $\phi_\Lambda - \Psi_1 = 0$  the helicity efficiency should have no effect since  $\sin(\Psi_1 - \phi_\Lambda^*)$  vs.  $\Psi_1 - \phi_\Lambda$  for  $\phi_\Lambda - \Psi_1 = \pi$  is also zero. The same thing is effectively true for a Lambda emitted in  $\phi_\Lambda - \Psi_1 = \pi$ . If, however the  $\Lambda(\bar{\Lambda})$  is emitted such that  $0 < \phi_\Lambda - \Psi_1 < \pi$  the efficiency will generate a large negative (positive)  $\sin(\Psi_1 - \phi_\Lambda^*)$ . Naturally the opposite is true for emission in  $\pi < \phi_\Lambda - \Psi_1 < \pi$ .

Let's start over with a  $\Lambda$  with  $\phi_\Lambda - \Psi_1 = 0$  decaying with the STAR magnetic field on FF (as we have in 27GeV data). The decay point resolution of the Lambda is finite so we do not know exactly where the proton daughter was born. The magnetic field points in  $+\hat{z}$  so the proton will appear to be bent slightly towards positive  $\hat{y}$  which means negative  $\hat{L}$ . This imperfection leads to a negative value of  $\sin(\Psi_1 - \phi_\Lambda^*)$  for such  $\Lambda$ s. This effect is the same for  $\bar{\Lambda}$ s since the antiproton curves the opposite direction and also denotes the opposite direction of spin - so two negatives cancel. This effect persists as you go about  $\phi^*$  so at  $\Lambda$  with  $\phi_\Lambda - \Psi_1 = \pi$  you end up with a positive number from the magnetic field.

Finally I want to compare these results to HIJING data

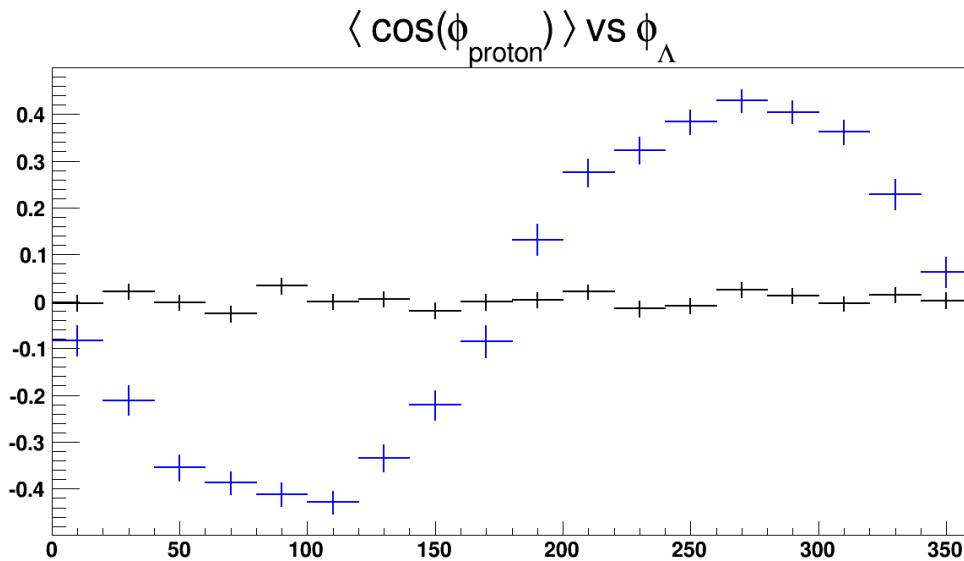


**Fig. 81:** As in Fig. 3.4.1 the black curve is from pure simulation  $\Lambda$ s. The blue curve is made from requiring basic reconstruction cuts. This has the assumption that the  $\Psi_1 = 0$ . **The same sign error is in these HIJING results.**

615 To understand how this efficiency creates an asymmetry in the final results see the flowing plots which  
 show the  $\eta_\Lambda$  dependence of our polarization parameter. In this version I am plotting  $S_y = \vec{S}_\Lambda \cdot \hat{L}$  which  
 differs by a factor of two from  $\sin(\Psi_1 - \phi_\Lambda^*)$  and also includes a boosting of the spin vector. In principle  
 this could make a difference but in practice the  $S_y$  results have been consistent (accounting for the factor  
 of two) with  $\sin(\Psi_1 - \phi_\Lambda^*)$ , so it seems to be an ignorable difference. At the very least I am confident  
 620 that the qualitative arguments presented here are correct.

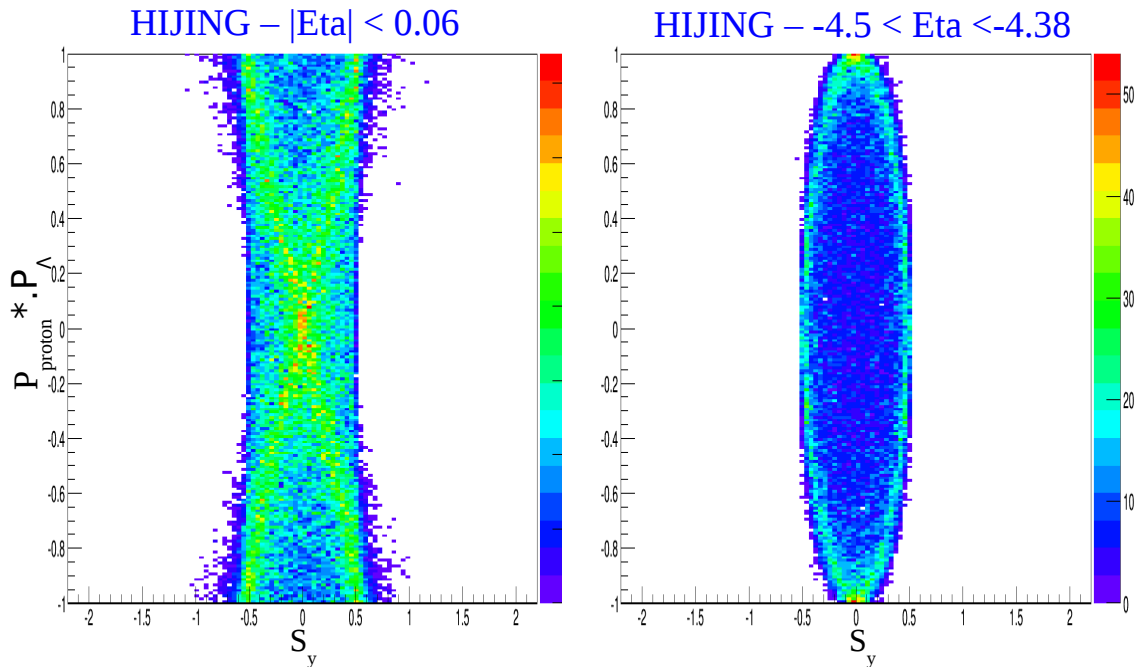


**Fig. 82:** As in Fig. 3.4.1 The figure on the left is a  $S_y$  for a narrow slice  $\eta_\Lambda$  at mid-rapidity while the figure on the right is a narrow slice very backward in  $\eta$ . For the first case the  $\Lambda$  is emitted in the same  $x - y$  plane as  $\hat{L}$  in the second figure it is almost perpendicular to  $\hat{L}$ . Since the proton tends to be emitted with basically the same momentum as the Lambda these tendencies make sense. **The same sign error is in these HIJING results.**

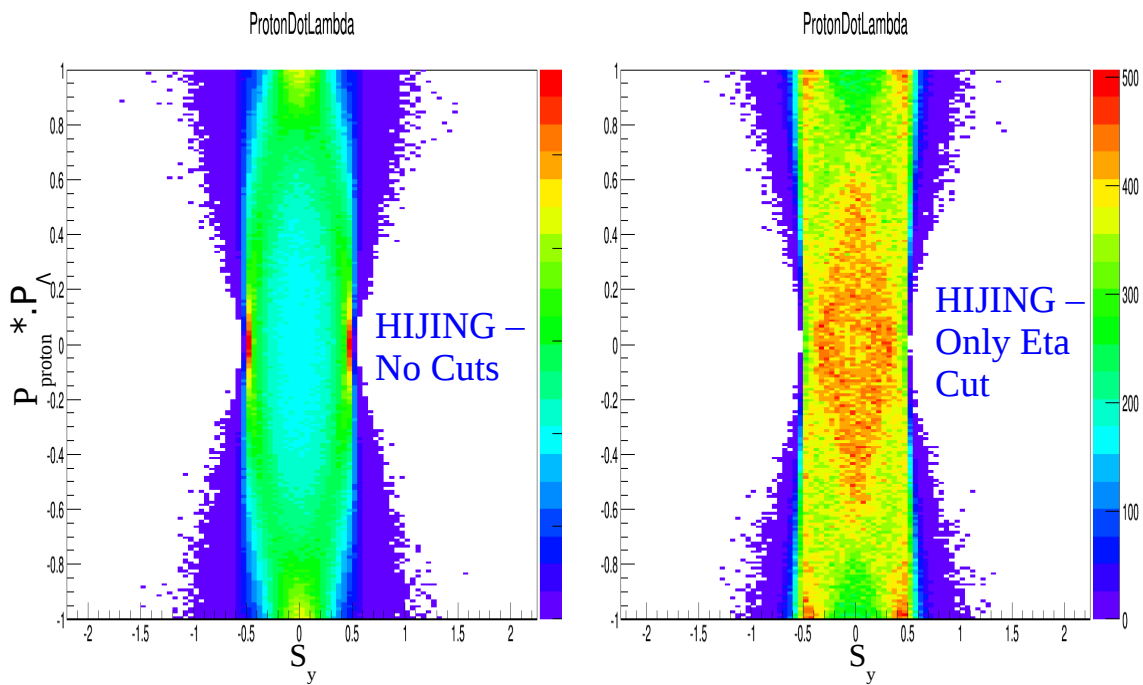


**Fig. 83:** As in Fig. 3.4.1 Fig. 3.4.1 tells us how looking at  $S_y$  within the STAR  $\eta$  range changes the underlying distribution. The same sign error is in these HIJING results.

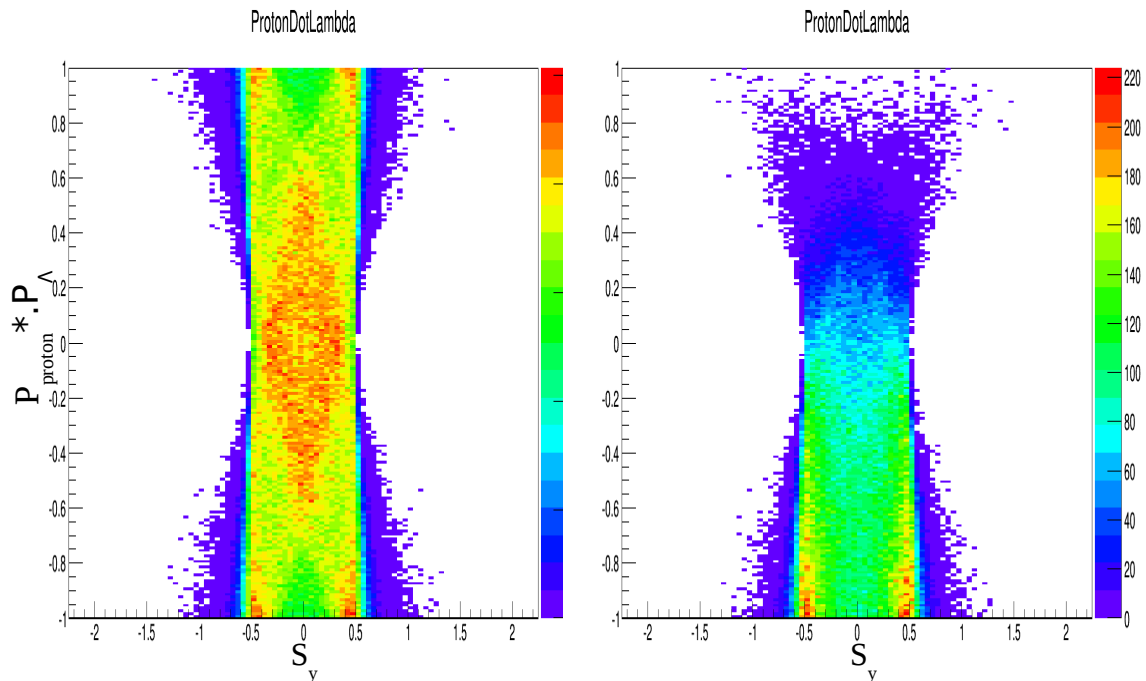


**Fig. 84:** Finally we see what the effect the helicity efficiency (Fig 3.4.1) has on the underlying distribution (Fig. 3.4.1). Now we see an asymmetry in the  $S_y$  distribution from the efficiency. **The same sign error is in these HIJING results.**

### 3.4.2 Helicity efficiency effect

In the previous section I described the helicity efficiency should average out when performing the analysis over all Lambda  $\phi$ . Something which may not be immediately obvious is that there is essentially a coupling at higher harmonics of the  $\phi$  distribution between the polarization (a zeroth order in trigonometric functions) and the aforementioned efficiency (a first order in trigonometric functions). Naturally I am assuming that the polarization is not phi dependant - an assumption which is seemingly born out in data (it is at least fair to say that such a dependence, if it exists, must be small compared to the phi-averaged polarization measured here).

Remember first that the sign of fig. 3.4.1 is wrong. we know from fig. 3.4.1 that negative (positive) helicity Lambdas (AntiLambdas) will have higher efficiency. If the Lambdas are actually polarized then a sample of Lambdas at  $\pi/2$  has polarization in  $-\hat{y}$  as well as an efficiency (independant of polarization) that tends to align spins along  $-\hat{y}$ . This will lead to an *increased* efficiency relative to Lambdas from any other  $\phi$ . Similarly Lambdas at  $-\pi/2$  have polarization anti-aligning with the efficiency effect, and thus a *decreased* efficiency. This coupling will make the first hump in 3.4.1 larger and the second hump smaller which means averaged over all of  $\phi$  the polarization you will measure is *larger* than the nominal polarization of the sample.

Attached is a BulkCorr presentation detailing a simple simulation. In the simulation the azimuthal distribution of the Lambda daughters are chosen by sampling the polarization distribution with a given polarization. Additionally there are minimum  $p_T$  cuts on the daughters to get the efficiency effect (the Lambda momentum is chosen by sampling a real Lambda momentum distribution).

The result of all of this is a 7% scaling (that is a division of 1.07) for the polarization measure.

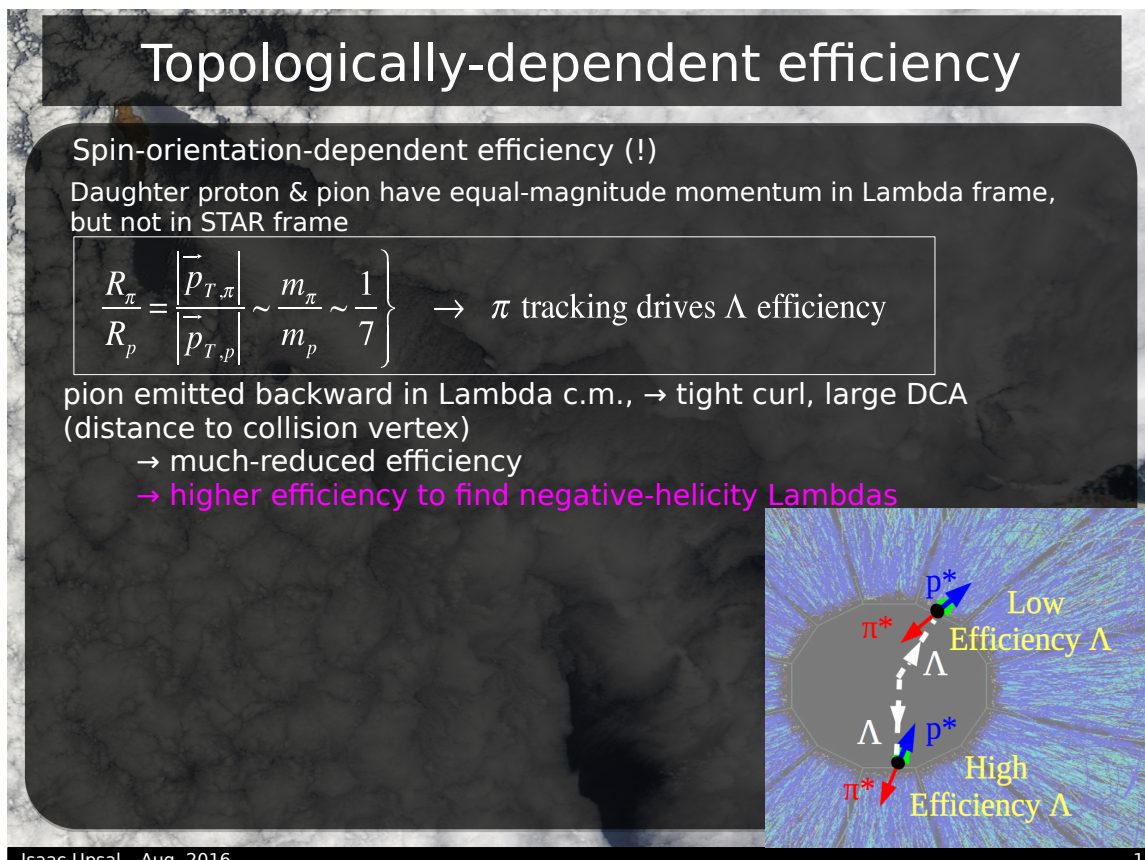


**Fig. 85:** Presentation on the effect of helicity efficiency on the polarization analysis p1.

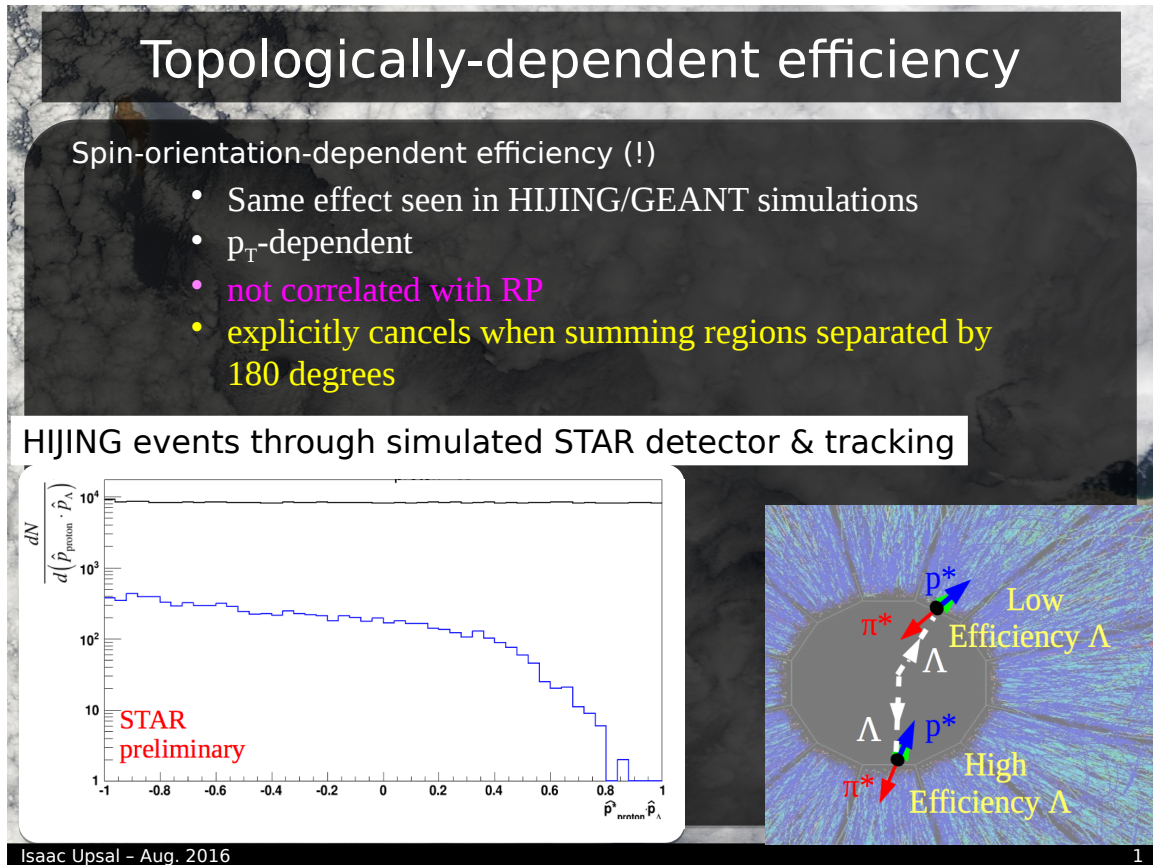


**Fig. 86:** Presentation on the effect of helicity efficiency on the polarization analysis p2.

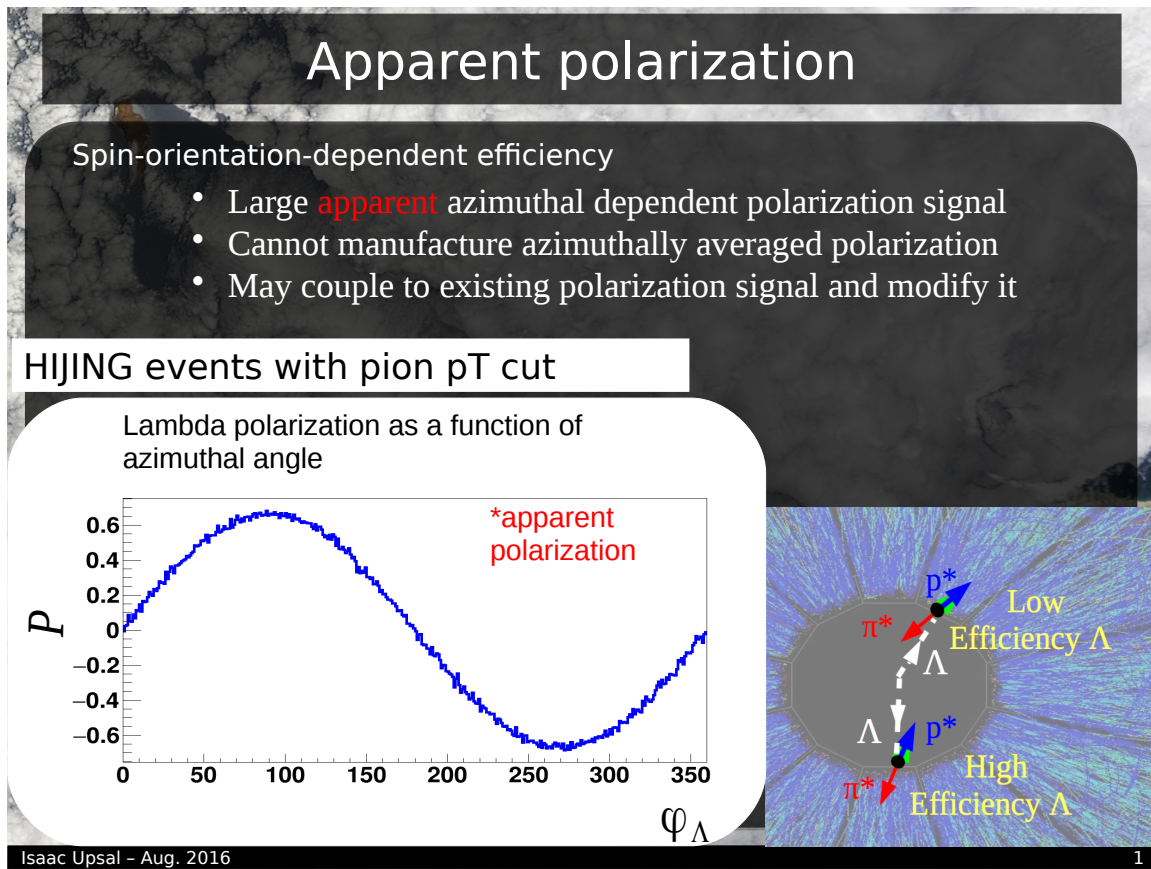


**Fig. 87:** Presentation on the effect of helicity efficiency on the polarization analysis p3.

## Spin alignment from polarization

- Azimuthally independent polarization
- No detector!
- Spins in ensemble align with  $\hat{L}$
- True for any ensemble of  $\varphi_\Lambda$

Isaac Upsal - Aug. 2016

1

**Fig. 88:** Presentation on the effect of helicity efficiency on the polarization analysis p4.

## Spin alignment from efficiency

- No real polarization – only detector effects
- Lose Lambdas with spins in **ensemble** which align with  $\hat{p}$

Isaac Upsal - Aug. 2016

1

**Fig. 89:** Presentation on the effect of helicity efficiency on the polarization analysis p5.

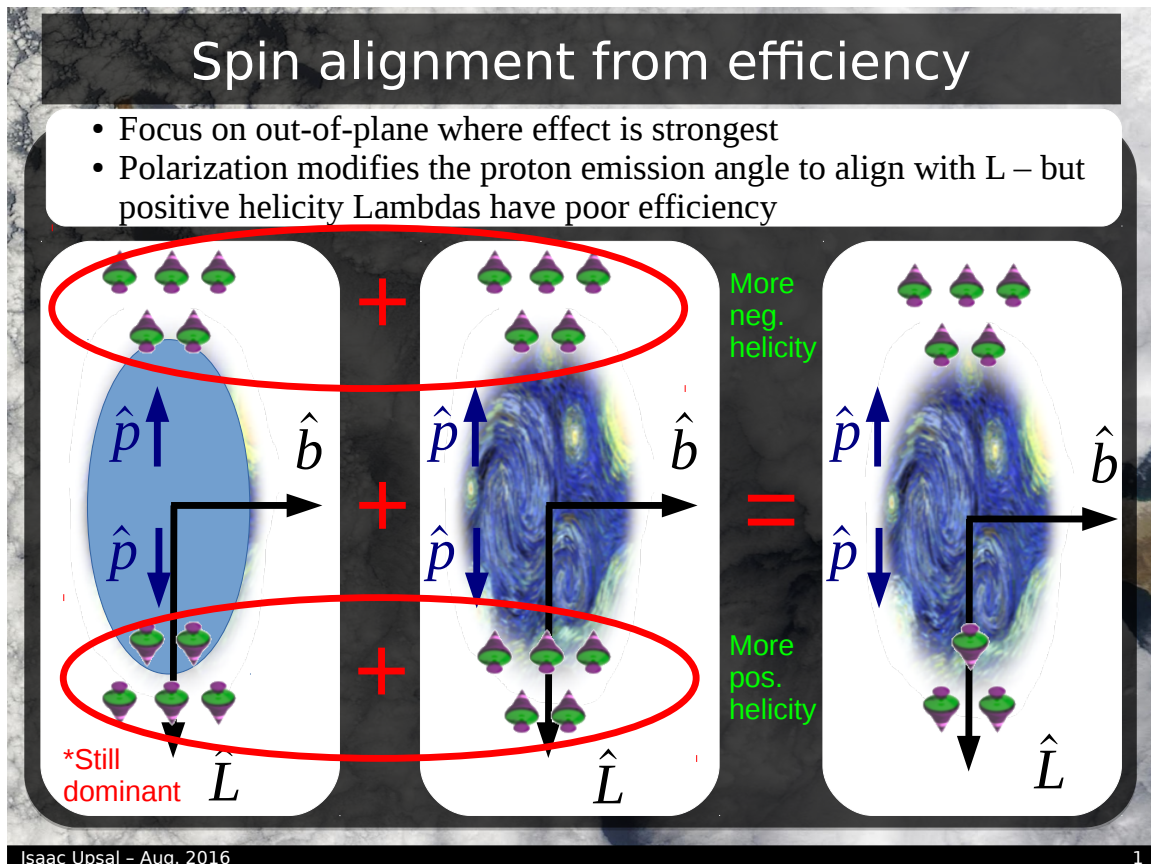


**Fig. 90:** Presentation on the effect of helicity efficiency on the polarization analysis p6.

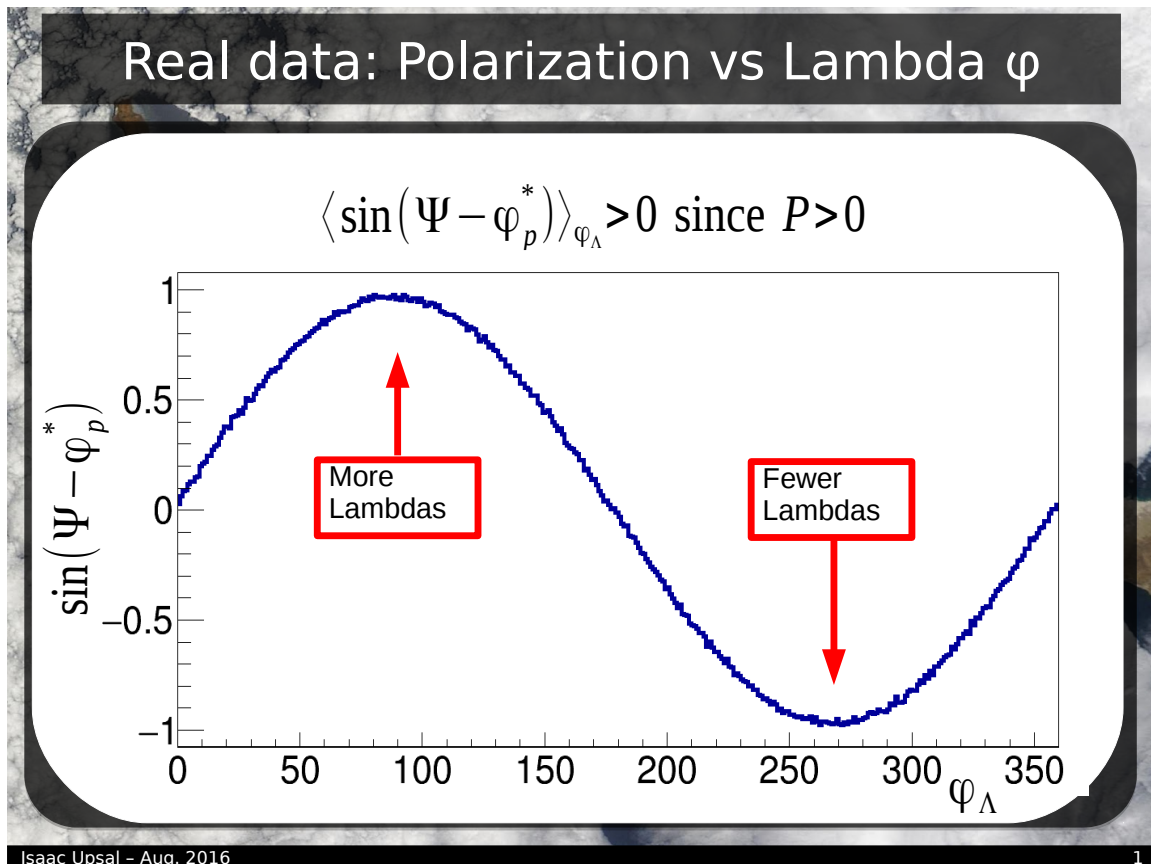
## Spin alignment from efficiency

- Introduces azimuthally dependent efficiency
- More Lambdas with spins aligning with angular momentum than anti-aligned
- Makes **real** polarization signal look bigger
- For AntiLambdas flip spins and efficiencies – ultimately the same effect
- Scaling and systematic error

Isaac Upsal - Aug. 2016

1

**Fig. 91:** Presentation on the effect of helicity efficiency on the polarization analysis p7.



Isaac Upsal - Aug. 2016

1

**Fig. 92:** Presentation on the effect of helicity efficiency on the polarization analysis p8.

## Test consequence of efficiency

- Simple simulation, get proton decay direction by sampling distribution for different polarizations

$$1 + \alpha P \cos(\theta^*)$$

- Then make pion pt cut and check and compare “measured” polarization to input polarization

**Fig. 93:** Presentation on the effect of helicity efficiency on the polarization analysis p9.

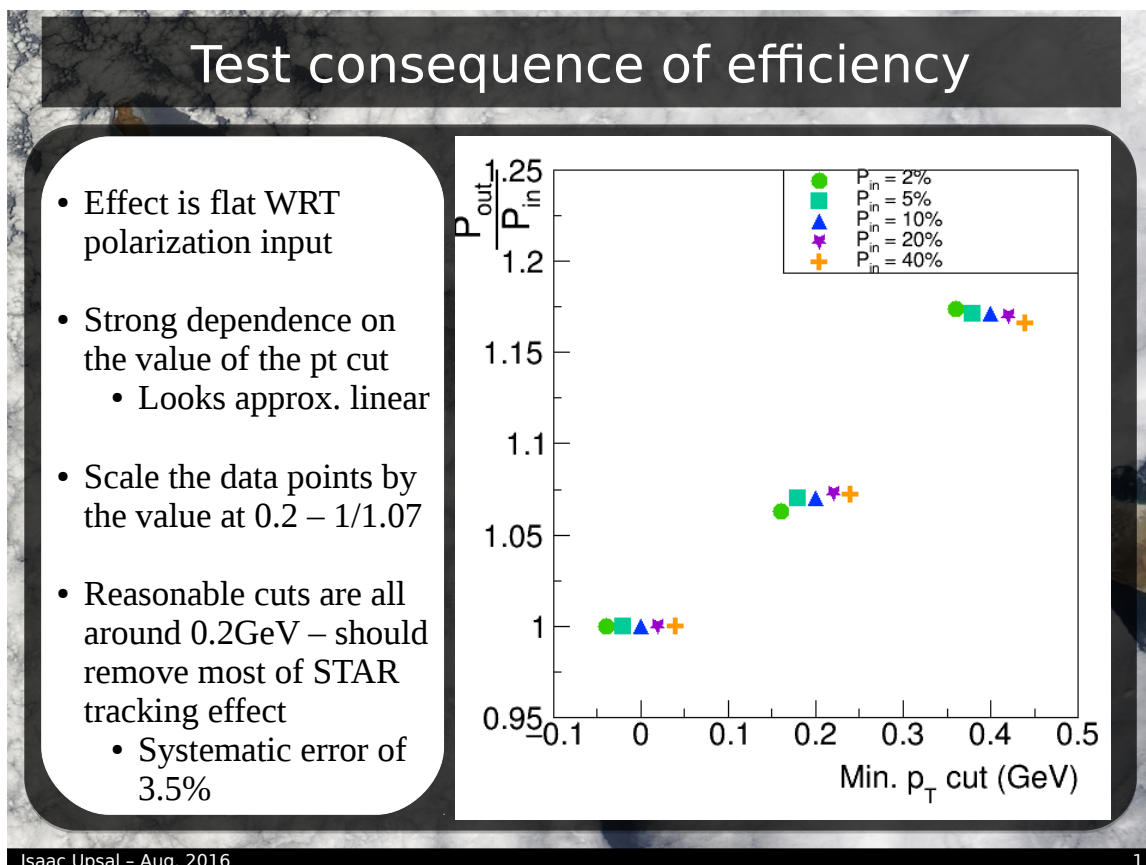


**Fig. 94:** Presentation on the effect of helicity efficiency on the polarization analysis p10.

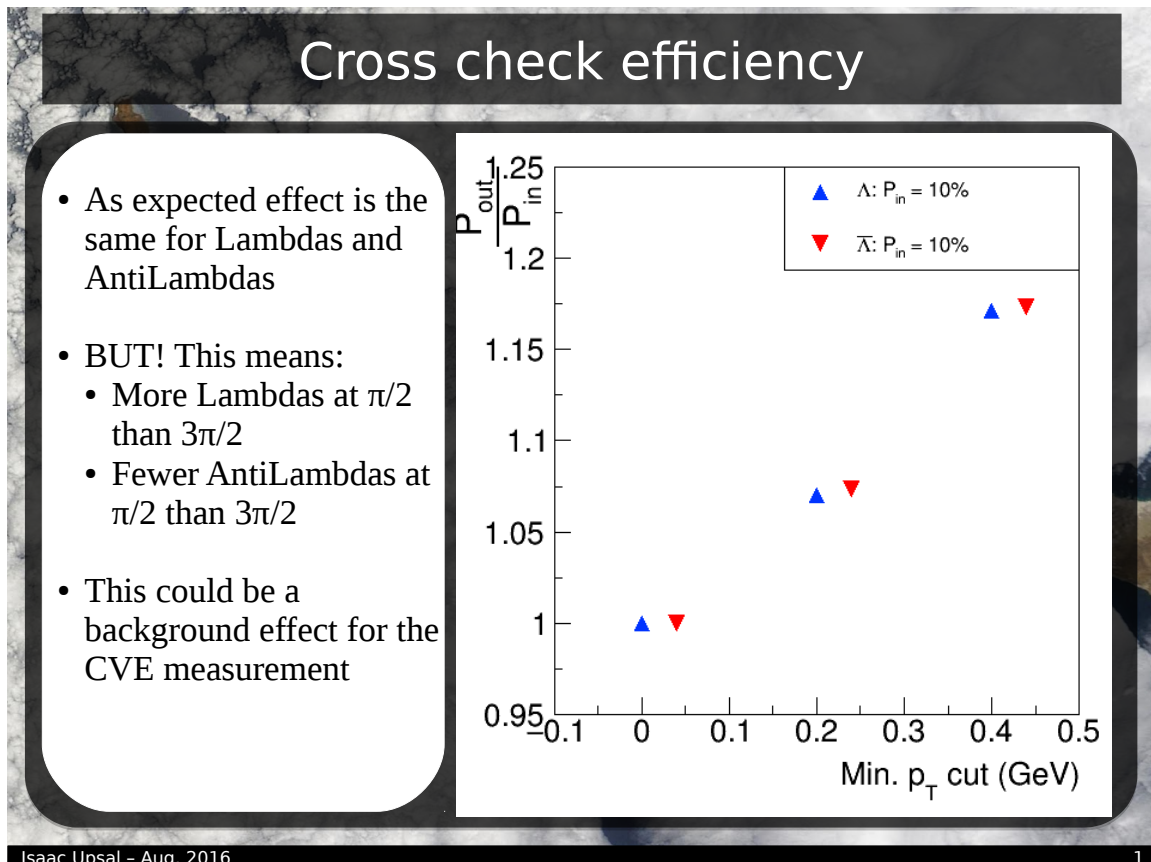


**Fig. 95:** Presentation on the effect of helicity efficiency on the polarization analysis p11.

### 3.5 Feed-down correction

This section is about feed-down correction which only applies to separating the vortical/magnetic components of the polarization. Perhaps the best resource is a paper we wrote along with Francesco Becattini and Iurii Karpenko specifically to address this:  
645

<https://arxiv.org/abs/1610.02506>

I'm basically going to just copy down a document Mike wrote about this as part of communications for the paper writing process. Because of this there is a possibility that certain statements make sense more in that context than this one. I'm going to copy the subsections of the document as well. I also plan on  
650 posting a document called "FeeddownCorrection.pdf" which has the same information as this section.

#### 3.5.1 Abstract for feeddown

A majority ( $\sim 75\%$ ) of  $\Lambda$  ( $\bar{\Lambda}$ ) hyperons in our data sample are not primary particles, but rather feeddown daughters of heavier particles, especially  $\Sigma^0, \Sigma^*, \Xi$ . To extract vorticity and magnetic field from the data, we must account for this feeddown. The formalism to do this in a thermal model has recently  
655 been published by Becattini, Karpenko, Lisa, Upsal and Voloshin. In this note, I detail how we use the THERMUS model yields to this effect.

#### 3.5.2 Correction procedure and definitions

If vortical and/or magnetic effects generate polarization in  $\Lambda$  and  $\bar{\Lambda}$  emitted from heavy ion collisions, then presumably all other hadrons are polarized, as well. Since more than 75% of measured  $\Lambda$  and  $\bar{\Lambda}$  are  
660 daughters of other particles, we need to account for the effects of "polarized feed-down."

The formalism for doing this has recently been published [?], and for small polarization the thermal vorticity  $\bar{\omega}$  and magnetic field are related to the measured polarizations according to

$$\begin{pmatrix} \bar{\omega}_c \\ B_c/T \end{pmatrix} = \begin{bmatrix} \frac{2}{3} \sum_R (f_{\Lambda R} C_{\Lambda R} - \frac{1}{3} f_{\Sigma^0 R} C_{\Sigma^0 R}) S_R (S_R + 1) & \frac{2}{3} \sum_R (f_{\Lambda R} C_{\Lambda R} - \frac{1}{3} f_{\Sigma^0 R} C_{\Sigma^0 R}) (S_R + 1) \mu_R \\ \frac{2}{3} \sum_{\bar{R}} (f_{\bar{\Lambda} \bar{R}} C_{\bar{\Lambda} \bar{R}} - \frac{1}{3} f_{\bar{\Sigma}^0 \bar{R}} C_{\bar{\Sigma}^0 \bar{R}}) S_{\bar{R}} (S_{\bar{R}} + 1) & \frac{2}{3} \sum_{\bar{R}} (f_{\bar{\Lambda} \bar{R}} C_{\bar{\Lambda} \bar{R}} - \frac{1}{3} f_{\bar{\Sigma}^0 \bar{R}} C_{\bar{\Sigma}^0 \bar{R}}) (S_{\bar{R}} + 1) \mu_{\bar{R}} \end{bmatrix}^{-1} \begin{pmatrix} P_{\Lambda}^{\text{meas}} \\ P_{\bar{\Lambda}}^{\text{meas}} \end{pmatrix} \quad (12)$$

Here,  $f_{\Lambda R}$  ( $f_{\bar{\Lambda} \bar{R}}$ ) is the fraction of measured  $\Lambda$ s ( $\bar{\Lambda}$ s) that arise from the direct decay of a baryon  $R \rightarrow \Lambda + X$  ( $\bar{R} \rightarrow \bar{\Lambda} + X$ ). Similarly,  $f_{\Sigma^0 R}$  ( $f_{\bar{\Sigma}^0 \bar{R}}$ ) is the fraction of measured  $\Lambda$ s ( $\bar{\Lambda}$ s) that arise from the direct decay  
665  $R \rightarrow \Sigma^0 + X \rightarrow \Lambda + \gamma + X$  ( $\bar{R} \rightarrow \bar{\Sigma}^0 + X \rightarrow \bar{\Lambda} + \gamma + X$ ). (Note carefully the last sentence:  $f_{\Sigma^0 R}$  does not give the fraction of *Sigmas* coming from parent  $R$ , but the fraction of *Lambdas* coming from (grand)parent  $R$ .) The branching ratio for  $\Sigma^0 \rightarrow \Lambda + \gamma$  is essentially 100%.

The constants  $C$  are the spin transfer coefficients, listed in table 2, and  $S_R$  and  $\mu_R$  are the spin and magnetic moment of particle  $R$ . For the antibaryons,  $S_{\bar{R}} = S_R$ ,  $C_{\bar{X}Y} = C_{XY}$ , and  $\mu_{\bar{R}} = -\mu_R$ .

670 The sums in equation 12 are understood to include the contributions of *primary*  $\Lambda$ s and  $\Sigma^0$ s, too.

#### 3.5.3 Which particles are included?

The number of individual contributors to the measured  $\Lambda$  yield is huge. However, the primary ones are listed in table 3. Primary  $\Lambda$ s make up about 25% of that yield. The daughters from  $\Xi, \Sigma^0, \Sigma^*$  make up another 60% and then there are  $\sim 15\%$  more, which we will call "other." These include things like  
675  $\Lambda(1405)$  and  $\Lambda(1530)$ . In fact, these two that I mention each contribute about 1% of the yield. Others contribute less. (Bill Llope's files list the contributors in decreasing order of contribution, and these two are the last ones he lists before truncating.)

Decay	$C$
parity-conserving: $\frac{1}{2}^+ \rightarrow \frac{1}{2}^+ 0^-$	-1/3
parity-conserving: $\frac{1}{2}^- \rightarrow \frac{1}{2}^+ 0^-$	1
parity-conserving: $\frac{3}{2}^+ \rightarrow \frac{1}{2}^+ 0^-$	1/3
parity-conserving: $\frac{3}{2}^- \rightarrow \frac{1}{2}^+ 0^-$	-1/5
$\Xi^0 \rightarrow \Lambda + \pi^0$	+0.900
$\Xi^- \rightarrow \Lambda + \pi^-$	+0.927
$\Sigma^0 \rightarrow \Lambda + \gamma$	-1/3

**Table 2:** Polarization transfer factors  $C$  for important decays  $X \rightarrow \Lambda(\Sigma)\pi$

This 15% we will consider as unpolarized. If there were no magnetic field, but only vortical-induced polarization, we [?] have checked that the alternating signs of the spin transfer coefficients  $C$  effectively 680 make all their contributions cancel each other out; so, our assumption of (effective) zero polarization is justified. To definitively say what would happen if there *is* a magnetic field, we would have to know the magnetic moments of these contributors, and they are not measured. It is very reasonable to assume, however, that, as in the vortical case, they would effectively cancel each other out. In any event, these “other” parents are assumed to be a zero-polarization component to the measured As. Hence, they 685 suppress the signal by “diluting” it by  $\sim 15\%$ .

The relevant values of  $f_{\Lambda R}$ ,  $f_{\bar{\Lambda}\bar{R}}$ ,  $f_{\Sigma^0 R}$ , and  $f_{\bar{\Sigma}^0\bar{R}}$ , using the THERMUS yields, are given in table 4. Appendix 3.5.7 discusses how to extract these constants  $f$  from the THERMUS files.

index $i$	particle	$J^P$	$\mu (\mu_N)$	$\text{BR} \rightarrow \Lambda + X$	$\text{BR} \rightarrow \Sigma^0 + X$
0	$\Lambda'$	$\frac{1}{2}^+$	-0.613 [?]	(100%)	-
1	$\Sigma^0$	$\frac{1}{2}^+$	+0.79 (quark model [?])	100%	-
2	$\Xi^-$	$\frac{1}{2}^+$	-0.651 [?]	100%	0
3	$\Xi^0$	$\frac{1}{2}^+$	-1.25 [?]	100%	0
4	$\Sigma^{*-}$	$\frac{3}{2}^+$	-2.41 [?]	87%	7%
5	$\Sigma^{*0}$	$\frac{3}{2}^+$	+0.30 [?]	87%	1%
6	$\Sigma^{*+}$	$\frac{3}{2}^+$	+3.02 [?]	87%	7%

**Table 3:** Particles that may feed down to our  $\Lambda$  sample.  $\Lambda'$  refers to primary  $\Lambda$ s. The index,  $i$ , is used in the computer code implementation of this calculation; it is included just for reference. Magnetic moments,  $\mu$ , are given in units of the nuclear magneton,  $\mu_N$ . Branching ratios to  $\Lambda$  and  $\Sigma^0$  baryons are needed to calculate  $f$  factors in equation 12.

### 3.5.4 Feed-down matrices

The numbers in table 4 may be plugged into equation 12, to get the matrix elements listed in table 5. To 690 be very clear, these are the matrix elements of the *inverted* matrix. In other words, to get the physical quantities of interest, use equation 13, below, with the values of  $a, b, c, d$  from table 5.

$$\begin{pmatrix} \bar{\omega}_c \\ B_c/T \end{pmatrix} = \begin{bmatrix} a & b \\ c & d \end{bmatrix} \begin{pmatrix} P_\Lambda^{\text{meas}} \\ P_{\bar{\Lambda}}^{\text{meas}} \end{pmatrix}. \quad (13)$$

### 3.5.5 Application to STAR data

The STAR measurements on hyperon polarization are listed in table 6. Applying equation 13 with the matrix elements listed in table 5 yields the physical parameters, listed in table 7.

$f$	7.7 GeV	11.5 GeV	14.5 GeV	19.6 GeV	27 GeV	39 GeV	62.4 GeV	200 GeV
$f_{\Lambda'}$	2.800e-01	2.492e-01	2.418e-01	2.350e-01	2.313e-01	2.273e-01	2.239e-01	2.183e-01
$f_{\Lambda\Sigma^0}$	1.806e-01	1.666e-01	1.627e-01	1.591e-01	1.569e-01	1.547e-01	1.524e-01	1.493e-01
$f_{\Lambda\Sigma^{*+}}$	1.044e-01	1.052e-01	1.045e-01	1.037e-01	1.027e-01	1.022e-01	1.007e-01	9.984e-02
$f_{\Lambda\Sigma^{*0}}$	1.039e-01	1.047e-01	1.040e-01	1.032e-01	1.023e-01	1.017e-01	1.002e-01	9.938e-02
$f_{\Lambda\Sigma^{*-}}$	1.018e-01	1.028e-01	1.020e-01	1.013e-01	1.004e-01	9.987e-02	9.840e-02	9.763e-02
$f_{\Lambda\Sigma^0}$	4.056e-02	4.992e-02	5.438e-02	5.842e-02	6.208e-02	6.464e-02	6.970e-02	7.308e-02
$f_{\Lambda\Sigma^-}$	3.906e-02	4.822e-02	5.256e-02	5.649e-02	6.004e-02	6.254e-02	6.743e-02	7.073e-02
$f_{\Sigma^0\Sigma^{*+}}$	8.402e-03	8.466e-03	8.405e-03	8.343e-03	8.267e-03	8.220e-03	8.099e-03	8.033e-03
$f_{\Sigma^0\Sigma^{*0}}$	1.194e-03	1.204e-03	1.195e-03	1.186e-03	1.175e-03	1.169e-03	1.152e-03	1.142e-03
$f_{\Sigma^0\Sigma^{*-}}$	8.188e-03	8.268e-03	8.211e-03	8.154e-03	8.080e-03	8.036e-03	7.917e-03	7.855e-03
$f_{\Lambda,\text{other}}$	1.319e-01	1.555e-01	1.602e-01	1.650e-01	1.667e-01	1.696e-01	1.701e-01	1.746e-01
$\bar{f}_{\Lambda'}$	2.327e-01	2.192e-01	2.162e-01	2.143e-01	2.153e-01	2.144e-01	2.175e-01	2.159e-01
$\bar{f}_{\Lambda\Sigma^0}$	1.502e-01	1.465e-01	1.455e-01	1.451e-01	1.461e-01	1.459e-01	1.480e-01	1.477e-01
$\bar{f}_{\Lambda\Sigma^{*+}}$	8.681e-02	9.254e-02	9.341e-02	9.454e-02	9.567e-02	9.638e-02	9.774e-02	9.871e-02
$\bar{f}_{\Lambda\Sigma^{*0}}$	8.636e-02	9.210e-02	9.297e-02	9.409e-02	9.522e-02	9.593e-02	9.729e-02	9.826e-02
$\bar{f}_{\Lambda\Sigma^-}$	8.461e-02	9.037e-02	9.126e-02	9.239e-02	9.350e-02	9.421e-02	9.555e-02	9.652e-02
$\bar{f}_{\Sigma^0\Sigma^-}$	1.071e-01	9.659e-02	9.200e-02	8.909e-02	8.565e-02	8.373e-02	7.931e-02	7.675e-02
$\bar{f}_{\Sigma^0\Sigma^{*+}}$	1.031e-01	9.329e-02	8.892e-02	8.614e-02	8.283e-02	8.100e-02	7.672e-02	7.428e-02
$\bar{f}_{\Sigma^0\Sigma^{*-}}$	6.985e-03	7.446e-03	7.516e-03	7.606e-03	7.697e-03	7.754e-03	7.864e-03	7.942e-03
$\bar{f}_{\Sigma^0\Sigma^{*0}}$	9.926e-04	1.059e-03	1.069e-03	1.082e-03	1.094e-03	1.103e-03	1.118e-03	1.129e-03
$\bar{f}_{\bar{\Sigma}^0\bar{\Sigma}^{*+}}$	6.807e-03	7.271e-03	7.343e-03	7.433e-03	7.523e-03	7.580e-03	7.688e-03	7.766e-03
$\bar{f}_{\bar{\Lambda},\text{other}}$	1.344e-01	1.536e-01	1.637e-01	1.683e-01	1.694e-01	1.719e-01	1.713e-01	1.751e-01

**Table 4:** f's from THERMUS.

$f$	7.7 GeV	11.5 GeV	14.5 GeV	19.6 GeV	27 GeV	39 GeV	62.4 GeV	200 GeV
a	1.4601	1.4260	1.4038	1.3856	1.3635	1.3512	1.3195	1.3029
b	1.0462	1.0930	1.1274	1.1513	1.1752	1.1913	1.2230	1.2456
c	-1.7853	-1.9134	-1.9357	-1.9539	-1.9616	-1.9722	-1.9709	-1.9877
d	1.7928	1.9162	1.9503	1.9676	1.9726	1.9817	1.9757	1.9898

**Table 5:** The matrix elements of the INVERTED matrix. Multiply this by the polarization “vector” as per equation 13.

In table 8 are listed the physical parameters *if feeddown is neglected*. This is obviously for comparison only. In this case,  $f_{\Lambda'} = \bar{f}_{\Lambda'} = 1$  and all other f's are zero, so that for every energy, the matrix is

$$\begin{bmatrix} a & b \\ c & d \end{bmatrix}_{\text{no feeddown}} = \begin{bmatrix} 0.5 & -0.613 \\ 0.5 & 0.613 \end{bmatrix}^{-1} = \begin{bmatrix} 1 & 1 \\ -0.8157 & +0.8157 \end{bmatrix} \quad (14)$$

Comparing tables 7 and 8 shows that accounting for feed-down increases  $\bar{\omega}$  by  $\sim 20\%$ , and increases  $B$  by a factor of 2.

**About units** As is common, we have been using units such that  $\hbar = c = k_B = 1$ . Furthermore, we've used  $\mu_N = 1$ . In this case,  $\bar{\omega}_c = \omega_c/T$  and  $B/T$  are both dimensionless. That's why they are quantified in percentages in the second and third columns of tables 7 and 8.

In human units, vorticity is measured in  $s^{-1}$  (usually not written as Hz) and  $B$  in Tesla. In order to get to these units, we will need to assume a temperature. Here, we will assume  $k_B T = 160$  MeV.

The conversions are

$$\omega [\text{in } \text{s}^{-1}] = (k_B T) \cdot \left( \frac{\omega}{T} [\text{dimensionless}] \right) / \hbar \quad (15)$$

$$B [\text{in Tesla}] = (k_B T) \cdot \left( \frac{B}{T} [\text{dimensionless}] \right) / \mu_N \quad (16)$$

Explicitly,  $\hbar = 6.58 \times 10^{-22} \text{ MeV} \cdot \text{s}$  and  $\mu_N = 3.15 \times 10^{-14} \text{ MeV/Tesla}$ .

<sup>705</sup> (To make the connection to equation 12, the  $\frac{2}{3}$  in front of everything is basically  $1/(S_\Lambda + 1)$ . The units of this cancel with the  $(S_R + 1)$  factor found inside of every sum. That leaves  $S_R$  in the left columns; this is the spin of particle  $R$ . In our matrix, we have been using, e.g.,  $S_{\Sigma^*} = \frac{3}{2}$ , when in reality it is  $S_{\Sigma^*} = \frac{3}{2}\hbar$ . Likewise, in our matrix, we have been using, e.g.  $\mu_{\Sigma^{*+}} = +3.02$ , when in reality it is  $\mu_{\Sigma^{*+}} = +3.02\mu_N$ .)

$\sqrt{s_{NN}}$ (GeV)	$\bar{P}_\Lambda$ (%)	$\bar{P}_{\bar{\Lambda}}$ (%)
7.7	2.27 +/- 0.63	7.56 +/- 3.61
11.5	1.38 +/- 0.40	2.63 +/- 1.27
14.5	1.17 +/- 0.49	1.42 +/- 1.31
19.6	0.96 +/- 0.31	1.45 +/- 0.61
27.0	1.03 +/- 0.28	1.41 +/- 0.47
39.0	0.49 +/- 0.42	1.06 +/- 0.61
62.4	1.25 +/- 1.09	1.60 +/- 1.49
200.0	0.12 +/- 0.95	-0.73 +/- 1.08

**Table 6:** STAR measurements on polarization for 20-50% centrality Au+Au collisions.

$\sqrt{s_{NN}}$ (GeV)	$\bar{\omega}_c$ (%)	$B/T$ (%)	$\omega$ ( $\text{s}^{-1}$ )	$B$ (Tesla)
7.7	11.23 +/- 3.89	9.49 +/- 6.58	2.7e+22 +/- 9.5e+21	4.8e+14 +/- 3.3e+14
11.5	4.85 +/- 1.50	2.40 +/- 2.55	1.2e+22 +/- 3.7e+21	1.2e+14 +/- 1.3e+14
14.5	3.24 +/- 1.63	0.51 +/- 2.73	7.9e+21 +/- 4.0e+21	2.6e+13 +/- 1.4e+14
19.6	2.99 +/- 0.82	0.98 +/- 1.34	7.3e+21 +/- 2.0e+21	5.0e+13 +/- 6.8e+13
27.0	3.06 +/- 0.68	0.76 +/- 1.09	7.5e+21 +/- 1.6e+21	3.8e+13 +/- 5.5e+13
39.0	1.93 +/- 0.93	1.13 +/- 1.48	4.7e+21 +/- 2.3e+21	5.8e+13 +/- 7.5e+13
62.4	3.60 +/- 2.32	0.70 +/- 3.64	8.8e+21 +/- 5.6e+21	3.6e+13 +/- 1.8e+14
200.0	-0.75 +/- 1.83	-1.68 +/- 2.86	-1.8e+21 +/- 4.4e+21	-8.5e+13 +/- 1.5e+14

**Table 7:** The vorticities and magnetic fields extracted from STAR polarization data, using equation 13 and the matrix elements from table 5.

$\sqrt{s_{NN}}$ (GeV)	$\bar{\omega}_c$ (%)	$B/T$ (%)	$\omega$ ( $\text{s}^{-1}$ )	$B$ (Tesla)
7.7	9.83 +/- 3.67	4.31 +/- 2.99	2.4e+22 +/- 8.9e+21	2.2e+14 +/- 1.5e+14
11.5	4.02 +/- 1.33	1.02 +/- 1.09	9.8e+21 +/- 3.2e+21	5.2e+13 +/- 5.5e+13
14.5	2.58 +/- 1.40	0.21 +/- 1.14	6.3e+21 +/- 3.4e+21	1.0e+13 +/- 5.8e+13
19.6	2.40 +/- 0.68	0.40 +/- 0.56	5.8e+21 +/- 1.7e+21	2.0e+13 +/- 2.8e+13
27.0	2.44 +/- 0.55	0.31 +/- 0.45	5.9e+21 +/- 1.3e+21	1.6e+13 +/- 2.3e+13
39.0	1.55 +/- 0.75	0.46 +/- 0.61	3.8e+21 +/- 1.8e+21	2.4e+13 +/- 3.1e+13
62.4	2.85 +/- 1.84	0.29 +/- 1.50	6.9e+21 +/- 4.5e+21	1.5e+13 +/- 7.6e+13
200.0	-0.61 +/- 1.44	-0.69 +/- 1.17	-1.5e+21 +/- 3.5e+21	-3.5e+13 +/- 6.0e+13

**Table 8:** The vorticities and magnetic fields extracted from STAR polarization data, using equation 13 but a matrix that ignores feeddown, i.e.  $f_{\Lambda'} = \bar{f}_{\bar{\Lambda}'} = 1$  and all other  $f$ s are zero. The matrix used is given in equation 14. See text for details.

### 3.5.6 Acknowledgements

<sup>710</sup> We thank Bill Llope for producing and interpreting UrQMD and THERMUS yields for all energies used here.

### 3.5.7 Extracting feed-down fractions from Bill Llope's THERMUS file

Bill Llope very kindly produced UrQMD and THERMUS output files for us, putting in way more work than we should have asked of him as a non-PA. Since the contribution of  $\Sigma^*$  is very important, and this <sup>715</sup> information is not retained in the UrQMD files, I will focus on the THERMUS files.

Getting the  $f_i$  values from these files is non-trivial, so here I explain the procedure in excruciating detail. In subsubsections 3.5.7 and 3.5.7, I discuss extracting the fractions for the baryons and antibaryons explicitly. I will refer to the numbers for the 7.7 GeV calculation in this discussion.

In subsubsection 3.5.7, I provide the THERMUS file verbatim. And if you are still up for it, I include <sup>720</sup> the actual root macro code used to extract the  $f$  values and the matrix elements in subsubsection 3.5.7.

#### Baryons

**Primary  $\Lambda$ s** The way Bill formatted these files was to give the primary yield of every particle *per primary  $\Lambda$* . The rate (number per event) of primary  $\Lambda$ s for 7.7 GeV collisions is 0.00410527, as given by the line

<sup>725</sup> rate information: Primary Lambda = 0.00410527

**From primary  $\Sigma^0$ s** The line 7.7 20 Sigma0 0.645168

tells us that there are 0.645168  $\Sigma^0$  per primary  $\Lambda$ ; i.e.  $0.645168 \times 0.00410527 = 0.00264858883536$   $\Sigma^0$ s per event.

Since the branching ratio for  $\Sigma^0 \rightarrow \Lambda + \gamma$  is 100%, that means there are 0.00264858883536  $\Lambda$ s originating <sup>730</sup> from primary  $\Sigma^0$  per event, consistent with the line

rate information: Lambda<-Sigma0 = 0.00264859 running decay total (%) = 28.2045.)

**Primary  $\Sigma^*$  contributions to  $\Lambda$ , both directly and through  $\Sigma^0$**  Bill puts his line numbers in kind of a weird order, but lower down, we see the same information for  $\Sigma^{*-}$ ,

7.7 103 Sigma\*- 0.417829

<sup>735</sup> which gives the number of  $\Sigma^{*-}$  per primary  $\Lambda$ , per event.

Now then,  $\Sigma^*$  will contribute to the  $\Lambda$  yield two ways: (1) directly and (2) through the  $\Sigma^0$ . As discussed above, we deal with these separately.

The BR for  $\Sigma^* \rightarrow \Lambda + \pi$  is 87%, meaning that the number of  $\Lambda$  coming *directly* from  $\Sigma^*$  decay is  $0.87 \times 0.417829 \times 0.00410527 = 0.00149231174718$ .

The BR for  $\Sigma^* \rightarrow \Sigma + \pi$  is 11.7%. However, we only care about the  $\Sigma^* \rightarrow \Sigma^0$  decay, since  $\Sigma^\pm$  does not decay to  $\Lambda$ . Unfortunately, the PDG does not specify the BR for  $\Sigma^* \rightarrow \Sigma^0 + \pi$ , so I had to do a little fiddling with numbers to figure out that the BRs that THERMUS uses are

$$BR[\Sigma^{*\pm} \rightarrow \Sigma^0 + \pi^\pm] = 7\% \quad \text{and} \quad BR[\Sigma^{*0} \rightarrow \Sigma^0 + \pi^0] = 1\%$$

<sup>740</sup> That means the rate of  $\Lambda$ s coming from  $\Sigma^{*-} \rightarrow \Sigma^0 \rightarrow \Lambda$  is  $0.07 \times 0.417829 \times 0.00410527 = 0.00012007106012$ .

Now then, when THERMUS reports the contribution of a parent (like  $\Sigma^{*-}$ ) to a stable daughter (like  $\Lambda$ ), *it includes all multi-generational branches*. (See the email from Jean Cleymans in subsubsection 3.5.8.) Therefore, to check consistency with the line

rate information: Lambda<-Sigma\*- = 0.00161238 running decay total (%) = 79.4

<sup>745</sup> we have to *add* these two routes:  $0.00149231174718 + 0.00012007106012 = 0.0016123828073$ , and find that it is, indeed, consistent.

**Primary  $\Xi \rightarrow \Lambda$  contributions** Isaac's simulations say that the DCA cuts do almost nothing to discriminate  $\Lambda$ s coming from the weak decay  $\Xi \rightarrow \Lambda + \pi$ , so we need to use the line

7.7 22 Xi0 0.14489.

<sup>750</sup> The branching ratio for  $\Xi \rightarrow \Lambda + \pi$  is 100%, so the  $\Xi^0$  rate is  $0.14489 \times 0.00410527 = 0.0005948125703$ . Since THERMUS treats weakly-decaying particles as stable, there is no line that begins rate information: Lambda<-Xi0 = ....

**“Other” contributions** As discussed in subsubsection 3.5.3, anything beyond the  $\Sigma^*$  we consider as “other.” There is a large number of such parents, and they individually contribute a few percent or less to the  $\Lambda$  yield.

We now have to discuss the so-called “**running decay total**” that one sees in Bill’s files. As he lists decay contributions, he is keeping a running tally of the percentage of *strong and electromagnetic decay* contributions that have been listed up until that point. In other words, the lines

rate information: Lambda<-Sigma0 = 0.00290201 running decay total (%) = 25.5247

<sup>760</sup> rate information: Lambda<-Sigma\*+ = 0.00198037 running decay total (%) = 42.9432

rate information: Lambda<-Sigma\*0 = 0.00184499 running decay total (%) = 59.1709

rate information: Lambda<-Sigma\*- = 0.00193394 running decay total (%) = 76.181

rate information: Lambda<-Lambda(1405) = 0.00025601 running decay total (%) = 82.1262

rate information: Lambda<-Lambda(1520) = 0.000198498 running decay total (%) = 84.24

<sup>765</sup> tell us that the  $\Sigma^0$  contributes 25.5247% of the  $\Lambda$ s that originate from strong and EM decay. And that the  $\Sigma^{*+}$  and  $\Sigma^0$  together account for 42.9432% of the  $\Lambda$ s that originate from strong and EM decay. Et cetera.

So, the percentage of the  $\Lambda$ s that originate from strong and EM decay “beyond”  $\Sigma^{*-}$  is  $100\% - 76.181\% = 23.819\%$ . The rate of “other,” then, is

$$\text{other rate} = \frac{100\% - 76.181\%}{76.181\%} \times (0.00290201 + 0.00198037 + 0.00184499 + 0.00193394) = 0.002708$$

The most significant contributor is  $\Lambda(1405)$ , which contributes  $84.24\% - 82.162\% = 2.078\%$  of the  $\Lambda$ s, as one finds by examining these lines:

<sup>770</sup> rate information: Lambda<-Lambda(1405) = 0.00025601 running decay total (%) = 82.1262

rate information: Lambda<-Lambda(1520) = 0.000198498 running decay total (%) = 84.24

**Getting  $fs$**  Okay, from subsubsections 3.5.7-3.5.7, we see how to get the *rates*. The value of a given fraction ( $f$ ) listed in table 4 is simply the rate divided by the sum of all the rates.

**$\bar{\Lambda}$  hyperons** For  $\bar{\Lambda}$ , the situation is slightly more complex, since for the lines that do not begin with “rate information”, the yield is *always* given as a fraction of the number of primary  $\Lambda$ , not  $\bar{\Lambda}$ . So,

$$\text{rate for: } \bar{\Lambda} \leftarrow \Xi^0 = \underbrace{0.00863487}_{\#\bar{\Xi}^0 / \#\Lambda} \times \underbrace{0.0187703^{-1}}_{(\#\bar{\Lambda} / \#\Lambda)^{-1}} \times \underbrace{7.70574e-05}_{\text{primary } \bar{\Lambda} \text{ rate}} = 0.00003544858801$$

$$\text{rate for: } \bar{\Lambda} \leftarrow \Xi^+ = \underbrace{0.00831551}_{\#\bar{\Xi}^+ / \#\Lambda} \times \underbrace{0.0187703^{-1}}_{(\#\bar{\Lambda} / \#\Lambda)^{-1}} \times \underbrace{7.70574e-05}_{\text{primary } \bar{\Lambda} \text{ rate}} = 0.00003413752471$$

<sup>775</sup> But as far as everything else, it is the same as for the  $\Lambda$ s.

```
780 +-----  
root-s = 7.7  
+-----  
785      rate information: Primary Lambda = 0.00410527  
          rate information: Lambda<-Sigma0 = 0.00264859      running decay total (%) =  
          28.2045  
790      rate information: Lambda<-Sigma*+ = 0.00165448      running decay total (%) =  
          45.8229  
          rate information: Lambda<-Sigma*0 = 0.00154073      running decay total (%) =  
795          62.2299  
          rate information: Lambda<-Sigma*- = 0.00161238      running decay total (%) = 79.4  
          rate information: Lambda<-Lambda(1405) = 0.00025601      running decay total (%) =  
800          82.1262  
          rate information: Lambda<-Lambda(1520) = 0.000198498      running decay total (%) =  
          84.24  
805 7.7 19 Sigma+      0.657359  
    7.7 20 Sigma0      0.645168  
    7.7 21 Sigma-      0.627637  
810 7.7 22 Xi0      0.14489  
    7.7 23 Xi-      0.139531  
815 7.7 24 Omega-      0.0158781  
    7.7 26 Antilambda      0.0187703  
          rate information: Primary Antilambda = 7.70574e-05  
820      rate information: Antilambda<-Antisigma0 = 4.9715e-05      running decay total (%) =  
          26.9547  
          rate information: Antilambda<-AntiSigma*- = 3.10552e-05      running decay total (%) =  
825          43.7924  
          rate information: Antilambda<-AntiSigma*0 = 2.89201e-05      running decay total (%) =  
          59.4724  
830      rate information: Antilambda<-AntiSigma*+ = 3.0265e-05      running decay total (%) =  
          75.8816
```

rate information: Antilambda<-AntiLambda(1405) = 4.8054e-06 running decay total  
(%) = 78.487  
835

rate information: Antilambda<-AntiLambda(1520) = 3.72587e-06 running decay total  
(%) = 80.5071

7.7 27 Antisigma- 0.0123389  
840

7.7 28 Antisigma0 0.01211

7.7 29 Antisigma+ 0.011781

845 7.7 30 Antixi0 0.00863487

7.7 31 Antixi+ 0.00831551

7.7 32 Antiomega+ 0.00300444  
850

7.7 101 Sigma\*+ 0.428739

7.7 102 Sigma\*0 0.426484

855 7.7 103 Sigma\*- 0.417829

7.7 -101 AntiSigma\*- 0.00804757

7.7 -102 AntiSigma\*0 0.00800526  
860

7.7 -103 AntiSigma\*+ 0.00784279

7.7 111 Lambda(1405) 0.187103

865 7.7 112 Lambda(1520) 0.191493

7.7 -111 AntiLambda(1405) 0.00351199

7.7 -112 AntiLambda(1520) 0.00359439  
870

-----

root-s = 11.5  
875 -----

rate information: Primary Lambda = 0.00434062

rate information: Lambda<-Sigma0 = 0.00290201 running decay total (%) =  
880 25.5247

rate information: Lambda<-Sigma\*+ = 0.00198037 running decay total (%) =  
42.9432

rate information: Lambda<-Sigma\*0 = 0.00184499 running decay total (%) =  
885 59.1709

```
rate information: Lambda<-Sigma*- = 0.00193394    running decay total (%) =
76.181
890
rate information: Lambda<-Lambda(1405) = 0.000309771   running decay total (%) =
78.9056
895
rate information: Lambda<-Lambda(1520) = 0.000253256   running decay total (%) =
81.1331
11.5 19 Sigma+      0.68017
11.5 20 Sigma0      0.668569
900
11.5 21 Sigma-      0.651854
11.5 22 Xi0         0.200347
905 11.5 23 Xi-      0.19352
11.5 24 Omega-      0.0327139
11.5 26 Antilambda   0.0684347
910
rate information: Primary Antilambda = 0.000297049
rate information: Antilambda<-Antisigma0 = 0.000198598   running decay total (%)
= 24.5241
915
rate information: Antilambda<-AntiSigma*- = 0.000135526   running decay total (%)
= 41.2598
920
rate information: Antilambda<-AntiSigma*0 = 0.000126262   running decay total (%)
= 56.8513
rate information: Antilambda<-AntiSigma*+ = 0.000132349   running decay total (%)
= 73.1946
925
rate information: Antilambda<-AntiLambda(1405) = 2.11991e-05   running decay total (%)
= 75.8124
rate information: Antilambda<-AntiLambda(1520) = 1.73315e-05   running decay total (%)
= 77.9526
930
11.5 27 Antisigma-   0.0465472
11.5 28 Antisigma0    0.0457533
935 11.5 29 Antisigma+  0.0446094
11.5 30 Antixi0       0.03016
11.5 31 Antixi+       0.0291322
940
11.5 32 Antiomega+    0.0108331
11.5 101 Sigma*+      0.485364
```

945 11.5 102 Sigma\*0 0.483015  
11.5 103 Sigma\*- 0.473984  
11.5 -101 AntiSigma\*- 0.0332157  
950 11.5 -102 AntiSigma\*0 0.033055  
11.5 -103 AntiSigma\*+ 0.032437  
955 11.5 111 Lambda(1405) 0.214118  
11.5 112 Lambda(1520) 0.231072  
11.5 -111 AntiLambda(1405) 0.0146531  
960 11.5 -112 AntiLambda(1520) 0.0158133  
+-----  
965 root-s = 14.5  
+-----  
rate information: Primary Lambda = 0.00377269  
970 rate information: Lambda<-Sigma0 = 0.00253881 running decay total (%) =  
24.9878  
rate information: Lambda<-Sigma\*+ = 0.00176082 running decay total (%) =  
975 42.3184  
rate information: Lambda<-Sigma\*0 = 0.00164057 running decay total (%) =  
58.4654  
rate information: Lambda<-Sigma\*- = 0.00172018 running decay total (%) =  
980 75.396  
rate information: Lambda<-Lambda(1405) = 0.000275975 running decay total (%) =  
78.1122  
985 rate information: Lambda<-Lambda(1520) = 0.000227828 running decay total (%) =  
80.3546  
14.5 19 Sigma+ 0.684432  
990 14.5 20 Sigma0 0.672946  
14.5 21 Sigma- 0.656389  
995 14.5 22 Xi0 0.224899  
14.5 23 Xi- 0.217355  
14.5 24 Omega- 0.0417916

1000            14.5 26 Antilambda        0.120935  
rate information: Primary Antilambda = 0.000456251  
1005            rate information: Antilambda<-Antisigma0 = 0.000307032    running decay total (%)  
                  = 24.1397  
rate information: Antilambda<-AntiSigma\*- = 0.000212945    running decay total (%)  
1010            = 40.8821  
rate information: Antilambda<-AntiSigma\*0 = 0.000198403    running decay total (%)  
1015            = 56.4811  
rate information: Antilambda<-AntiSigma\*+ = 0.000208031    running decay total (%)  
                  = 72.8371  
rate information: Antilambda<-AntiLambda(1405) = 3.33751e-05    running decay total (%)  
                  = 75.4612  
1020            rate information: Antilambda<-AntiLambda(1520) = 2.75524e-05    running decay total (%)  
                  = 77.6274  
14.5 27 Antisigma-        0.082772  
1025 14.5 28 Antisigma0        0.0813828  
14.5 29 Antisigma+        0.0793805  
14.5 30 Antixi0        0.0514521  
1030 14.5 31 Antixi+        0.0497262  
14.5 32 Antiomega+        0.018087  
1035 14.5 101 Sigma\*+        0.496519  
14.5 102 Sigma\*0        0.494154  
14.5 103 Sigma\*-        0.48506  
1040 14.5 -101 AntiSigma\*-        0.0600467  
14.5 -102 AntiSigma\*0        0.0597606  
1045 14.5 -103 AntiSigma\*+        0.0586609  
14.5 111 Lambda(1405)        0.219474  
14.5 112 Lambda(1520)        0.239163  
1050 14.5 -111 AntiLambda(1405) 0.0265422  
14.5 -112 AntiLambda(1520) 0.0289233  
1055 +-----

```
root-s = 19.6

+-----+
1060      rate information: Primary Lambda = 0.00332199
1065      rate information: Lambda<-Sigma0 = 0.0022491   running decay total (%) = 24.4789
1070      rate information: Lambda<-Sigma*+ = 0.00158353   running decay total (%) =
1075      rate information: Lambda<-Sigma*0 = 0.0014755   running decay total (%) =
1080      rate information: Lambda<-Sigma*- = 0.00154753   running decay total (%) =
1085      rate information: Lambda<-Lambda(1405) = 0.000248646   running decay total (%) =
1090      rate information: Lambda<-Lambda(1520) = 0.000207127   running decay total (%) =
1095      19.6 19 Sigma+          0.688414
1096      19.6 20 Sigma0         0.677035
1097      19.6 21 Sigma-         0.660628
1098      19.6 22 Xi0           0.248538
1099      19.6 23 Xi-           0.240325
1100      19.6 24 Omega-        0.0516924
1101      19.6 26 Antilambda     0.204605
1102      rate information: Primary Antilambda = 0.000679694
1103      rate information: Antilambda<-Antisigma0 = 0.000460177   running decay total (%) =
1104      = 23.763
1105      rate information: Antilambda<-AntiSigma*- = 0.000323998   running decay total (%) =
1106      = 40.4939
1107      rate information: Antilambda<-AntiSigma*0 = 0.000301894   running decay total (%) =
1108      = 56.0834
1109      rate information: Antilambda<-AntiSigma*+ = 0.000316631   running decay total (%) =
1110      = 72.4339
1111      rate information: Antilambda<-AntiLambda(1405) = 5.08741e-05   running decay total (%)
1112      = 75.061
1113      rate information: Antilambda<-AntiLambda(1520) = 4.23792e-05   running decay total
```

(%) = 77.2494

19.6 27 Antisigma-	0.140853
1115 19.6 28 Antisigma0	0.138525
19.6 29 Antisigma+	0.135168
1120 19.6 30 Antixi0	0.0850653
19.6 31 Antixi+	0.0822541
19.6 32 Antiomega+	0.0295958
1125 19.6 101 Sigma*+	0.507108
19.6 102 Sigma*0	0.504729
1130 19.6 103 Sigma*-	0.495578
19.6 -101 AntiSigma*-	0.103757
19.6 -102 AntiSigma*0	0.10327
1135 19.6 -103 AntiSigma*+	0.101398
19.6 111 Lambda(1405)	0.224568
1140 19.6 112 Lambda(1520)	0.246932
19.6 -111 AntiLambda(1405)	0.0459477
19.6 -112 AntiLambda(1520)	0.0505235
1145 +-----	
root-s = 27	
1150 +-----	
rate information: Primary Lambda	= 0.00295424
rate information: Lambda<-Sigma0	= 0.00200409 running decay total (%) =
1155 24.2655	
rate information: Lambda<-Sigma*+	= 0.001418 running decay total (%) = 41.4346
rate information: Lambda<-Sigma*0	= 0.00132129 running decay total (%) =
1160 57.4327	
rate information: Lambda<-Sigma*-	= 0.00138591 running decay total (%) = 74.2133
1165 rate information: Lambda<-Lambda(1405)	= 0.000222788 running decay total (%) = 76.9109

rate information: Lambda<-Lambda(1520) = 0.000186136 running decay total (%) =  
79.1646

1170  
27 19 Sigma+ 0.689723

27 20 Sigma0 0.67838

1175 27 21 Sigma- 0.662023

27 22 Xi0 0.268434

27 23 Xi- 0.259606

1180  
27 24 Omega- 0.0605516

27 26 Antilambda 0.284925

1185 rate information: Primary Antilambda = 0.000841737

rate information: Antilambda<-Antisigma0 = 0.000571017 running decay total (%)  
= 23.7083

1190 rate information: Antilambda<-AntiSigma\*- = 0.000404023 running decay total (%)  
= 40.4832

rate information: Antilambda<-AntiSigma\*0 = 0.000376468 running decay total (%)  
= 56.114

1195 rate information: Antilambda<-AntiSigma\*+ = 0.000394882 running decay total (%)  
= 72.5092

rate information: Antilambda<-AntiLambda(1405) = 6.34779e-05 running decay total  
(%) = 75.1448

1200 rate information: Antilambda<-AntiLambda(1520) = 5.30349e-05 running decay total  
(%) = 77.3468

1205 27 27 Antisigma- 0.19652

27 28 Antisigma0 0.193288

27 29 Antisigma+ 0.188627

1210  
27 30 Antixi0 0.113318

27 31 Antixi+ 0.109591

1215 27 32 Antiomega+ 0.0378719

27 101 Sigma\*+ 0.510625

27 102 Sigma\*0 0.508241

1220  
27 103 Sigma\*- 0.499072

27 -101 AntiSigma\*- 0.14549

```
1225 27 -102 AntiSigma*0    0.144811
      27 -103 AntiSigma*+    0.142198
      27 111 Lambda(1405)   0.226262
1230
      27 112 Lambda(1520)   0.249531
      27 -111 AntiLambda(1405) 0.0644677
1235 27 -112 AntiLambda(1520) 0.0710976
+
-----+
root-s = 39
1240
+
-----+
rate information: Primary Lambda = 0.00258929
1245 rate information: Lambda<-Sigma0 = 0.00176244      running decay total (%) =
      23.9675
      rate information: Lambda<-Sigma*+ = 0.00125746      running decay total (%) =
      41.0678
1250
      rate information: Lambda<-Sigma*0 = 0.00117175      running decay total (%) =
      57.0025
      rate information: Lambda<-Sigma*- = 0.00122925      running decay total (%) =
      73.7191
1255
      rate information: Lambda<-Lambda(1405) = 0.000197768  running decay total (%) =
      76.4085
      rate information: Lambda<-Lambda(1520) = 0.000166061  running decay total (%) =
      78.6668
      39 19 Sigma+        0.691946
1265 39 20 Sigma0        0.680664
      39 21 Sigma-        0.664391
      39 22 Xi0          0.284404
1270
      39 23 Xi-          0.27513
      39 24 Omega-        0.0684525
1275 39 26 Antilambda    0.430029
      rate information: Primary Antilambda = 0.00111347
      rate information: Antilambda<-Antisigma0 = 0.0007579  running decay total (%) =
```

1280                    23.508

rate information: Antilambda<-AntiSigma\*- = 0.000540746 running decay total (%)  
= 40.2805

1285                    rate information: Antilambda<-AntiSigma\*0 = 0.000503886 running decay total (%)  
= 55.9096

rate information: Antilambda<-AntiSigma\*+ = 0.000528614 running decay total (%)  
= 72.3058

1290                    rate information: Antilambda<-AntiLambda(1405) = 8.50459e-05 running decay total (%) = 74.9437

rate information: Antilambda<-AntiLambda(1520) = 7.14112e-05 running decay total (%) = 77.1587

1295

39 27 Antisigma-    0.297557

39 28 Antisigma0    0.292705

1300 39 29 Antisigma+    0.285708

39 30 Antixi0    0.167933

1305 39 31 Antixi+    0.162457

39 32 Antiomega+    0.0555001

39 101 Sigma\*+    0.516638

1310 39 102 Sigma\*0    0.514246

39 103 Sigma\*-    0.505046

1315 39 -101 AntiSigma\*-    0.222169

39 -102 AntiSigma\*0    0.221141

39 -103 AntiSigma\*+    0.217185

1320 39 111 Lambda(1405)    0.22916

39 112 Lambda(1520)    0.253995

1325 39 -111 AntiLambda(1405) 0.0985454

39 -112 AntiLambda(1520) 0.109225

+-----

1330 root-s = 62.4

+-----

1335                    rate information: Primary Lambda = 0.00223124

```
rate information: Lambda<-Sigma0 = 0.00151873      running decay total (%) =
23.8575

1340      rate information: Lambda<-Sigma*+ = 0.00108358      running decay total (%) =
40.8793

      rate information: Lambda<-Sigma*0 = 0.00100972      running decay total (%) =
56.7408

1345      rate information: Lambda<-Sigma*- = 0.00105927      running decay total (%) =
73.3807

      rate information: Lambda<-Lambda(1405) = 0.00017042      running decay total (%) =
76.0579

1350      rate information: Lambda<-Lambda(1520) = 0.000143098      running decay total (%) =
78.3058

1355 62.4 19 Sigma+      0.691946
      62.4 20 Sigma0      0.680664
      62.4 21 Sigma-      0.664391
1360      62.4 22 Xi0      0.311249
      62.4 23 Xi-      0.301099
1365 62.4 24 Omega-      0.0819849
      62.4 26 Antilambda    0.591916

      rate information: Primary Antilambda = 0.00132071
1370      rate information: Antilambda<-Antisigma0 = 0.000898958      running decay total (%) =
23.6245

      rate information: Antilambda<-AntiSigma*- = 0.000641388      running decay total (%) =
40.4801

1375      rate information: Antilambda<-AntiSigma*0 = 0.000597668      running decay total (%) =
56.1868

      rate information: Antilambda<-AntiSigma*+ = 0.000626998      running decay total (%) =
72.6642

      rate information: Antilambda<-AntiLambda(1405) = 0.000100874      running decay total (%)
= 75.3152

1385      rate information: Antilambda<-AntiLambda(1520) = 8.4702e-05      running decay total (%)
= 77.5412

      62.4 27 Antisigma-    0.409574
1390      62.4 28 Antisigma0    0.402896
```

62.4 29 Antisigma+ 0.393264  
1395 62.4 30 Antixi0 0.215884  
62.4 31 Antixi+ 0.208844  
62.4 32 Antiomega+ 0.0666342  
1400  
62.4 101 Sigma\*+ 0.516638  
62.4 102 Sigma\*0 0.514246  
1405 62.4 103 Sigma\*- 0.505046  
62.4 -101 AntiSigma\*- 0.305806  
62.4 -102 AntiSigma\*0 0.30439  
1410 62.4 -103 AntiSigma\*+ 0.298945  
62.4 111 Lambda(1405) 0.22916  
1415 62.4 112 Lambda(1520) 0.253995  
62.4 -111 AntiLambda(1405) 0.135643  
62.4 -112 AntiLambda(1520) 0.150344  
1420 +-----  
root-s = 200  
1425 +-----  
rate information: Primary Lambda = 0.00209703  
1430 rate information: Lambda<-Sigma0 = 0.00143445 running decay total (%) =  
23.413  
rate information: Lambda<-Sigma\*+ = 0.00103611 running decay total (%) =  
40.3242  
1435 rate information: Lambda<-Sigma\*0 = 0.000965538 running decay total (%) =  
56.0836  
rate information: Lambda<-Sigma\*- = 0.00101315 running decay total (%) =  
72.6201  
1440 rate information: Lambda<-Lambda(1405) = 0.000163199 running decay total (%) =  
75.2838  
rate information: Lambda<-Lambda(1520) = 0.000138048 running decay total (%) =  
77.537  
200 19 Sigma+ 0.695232

200 20 Sigma0 0.68404  
1450 200 21 Sigma- 0.667893  
200 22 Xi0 0.334738  
1455 200 23 Xi- 0.323959  
200 24 Omega- 0.0958179  
200 26 Antilambda 0.824479  
1460  
rate information: Primary Antilambda = 0.00172896  
rate information: Antilambda<-Antisigma0 = 0.00118268 running decay total (%)  
= 23.3221  
1465 rate information: Antilambda<-AntiSigma\*- = 0.000854248 running decay total (%)  
= 40.1676  
rate information: Antilambda<-AntiSigma\*0 = 0.000796066 running decay total (%)  
1470 = 55.8658  
rate information: Antilambda<-AntiSigma\*+ = 0.00083532 running decay total (%)  
= 72.3381  
1475 rate information: Antilambda<-AntiLambda(1405) = 0.000134554 running decay total (%) = 74.9915  
rate information: Antilambda<-AntiLambda(1520) = 0.000113818 running decay total (%) = 77.236  
1480 200 27 Antisigma- 0.573204  
200 28 Antisigma0 0.563977  
1485 200 29 Antisigma+ 0.550664  
200 30 Antixi0 0.293143  
200 31 Antixi+ 0.283702  
1490 200 32 Antiomega+ 0.089128  
200 101 Sigma\*+ 0.525619  
1495 200 102 Sigma\*0 0.523216  
200 103 Sigma\*- 0.513973  
200 -101 AntiSigma\*- 0.433362  
1500 200 -102 AntiSigma\*0 0.431381  
200 -103 AntiSigma\*+ 0.42376

```

1505 200 111 Lambda(1405) 0.233495
      200 112 Lambda(1520) 0.260714
      200 -111 AntiLambda(1405) 0.192511
1510 200 -112 AntiLambda(1520) 0.214953

```

**Mike's code to calculate  $f$ 's from Bill's THERMUS files** Look, I know that what I have described is a painful process, believe me. You might doubt that I did it right, and I wouldn't blame you for wanting 1515 to check. (If it makes you feel better, Iurii Karpenko did it also, though with a different thermal model (Becattini's) and no magnetic field and got very similar results.)

Here is the relevant snippet of code where I calculate the  $f$ 's and then the matrix elements. My philosophy here was to be super-explicit in the variable names, to make it as readable as possible. I fear that I overdid it. The variable names are too long. If I wasn't worrying about you, dear reader, then I would have made 1520 an array and done loops. As it is, I am doing explicit sums of variables with long names. I am aware that this is often a recipe for disaster, but I was super careful and double-checked my work along the way with an excel spreadsheet.

```

void MikeCodeSnippet() {

1525 // this is simply the numbers from Bill Llope's files, distilled into a form amenable to
      // numeric manipulation
// I extracted these numbers partially "by hand," being as careful as I could...
Double_t roots[8]
    = {7.7      , 11.5     , 14.5     , 19.6     , 27       , 39       , 62.4     , 200
1530      };

Double_t PrimaryLambdaRate[8]
    = {0.00410527, 0.00434062, 0.00377269, 0.00332199, 0.00295424, 0.00258929,
      0.00223124, 0.00209703};

1535 Double_t SigmaZeroToLambda[8]
    = {0.645168 , 0.668569 , 0.672946 , 0.677035 , 0.67838  , 0.680664 , 0.680664 ,
      0.68404  };

Double_t SigmaStarPlusToLambda[8]
    = {0.428739 , 0.485364 , 0.496519 , 0.507108 , 0.510625 , 0.516638 , 0.516638 ,
      0.525619 };

1540 Double_t SigmaStarZeroToLambda[8]
    = {0.426484 , 0.483015 , 0.494154 , 0.504729 , 0.508241 , 0.514246 , 0.514246 ,
      0.523216 };

Double_t SigmaStarMinusToLambda[8]
1545    = {0.417829 , 0.473984 , 0.48506  , 0.495578 , 0.499072 , 0.505046 , 0.505046 ,
      0.513973 };

Double_t XiZeroToLambda[8]
    = {0.14489 , 0.200347 , 0.224899 , 0.248538 , 0.268434 , 0.284404 , 0.311249 ,
      0.334738 };

1550 Double_t XiMinusToLambda[8]
    = {0.139531 , 0.19352 , 0.217355 , 0.240325 , 0.259606 , 0.27513 , 0.301099 ,
      0.323959 };

Double_t RunningDecayTotalAtSigmaStarMinus[8]
    = {79.4     , 76.181   , 75.396   , 74.616   , 74.2133  , 73.7191  , 73.3807 ,
      72.6201  };

```

```

Double_t AntiPrimaryLambdaToLambda[8]
= {0.0187703, 0.0684347, 0.120935, 0.204605, 0.284925, 0.430029, 0.591916,
  0.824479};
1560 Double_t AntiSigmaZeroToLambda[8]
= {0.01211, 0.0457533, 0.0813828, 0.138525, 0.193288, 0.292705, 0.402896,
  0.563977};
Double_t AntiSigmaStarMinusToLambda[8]
= {0.00804757, 0.0332157, 0.0600467, 0.103757, 0.14549, 0.222169, 0.305806,
1565 0.433362};
Double_t AntiSigmaStarZeroToLambda[8]
= {0.00800526, 0.033055, 0.0597606, 0.10327, 0.144811, 0.221141, 0.30439,
  0.431381};
Double_t AntiSigmaStarPlusToLambda[8]
= {0.00784279, 0.032437, 0.0586609, 0.101398, 0.142198, 0.217185, 0.298945,
  0.42376};
Double_t AntiXiPlusToLambda[8]
= {0.00831551, 0.0291322, 0.0497262, 0.0822541, 0.109591, 0.162457, 0.208844,
  0.283702};
1575 Double_t AntiXiZeroToLambda[8]
= {0.00863487, 0.03016, 0.0514521, 0.0850653, 0.113318, 0.167933, 0.215884,
  0.293143};
Double_t RunningDecayTotalAtAntiSigmaStarPlus[8]
= {75.8816, 74.0, 72.8371, 72.4339, 72.5092, 72.3058, 72.6642,
1580 72.3381};

// okay now make the f's. This is more painful than one might guess.

1585 Double_t f_Lprimary[8], f_LSig0[8], f_LSigStarPlus[8], f_LSigStarZero[8],
  f_LSigStarMinus[8], f_LXiZero[8], f_LXiMinus[8];
Double_t f_SSigStarMinus[8], f_SSigStarZero[8], f_SSigStarPlus[8], f_Lother[8];

Double_t fBar_AntiLprimary[8], fBar_AntiLAntiSig0[8], fBar_AntiLAntiSigStarPlus[8],
1590  fBar_AntiLAntiSigStarZero[8];
Double_t fBar_AntiLAntiSigStarMinus[8], fBar_AntiLAntiXiZero[8], fBar_AntiLAntiXiPlus[8];
Double_t fBar_AntiSAntiSigStarMinus[8], fBar_AntiSAntiSigStarZero[8],
  fBar_AntiSAntiSigStarPlus[8], fBar_AntiLother[8];

1595 for (Int_t iroots=0; iroots<8; iroots++) {
  Double_t sum=0.0;
  Double_t sum2=0.0;
  sum += f_Lprimary[iroots] = PrimaryLambdaRate[iroots];
  sum2 += f_LSig0[iroots] = SigmaZeroToLambda[iroots]*PrimaryLambdaRate[iroots];
1600  sum2 += f_LSigStarPlus[iroots] = SigmaStarPlusToLambda[iroots]*PrimaryLambdaRate[iroots
    ]*0.87;
  sum2 += f_LSigStarZero[iroots] = SigmaStarZeroToLambda[iroots]*PrimaryLambdaRate[iroots
    ]*0.87;
  sum2 += f_LSigStarMinus[iroots] = SigmaStarMinusToLambda[iroots]*PrimaryLambdaRate[
    iroots]*0.87;
  sum2 += f_SSigStarPlus[iroots] = SigmaStarPlusToLambda[iroots]*PrimaryLambdaRate[iroots
    ]*0.07; // note 2-step decay thru Sigma0
  sum2 += f_SSigStarZero[iroots] = SigmaStarZeroToLambda[iroots]*PrimaryLambdaRate[iroots
    ]*0.01; // note 2-step decay thru Sigma0
1610  sum2 += f_SSigStarMinus[iroots] = SigmaStarMinusToLambda[iroots]*PrimaryLambdaRate[
    iroots]*0.07; // note 2-step decay thru Sigma0

```

```

sum += sum2;
sum += f_LXiZero[iroots]      = XiZeroToLambda[iroots]*PrimaryLambdaRate[iroots];
sum += f_LXiMinus[iroots]     = XiMinusToLambda[iroots]*PrimaryLambdaRate[iroots];
1615 sum += f_Lother[iroots]
= sum2*(100.0-RunningDecayTotalAtSigmaStarMinus[iroots])/ 
    RunningDecayTotalAtSigmaStarMinus[iroots];

f_Lprimary[iroots] /= sum;
1620 f_LSig0[iroots] /= sum;
f_LSigStarPlus[iroots] /= sum;
f_LSigStarZero[iroots] /= sum;
f_LSigStarMinus[iroots] /= sum;
f_SSigStarPlus[iroots] /= sum;
1625 f_SSigStarZero[iroots] /= sum;
f_SSigStarMinus[iroots] /= sum;
f_LXiZero[iroots] /= sum;
f_LXiMinus[iroots] /= sum;
f_Lother[iroots] /= sum;
1630 }

1635 for (Int_t iroots=0; iroots<8; iroots++) {
Double_t sum=0.0;
Double_t sum2=0.0;
sum += fBar_AntiLprimary[iroots]
= AntiPrimaryLambdaToLambda[iroots]*PrimaryLambdaRate[iroots];
1640 sum2 += fBar_AntiLAntiSig0[iroots]
= AntiSigmaZeroToLambda[iroots]*PrimaryLambdaRate[iroots];
sum2 += fBar_AntiLAntiSigStarPlus[iroots]
= AntiSigmaStarPlusToLambda[iroots]*PrimaryLambdaRate[iroots]*0.87;
sum2 += fBar_AntiLAntiSigStarZero[iroots]
= AntiSigmaStarZeroToLambda[iroots]*PrimaryLambdaRate[iroots]*0.87;
1645 sum2 += fBar_AntiLAntiSigStarMinus[iroots]
= AntiSigmaStarMinusToLambda[iroots]*PrimaryLambdaRate[iroots]*0.87;
sum2 += fBar_AntiSAntiSigStarPlus[iroots]
= AntiSigmaStarPlusToLambda[iroots]*PrimaryLambdaRate[iroots]*0.07; // note 2-step
1650 decay thru Sigma0
sum2 += fBar_AntiSAntiSigStarZero[iroots]
= AntiSigmaStarZeroToLambda[iroots]*PrimaryLambdaRate[iroots]*0.01; // note 2-step
decay thru Sigma0
sum2 += fBar_AntiSAntiSigStarMinus[iroots]
= AntiSigmaStarMinusToLambda[iroots]*PrimaryLambdaRate[iroots]*0.07; // note 2-step
1655 decay thru Sigma0
sum += sum2;
sum += fBar_AntiLAntiXiZero[iroots]
= AntiXiZeroToLambda[iroots]*PrimaryLambdaRate[iroots];
1660 sum += fBar_AntiLAntiXiPlus[iroots]
= AntiXiPlusToLambda[iroots]*PrimaryLambdaRate[iroots];
sum += fBar_AntiLother[iroots]
= sum2*(100.0-RunningDecayTotalAtAntiSigmaStarPlus[iroots])/ 
    RunningDecayTotalAtAntiSigmaStarPlus[iroots];

1665 fBar_AntiLprimary[iroots] /= sum;
fBar_AntiLAntiSig0[iroots] /= sum;

```

```

fBar_AntiLAntiSigStarPlus[iroots] /= sum;
fBar_AntiLAntiSigStarZero[iroots] /= sum;
1670 fBar_AntiLAntiSigStarMinus[iroots] /= sum;
fBar_AntiSAntiSigStarPlus[iroots] /= sum;
fBar_AntiSAntiSigStarZero[iroots] /= sum;
fBar_AntiSAntiSigStarMinus[iroots] /= sum;
fBar_AntiLAntiXiZero[iroots] /= sum;
1675 fBar_AntiLAntiXiPlus[iroots] /= sum;
fBar_AntiLother[iroots] /= sum;

}

1680 // Now let's make the matrix!

//-----
1685 Double_t a[8],b[8],c[8],d[8];

for (int i=0; i<8; i++){
    a[i] = (2.0/3.0)*(1.0*
        f_Lprimary[i]      * 1.0          * (3.0/4.0)
1690    + f_LSig0[i]       * (-1.0/3.0) * (3.0/4.0)
        + f_LSigStarPlus[i] * (1.0/3.0) * (15.0/4.0)
        + f_LSigStarZero[i] * (1.0/3.0) * (15.0/4.0)
        + f_LSigStarMinus[i] * (1.0/3.0) * (15.0/4.0)
        + f_LXiZero[i]     * (0.900)   * (3.0/4.0)
1695    + f_LXiMinus[i]   * (0.927)   * (3.0/4.0)
        )
        -(1.0/3.0)*(
            f_SSigStarPlus[i] * (1.0/3.0) * (15.0/4.0)
            + f_SSigStarZero[i] * (1.0/3.0) * (15.0/4.0)
1700    + f_SSigStarMinus[i] * (1.0/3.0) * (15.0/4.0)
        )
    );
    b[i] = (2.0/3.0)*(1.0*
        f_Lprimary[i]      * 1.0          * (3.0/2.0) * (-0.613)
1705    + f_LSig0[i]       * (-1.0/3.0) * (3.0/2.0) * (+0.79)
        + f_LSigStarPlus[i] * (1.0/3.0) * (5.0/2.0) * (+3.02)
        + f_LSigStarZero[i] * (1.0/3.0) * (5.0/2.0) * (+0.30)
        + f_LSigStarMinus[i] * (1.0/3.0) * (5.0/2.0) * (-2.41)
1710    + f_LXiZero[i]     * (0.900)   * (3.0/2.0) * (-1.25)
        + f_LXiMinus[i]   * (0.927)   * (3.0/2.0) * (-0.651)
        )
        -(1.0/3.0)*(
            f_SSigStarPlus[i] * (1.0/3.0) * (5.0/2.0) * (+3.02)
            + f_SSigStarZero[i] * (1.0/3.0) * (5.0/2.0) * (+0.30)
1715    + f_SSigStarMinus[i] * (1.0/3.0) * (5.0/2.0) * (-2.41)
        )
    );
    c[i] = (2.0/3.0)*(1.0*
        fBar_AntiLprimary[i]      * 1.0          * (3.0/4.0)
        + fBar_AntiLAntiSig0[i]   * (-1.0/3.0) * (3.0/4.0)
        + fBar_AntiLAntiSigStarPlus[i] * (1.0/3.0) * (15.0/4.0)

```

```

1725
    + fBar_AntiLAntiSigStarZero[i] * (1.0/3.0) * (15.0/4.0)
    + fBar_AntiLAntiSigStarMinus[i] * (1.0/3.0) * (15.0/4.0)
    + fBar_AntiLAntiXiZero[i]     * (0.900)   * (3.0/4.0)
    + fBar_AntiLAntiXiPlus[i]    * (0.927)   * (3.0/4.0)
    )
    -(1.0/3.0)*(
        fBar_AntiSAntiSigStarPlus[i] * (1.0/3.0) * (15.0/4.0)
        + fBar_AntiSAntiSigStarZero[i] * (1.0/3.0) * (15.0/4.0)
        + fBar_AntiSAntiSigStarMinus[i] * (1.0/3.0) * (15.0/4.0)
        )
    );
1735
d[i] = (2.0/3.0)*(1.0*(
    fBar_AntiLprimary[i]      * 1.0      * (3.0/2.0) * (+0.613)
    + fBar_AntiLAntiSig0[i]    * (-1.0/3.0) * (3.0/2.0) * (-0.79)
    + fBar_AntiLAntiSigStarPlus[i] * (1.0/3.0) * (5.0/2.0) * (-3.02)
    + fBar_AntiLAntiSigStarZero[i] * (1.0/3.0) * (5.0/2.0) * (-0.30)
    + fBar_AntiLAntiSigStarMinus[i] * (1.0/3.0) * (5.0/2.0) * (+2.41)
    + fBar_AntiLAntiXiZero[i]   * (0.900)   * (3.0/2.0) * (+1.25)
    + fBar_AntiLAntiXiPlus[i]  * (0.927)   * (3.0/2.0) * (+0.651)
    )
    -(1.0/3.0)*(
        fBar_AntiSAntiSigStarPlus[i] * (1.0/3.0) * (5.0/2.0) *
        (-3.02)
        + fBar_AntiSAntiSigStarZero[i] * (1.0/3.0) * (5.0/2.0) *
        (-0.30)
        + fBar_AntiSAntiSigStarMinus[i] * (1.0/3.0) * (5.0/2.0) *
        (+2.41)
        )
    );
1745
)
1755
}
// ----- what we want is the INVERTED matrix -----
1760 Double_t aInv[8],bInv[8],cInv[8],dInv[8];
for (Int_t i=0; i<8; i++){
    Double_t det = a[i]*d[i] - b[i]*c[i];
    aInv[i] = d[i]/det;
    bInv[i] = -b[i]/det;
    1765 cInv[i] = -c[i]/det;
    dInv[i] = a[i]/det;
}
1770 }

```

### 3.5.8 Communication with Jean Cleymans

This subsubsection contains an email exchange with Jean Cleymans, the author of THERMUS. Basically, I wanted to make sure I understood how to interpret the output of the code. From this exchange, I understand that when I see the line

1775 rate information: Lambda<-Lambda(1405) = 0.00025601 running decay total (%) = 82.1262  
 that tells me the number of As, per event, that have their origin as a *primary*  $\Lambda(1405)$ . That primary  $\Lambda(1405)$  could be a parent, a grandparent, a great-grandparent, whatever.

At the end of Jean's mail, he tells me that he will get back to me "today," but he never did. Which is fine; I got the information I needed.

1780 Dear Lisa,

Great to hear that you are finding THERMUS useful. The main author Spencer Wheaton wrote the following:

Yes, the grandparents are included too. Essentially, in the decay chain, all decay  
1785 products are allowed to decay down until they reach particles that are considered stable.

Regards  
Spencer

1790 I will look more specifically at your question and get back to you later today.  
With best regards  
Jean

1795 From: Lisa, Michael <lisa@physics.osu.edu>  
Sent: 13 July 2016 05:38:45 PM  
To: Jean Cleymans  
Subject: question about THERMUS

1800 Dear Jean,

We are using THERMUS for some feed-down studies, and it is incredibly useful!

I have an important question that I hope you can answer. If I look at section 2.2  
1805 of your paper <https://arxiv.org/pdf/hep-ph/0407174v2.pdf>, you discuss that the code will decay unstable hadrons to the stable ones (like pions, protons, Lambdas) which is crucial for us experimentalists.

So, Delta++ ---> p + pi+ will occur, and the pi+ distribution at the end will include  
1810 contributions from Delta++ decay. Great! My question is, what about multi-step decays, for example Sigma(1775)-->Sigma(1385)+pion and then the Sigma(1385)-->Sigma+pion, and then Sigma-->Lambda+gamma.

Equation (30) of your paper seems to say that there is a loop over primordial particles,  
1815 which are allowed to decay, but in the above example, the Sigma(1385) would not be "primordial," correct? (I do understand that, naturally, there are ALSO primordial Sigma(1385) baryons from the model.) And also the Sigma is not "primordial."

My confusion comes from the text above equation (30) that reads "the primordial hadrons  
1820 are allowed to decay to particles considered stable..." as well as the "(prim)"  
superscript  
in equation (30) itself.

My question may boil down to ask: in my above example, do the final Lambdas have the  
1825 contribution whose "grandparent" is Sigma(1775)?

I hope my question is clear. Can you help me understand?

Thank you very much, and best regards,

1830 Mike

### 3.5.9 Notes on Bill's THERMUS

The parameters for THERMUS were chosen by Bill from Sabita Das' thesis [https://drupal.star.bnl.gov/STAR/system/files/Thesis\\_SabitaDas\\_26thOct.pdf](https://drupal.star.bnl.gov/STAR/system/files/Thesis_SabitaDas_26thOct.pdf). Quantities of interest are enumerated in "Table 4.4: Freeze-out parameters obtained from yields in GCE and SCE ( $\mu_Q = 0$ ).". Naturally numbers were chosen to match the 20-50% of the analysis. Sabita uses THERMUS for the STAR results so it is not a surprise that they match.

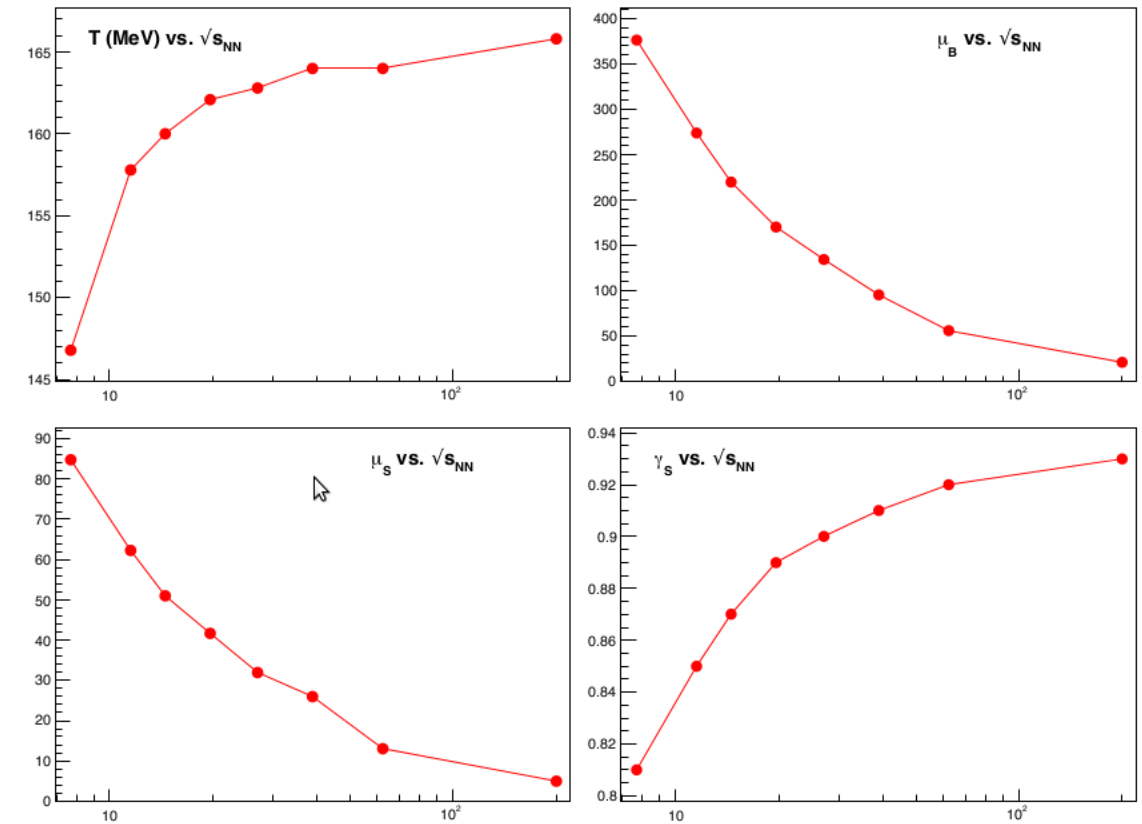


**Fig. 96:** Input numbers for THERMUS simulation

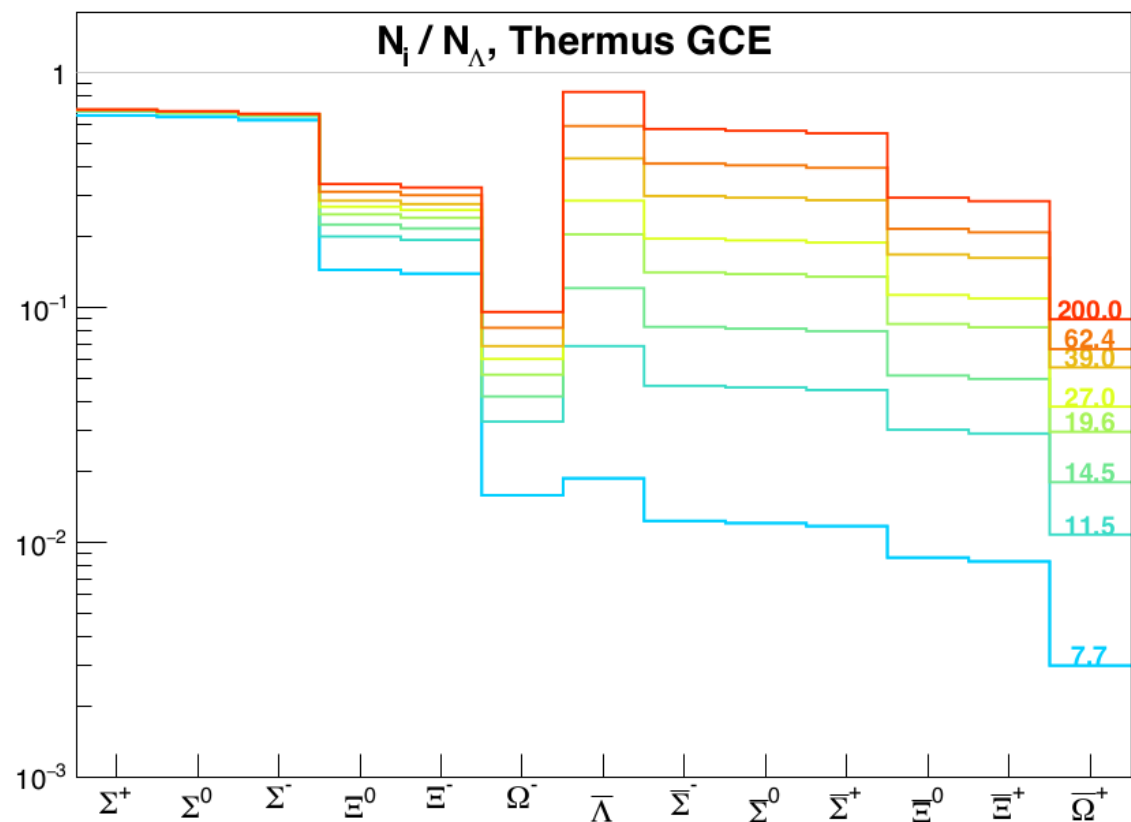


**Fig. 97:** Output particle ratios for THERMUS simulation, unfortunately these do not include  $\Sigma^*$  baryons.

### 3.5.10 Sanity check

For  $\Xi^-\left[\frac{1}{2}^+\right] \rightarrow \Lambda\left[\frac{1}{2}^+\right] + \pi^-[0^-]$ , parity is conserved for p-wave decay and violated for s-wave decay. In the weak decay of these baryons, the  $\gamma$  factor quantifies the degree by which parity is violated.

$$\gamma = \frac{S^2 - P^2}{S^2 + P^2} \quad (17)$$

<sup>1840</sup> As an electromagnetic process,  $\Sigma^0 \rightarrow \Lambda + \gamma$  conserves parity, so is p-wave. This would correspond to  $\gamma_{\Xi^-} = -1$ , in which case  $F_{\Xi^-} = -\frac{1}{3}$ , which is the same as  $F_{\Sigma^0}$ . This is consistent with equation ??.

$\gamma_{\Xi^-} = +1$  corresponds to the parity-violating s-wave decay mode, for which the spin of the  $\Lambda$  daughter must point in the same direction as the  $\Xi^-$  parent ( $F_{\Xi^-} = +1$ ), by angular momentum conservation. Again, this is consistent with equation ??.

<sup>1845</sup> **3.5.11 HIJING efficiency**

We do not use the results of this section in the feed-down correction

Different particles have different decay kinematics which can lead to different efficiencies. Since the  $\Sigma^0$  decay is electromagnetic the  $\Lambda$  daughter has basically the same decay kinematics as a primary  $\Lambda$ . On the other hand, weak decays like the  $\Xi^-$ ,  $\Xi^0$ , and the  $\Omega^0$  have lifetimes similar to the  $\Lambda$ . Because of this the the *apparent* decay length of the  $\Lambda$  which is a daughter of one of these multi-strange particles is longer than average decay length of actual primary  $\Lambda$ . Similarly such a secondary  $\Lambda$  would have a larger reconstructed DCA and (generally) larger DCA of each secondary  $\Lambda$  daughter to the primary vertex. In order to account for this effect we used HIJING data and compared the efficiency of the multi-strange hadrons to the efficiency of the Lambdas. This relative efficiency was used because the yields we got from UrQMD and THERMUS are with respect to Lambdas. Quoting the yields this way somewhat mitigates the tendency for models like UrQMD to underestimate strangeness. These efficiencies are taken into account when quoting yields in in section ??.

In order to get the efficiency for reconstructing a  $\Xi^-$  relative to reconstructing a primary  $\Lambda$  we first get a  $\Xi^-$  efficiency. This is accomplished by dividing the number of MC  $\Xi^-$  tracks in the HIJING by the number of HIJING  $\Xi^-$ 's that are associated via the association maker and pass our normal reconstruction cuts. This quantity is then divided by the same thing (# pure MC tracks/# reconstructed  $\Lambda$ ) for primary  $\Lambda$ s. The corollary is done for antiparticles (that is efficiency is quoted with respect to the  $\bar{\Lambda}$ ). All such efficiencies were calculated with STAR productionHIJING events at 19GeV. It is assumed that it should not vary significantly for different values of  $\sqrt{s_{NN}}$ . These final efficiencies can then be multiplied by the yields of  $\Xi^-$  per  $\Lambda$  that we have for the UrQMD and THERMUS.

Particle	relative efficiency
$\Xi^-$	1.12728
$\Xi^0$	1.01695
$\Omega^0$	0.97769
$\Xi^+$	1.09458
$\Xi^0$	1.00359
$\Omega^0$	1.00907

**Table 9:** Relative efficiency [(# Multi-strange particle passing cuts)/(# Multi-strange particle simulated)]/[(# primary Lambda passing cuts)/(# primary Lambda simulated)]

### 3.5.12 Old feed-down correction using only $\Sigma^0$ s

This section is obsolete. It explains how we used to do the feed-down correction when only  $\Sigma^0$ s were considered.

One correction that has to be done is the effect of Sigma baryon feeddown from the electromagnetic decay  $\Sigma^0 \rightarrow \Lambda + \gamma$ . The lifetime of the Sigma is  $7.4 \cdot 10^{-20}$  s so it effectively doesn't change the decay topology of the Lambda. If a collection of  $\Sigma^0$  has spin aligned in one direction the  $\Lambda$  daughter will, on average, receive a  $-1/3$  of the spin of the  $\Sigma^0$  because of the spin 1 photon. If the global  $\Lambda$  polarization originates from spin coupling in the fireball one would expect that all particles emitted from the fireball share this global polarization. Therefore the Lambda polarization we're measuring appears smaller than it actually is due to this  $\Sigma^0$  feeddown. In the following equation the subscript " $\Lambda$ " means *primary* Lambdas - or at least those not from  $\Sigma^0$ s - while " $\Sigma^0$ " means Lambdas from  $\Sigma^0$  feeddown

$$\langle \sin(\Psi_1 - \phi_\Lambda^*) \rangle_{\text{Measured}} = \frac{N_\Lambda}{N_\Lambda + N_{\Sigma^0}} \langle \sin(\Psi_1 - \phi_\Lambda^*) \rangle_\Lambda + \frac{N_{\Sigma^0}}{N_\Lambda + N_{\Sigma^0}} \langle \sin(\Psi_1 - \phi_\Lambda^*) \rangle_{\Sigma^0} \quad (18)$$

As mentioned above

$$\langle \sin(\Psi_1 - \phi_\Lambda^*) \rangle_{\Sigma^0} = -\frac{1}{3} \langle \sin(\Psi_1 - \phi_\Lambda^*) \rangle_\Lambda \quad (19)$$

Therefore

$$\begin{aligned} \langle \sin(\Psi_1 - \phi_\Lambda^*) \rangle_\Lambda &= \frac{1 + \frac{N_{\Sigma^0}}{N_\Lambda}}{1 - \frac{1}{3} \frac{N_{\Sigma^0}}{N_\Lambda}} \langle \sin(\Psi_1 - \phi_\Lambda^*) \rangle_{\text{Measured}} \\ &\approx \frac{1 + e^{-\Delta m/T}}{1 - \frac{1}{3} e^{-\Delta m/T}} \langle \sin(\Psi_1 - \phi_\Lambda^*) \rangle_{\text{Measured}} \end{aligned} \quad (20)$$

Where in Eq. 20 we can approximate the ratio  $N_{\Sigma^0}/N_\Lambda$  using a simple thermal distribution so that  $\frac{N_{\Sigma^0}}{N_\Lambda} \sim e^{-\frac{m_{\Sigma^0} - m_\Lambda}{T}}$ . The temperature should be about 140 MeV and deviations of  $\pm 10$  MeV seem to only alter the scaling by about 4%.

### 3.6 Discussion of statistical error

There is not much to discuss in this section but I want to clearly enumerate the sources of statiscal error. Systematic errors are discussed in sec. 4.

- 1885 Of course the first thing is the statistical error itself coming from filling the TProfiles as described in the bulleted list at the beginning of this section (sec. 3). Of course the error bars are appropriately scaled with the various scalings and corrections we do to the data. The errors on these scalings make up the systematic error of the measurement. A detailed discussion on the error for the mass purity correction can  
1890 and the acceptance correction) all have associated errors which fall under systematics, and are discussed in sec. 4.3.

## 4 Systematic errors

Summary of systematic errors to be discussed in detail later in this section

- Mass purity/residual mass background correction (sec. 4.2). This is the primary source of errors.
- 1895 – Error in  $\alpha_H$  (sec. 4.3) –  $\sim 2\%$  scaling error.
- Error in resolution correction (sec. 2.2.1 and 4.3) –  $< 1\%$
- Error in  $A_0$  determination (table 1 and 4.3) –  $< 0.03\%$
- There is an error in the helicity efficiency effect on the data (sec. 3.4.2 and 4.3) –  $< 3.5\%$
- Error in resolution correction from momentum conservation effects (sec. 4.4) –  $\sim 2\%$
- 1900 – For feed down corrected results (vorticity and magnetic field) there is a factor 2 systematic error coming from uncertainty in the temperature  $T$  (sec. 3.5)

### 4.1 Topological cut dependencies

A typical source of systematic errors in the cuts. In this section I'll go over the analysis to find systematic errors from the topology cuts we use to find Lambdas. The nominal cuts used in the analysis can be found in section 2.4.2. The first thing we tried doing was making each cut individually tighter or looser so we had  $\pm 25\%$  of the number of Lambdas used in the analysis. The idea was that we could estimate the systematic error by comparing the tight-cut and the loose-cut results. The difference turned out to be possible contributable to statistical error (see section 4.1.4). In order to get a finer handle on this difference we tried to look at the covariance of the polarization with the topological cuts. The result from this study is that “systematic errors are smaller than statistical”. The statistical fluctuations simply dominate any deviation from zero covariance that we can see

#### 4.1.1 Covariance method idea

The covariance of two variables (say  $P$  for polarization and  $X$  for some cut quantity e.g. pion DCA) is defined to be

$$\text{Cov}(P, X) = \langle PX \rangle - \langle P \rangle \langle X \rangle. \quad (21)$$

1915 This, of course, tells us how the cut quantities and the polarization measure co-vary. We look at each covariation with each variable separately. The advantage here is that we can use much more Lambda candidates that wouldn't pass the nominal cuts in order to understand a trend rather than a simple difference. What we really want to get systematic errors is a description of how the polarization depends on the variable. A slope parameter can be made that treats the variation as approximately linear

$$\begin{aligned} \text{Slope}(P(X)) &= \frac{\text{Covariance}(P, X)}{\text{Variance}(X)} \\ &= \frac{\langle PX \rangle - \langle P \rangle \langle X \rangle}{\langle X^2 \rangle - \langle X \rangle^2} \end{aligned} \quad (22)$$

1920 Once we have a slope that describes the variation of the polarization with  $X$  we can get the systematic error by multiplying by a *reasonable* range in the cut quantity ( $\Delta X$ )

$$\text{Error} = \Delta X * \text{Slope} \quad (23)$$

A reasonable range for  $\Delta X$  is, for each cut, the difference between where you might make the a loose version and a tight version of the cut. As it happens the  $\Delta X$  is just a scaling and, since we don't get a significant slope value, it is not necessary to use when we find no clear non-statistican deviation from zero for the slope.

There is a subtlety here I've glossed over which is that the apparent magnitude of the polarization depends on the purity of Lambda sample which, in turn, depends on the value of the quantity I'm cutting on. To account for this I can scale the slope by the purity of the mass distribution. Doing this requires a characterization of the slope of the purity distribution. For example suppose I want to know the covariance of the polarization with the pion DCA. If I look in bins of pion DCA for Lambda candidates the ones with the largest DCA have the purest Lambda distribution. Since we normally scale the measured polarization by  $(S+B)/S$  (assuming zero polarization in the mass background) the polarization will be of a greater magnitude than that measured at low pion DCA. So we have done no purity correction to the data if it has the same positive polarization at a bin of low pion DCA as it does for a different bin a high pion DCA, the high pion DCA bin will have a larger *apparent* polarization and a positive covarianc will be seen. Given that we have a positive net polarization we might expect a trivial positive covariance for pion DCA to appear just from variation of the purity with pion DCA.

What we measure without correcting for the purity is the so called “measured” slope, we can recast 22 as

$$\text{Slope}(P(X))^M = \frac{d}{dX} P^M \quad (24)$$

where  $M$  denotes the “measured” quantity and  $T$  denotes a “true” quantity. We can relate this to the true polarization which we get from purity correcting the measured values, provided we assume that we can describe the variation of  $S/(S+B)$  with  $X$  by a linear function with slope  $m_X$

$$\begin{aligned} \text{Slope}(P(X))^M &= \frac{d}{dX} \left( \frac{S}{S+B} P^T \right) \\ &= \frac{S}{S+B} \frac{d}{dX} P^T + \left( \frac{d}{dX} \frac{S}{S+B} \right) P^T \\ &= \frac{S}{S+B} \text{Slope}^T + m_X P^T \\ &\approx \left\langle \frac{S}{S+B} \right\rangle \text{Slope}^T + m_X \langle P^T \rangle \end{aligned} \quad (25)$$

#### 4.1.2 Mass purity

An example of purity changing with a cut quantity:

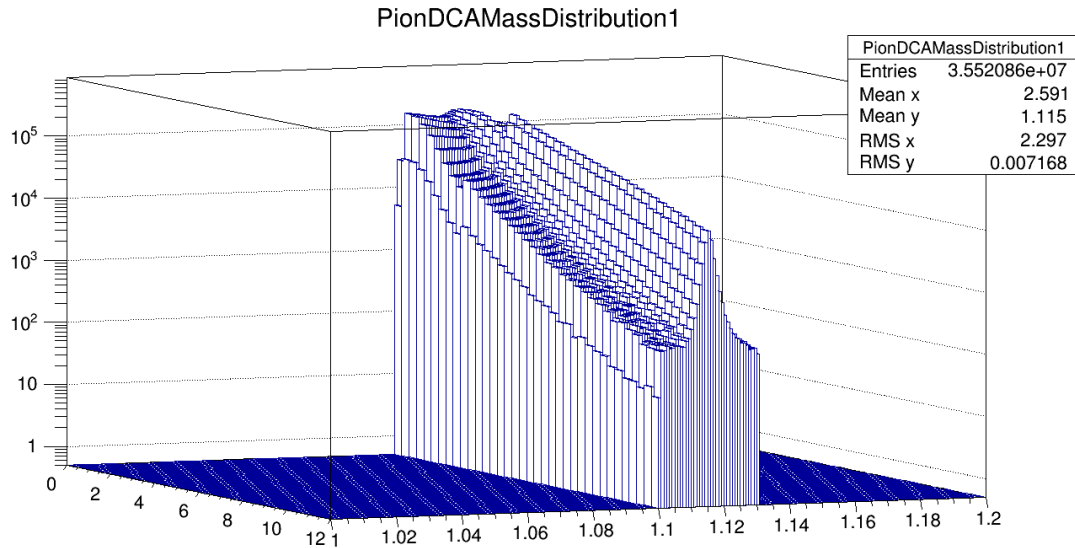


**Fig. 98:** Invariant mass (GeV – right axis) as a function of pion DCA (cm – left axis) for cut index 1 (proton has ToF info, pion does not). Vertical axis is counts. Cutoff in invariant mass is an artifact of what I save in my PicoDst files – higher/lower mass is not necessary for purity estimation.

1945 A linear fit of the purity for various quantities can be seen below

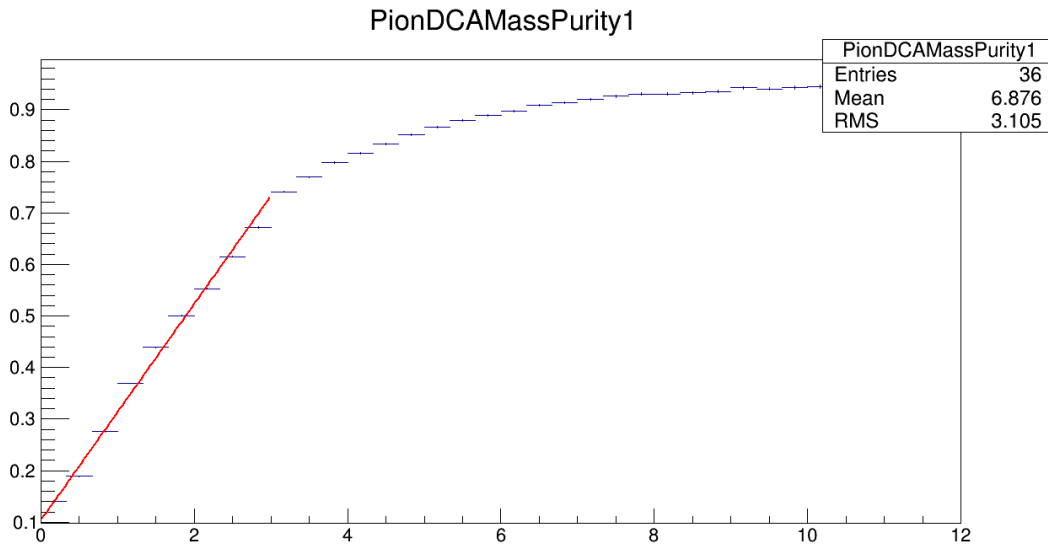


**Fig. 99:** Lambda invariant mass purity as a function of pion DCA fit with a linear function ( $p_0 + p_1 * x$ ) for cut index 1

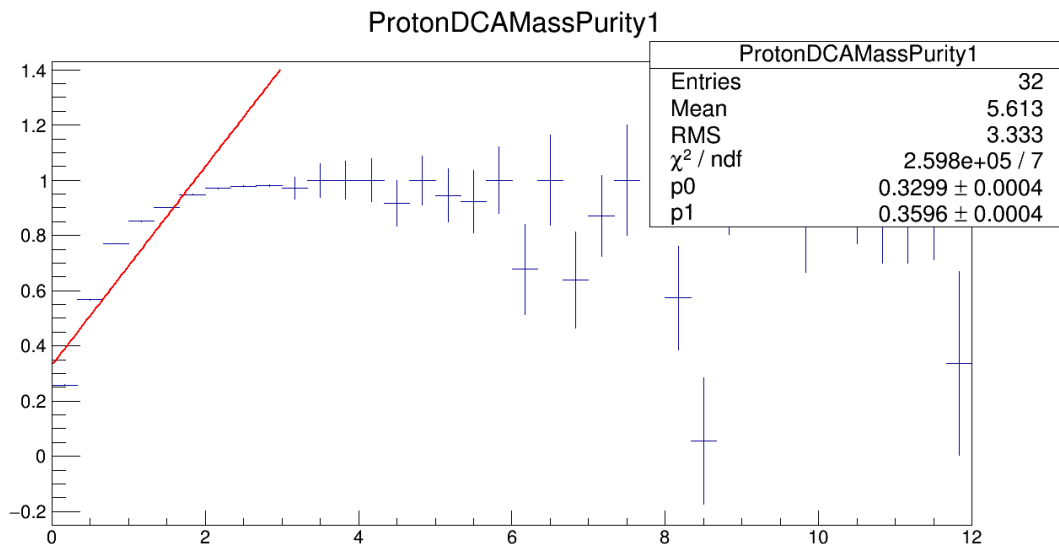


**Fig. 100:** Lambda invariant mass purity as a function of proton DCA fitted with a linear function ( $p_0 + p_1 * x$ ) for cut index 1

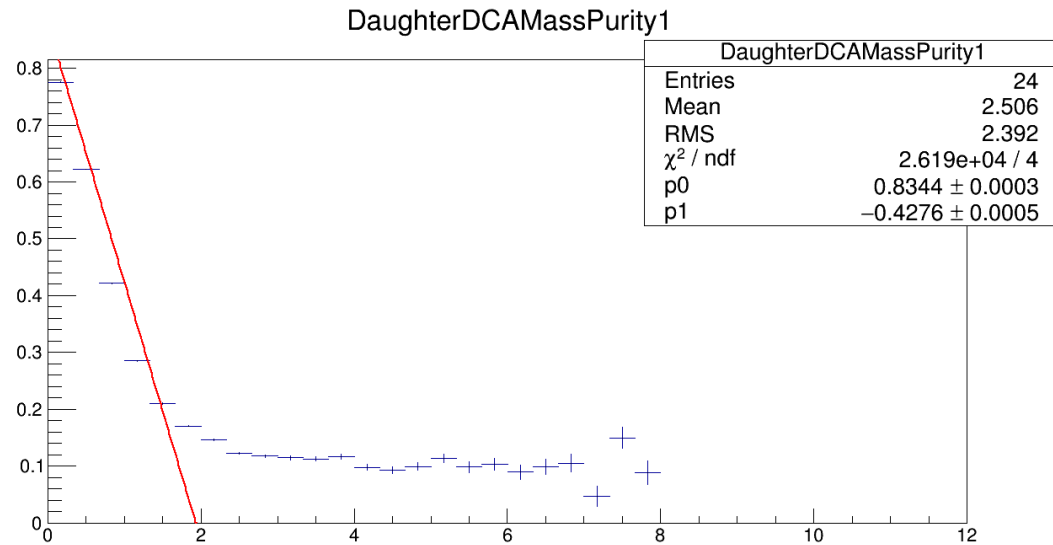


**Fig. 101:** Lambda invariant mass purity as a function of daughter DCA fit with a linear function ( $p_0 + p_1 * x$ ) for cut index 1

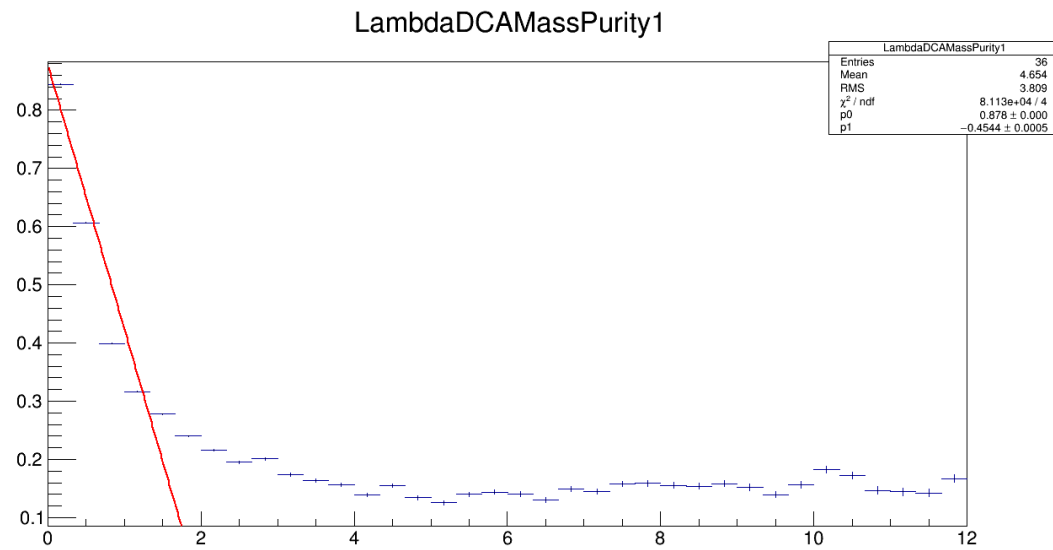


**Fig. 102:** Lambda invariant mass purity as a function of Lambda DCA fitted with a linear function ( $p_0 + p_1 * x$ ) for cut index 1

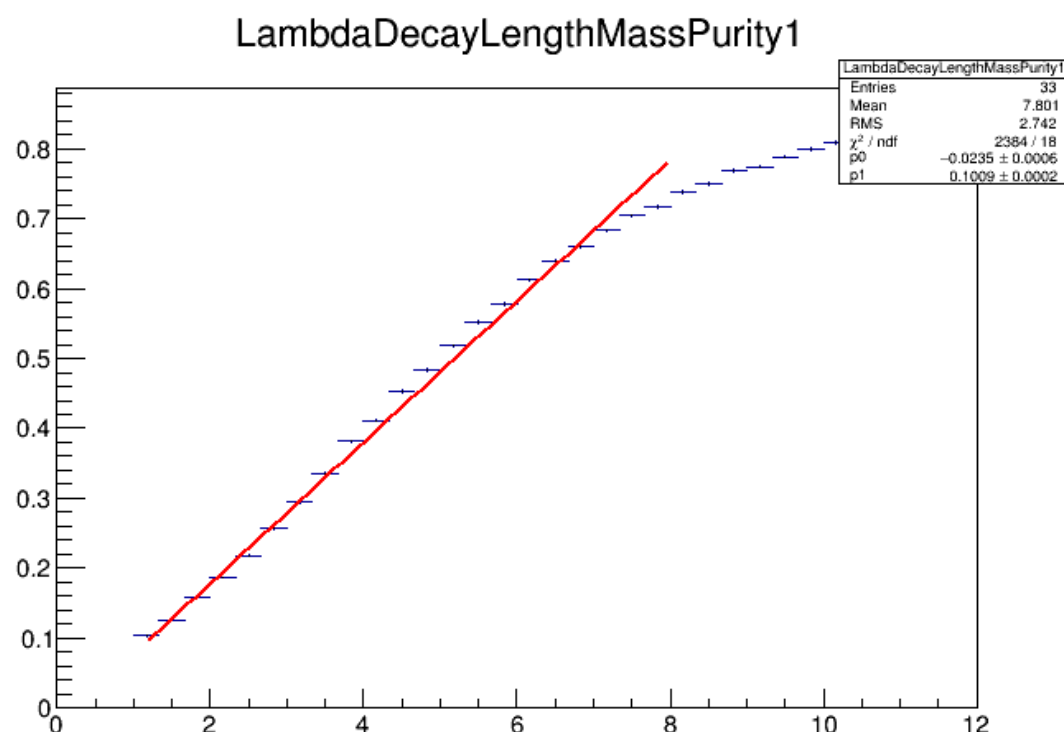


**Fig. 103:** Lambda invariant mass purity as a function of Lambda decay length fitted with a linear function ( $p_0 + p_1 * x$ ) for cut index 1

Clearly a linear approximation is not ideal for several of these functions. The only thing to be done is to change the range over which the fit is done and try to overestimate  $m_X$ . The range was varied but the nominal fit range for these functions is (where Min. refers to the lower value of the cut and max refers to the upper value)

Cut description	cut index 0	cut index 1	cut index 2	cut index 3
PionDCA min	0.0	0.0	0.5	0.5
PionDCA max	3.0	3.0	3.0	3.0
ProtonDCA min	0.0	0.0	0.0	0.0
ProtonDCA max	3.0	3.0	3.0	3.0
DaughterDCA min	0.0	0.0	0.0	0.0
DaughterDCA max	2.0	2.0	2.0	2.0
LambdaDCA min	0.0	0.0	0.0	0.0
LambdaDCA max	2.0	2.0	2.0	2.0
LambdaDecayLength min	1.167	1.167	3.0	3.0
LambdaDecayLength max	8.0	8.0	8.0	8.0

**Table 10:** Range of linear fit of mass purity as a function of respective cut quantity

1950 **4.1.3 Results**

1955 Since the error bars depend so much on which cut I'm considering and the cut index of the Lambda I may have to duplicate a few of the plots so zoomed in. What we're looking for is a clear non-statistical deviation of the slope. Each point on the following plots represents the covariance of the polarization with various cut quantities (e.g. pion DCA). There is a separate point for each type of Lambda (cut index 0, 1, 2, or 3).

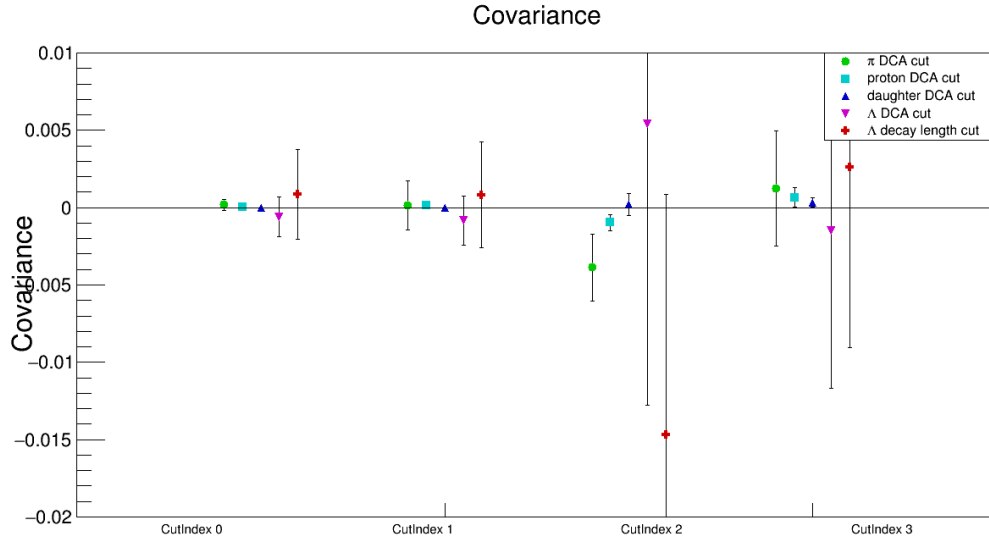


Fig. 104:  $\Lambda$  polarization covariance with cut quantities for each  $\Lambda$  cut index.

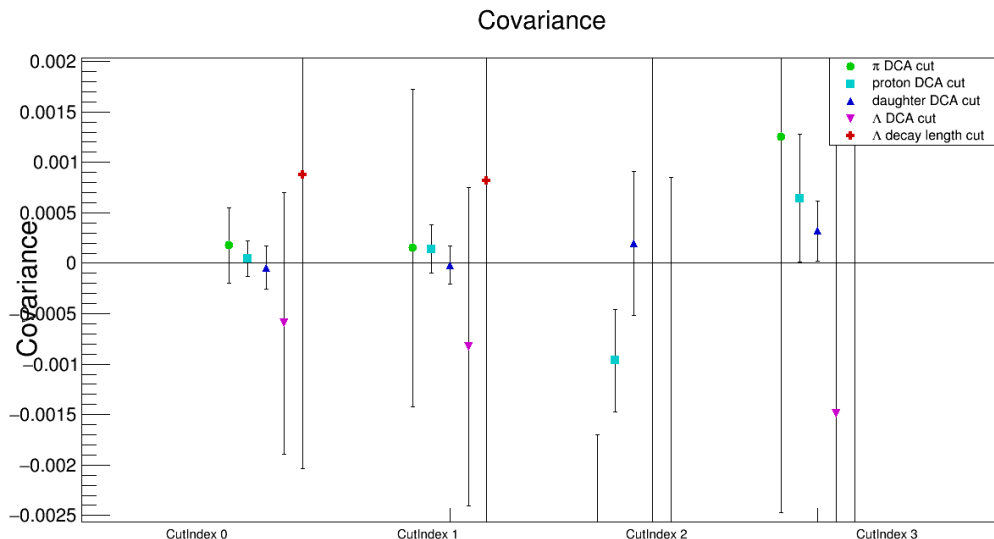
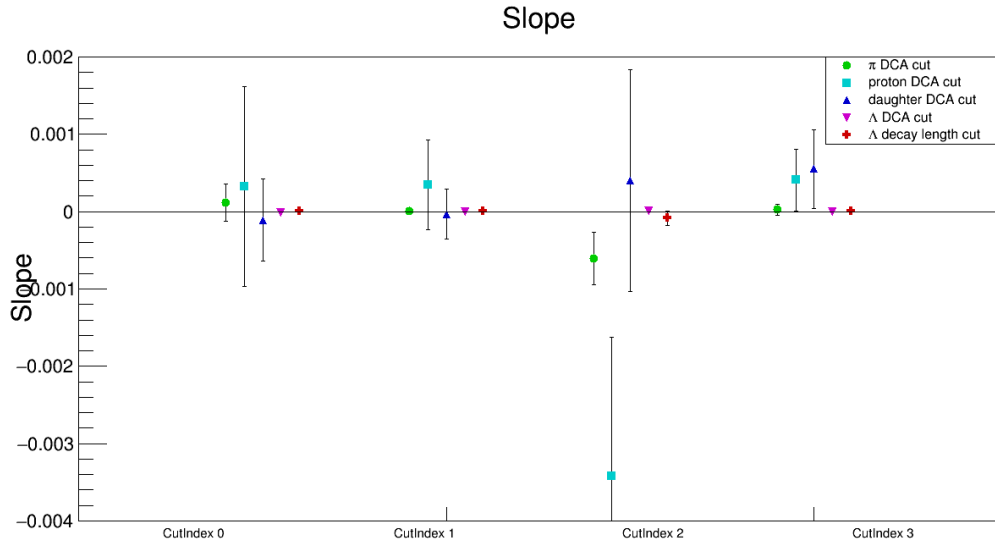
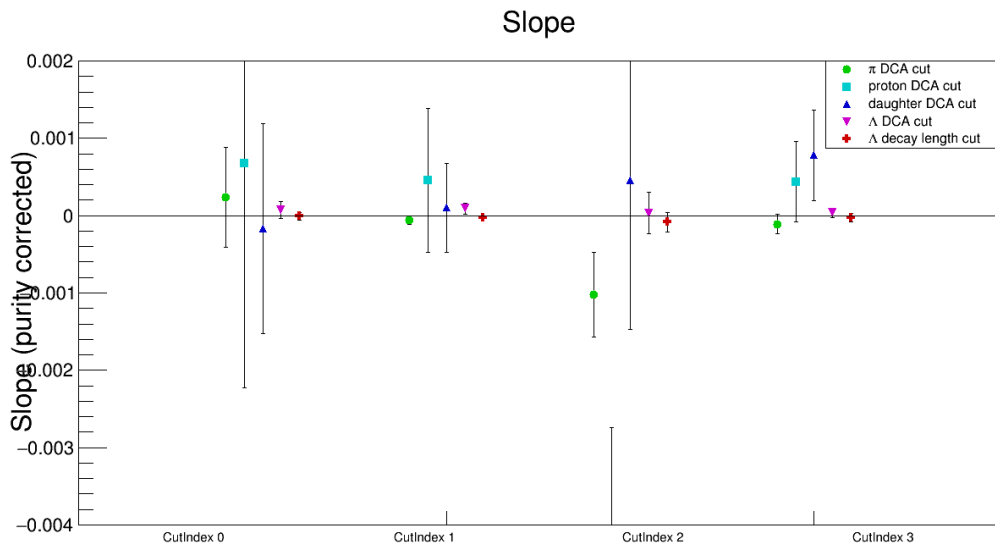


Fig. 105:  $\Lambda$  polarization covariance with cut quantities for each  $\Lambda$  cut index; zoomed in.



**Fig. 106:**  $\Lambda$  polarization “slope” from covariance with cut quantities for each  $\Lambda$  cut index. This is not corrected for mass purity.



**Fig. 107:**  $\Lambda$  polarization “slope” from covariance with cut quantities for each  $\Lambda$  cut index. This is corrected for mass purity.

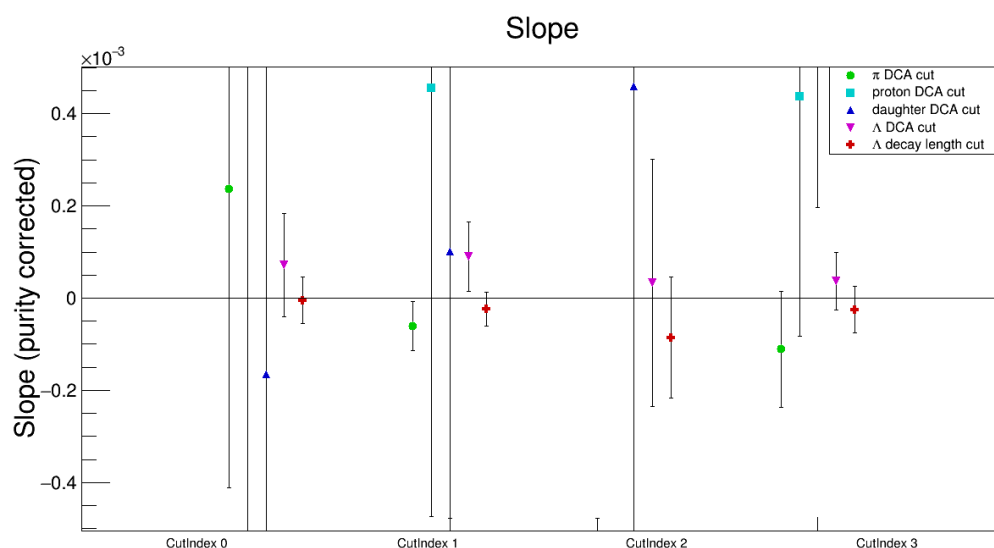


**Fig. 108:**  $\Lambda$  polarization “slope” from covariance with cut quantities for each  $\Lambda$  cut index; zoomed in. This is corrected for mass purity.

The only hints of non-statical deviation comes from cut index 2, but cut index 2 is only 3% of the data! Cut index 2 represents Lambda's whose daughter proton has no ToF information while the pion daughter does. This is a very poor quantity Lambda candidate and since it is such a small percentage of the total number of Lambdas we can throw these Lambdas out with impunity. There is no bias introduced here, these are simply poor quality Lambdas. Therefore (throwing out cut index 2 Lambdas) there is no non-statistical deviations from covaration of the polarization and any of the cut quantities. To double check this conclusion I've increased/decreased the maximum of the fit range for the purity slope  $m_X$ . In the following plots the the maximum of the fit is multiplied by a rangefactor.

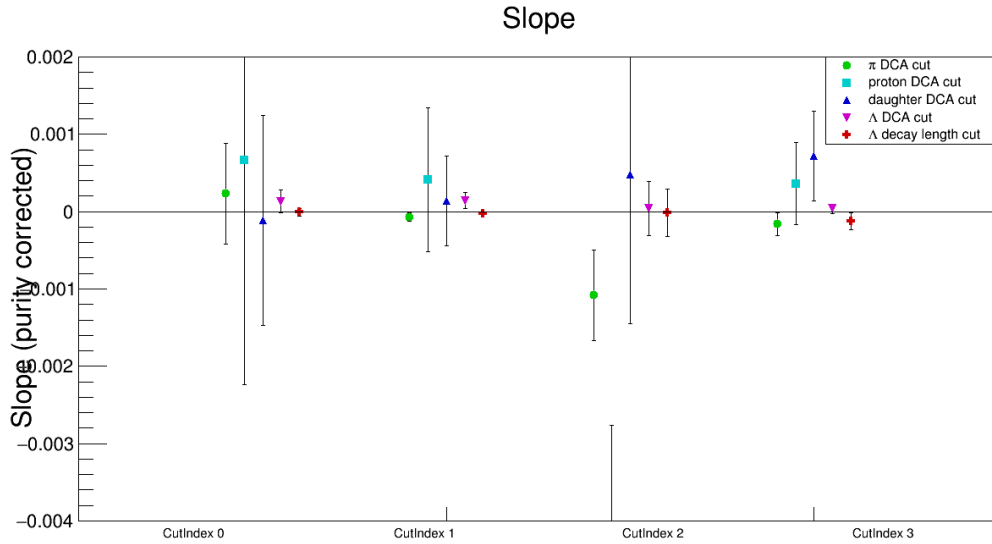


**Fig. 109:**  $\Lambda$  polarization “slope” from covariance with cut quantities for each  $\Lambda$  cut index. This is corrected for mass purity. The rangefactor is 0.5.

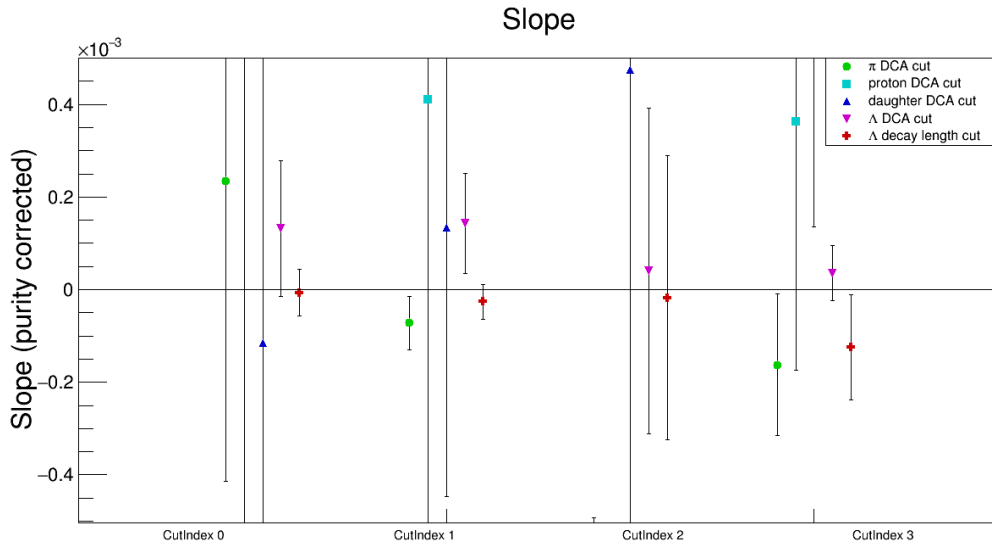


**Fig. 110:**  $\Lambda$  polarization “slope” from covariance with cut quantities for each  $\Lambda$  cut index; zoomed in. This is corrected for mass purity. The rangefactor is 0.5.

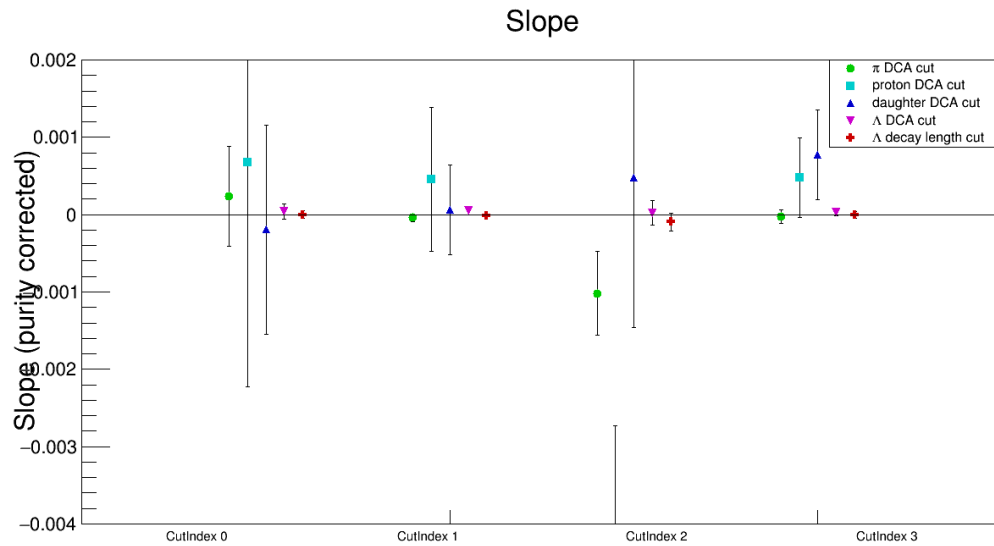


**Fig. 111:**  $\Lambda$  polarization “slope” from covariance with cut quantities for each  $\Lambda$  cut index. This is corrected for mass purity. The rangefactor is 2.

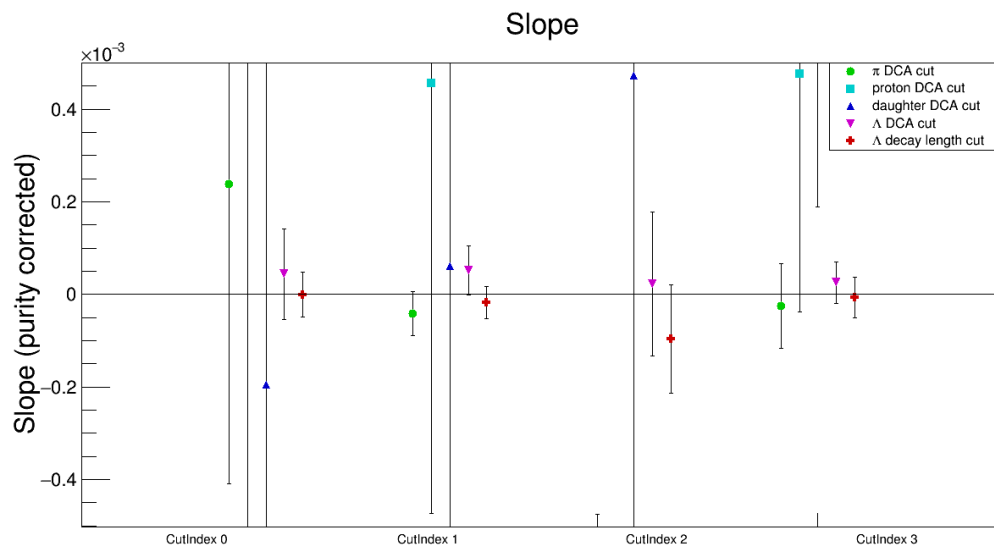


**Fig. 112:**  $\Lambda$  polarization “slope” from covariance with cut quantities for each  $\Lambda$  cut index; zoomed in. This is corrected for mass purity. The rangefactor is 2.

#### 4.1.4 Simple cut variation

1965 This section is for historical purposes. The results shown here do not provide final systematic errors.

I'll focus on errors from the topology cuts for the Lambda as they are the ones specific to my analysis. To get a handle on the errors I varied each cut for 19GeV by either making the cut tighter so that I had 75% of the Lambdas as would be found using nominal cuts or I made the cut looser so that 125% of the Lambdas were found. The result for each cut for both  $\Lambda$  and  $\bar{\Lambda}$  are shown below

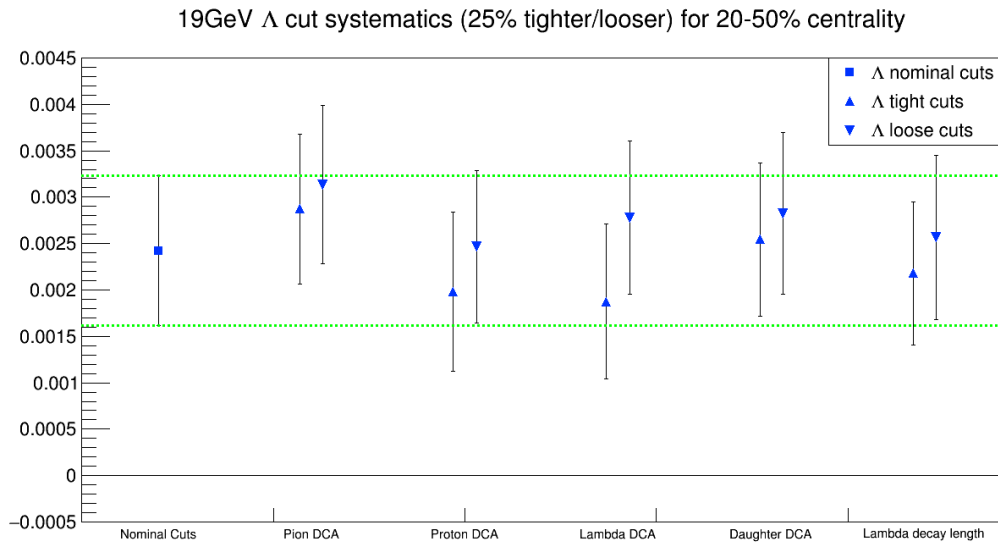


**Fig. 113:**  $\langle \sin(\Psi_1 - \phi_{\Lambda}^*) \rangle$  as a function of cut variation. One cut at a time is loosened or tightened so that 125% or 75% of the Lambdas are found.

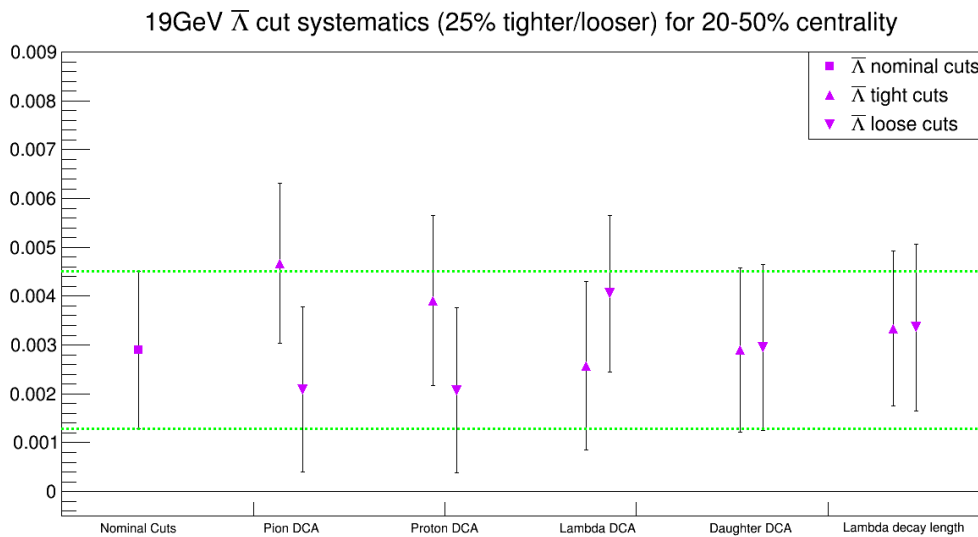


**Fig. 114:**  $\langle \sin(\Psi_1 - \phi_{\bar{\Lambda}}^*) \rangle$  as a function of cut variation. One cut at a time is loosened or tightened so that 125% or 75% of the Lambdas are found.

<sup>1970</sup> Note that in the previous two figures each data point is scaled by the (Signal+Background)/Signal of the mass distribution so that the results are not affected by the purity changes that would occur by loosening/tightening a cut. The systematic error is determined to be the largest variation between the tight cuts and loose cuts (eg. for  $\Lambda$  the difference between Lambda DCA tight and Lambda DCA loose). A covariance analysis is underway to get at these errors in a more sophisticated manner.

## 4.2 Residual effect

There is a systematic error from the residual signal we see in the wings of the mass distribution which should be in the mass background of the results (see section 3.2). In section 3.2 we posit that this small residual effect comes from Lambdas which have proton daughters that get matched up with pion who does not come from a Lambda. Many of the protons in an event come from Lambdas and it is a much smaller percent of the pions. A Lambda candidate made from these particles might well have a small residual polarization since the proton carries the larger percentage of the Lambda momentum, and thus a fair bit of the spin information. The following are corrected for resolution.

$\sqrt{s_{NN}}$ (GeV)	$P\Lambda_{\text{uncorrected}} (\%)$	$P\bar{\Lambda}_{\text{uncorrected}} (\%)$
7.7	1.6%	6.6%
11.5	1.0%	2.3%
14.5	0.6%	0.9%
19.6	0.7%	1.2%
27	0.7%	1.1%
39	0.3%	0.8%

**Table 11:** Uncorrected results for Au+Au 20-50%.

$\sqrt{s_{NN}}$ (GeV)	$P\Lambda_{\text{noresidual}} (\%)$	$P\bar{\Lambda}_{\text{noresidual}} (\%)$	Level of correction $\Lambda$	Level of correction $\bar{\Lambda}$
7.7	2.4%	8.1%	155.4%	121.8%
11.5	1.5%	2.8%	151.7%	123.8%
14.5	1.2%	1.5%	192.3%	168.7%
19.6	1.0%	1.5%	151.5%	129.1%
27	1.1%	1.5%	153.0%	134.2%
39	0.5%	1.1%	149.2%	135.4%

**Table 12:** Results for Au+Au 20-50% corrected for mass purity without taking into account residual mass background polarization.

$\sqrt{s_{NN}}$ (GeV)	$P\Lambda_{\text{withresidual}} (\%)$	$P\bar{\Lambda}_{\text{withresidual}} (\%)$	Level of correction $\Lambda$	Level of correction $\bar{\Lambda}$
7.7	2.3%	7.0%	148.5%	106.0%
11.5	1.2%	2.7%	125.0%	116.7%
14.5	0.9%	2.2%	142.2%	245.9%
19.6	0.9%	1.7%	129.0%	138.4%
27	1.0%	1.3%	136.3%	119.9%
39	0.3%	1.2%	95.2%	136.6%

**Table 13:** Results for Au+Au 20-50% corrected for mass purity while taking into account residual mass background polarization.

$\sqrt{s_{NN}}$ (GeV)	$P\Lambda_{\text{withresidual}}/P\Lambda_{\text{noresidual}}$	$P\bar{\Lambda}_{\text{withresidual}}/P\bar{\Lambda}_{\text{noresidual}}$	$P\Lambda_{\text{noresidual}} - P\Lambda_{\text{withresidual}}$	$P\bar{\Lambda}_{\text{noresidual}} - P\bar{\Lambda}_{\text{withresidual}}$
7.7	95.6%	87.0%	-0.11%	-1.05%
11.5	82.4%	94.3%	-0.26%	-0.16%
14.5	73.9%	145.8%	-0.33%	0.69%
19.6	85.1%	107.2%	-0.15%	0.11%
27	89.1%	89.3%	-0.12%	-0.16%
39	63.8%	100.9%	-0.18%	0.01%

**Table 14:** Comparison between residual and non-residual corrections to data.

There are large statistical error bars associated with scale of the residual background correction. In fact this difference between considering and not considering the residual effect is well within statistical errors<sup>1985</sup> but we would like to associate a systematic error to our lack of understanding about the correct way of dealing with this residual effect. We can roughly average over the difference of the ratio of the two scaling methods to get final systematic errors. 15GeV is a special energy that will have an exception, but the average ratio not including 15GeV  $\langle P\Lambda_{\text{withresidual}} / P\Lambda_{\text{noresidual}} \rangle \sim 0.85$  and  $\langle P\bar{\Lambda}_{\text{withresidual}} / P\bar{\Lambda}_{\text{noresidual}} \rangle \sim 0.95$ .

$\sqrt{s_{\text{NN}}}$ (GeV)	$P\Lambda_{\text{noresidual}}$ (%)	$P\bar{\Lambda}_{\text{noresidual}}$ (%)	$0.85P\Lambda_{\text{noresidual}}$	$0.95P\bar{\Lambda}_{\text{noresidual}}$ (%)	diff $\Lambda$	diff $\bar{\Lambda}$
7.7	2.4%	8.1%	2.019%	7.686%	0.4136%	0.4045%
11.5	1.5%	2.8%	1.228%	2.679%	0.2516%	0.1410%
14.5	1.2%	1.5%	1.036%	1.442%	0.2122%	0.0759%
19.6	1.0%	1.5%	0.8466%	1.471%	0.1734%	0.0774%
27	1.1%	1.5%	0.9172%	1.434%	0.1879%	0.0755%
39	0.5%	1.1%	0.4374%	1.083%	0.08959%	0.0570%

**Table 15:** Results for Au+Au 20-50% corrected for mass purity without taking into account residual mass background polarization. Diff is the difference between the first column and the previous relevant column.

Roughly averaging over the results in table 15 we get the following range of systematic errors (upper and lower)

$\sqrt{s_{NN}}$ (GeV)	$\Lambda$	$\Lambda$ up sys	$\Lambda$ down sys	$\bar{\Lambda}$	$\bar{\Lambda}$ up sys	$\bar{\Lambda}$ down sys
7.7	2.43%	0.00%	0.20%	8.09%	0.00%	1.00%
11.5	1.48%	0.00%	0.20%	2.82%	0.00%	0.15%
14.5	1.25%	0.00%	0.30%	1.52%	0.40%	0.15%
19.6	1.02%	0.00%	0.20%	1.55%	0.00%	0.15%
27	1.11%	0.00%	0.20%	1.51%	0.00%	0.15%
39	0.50%	0.00%	0.20%	1.14%	0.00%	0.15%

**Table 16:** Results for Au+Au 20-50% polarization results corrected for resolution correction and purity correction as well as systematic error.

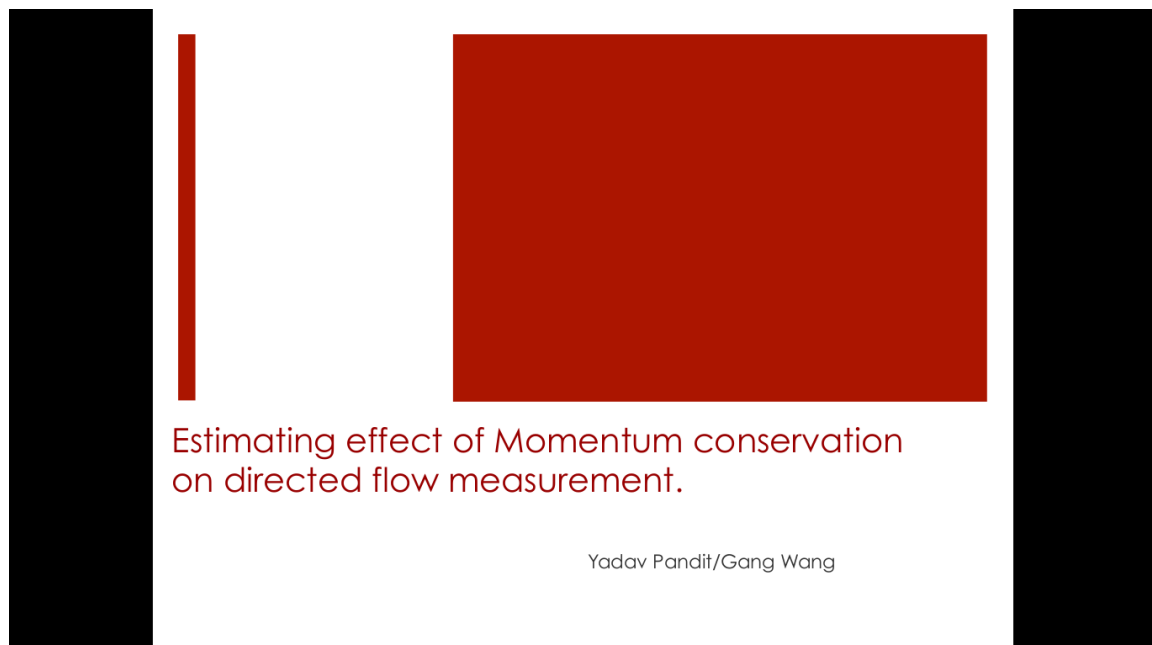
### 4.3 Scaling errors

As discussed in the beginning of sec. 3 the data is subject to a few scalings: that of  $\alpha_H = 0.647 \pm 0.013$  – the decay parameter, that of the resolution correction – as discussed in sec. 2.2.1, and the acceptance correction  $A_0$  – as seen in table 1. All of these have associated errors, which are very very small compared to the statistical error of the measure. The  $\alpha_H$  is the largest at 2%. These are included as a statement in the paper about the uncertainty in the scaling.

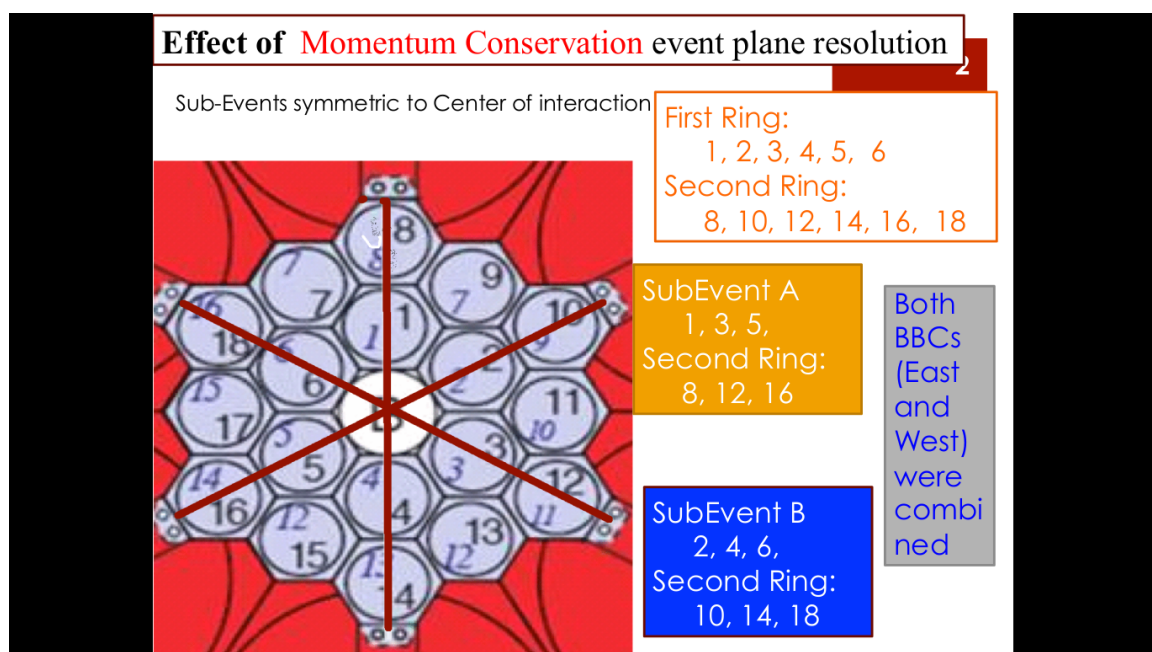
Additionally given the interplay between helicity efficiency and non-zero polarization (discussed in sec. 3.4.2) we know (from simple simulation) that we should scale the data by about  $7\% \pm 3.5\%$ . This error is quoted from fig. 3.4.2.

#### 2000 4.4 Conservation of momentum effects on event plane resolution

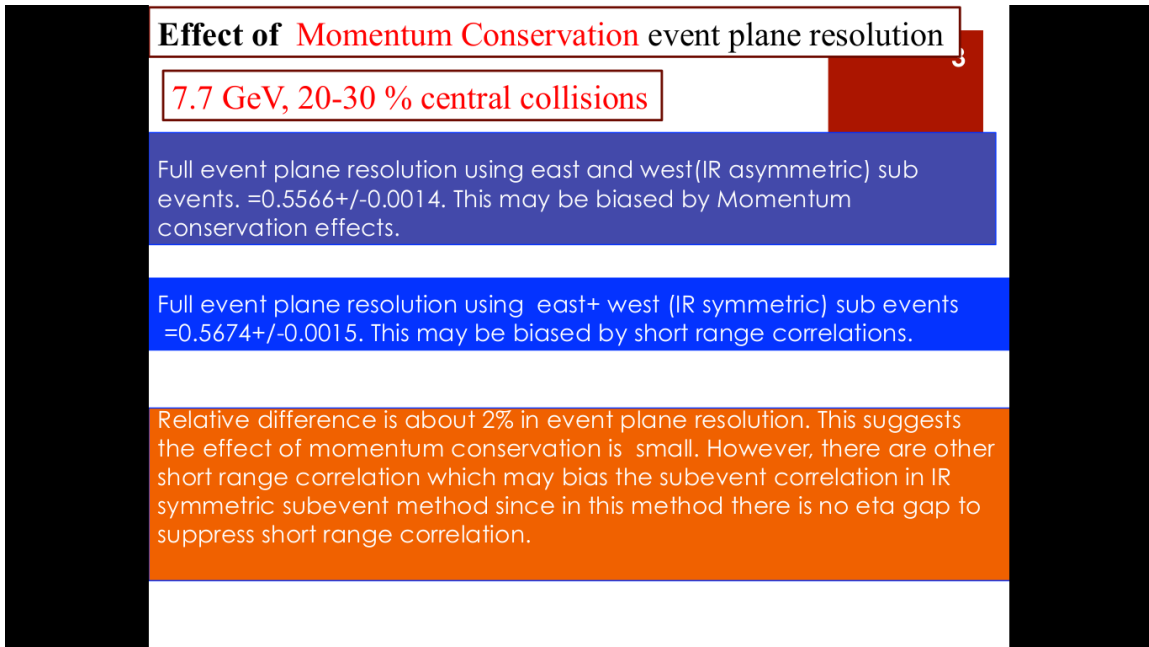
There are possible conservation of momentum (MC) effects on the event plane determination. This was studied by Yadav Pandit in the run up of the BES  $v_1$  paper using MevSim with and without MC (with the version used it could be turned off and on) using sub-event planes made by using different subsections of the BBC. As far as this analysis is concerned we expect this to be a roughly 2% systematic error  
 2005 on the event plane resolution for the BES. This study can be found on the paper webpage <http://www.star.bnl.gov/protected/bulkcorr/ypandit/BESv1Paper/> under “Support Documents” —> “Momentum Conservation Effects”. It is also copied below:



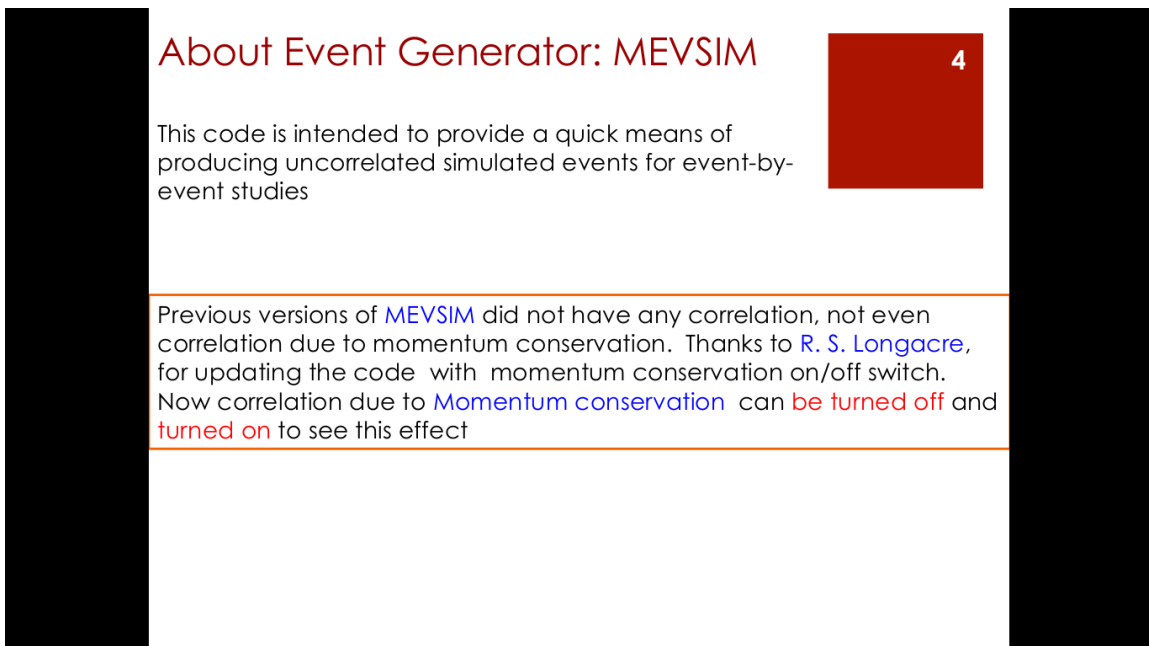
**Fig. 115:**



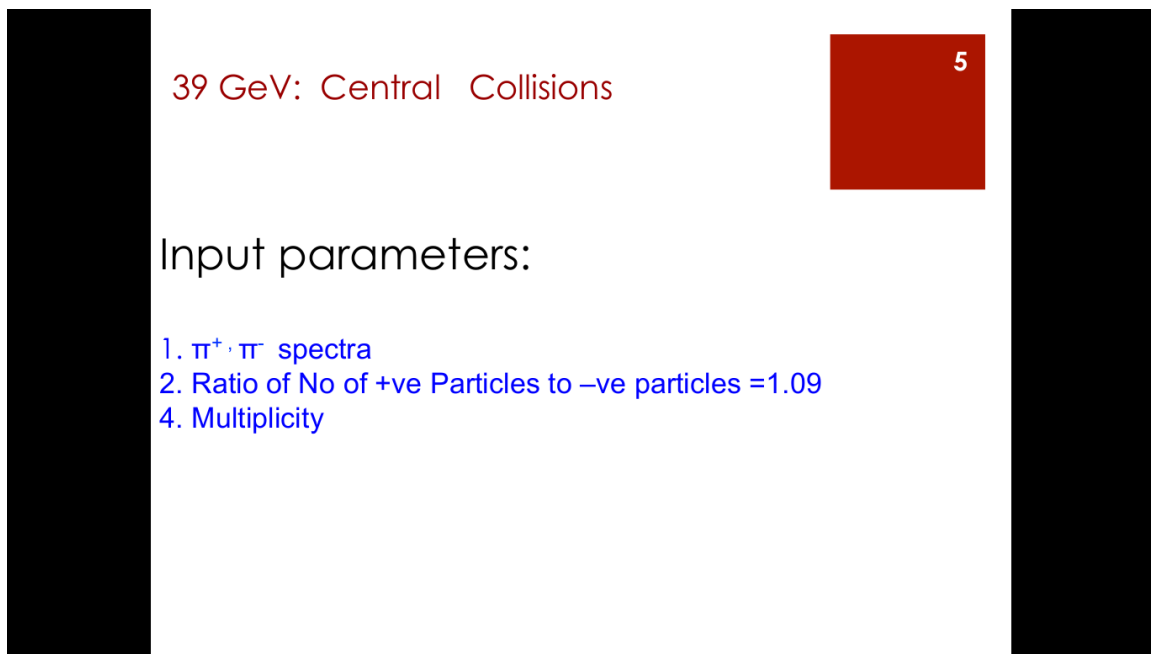
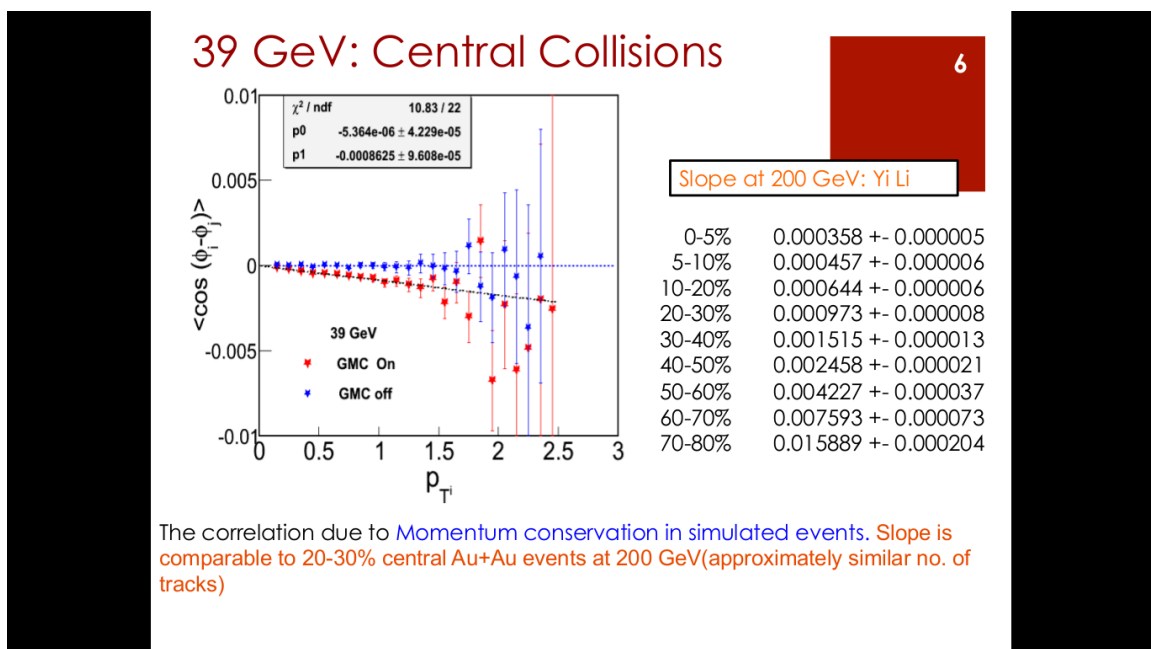
**Fig. 116:**



**Fig. 117:**

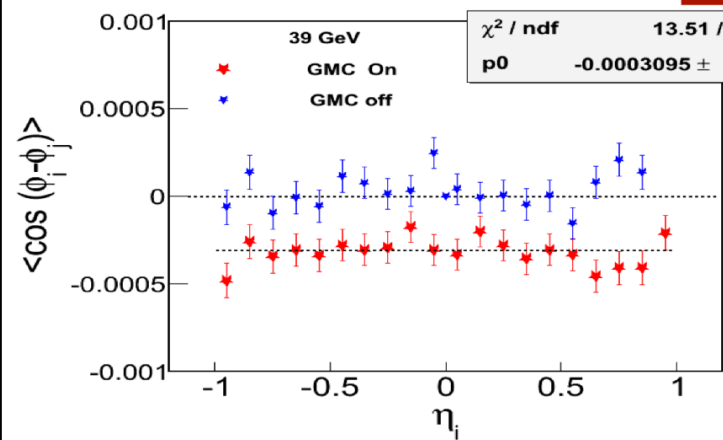


**Fig. 118:**

**Fig. 119:****Fig. 120:**

## 39 GeV: Central Collisions

7



The correlation due to Momentum conservation is flat in eta.

Fig. 121:

## Effect on event plane resolution

8

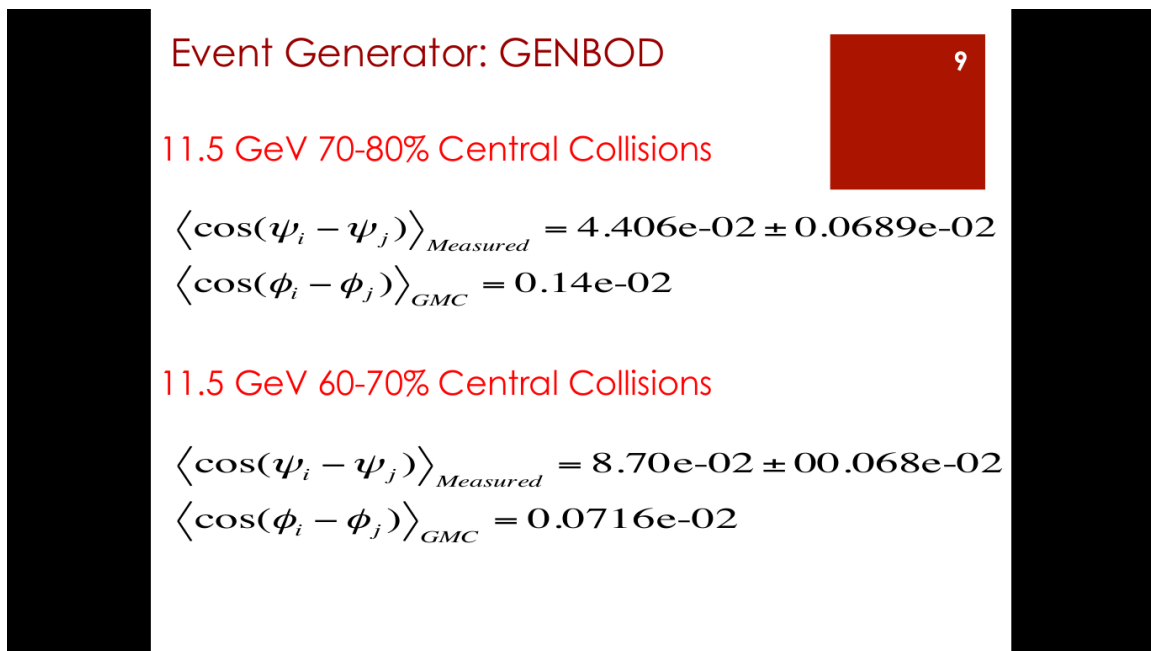
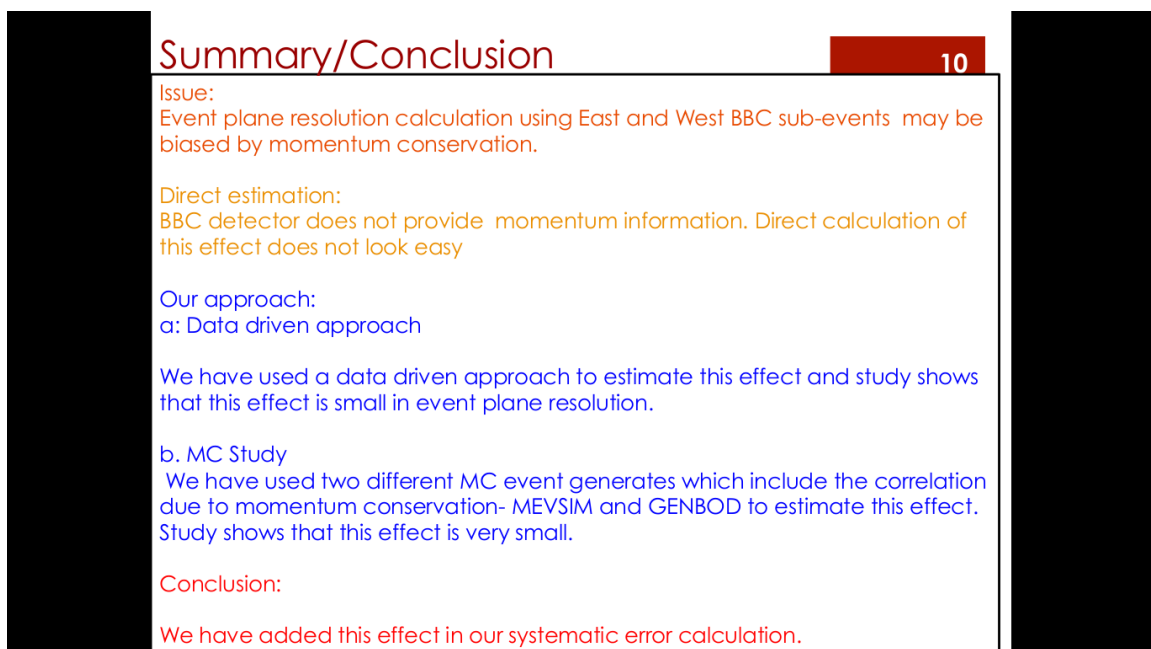
For 39 GeV, Central Collisions

$$\langle \cos(\psi_i - \psi_j) \rangle_{\text{Measured}} = 4.73e-03 \pm 0.67e-03$$

$$\langle \cos(\phi_i - \phi_j) \rangle_{\text{GMC}} = 0.31e-03$$

This effect is smaller than statistical error.

Fig. 122:

**Fig. 123:****Fig. 124:**

## 4.5 Feeddown

There is uncertainty with our estimation of the yields for particles that feeddown into Lambdas. The  
 2010 feeddown is discussed in detail in section 3.5. Initially yield discrepancies between UrQMD and THERMUS made our systematic errors. Now we are using a very explicitly thermal approach. We want to get a sense of how sensitive to the results are to the specifics of the THERMUS yields. Additional details of this study can be found at <https://drupal.star.bnl.gov/STAR/blog/iupsal/bulkcorr-presentation-feed-down-systematics>.

2015 For this study we will vary the  $f_{R\Lambda}$  (fractions of Lambdas coming from a given source) for each source species (primary Lambda ( $\Lambda'$ ),  $\Sigma^0$ ,  $\Xi^0$ ,  $\Xi^-$ ,  $\Sigma^{*-}$ ,  $\Sigma^{*0}$ ,  $\Sigma^{*+}$ , other) in accordance with the procedure in sec. 3.5. Naturally the same is done in parallel for the sources of  $\bar{\Lambda}$ . The variation is going to be from sampling a Gaussian distribution centered around 0, so

$$f_R = f_R^{\text{THERMUS}} (1 + \text{TRandom3.Gaus}(0, \sigma)) \quad (26)$$

2020 for some  $\sigma$  where  $\text{Gaus}(0, \sigma)$  is a function of a TRandom3 whereby a gaussian of width  $\sigma$  centered around 0 is sampled. Naturally once this has been done for all  $f_R$  one must renormalize them so that they are fractions again. There is always a finite chance that that  $f_R$  will be negative. To correct for this if( $f_R == 0$ ) $f_R = 0$ . Such a sampling is done many ( $10^7$ ) times to get a statistically significant value and repeated for different choices of  $\sigma$ . It has been found that the width of the  $\hbar\omega/k_B T$  or  $\mu_N B/k_B T$  distributions when fit by a gaussian of width  $\rho$  are proportional to  $\sigma$ , so that  $\rho_{N,\omega} \approx N \cdot \rho_\omega$ . This scaling seemed consistent  
 2025 event to fairly large  $\sigma$  (e.g.  $\sigma = 0.5$ ) where zeroing out  $f_{R\Lambda}$  could lead to more asymmetric vortical or magnetic distributions. The width of these distributions for different values of  $\sigma$  can be seen

The last step is to actually fit what is shown in figures 4.5 and 4.5. The width of the fit (discussed above as  $\rho$ ) is to be the systematic error from feed down for the final results. What is evident from the aforementioned figures is that the variation falls well within the statistical limits of the measurement, so  
 2030 this shouldn't be a dominant error. We have a fair level of trust in THERMUS so we use the  $\rho$  found for the  $\sigma = 0.2$  curve which we think should include any reasonably different particle production model. This fit can be seen below, the results of  $\rho$  numerically for  $\hbar\omega/k_B T$  or  $\mu_N B/k_B T$  as percentages in order of increasing  $\sqrt{s_{NN}}$  are:

```
float RhoVorticity[8] = {1.30, 0.19, 0.28, 0.18, 0.14, 0.12, 0.19, 0.18};  

2035 float RhoMagnetic[8] = {1.70, 0.29, 0.42, 0.28, 0.23, 0.18, 0.32, 0.29};
```

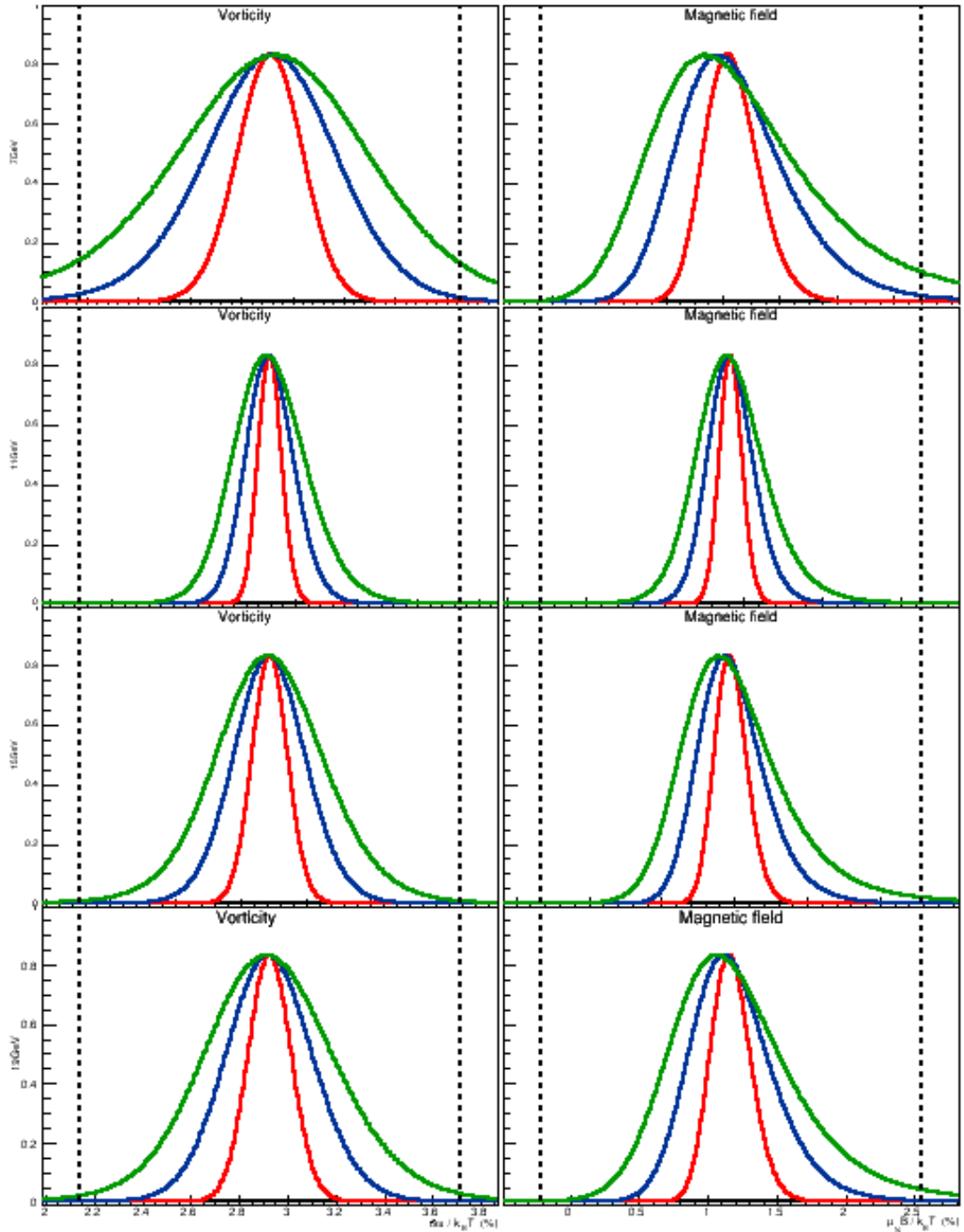


**Fig. 125:** Feed down variation away from THERMUS for low  $\sqrt{s_{NN}}$  with some width  $\sigma$ . Different widths can be seen in the colors for  $\sigma = 0.1$ ,  $\sigma = 0.2$ , and  $\sigma = 0.3$ . The left column depicts  $\hbar\omega/k_B T$  as  $\sqrt{s_{NN}}$  goes down and the right depicts  $\hbar\omega/k_B T$  or  $\mu_N B/k_B T$  (both are as percentages). The rows are, in descending order, for  $\sqrt{s_{NN}} = 7.7 \text{ GeV}$ ,  $\sqrt{s_{NN}} = 11.5 \text{ GeV}$ ,  $\sqrt{s_{NN}} = 14.5 \text{ GeV}$ , and  $\sqrt{s_{NN}} = 19.6 \text{ GeV}$ . The dashed lines represent the statistical errors of the measure for nominal  $f_R$ s. The y axis shows counts with the top bin normalized to 1/1.2, while the x axis is vorticity or magnetic field centered about the nominal measure.

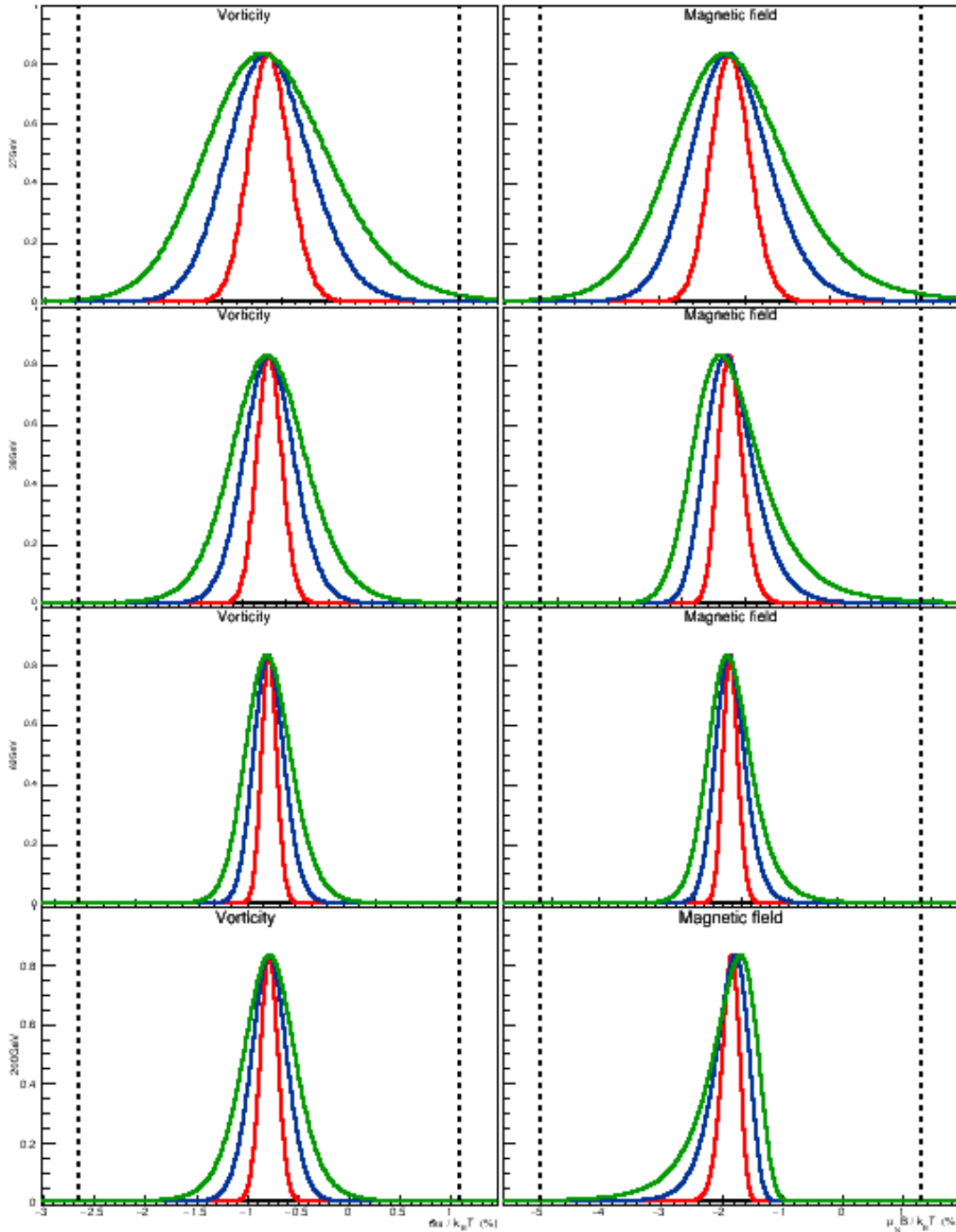


**Fig. 126:** Feed down variation away from THERMUS for high  $\sqrt{s_{\text{NN}}}$  with some width  $\sigma$ . Different widths can be seen in the colors for  $\sigma = 0.1$ ,  $\sigma = 0.2$ , and  $\sigma = 0.3$ . The left column depicts  $\hbar\omega/k_B T$  as  $\sqrt{s_{\text{NN}}}$  goes down and the right depicts  $\hbar\omega/k_B T$  or  $\mu_N B/k_B T$  (both are as percentages). The rows are, in descending order, for  $\sqrt{s_{\text{NN}}} = 27\text{GeV}$ ,  $\sqrt{s_{\text{NN}}} = 39\text{GeV}$ ,  $\sqrt{s_{\text{NN}}} = 62\text{GeV}$ , and  $\sqrt{s_{\text{NN}}} = 200\text{GeV}$ . The dashed lines represent the statistical errors of the measure for nominal  $f_{RS}$ . The y axis shows counts with the top bin normalized to 1/1.2, while the x axis is vorticity or magnetic field centered about the nominal measure.

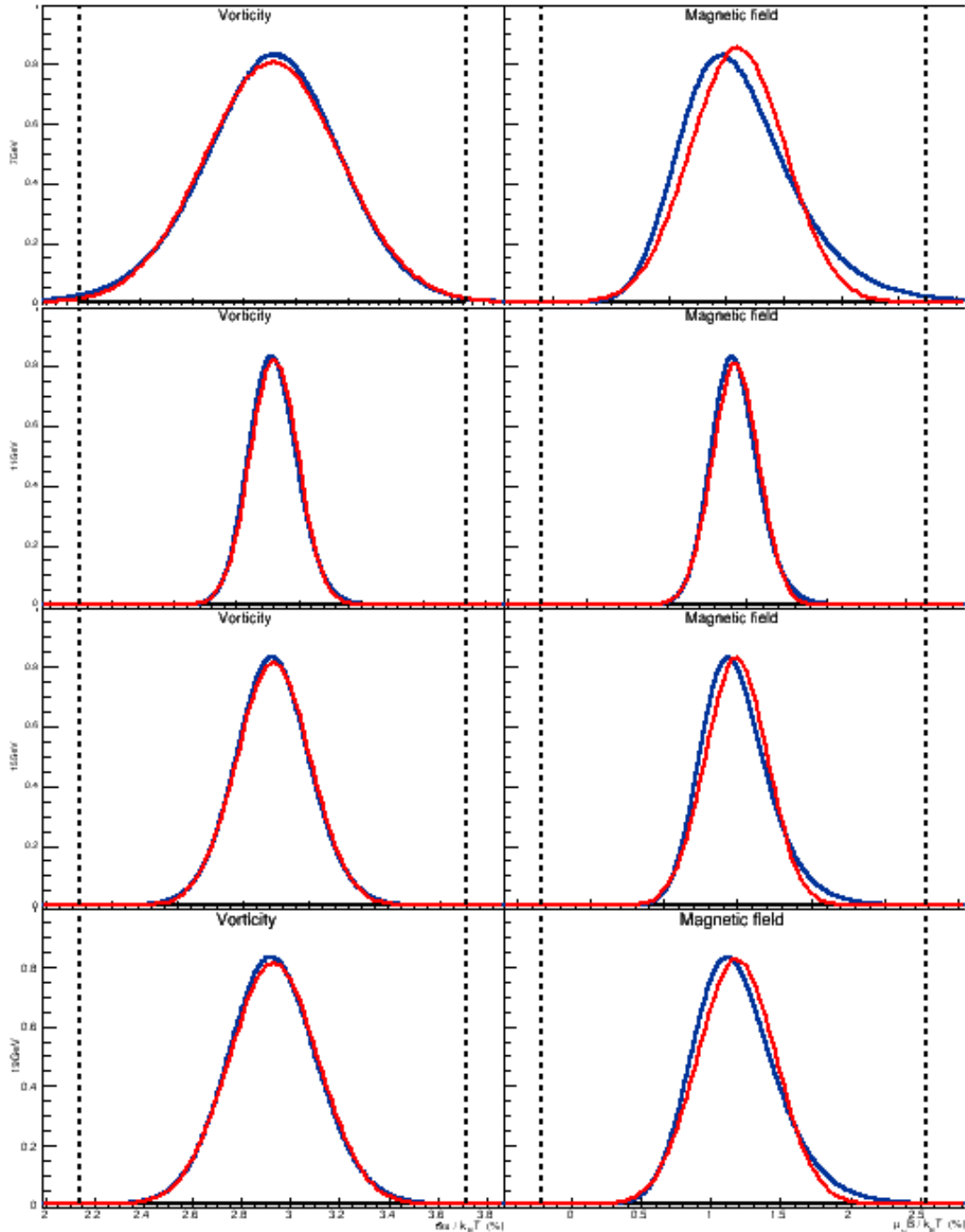


**Fig. 127:** Gaussian fits (shown in red) of the feed down variation away from THERMUS for low  $\sqrt{s_{NN}}$  with  $\sigma = 0.2$ . The left column depicts  $\hbar\omega/k_B T$  as  $\sqrt{s_{NN}}$  goes down and the right depicts  $\hbar\omega/k_B T$  or  $\mu_N B/k_B T$  (both are as percentages). The rows are, in decending order, for  $\sqrt{s_{NN}} = 7.7\text{GeV}$ ,  $\sqrt{s_{NN}} = 11.5\text{GeV}$ ,  $\sqrt{s_{NN}} = 14.5\text{GeV}$ , and  $\sqrt{s_{NN}} = 19.6\text{GeV}$ . The dashed lines represent the statistical errors of the measure for nominal  $f_{RS}$ . The y axis shows counts with the top bin normalized to 1/1.2, while the x axis is vorticity or magnetic field centered about the nominal measure.

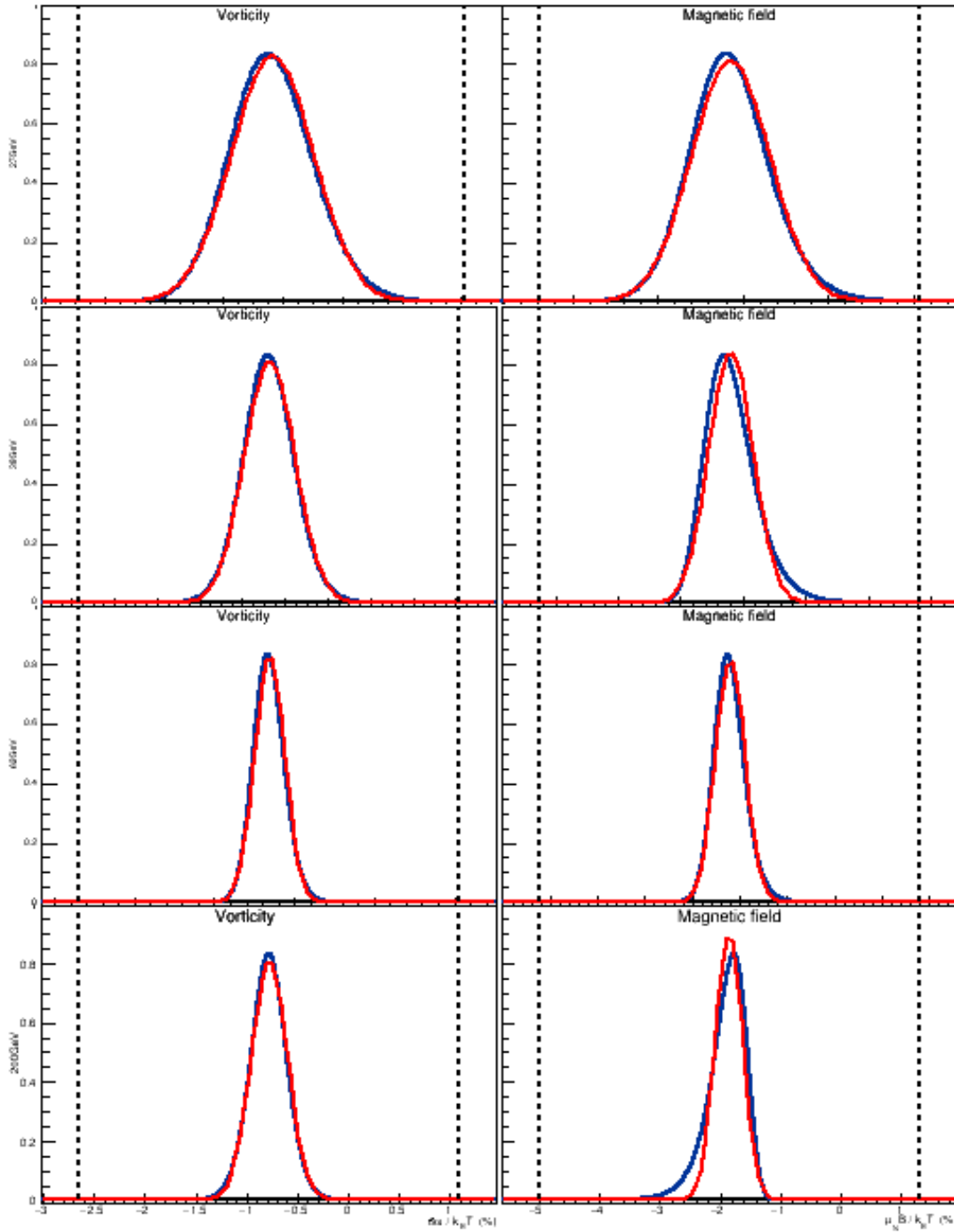


**Fig. 128:** Gaussian fits (shown in red) of the feed down variation away from THERMUS for high  $\sqrt{s_{NN}}$  with  $\sigma = 0.2$ . The left column depicts  $\hbar\omega/k_B T$  as  $\sqrt{s_{NN}}$  goes down and the right depicts  $\hbar\omega/k_B T$  or  $\mu_N B/k_B T$  (both are as percentages). The rows are, in descending order, for  $\sqrt{s_{NN}} = 27\text{GeV}$ ,  $\sqrt{s_{NN}} = 39\text{GeV}$ ,  $\sqrt{s_{NN}} = 62\text{GeV}$ , and  $\sqrt{s_{NN}} = 200\text{GeV}$ . The dashed lines represent the statistical errors of the measure for nominal  $f_{RS}$ . The y axis shows counts with the top bin normalized to 1/1.2, while the x axis is vorticity or magnetic field centered about the nominal measure.

## 5 Systematic Dependencies

In this section we intend to present any systematic dependency  $\langle \sin(\Psi_1 - \phi_\Lambda^*) \rangle$  has on various quantities of interest. It has been posited that the measure may increase for Lambdas emitted in plane and at large momentum. It has also been claimed that this will not depend greatly on rapidity. There certainly should be some centrality dependence to the result as it depends on system angular momentum and thermalization. Because the analysis is so statistics limited this has become more a consistency check than a check for real dependence. The results are all corrected only for resolution. Higher order corrections (mass purity) are not taken into account. Additionally the results are not scaled by the factor of  $8/(\pi\alpha)$ .

Some of the figures in here are really of  $\S_y \equiv \vec{S} \cdot \hat{L}$ , that is with a boosted spin vector. In practice this result is nearly identical to the polarization measure. It is reasonable to expect they would have the same systematic dependencies. If these are still in the document I do intend to replace them at some point.

### 5.1 Centrality

This section is to show the centrality dependence of the signal. Many centrality windows are shown. The most peripheral collisions have the largest angular momentum but what is most important is the amount of angular momentum that gets transferred to the fireball at mid-rapidity. Additionally one must consider how thermalized the system is to know how the particle spin gets distributed. Stopping and thermalization mechanics are complicated so the dependence on centrality may well be difficult to predict. As a bit of a compromise one might expect the largest signal for mid-central collisions.

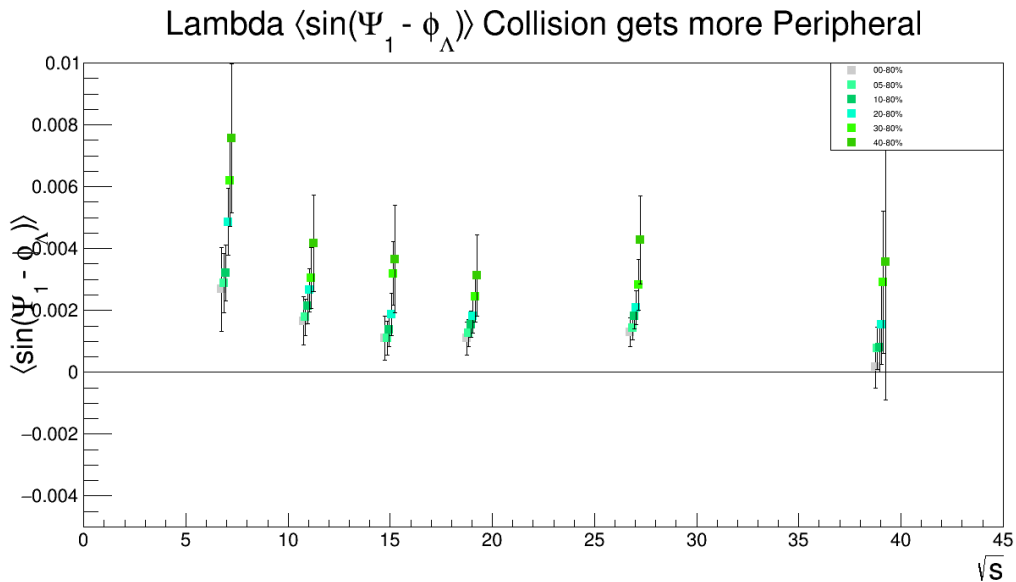


**Fig. 129:**  $\langle \sin(\Psi_1 - \phi_\Lambda^*) \rangle$  as the collision gets more peripheral

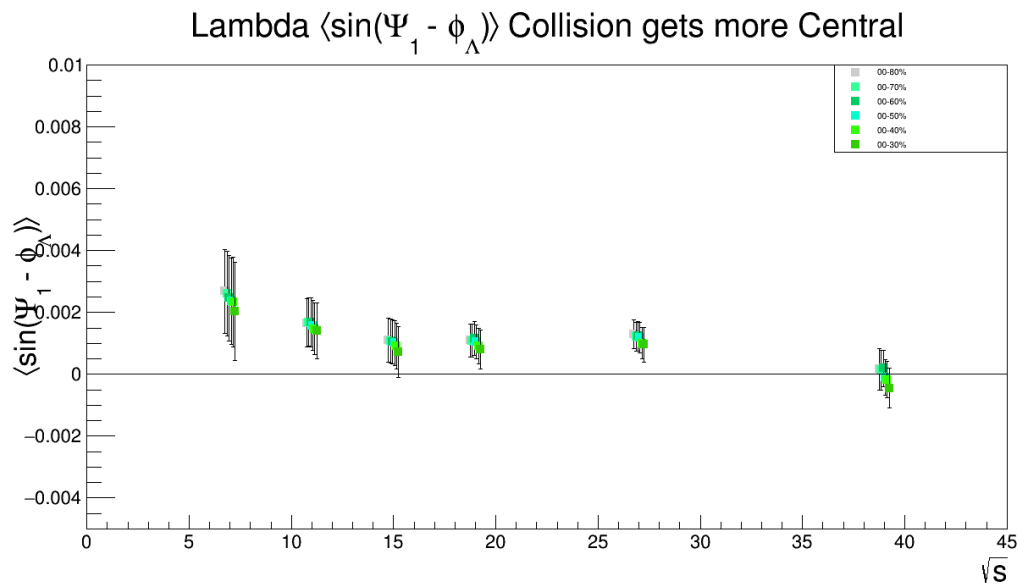


**Fig. 130:**  $\langle \sin(\Psi_1 - \phi_\Lambda^*) \rangle$  as the collision gets more central

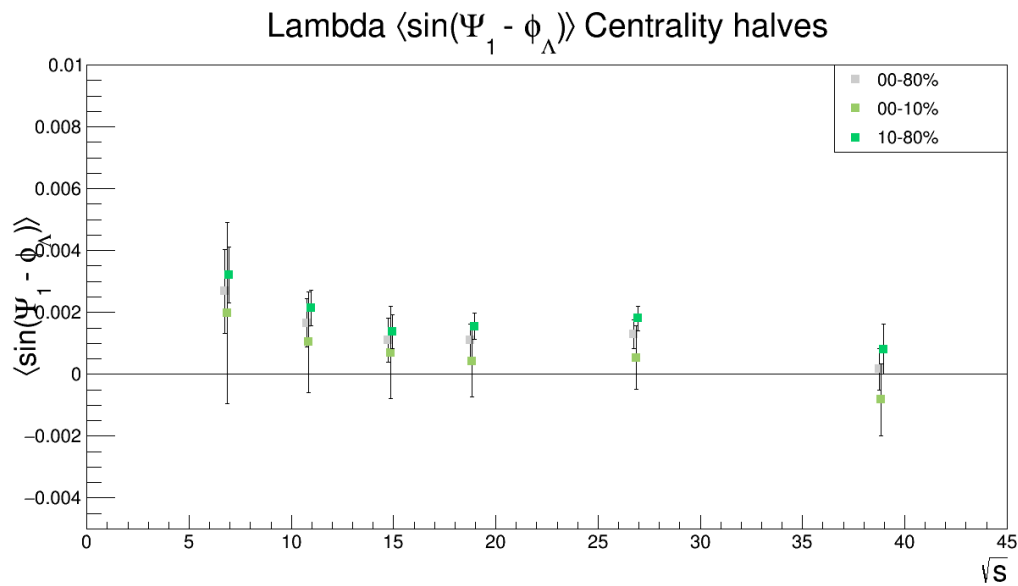


**Fig. 131:**  $\langle \sin(\Psi_1 - \phi_\Lambda^*) \rangle$  for rough halves of centrality by yield

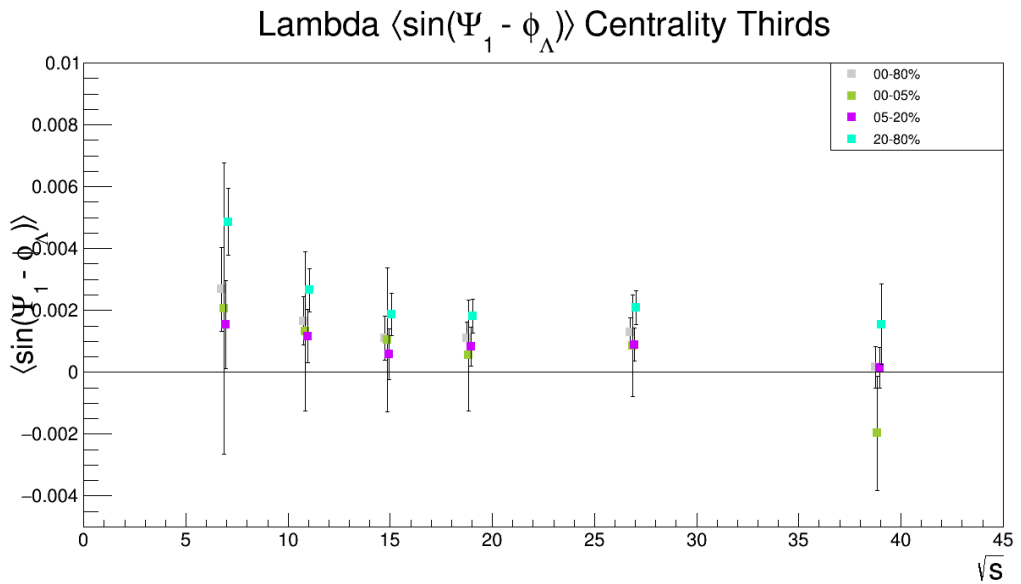


**Fig. 132:**  $\langle \sin(\Psi_1 - \phi_{\Lambda}^*) \rangle$  for rough thirds of centrality by yield

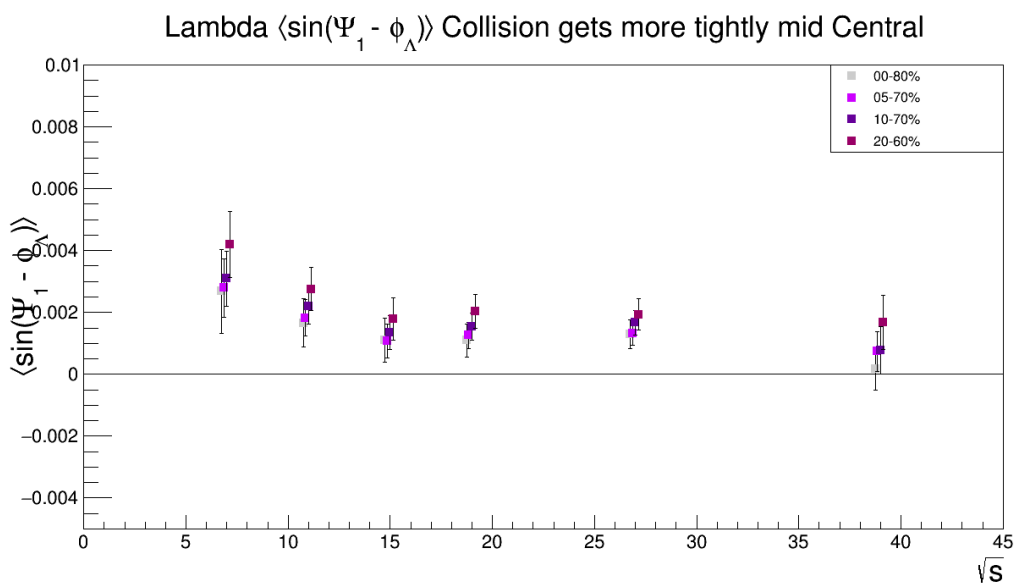


**Fig. 133:**  $\langle \sin(\Psi_1 - \phi_{\Lambda}^*) \rangle$  as collisions get more mid-central

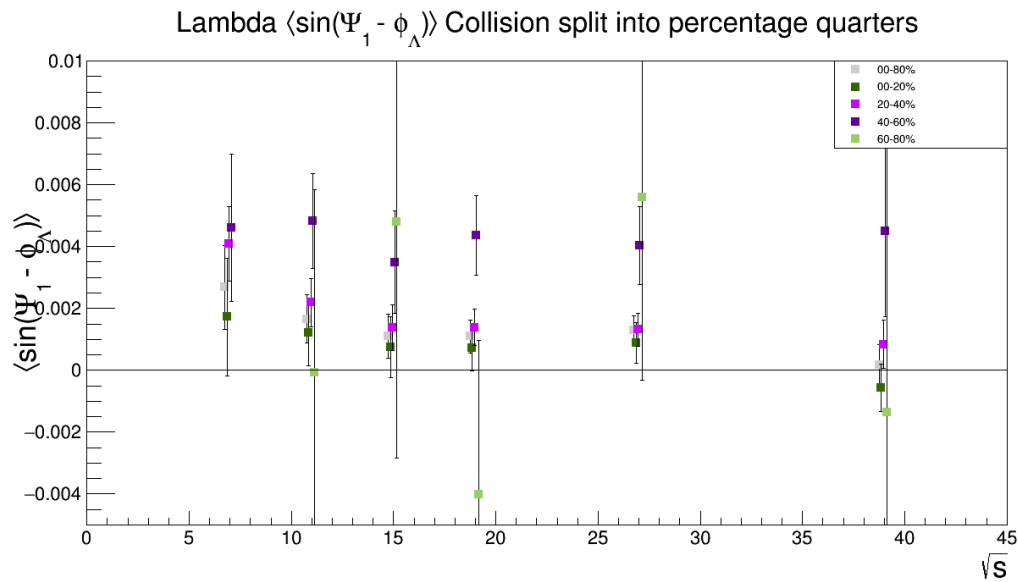


**Fig. 134:**  $\langle \sin(\Psi_1 - \phi_{\Lambda}^*) \rangle$  for bins of 20% centrality

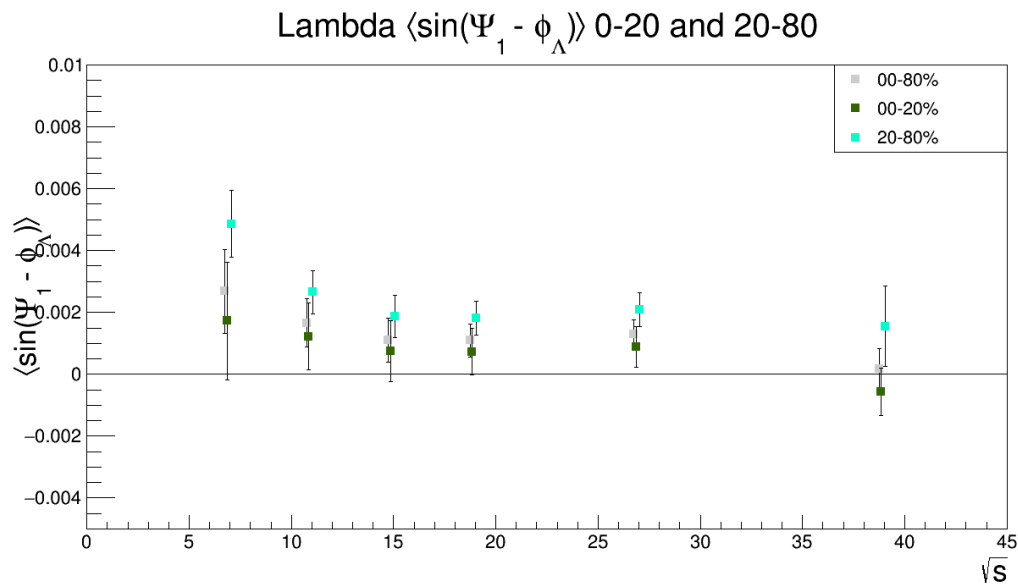


**Fig. 135:**  $\langle \sin(\Psi_1 - \phi_{\Lambda}^*) \rangle$  for 0-20% and 20-80% centrality

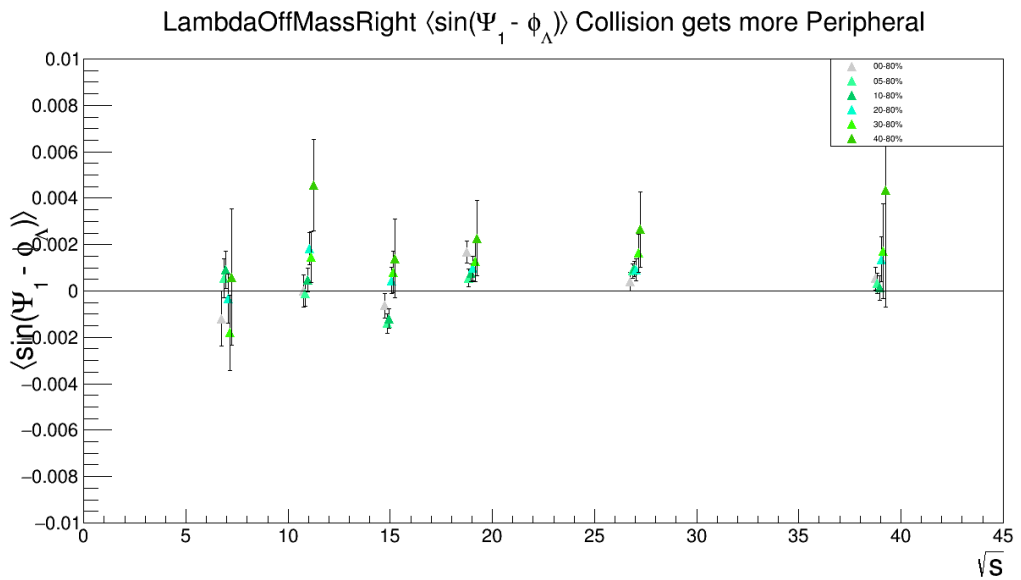


**Fig. 136:**  $\langle \sin(\Psi_1 - \phi_\Lambda^*) \rangle$  right of mass peak ( $m_{\text{inv}} > m_\Lambda$ ) as the collision gets more peripheral

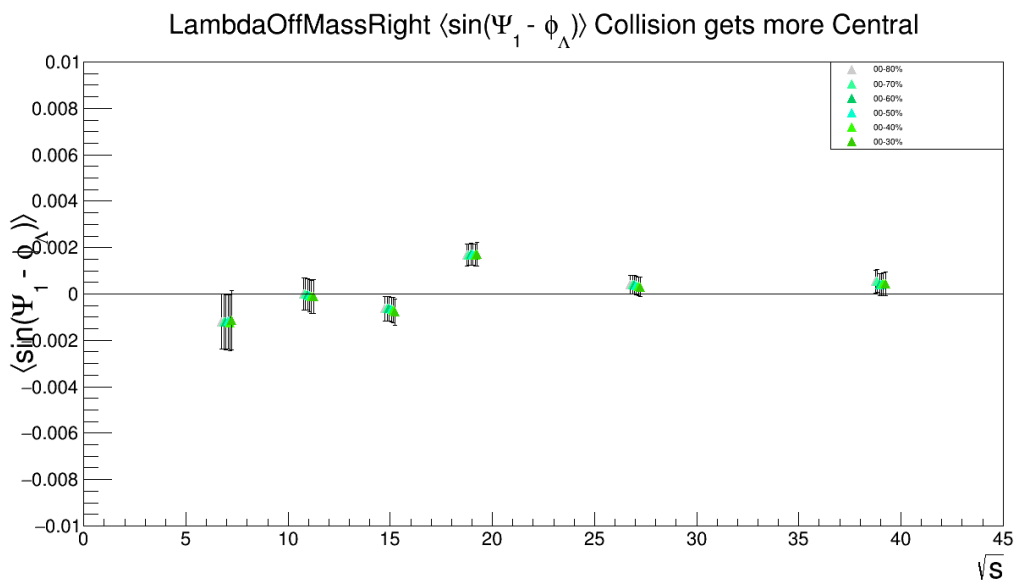


**Fig. 137:**  $\langle \sin(\Psi_1 - \phi_\Lambda^*) \rangle$  right of mass peak ( $m_{\text{inv}} > m_\Lambda$ ) as the collision gets more central

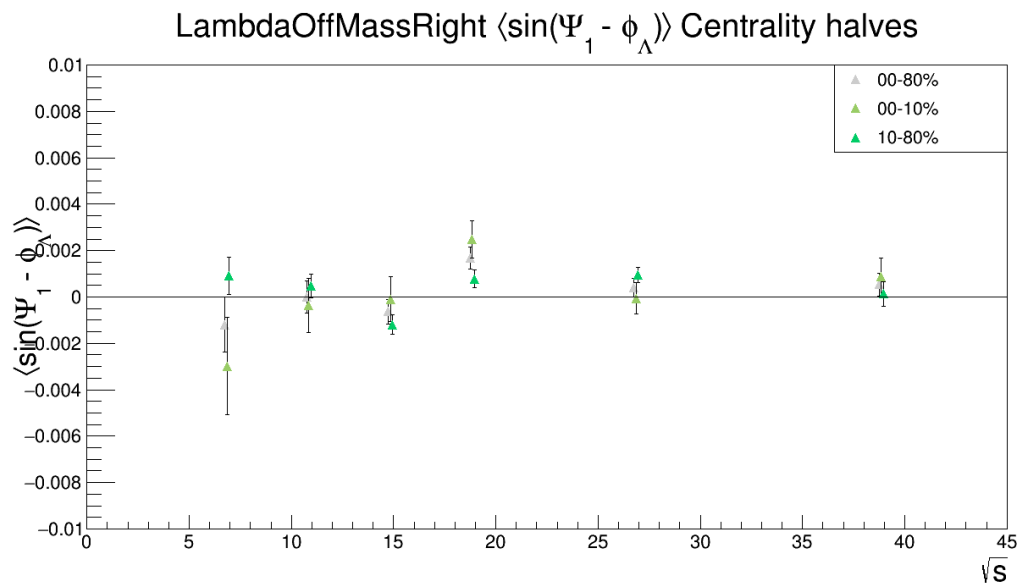


**Fig. 138:**  $\langle \sin(\Psi_1 - \phi_\Lambda^*) \rangle$  right of mass peak ( $m_{\text{inv}} > m_\Lambda$ ) for rough halves of centrality by yield

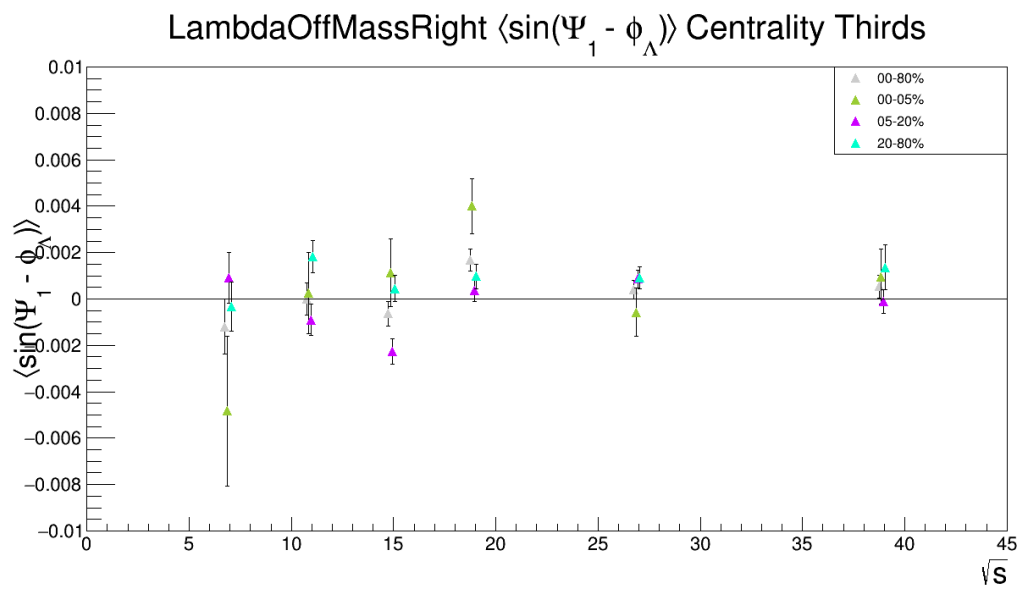


**Fig. 139:**  $\langle \sin(\Psi_1 - \phi_\Lambda^*) \rangle$  right of mass peak ( $m_{\text{inv}} > m_\Lambda$ ) for rough thirds of centrality by yield

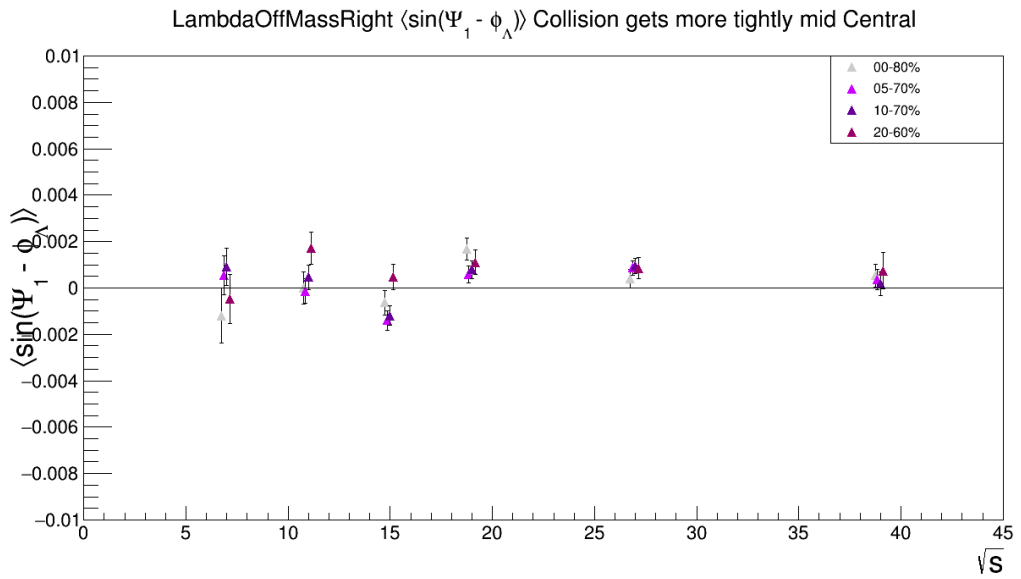


**Fig. 140:**  $\langle \sin(\Psi_1 - \phi_\Lambda^*) \rangle$  right of mass peak ( $m_{\text{inv}} > m_\Lambda$ ) as collisions get more mid-central

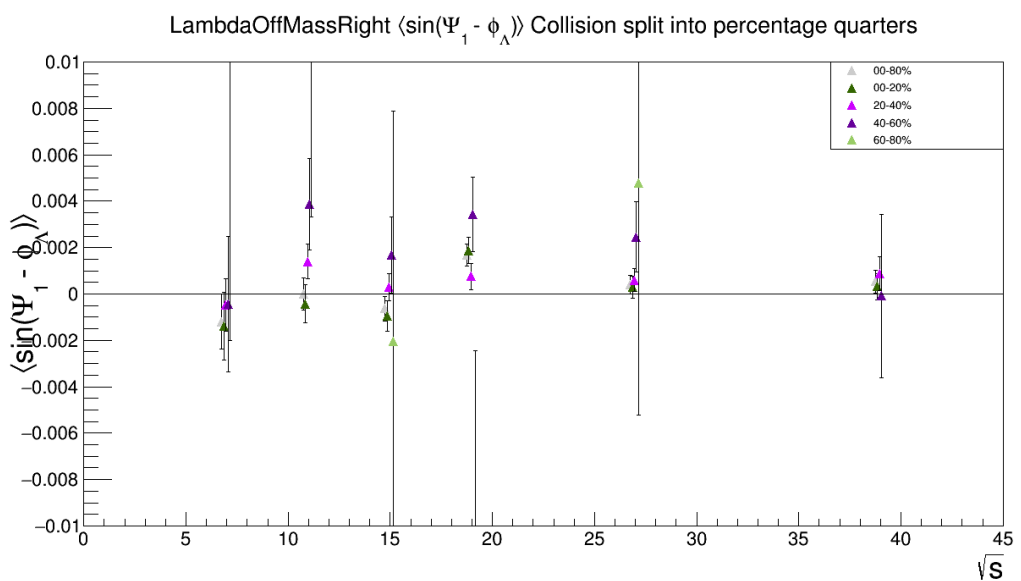


**Fig. 141:**  $\langle \sin(\Psi_1 - \phi_\Lambda^*) \rangle$  right of mass peak ( $m_{\text{inv}} > m_\Lambda$ ) for bins of 20% centrality

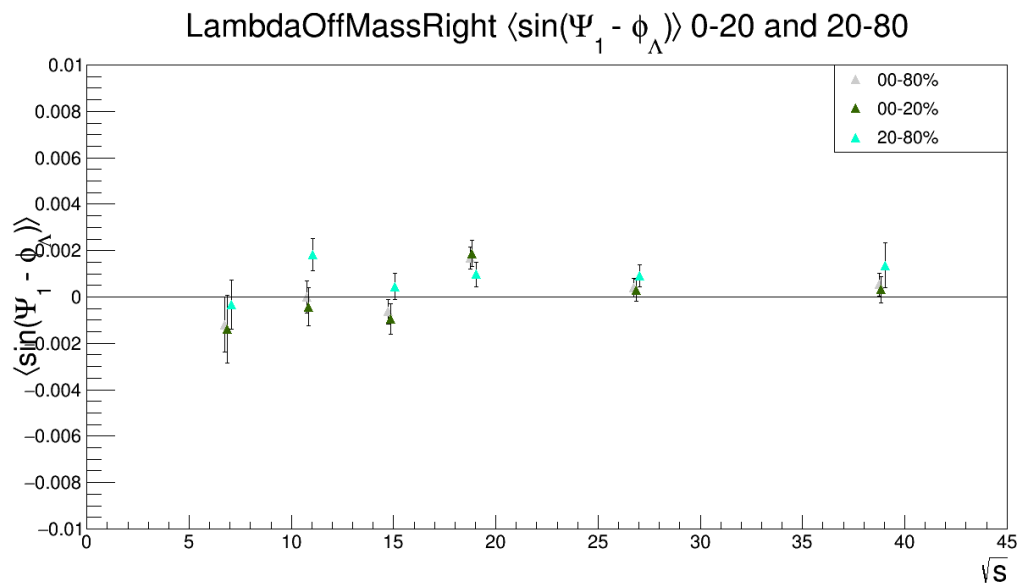


**Fig. 142:**  $\langle \sin(\Psi_1 - \phi_{\Lambda}^*) \rangle$  right of mass peak ( $m_{\text{inv}} > m_{\Lambda}$ ) for 0-20% and 20-80% centrality

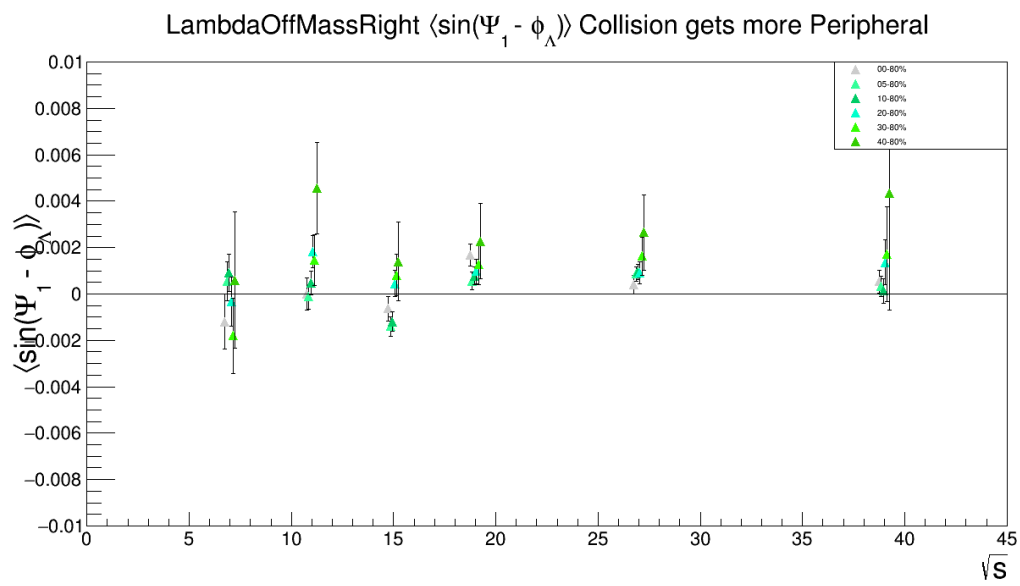


**Fig. 143:**  $\langle \sin(\Psi_1 - \phi_{\Lambda}^*) \rangle$  left of mass peak ( $m_{\text{inv}} < m_{\Lambda}$ ) as the collision gets more peripheral

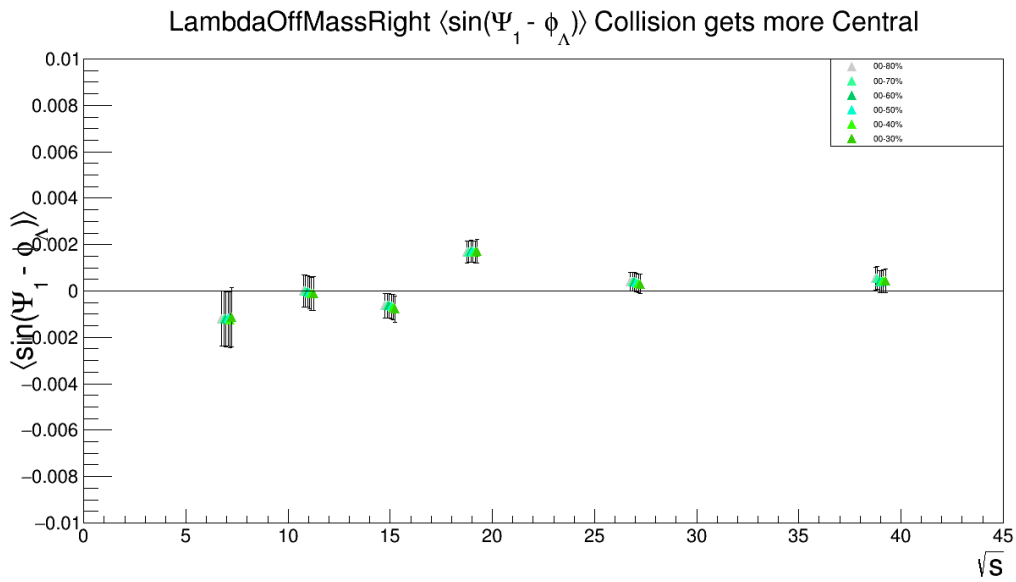


**Fig. 144:**  $\langle \sin(\Psi_1 - \phi_\Lambda^*) \rangle$  left of mass peak ( $m_{\text{inv}} < m_\Lambda$ ) as the collision gets more central

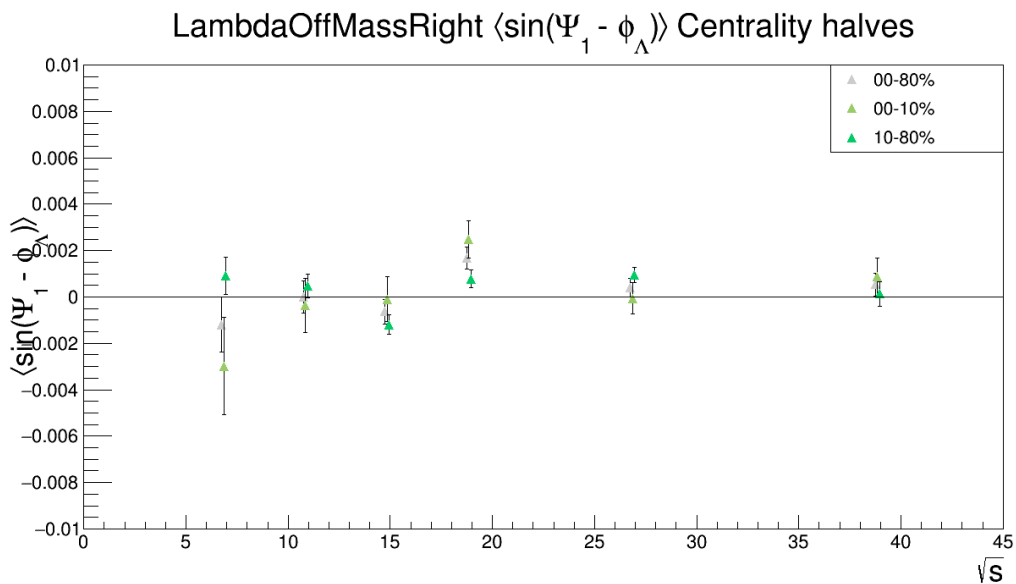


**Fig. 145:**  $\langle \sin(\Psi_1 - \phi_\Lambda^*) \rangle$  left of mass peak ( $m_{\text{inv}} < m_\Lambda$ ) for rough halves of centrality by yield

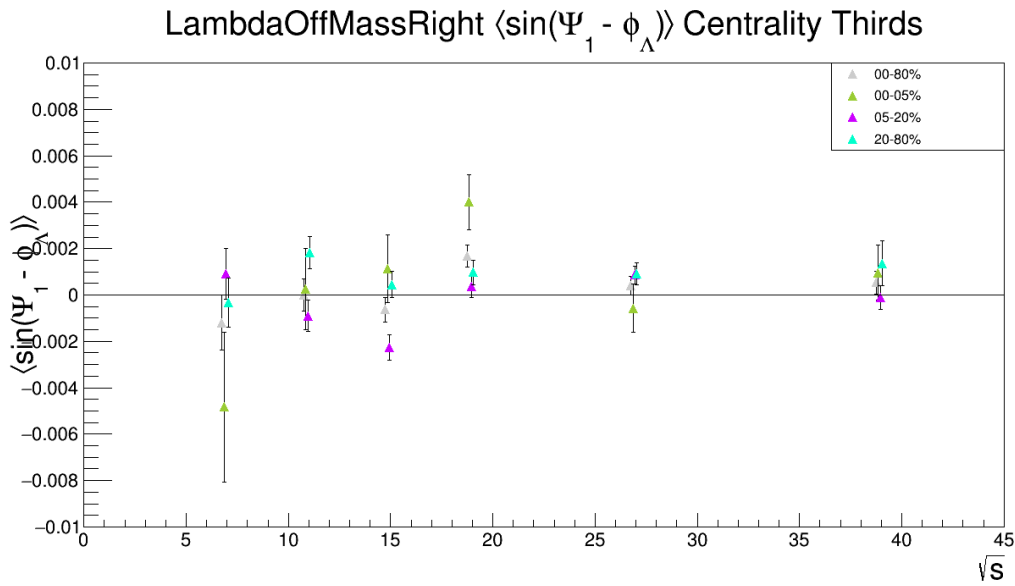


**Fig. 146:**  $\langle \sin(\Psi_1 - \phi_\Lambda^*) \rangle$  left of mass peak ( $m_{\text{inv}} < m_\Lambda$ ) for rough thirds of centrality by yield

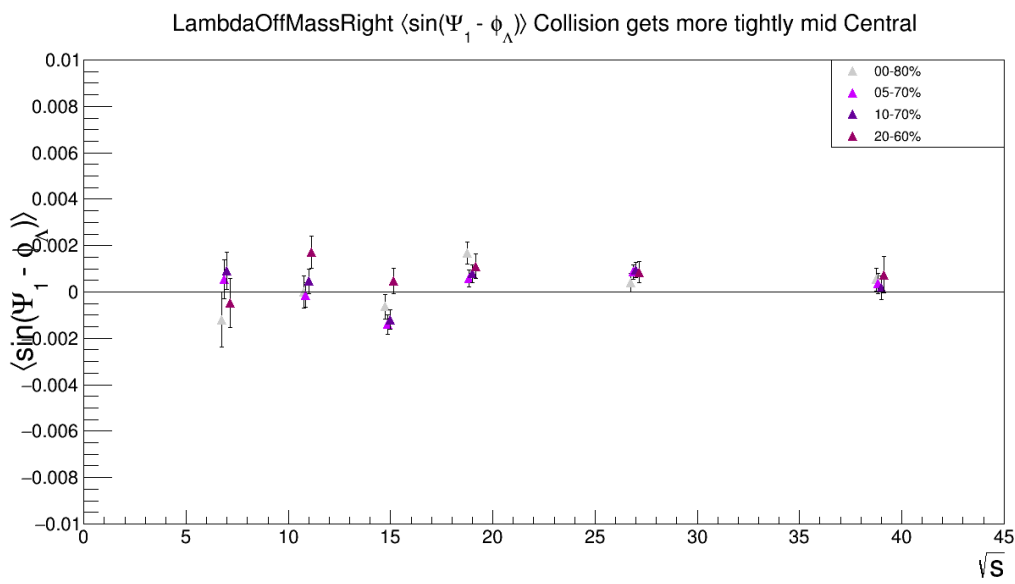


**Fig. 147:**  $\langle \sin(\Psi_1 - \phi_\Lambda^*) \rangle$  left of mass peak ( $m_{\text{inv}} < m_\Lambda$ ) as collisions get more mid-central

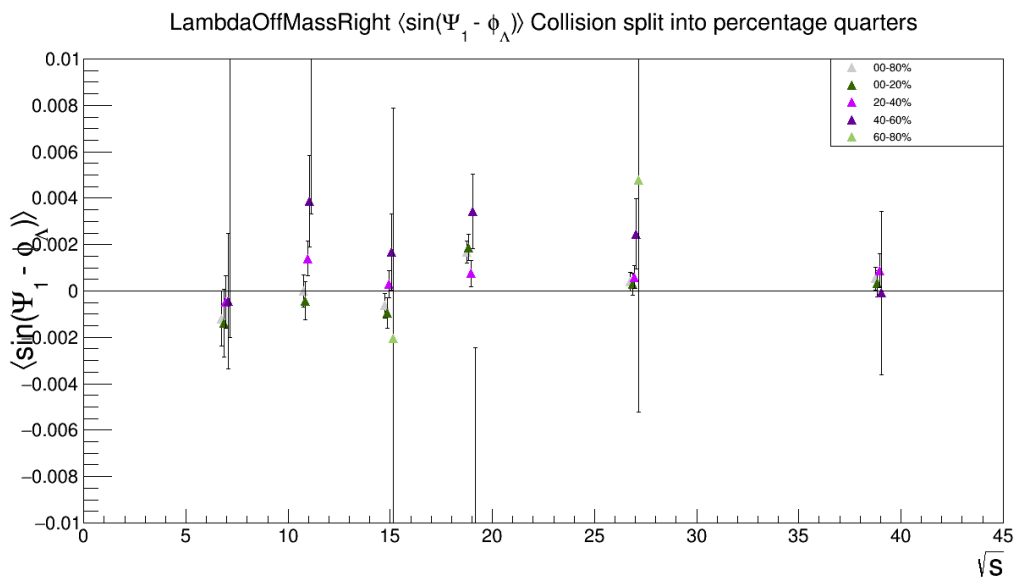


**Fig. 148:**  $\langle \sin(\Psi_1 - \phi_\Lambda^*) \rangle$  left of mass peak ( $m_{\text{inv}} < m_\Lambda$ ) for bins of 20% centrality

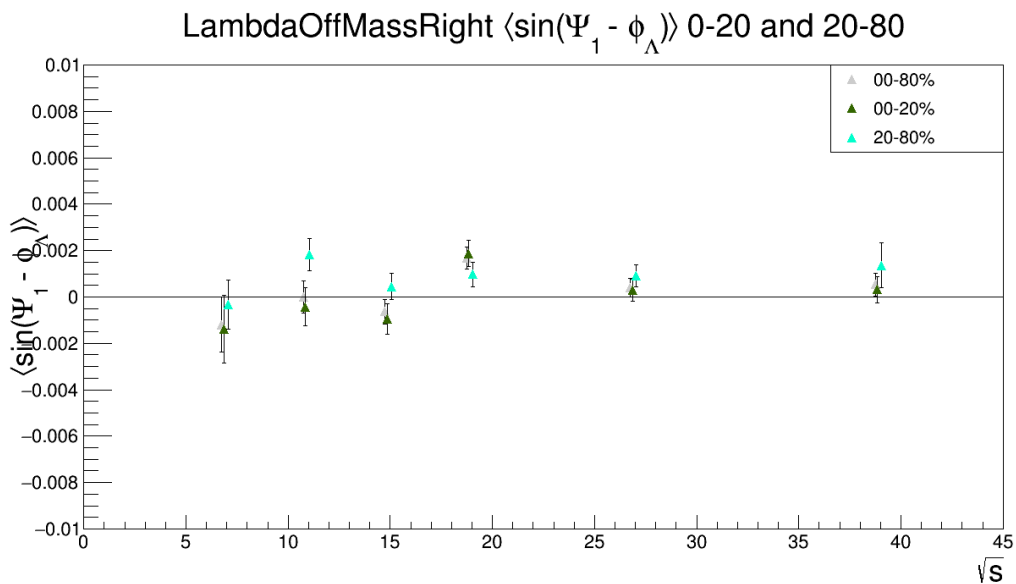


**Fig. 149:**  $\langle \sin(\Psi_1 - \phi_\Lambda^*) \rangle$  left of mass peak ( $m_{\text{inv}} < m_\Lambda$ ) for 0-20% and 20-80% centrality

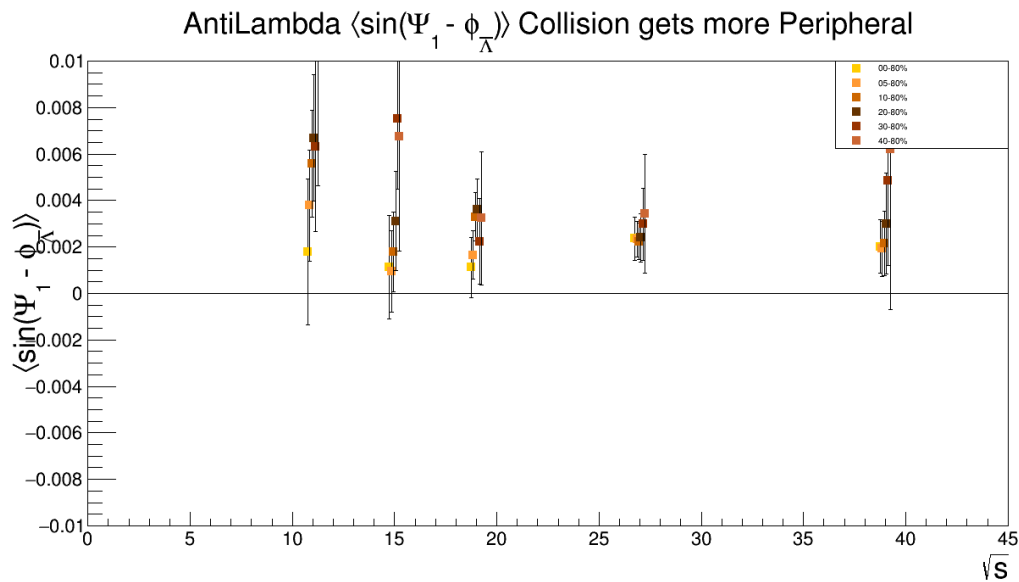


**Fig. 150:**  $\langle \sin(\Psi_1 - \phi_{\bar{\Lambda}}^*) \rangle$  as the collision gets more peripheral

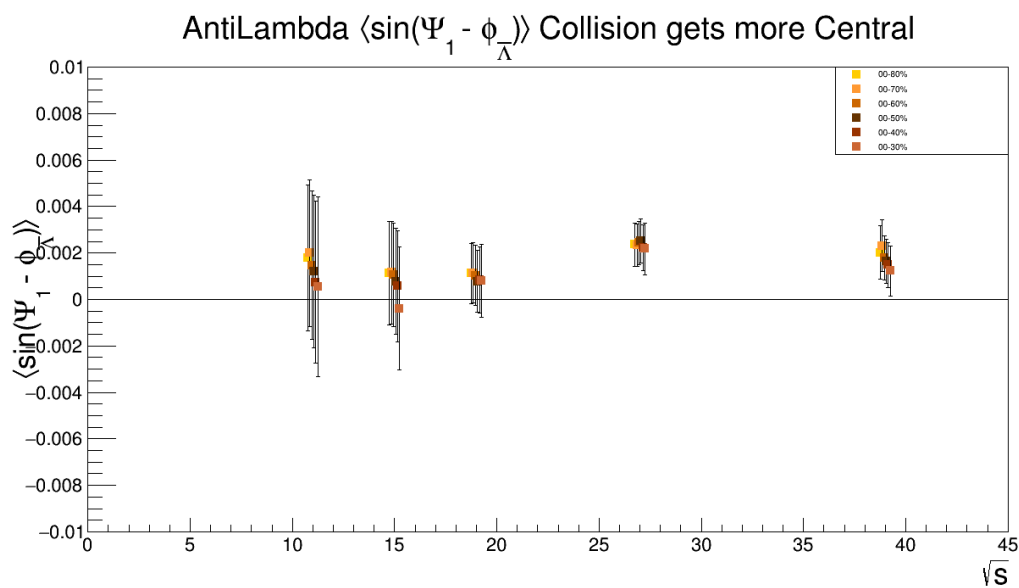


**Fig. 151:**  $\langle \sin(\Psi_1 - \phi_{\bar{\Lambda}}^*) \rangle$  as the collision gets more central

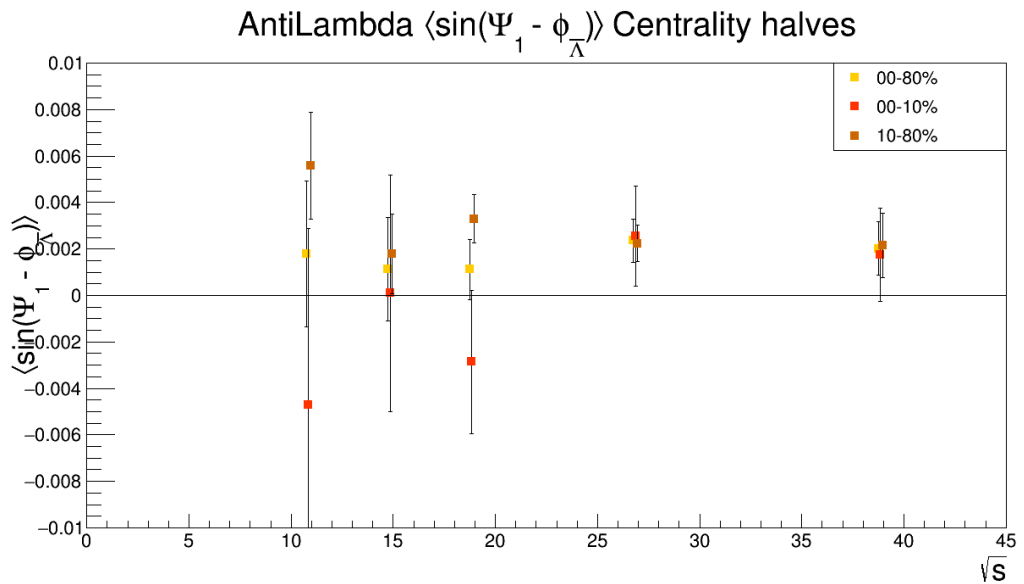


**Fig. 152:**  $\langle \sin(\Psi_1 - \phi_{\bar{\Lambda}}^*) \rangle$  for rough halves of centrality by yield

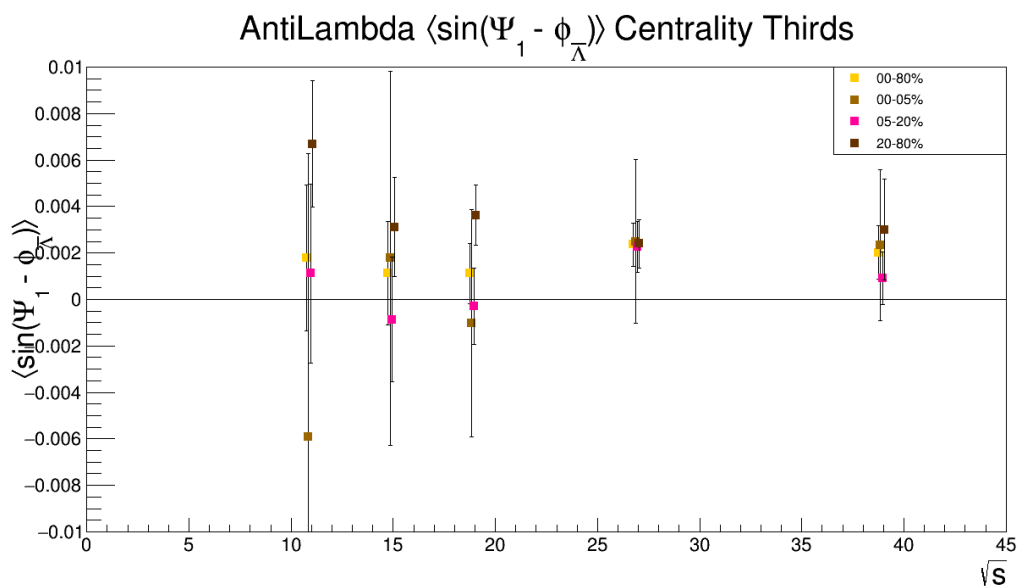


**Fig. 153:**  $\langle \sin(\Psi_1 - \phi_{\bar{\Lambda}}^*) \rangle$  for rough thirds of centrality by yield

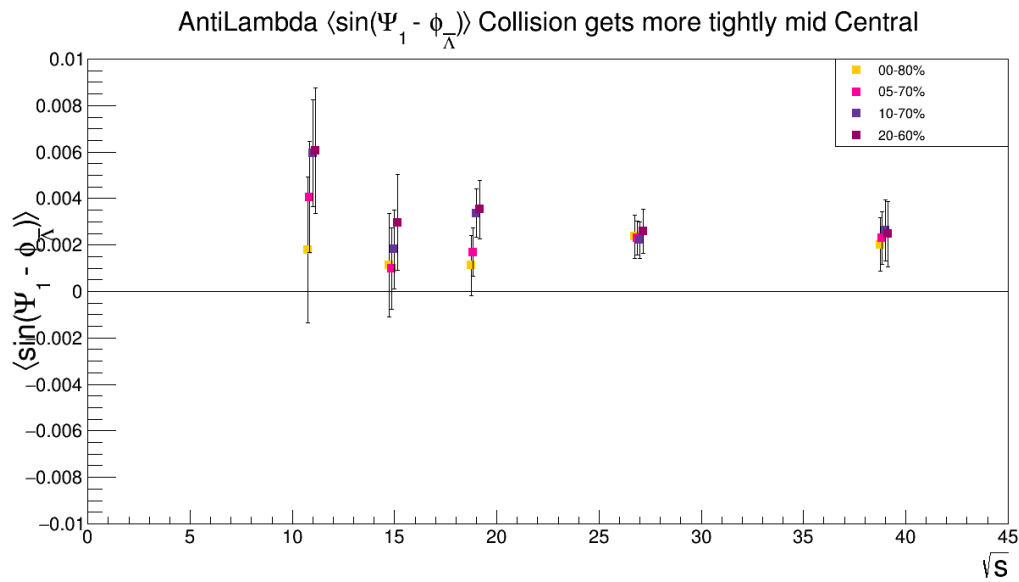


**Fig. 154:**  $\langle \sin(\Psi_1 - \phi_{\bar{\Lambda}}^*) \rangle$  as collisions get more mid-central

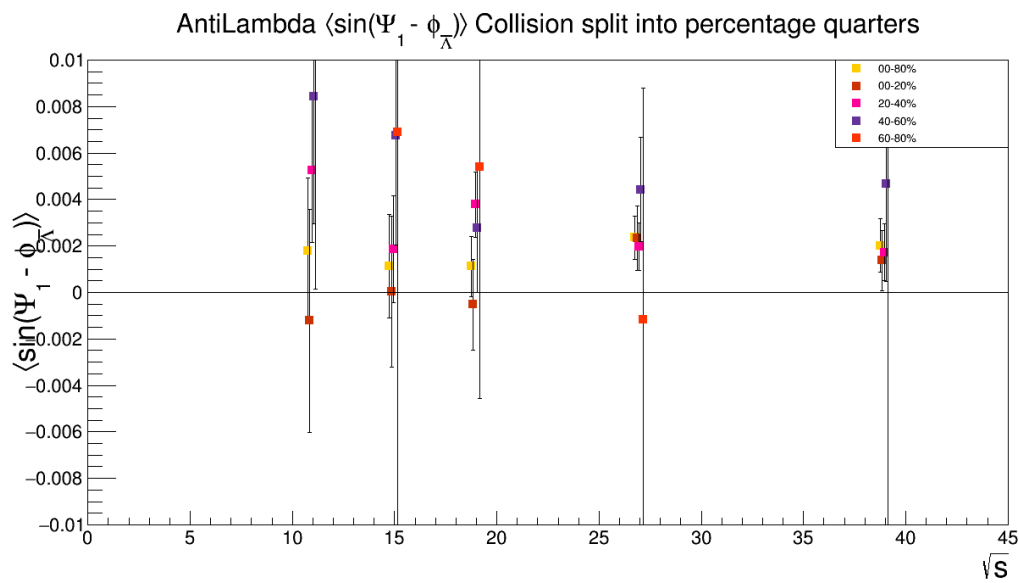


**Fig. 155:**  $\langle \sin(\Psi_1 - \phi_{\bar{\Lambda}}^*) \rangle$  for bins of 20% centrality

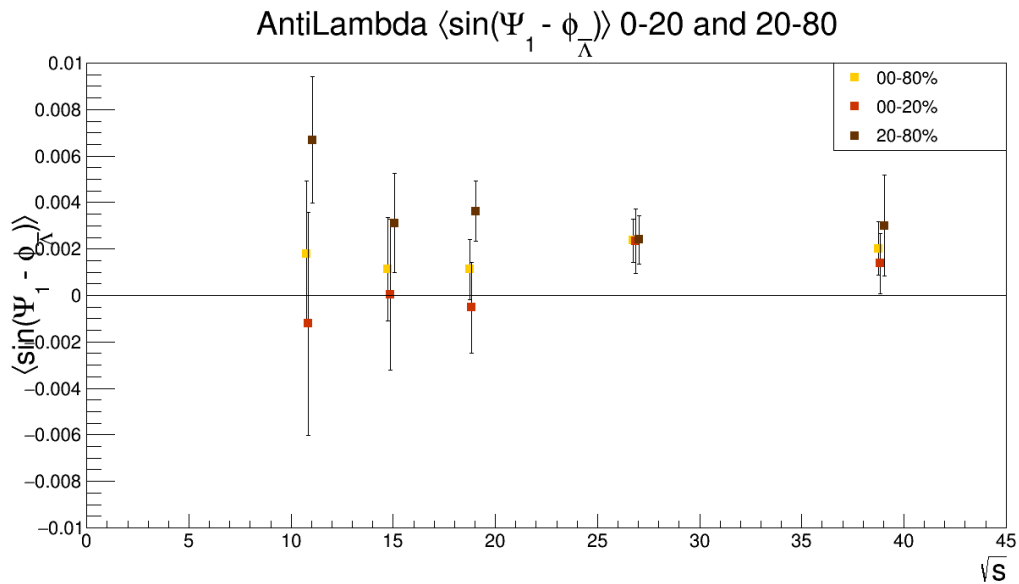


**Fig. 156:**  $\langle \sin(\Psi_1 - \phi_{\bar{\Lambda}}^*) \rangle$  for 0-20% and 20-80% centrality

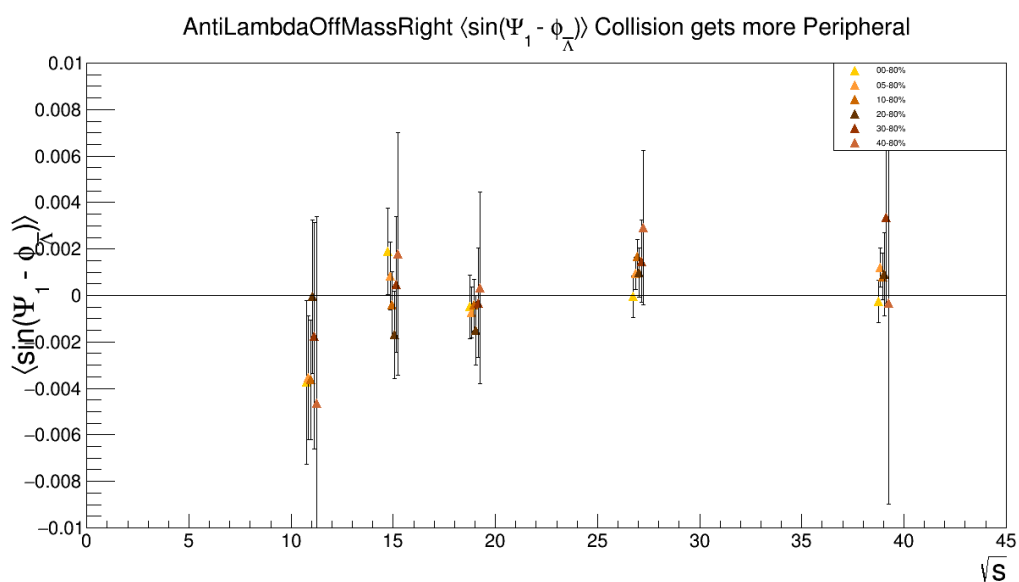


**Fig. 157:**  $\langle \sin(\Psi_1 - \phi_{\bar{\Lambda}}^*) \rangle$  right of mass peak ( $m_{\text{inv}} > m_{\bar{\Lambda}}$ ) as the collision gets more peripheral

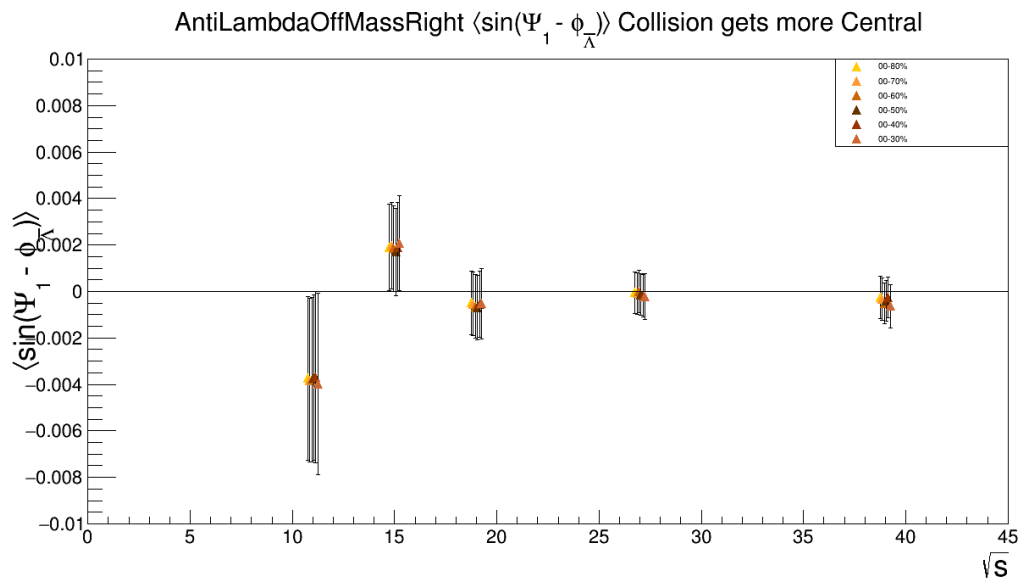


**Fig. 158:**  $\langle \sin(\Psi_1 - \phi_{\bar{\Lambda}}^*) \rangle$  right of mass peak ( $m_{\text{inv}} > m_{\Lambda}$ ) as the collision gets more central

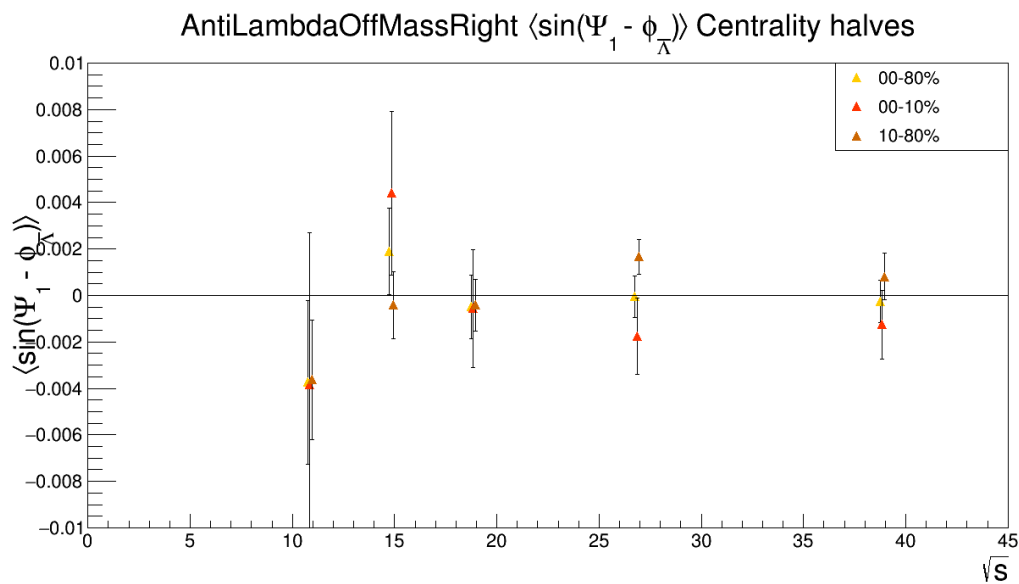


**Fig. 159:**  $\langle \sin(\Psi_1 - \phi_{\bar{\Lambda}}^*) \rangle$  right of mass peak ( $m_{\text{inv}} > m_{\Lambda}$ ) for rough halves of centrality by yield

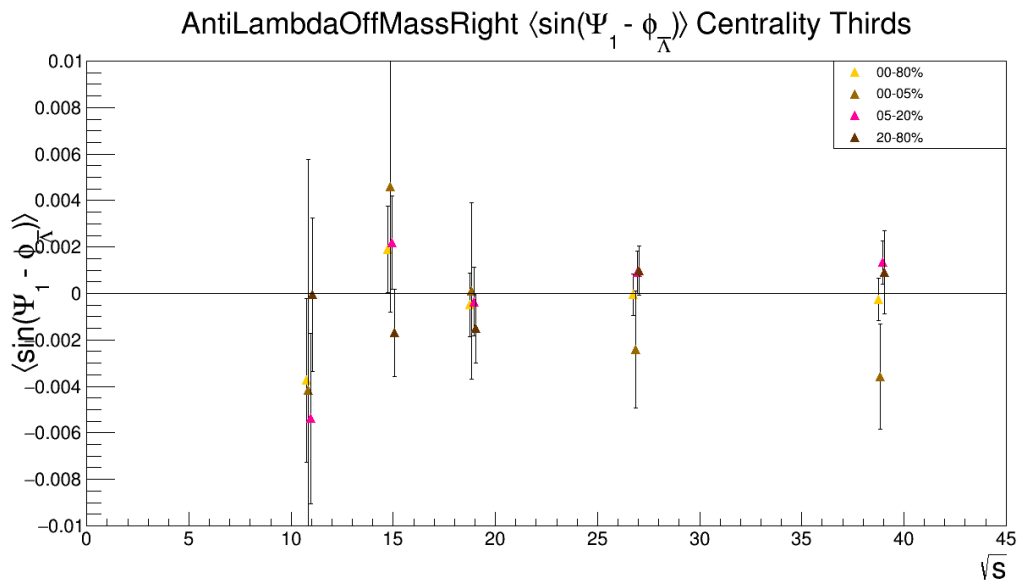


**Fig. 160:**  $\langle \sin(\Psi_1 - \phi_{\bar{\Lambda}}^*) \rangle$  right of mass peak ( $m_{\text{inv}} > m_{\Lambda}$ ) for rough thirds of centrality by yield

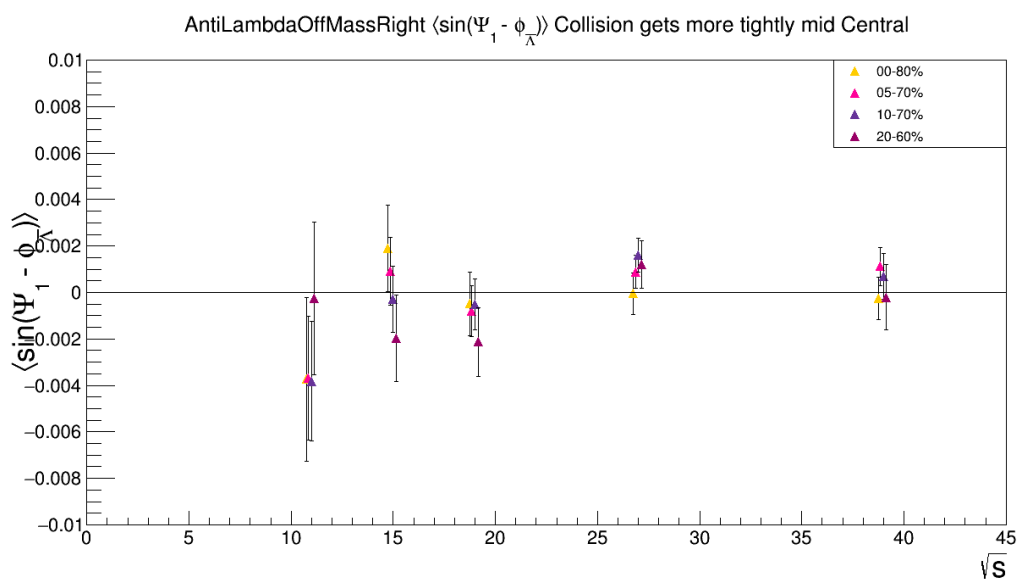


**Fig. 161:**  $\langle \sin(\Psi_1 - \phi_{\bar{\Lambda}}^*) \rangle$  right of mass peak ( $m_{\text{inv}} > m_{\Lambda}$ ) as collisions get more mid-central

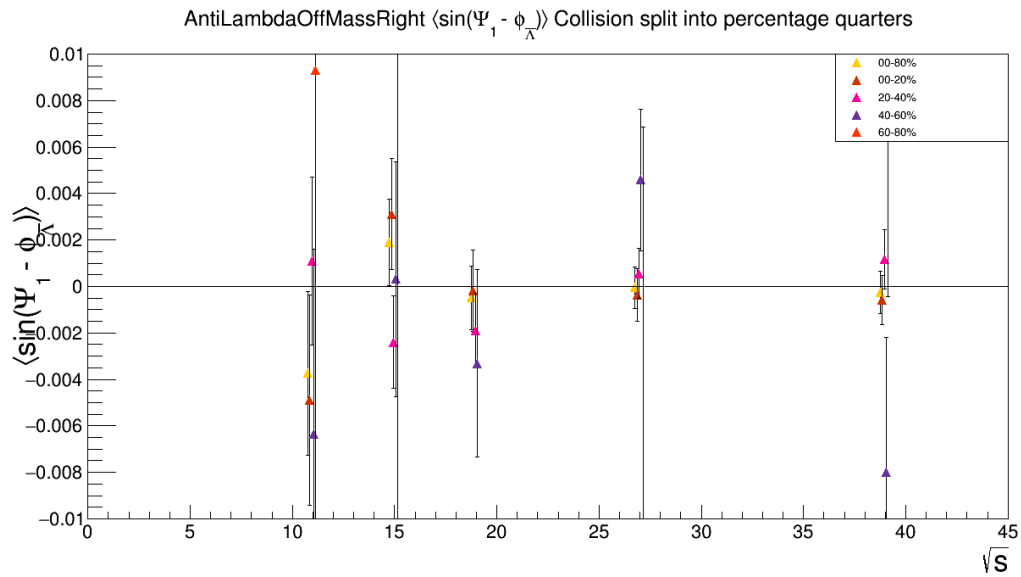


**Fig. 162:**  $\langle \sin(\Psi_1 - \phi_{\bar{\Lambda}}^*) \rangle$  right of mass peak ( $m_{\text{inv}} > m_{\Lambda}$ ) for bins of 20% centrality

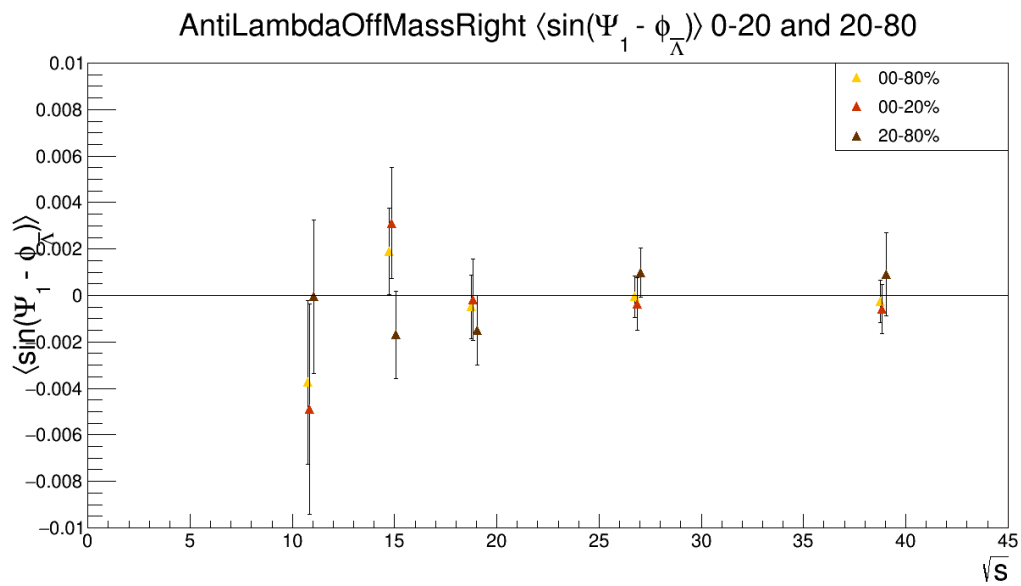


**Fig. 163:**  $\langle \sin(\Psi_1 - \phi_{\bar{\Lambda}}^*) \rangle$  right of mass peak ( $m_{\text{inv}} > m_{\Lambda}$ ) for 0-20% and 20-80% centrality

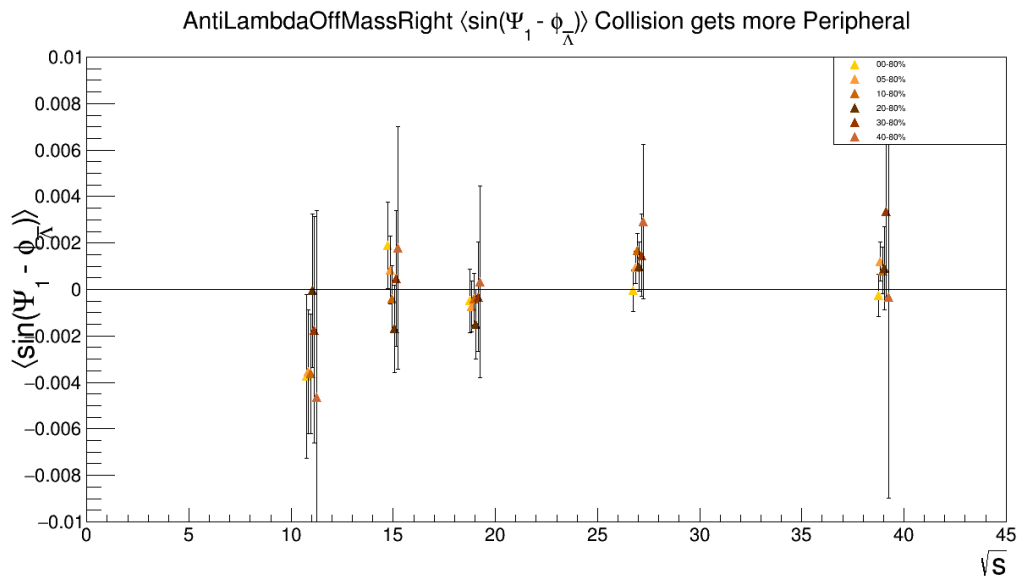


**Fig. 164:**  $\langle \sin(\Psi_1 - \phi_{\bar{\Lambda}}^*) \rangle$  left of mass peak ( $m_{\text{inv}} < m_{\Lambda}$ ) as the collision gets more peripheral

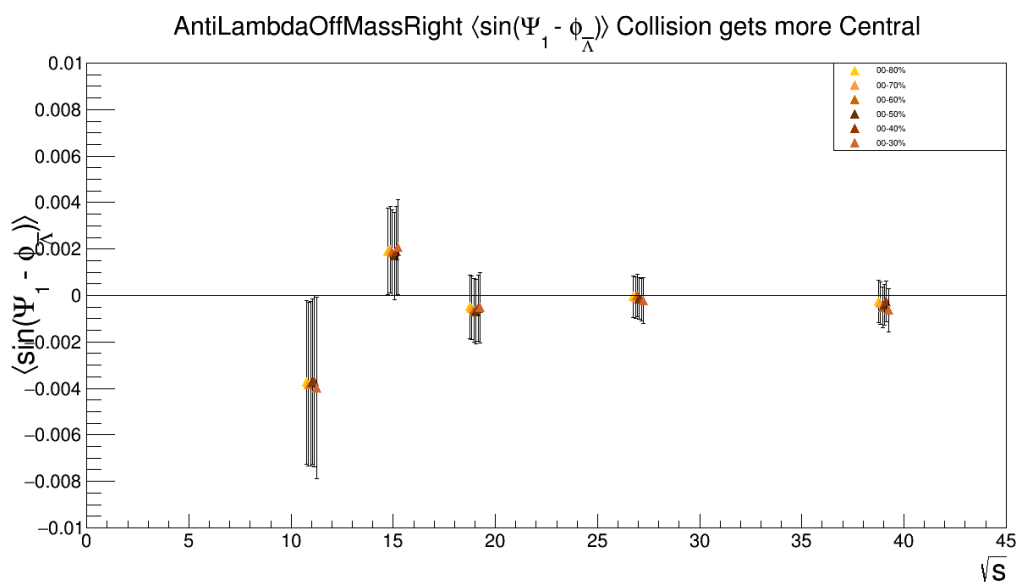


**Fig. 165:**  $\langle \sin(\Psi_1 - \phi_{\bar{\Lambda}}^*) \rangle$  left of mass peak ( $m_{\text{inv}} < m_{\Lambda}$ ) as the collision gets more central

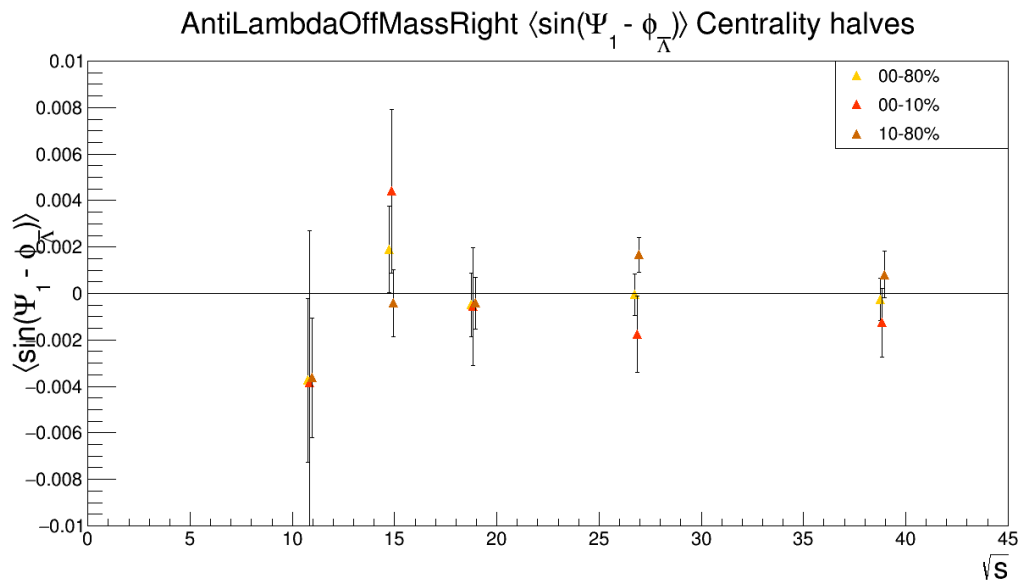


**Fig. 166:**  $\langle \sin(\Psi_1 - \phi_{\bar{\Lambda}}^*) \rangle$  left of mass peak ( $m_{\text{inv}} < m_{\Lambda}$ ) for rough halves of centrality by yield

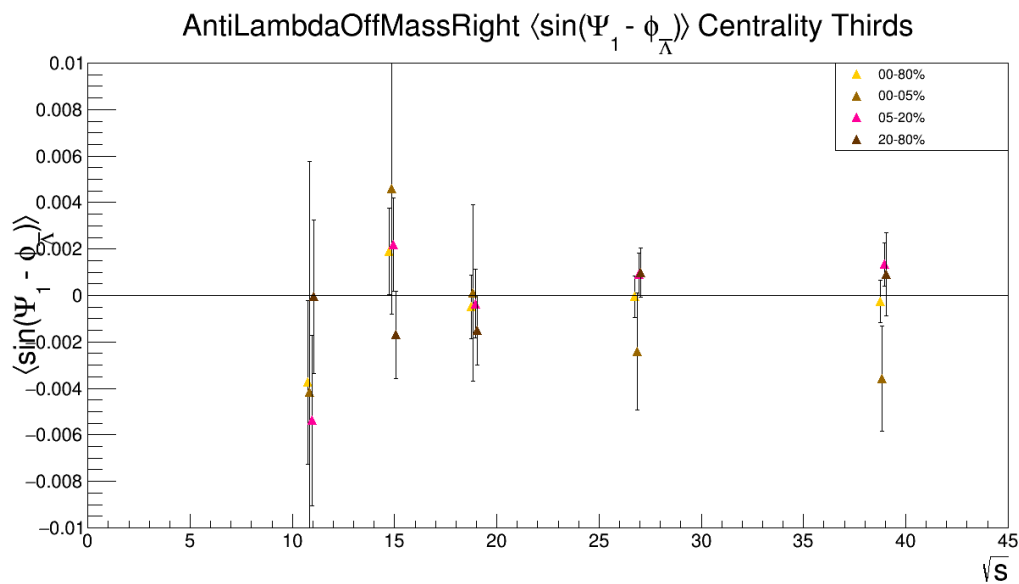


**Fig. 167:**  $\langle \sin(\Psi_1 - \phi_{\bar{\Lambda}}^*) \rangle$  left of mass peak ( $m_{\text{inv}} < m_{\Lambda}$ ) for rough thirds of centrality by yield

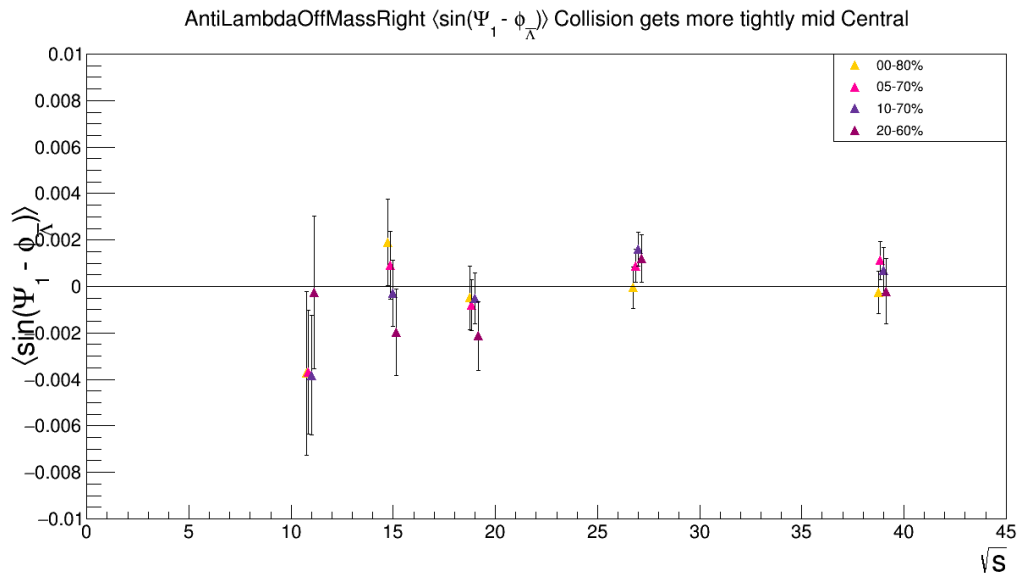


**Fig. 168:**  $\langle \sin(\Psi_1 - \phi_{\bar{\Lambda}}^*) \rangle$  left of mass peak ( $m_{\text{inv}} < m_{\Lambda}$ ) as collisions get more mid-central

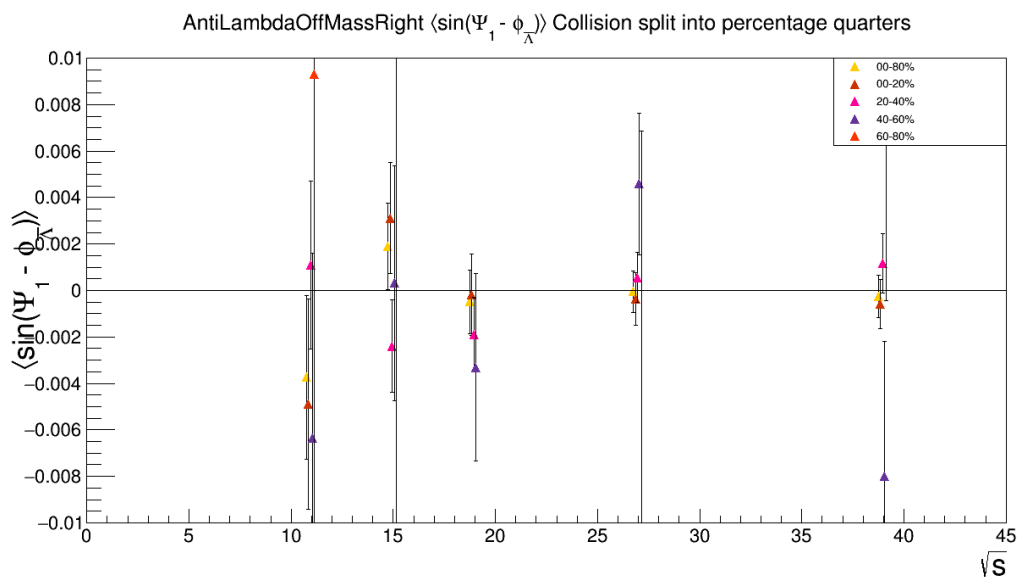


**Fig. 169:**  $\langle \sin(\Psi_1 - \phi_{\bar{\Lambda}}^*) \rangle$  left of mass peak ( $m_{\text{inv}} < m_{\Lambda}$ ) for bins of 20% centrality

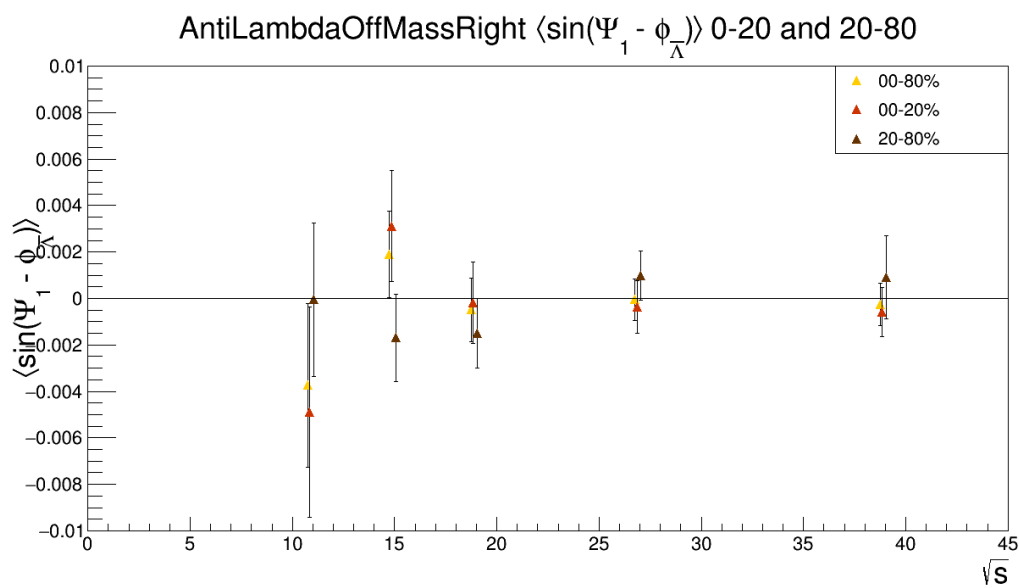


**Fig. 170:**  $\langle \sin(\Psi_1 - \phi_{\bar{\Lambda}}^*) \rangle$  left of mass peak ( $m_{\text{inv}} < m_{\Lambda}$ ) for 0-20% and 20-80% centrality

## 5.2 Energy

2055 Higher momentum Lambdas have the opportunity to carry away a large fraction of the excess of angular momentum of the fireball. This may be energetically favored. It is generally predicted that the signal would increase with energy. What is shown here is the results when an attempt is made to split the data into statistically equal halves and thirds of Lambda energy (in GeV). The intentions of these cuts to make equal fractions may not be particularly well borne out because the cuts were chosen via histograms (it is  
2060 a binning issue).

Lambda Average Sy For Different Ranges of E

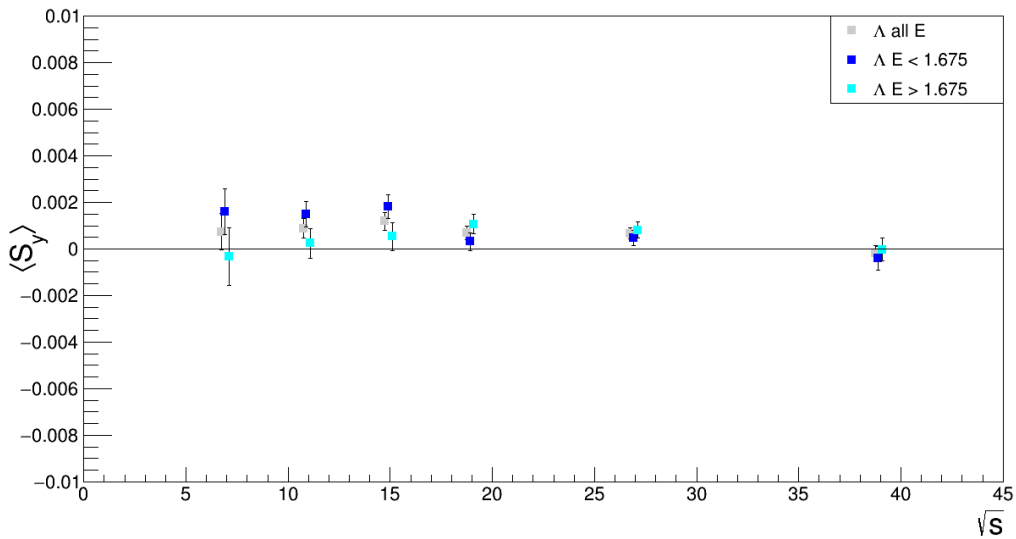


Fig. 171:  $\Lambda$  polarization cut into two energy bins. Energies quoted in legend are in GeV.

Lambda Average Sy For Different Ranges of E

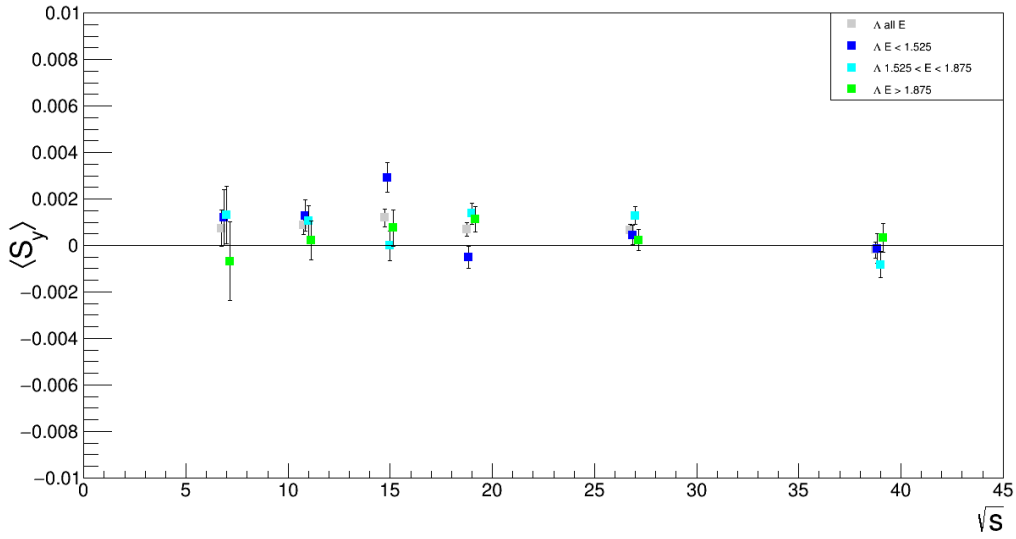
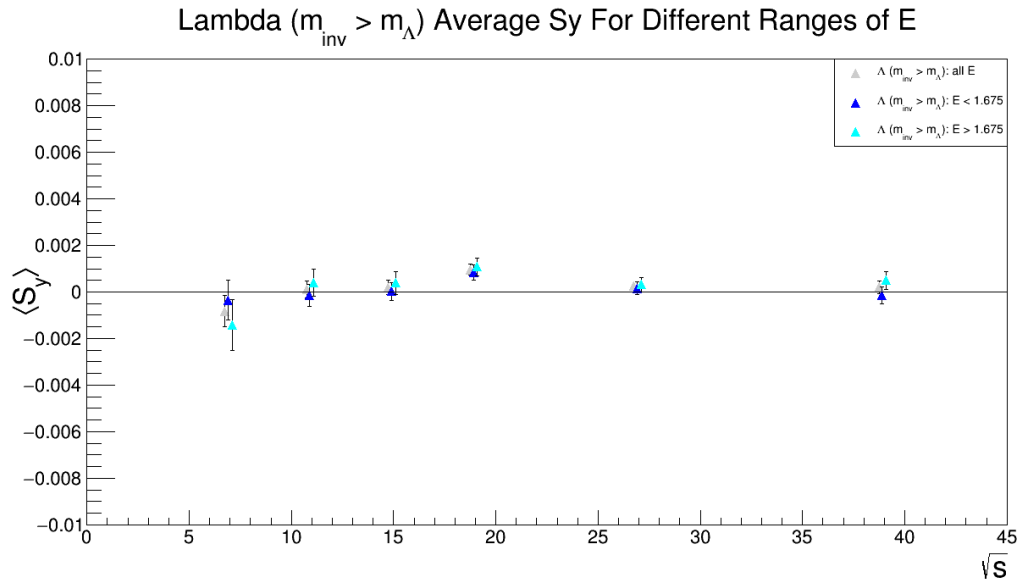
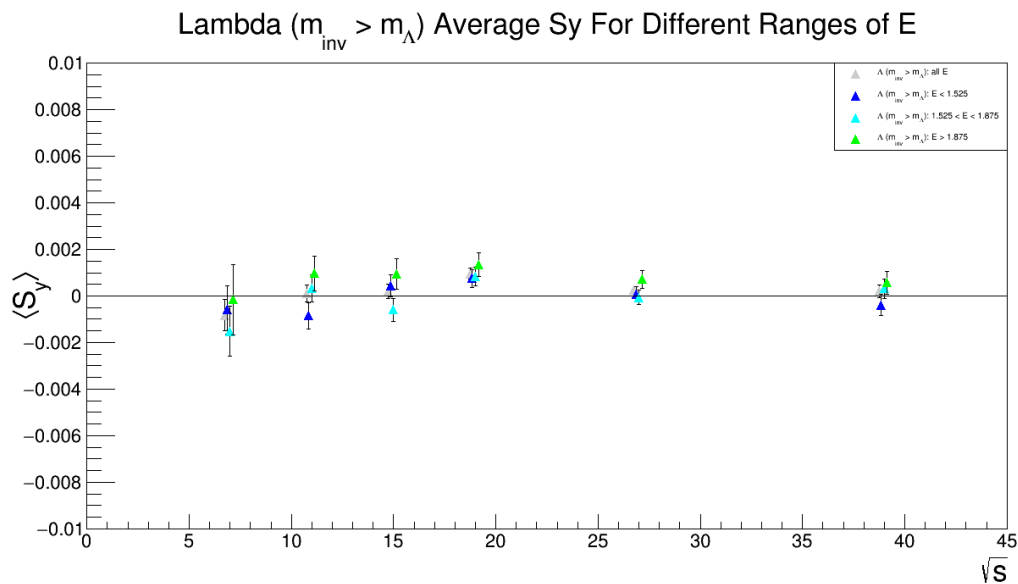


Fig. 172:  $\Lambda$  polarization cut into three energy bins. Energies quoted in legend are in GeV.



**Fig. 173:**  $\Lambda$  right of mass peak ( $m_{inv} > m_\Lambda$ ) polarization cut into two energy bins. Energies quoted in legend are in GeV.



**Fig. 174:**  $\Lambda$  right of mass peak ( $m_{inv} > m_\Lambda$ ) polarization cut into three energy bins. Energies quoted in legend are in GeV.

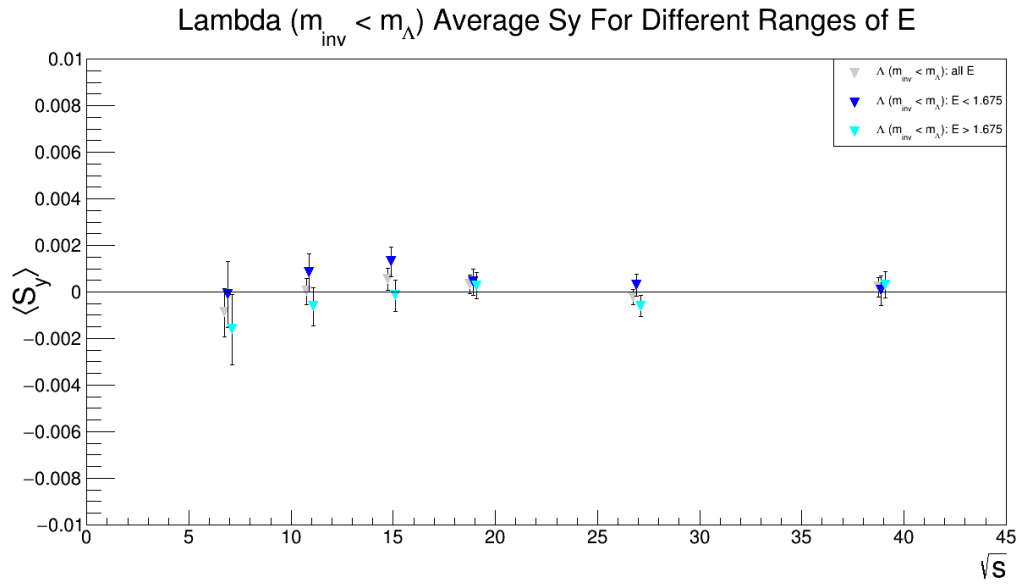


**Fig. 175:**  $\Lambda$  left of mass peak ( $m_{\text{inv}} < m_{\Lambda}$ ) polarization cut into two energy bins. Energies quoted in legend are in GeV.

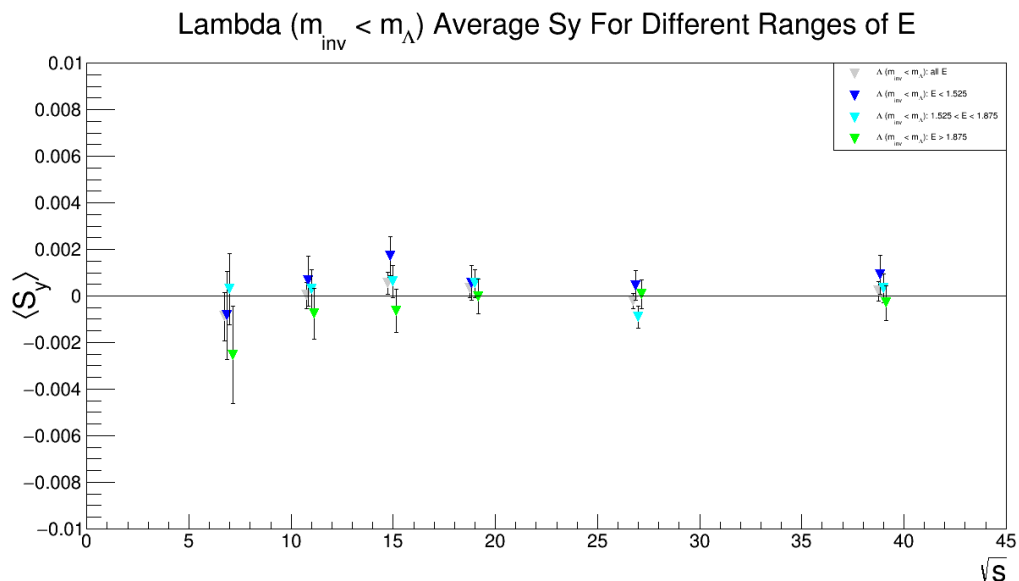


**Fig. 176:**  $\Lambda$  left of mass peak ( $m_{\text{inv}} < m_{\Lambda}$ ) polarization cut into three energy bins. Energies quoted in legend are in GeV.

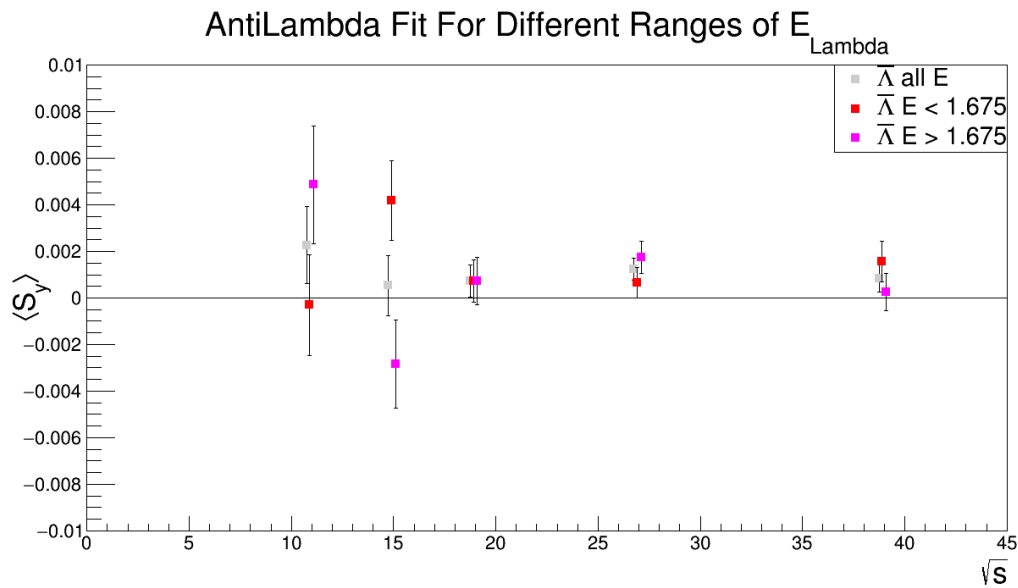


**Fig. 177:**  $\bar{\Lambda}$  polarization cut into two energy bins. Energies quoted in legend are in GeV.

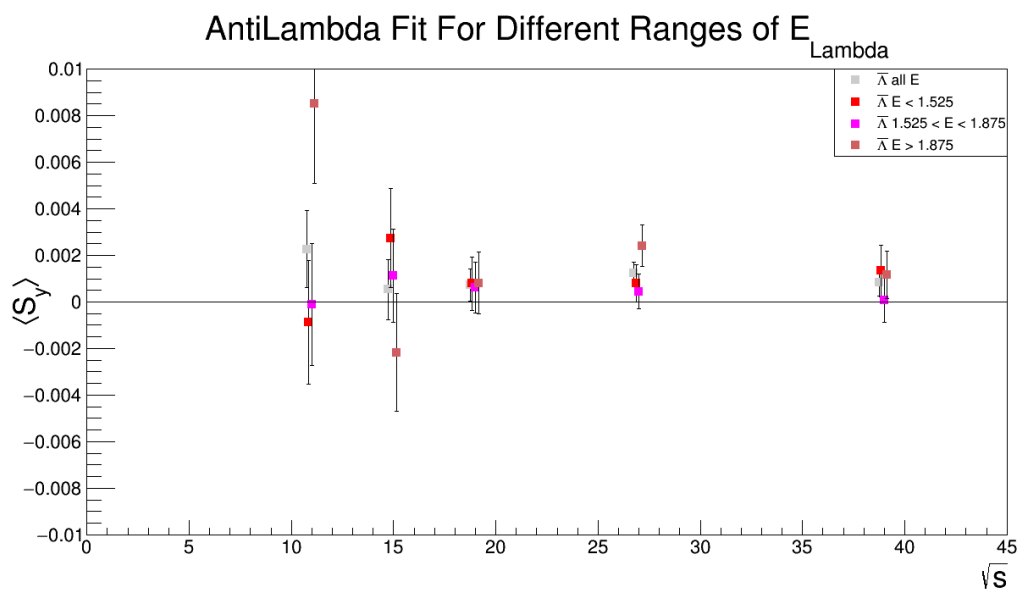


**Fig. 178:**  $\bar{\Lambda}$  polarization cut into three energy bins. Energies quoted in legend are in GeV.

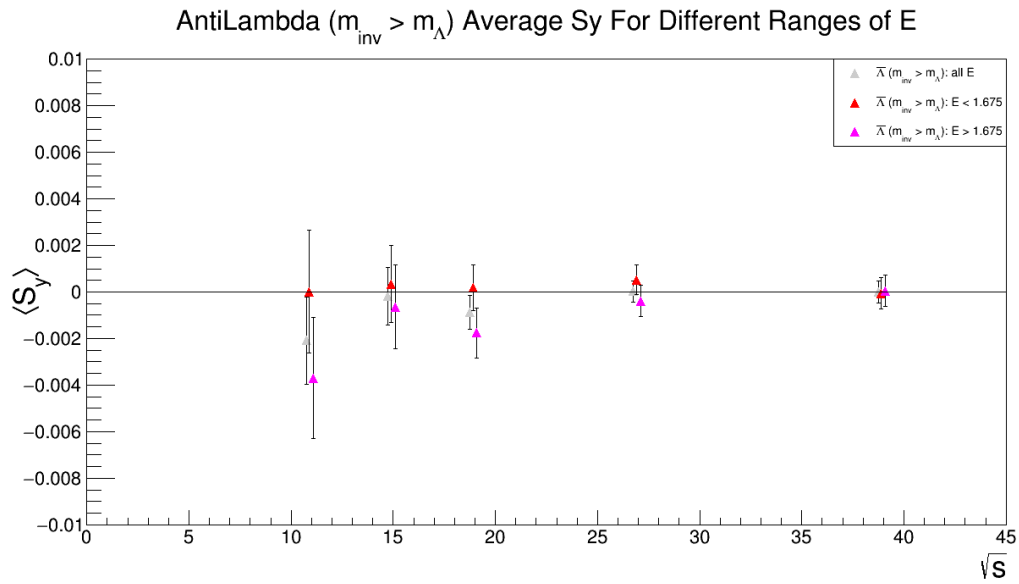


**Fig. 179:**  $\bar{\Lambda}$  right of mass peak ( $m_{inv} > m_\Lambda$ ) polarization cut into two energy bins. Energies quoted in legend are in GeV.

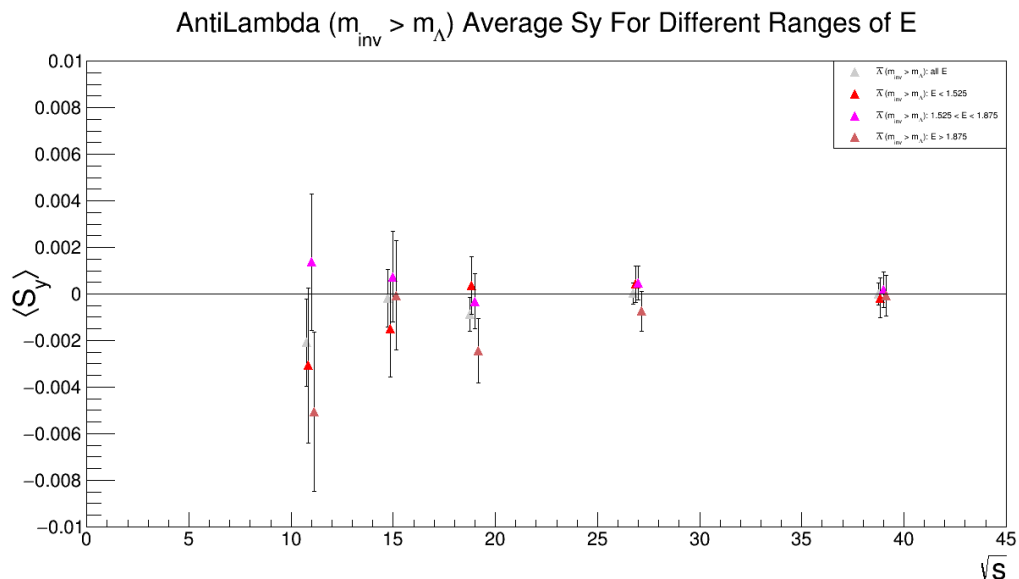


**Fig. 180:**  $\bar{\Lambda}$  right of mass peak ( $m_{inv} > m_\Lambda$ ) polarization cut into three energy bins. Energies quoted in legend are in GeV.

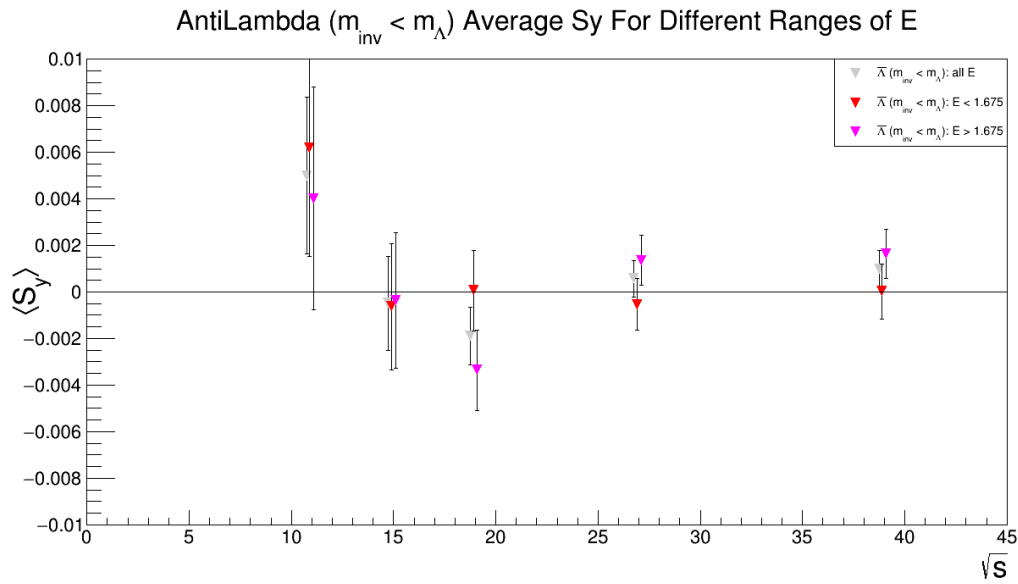


**Fig. 181:**  $\bar{\Lambda}$  left of mass peak ( $m_{inv} < m_\Lambda$ ) polarization cut into two energy bins. Energies quoted in legend are in GeV.

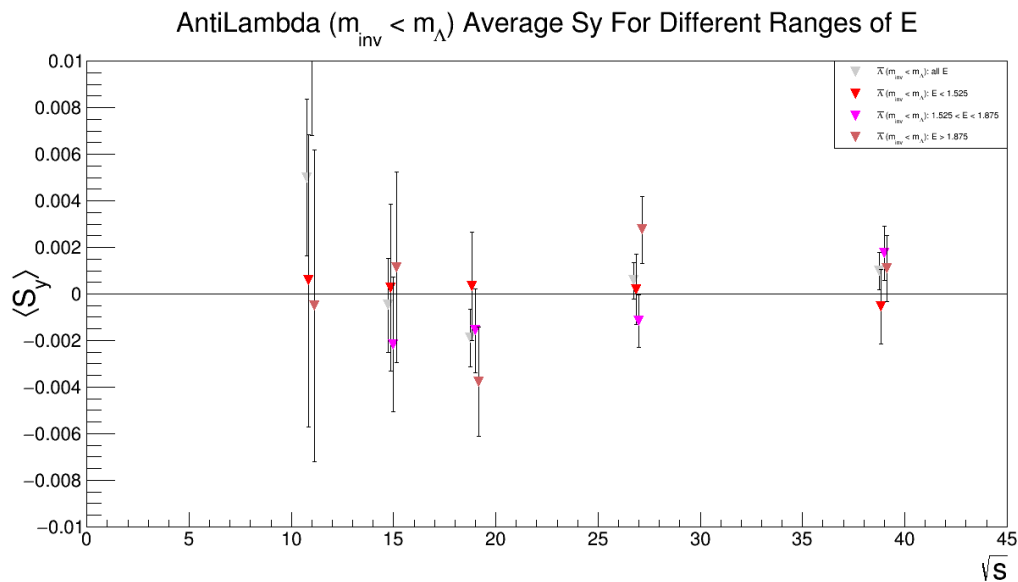


**Fig. 182:**  $\bar{\Lambda}$  left of mass peak ( $m_{inv} < m_\Lambda$ ) polarization cut into three energy bins. Energies quoted in legend are in GeV.

### 5.3 Rapidity

Hydrodynamic models see possible variation of the signal with Lambda rapidity magnitude. Naively the signal should not depend on the sign of the rapidity. It is possible that the production plane polarization coupled with first order flow could make this happen. What is shown here is the results when an attempt is made to split the data into statistically equal halves and thirds of Lambda rapidity. The intentions of these cuts to make equal fractions may not be particularly well borne out because the cuts were chosen via histograms (it is a binning issue).

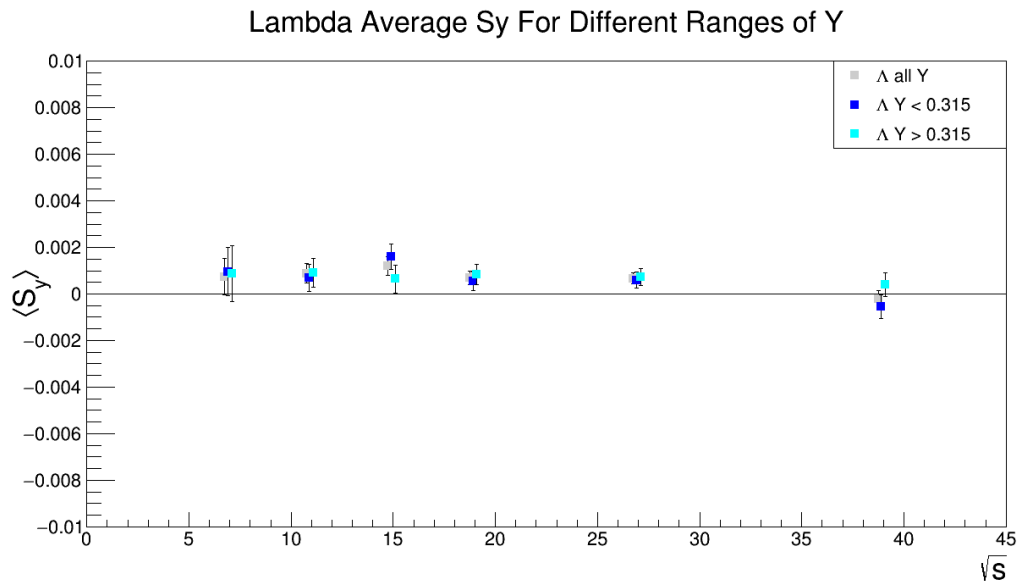


Fig. 183:  $\Lambda$  polarization cut into two rapidity bins.

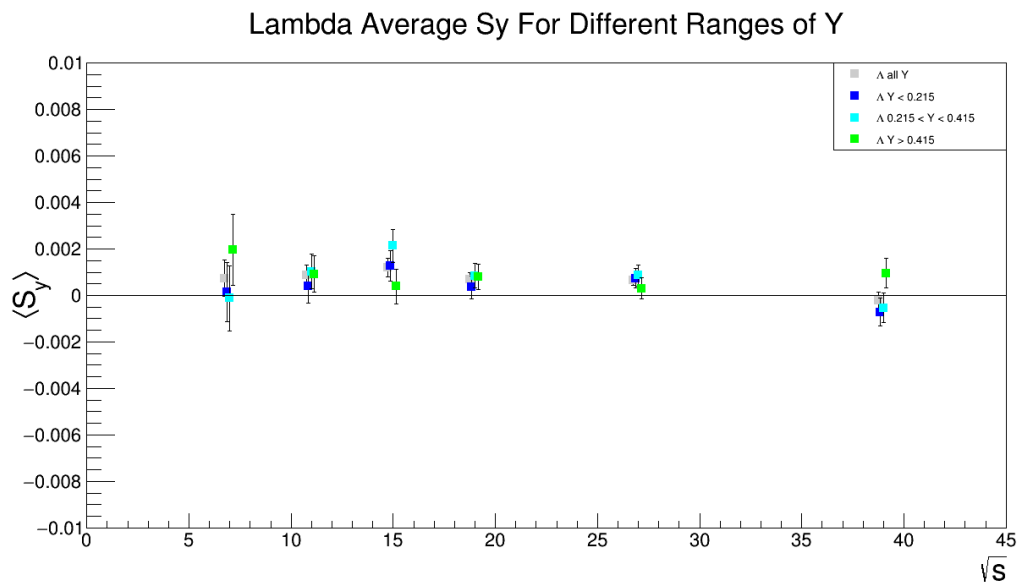
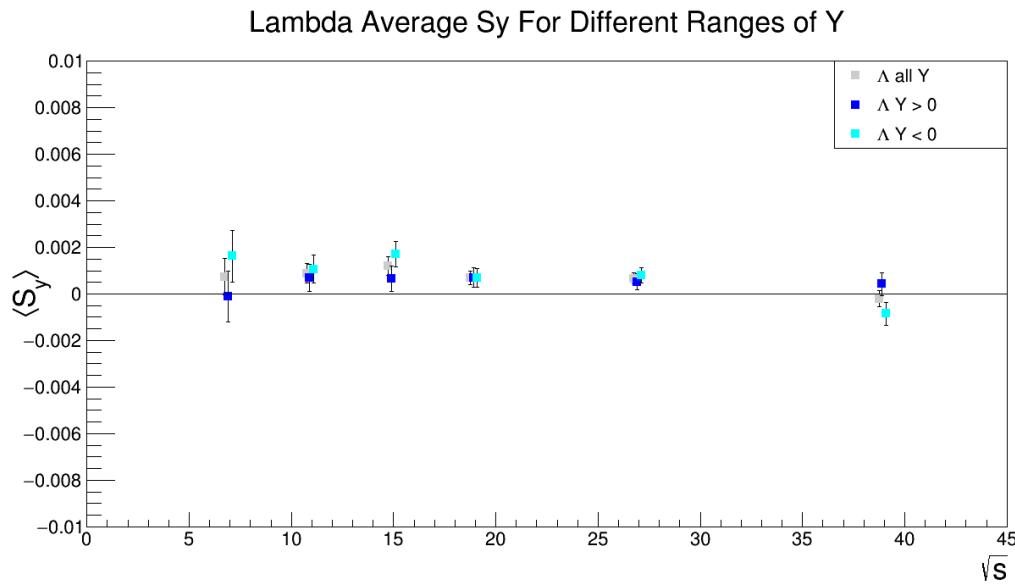
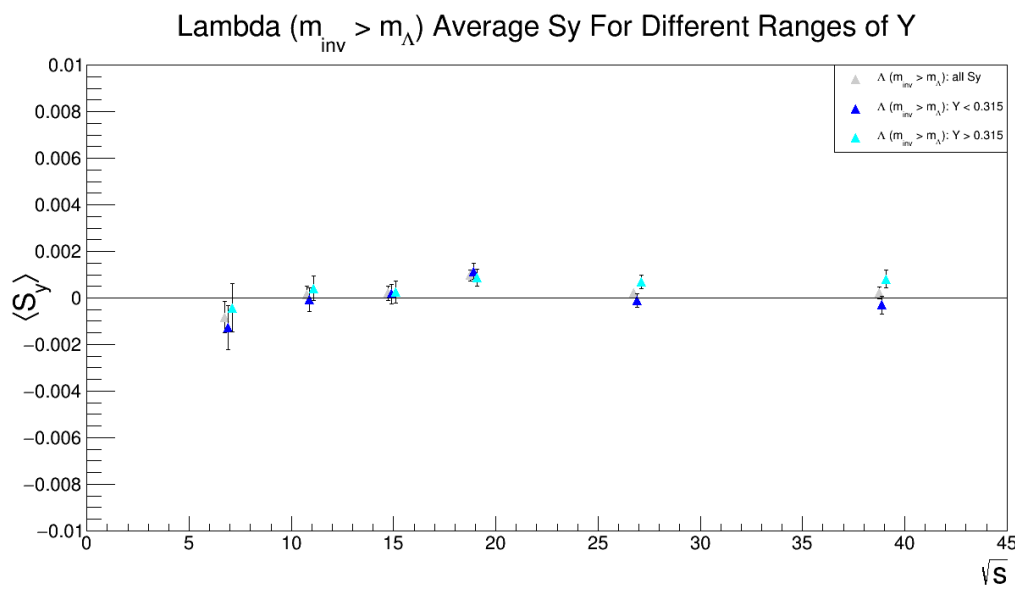


Fig. 184:  $\Lambda$  polarization cut into three rapidity bins.



**Fig. 185:**  $\Lambda$  polarization cut into positive and negative rapidity bins.



**Fig. 186:**  $\Lambda$  right of mass peak ( $m_{inv} > m_\Lambda$ ) polarization cut into two rapidity bins.

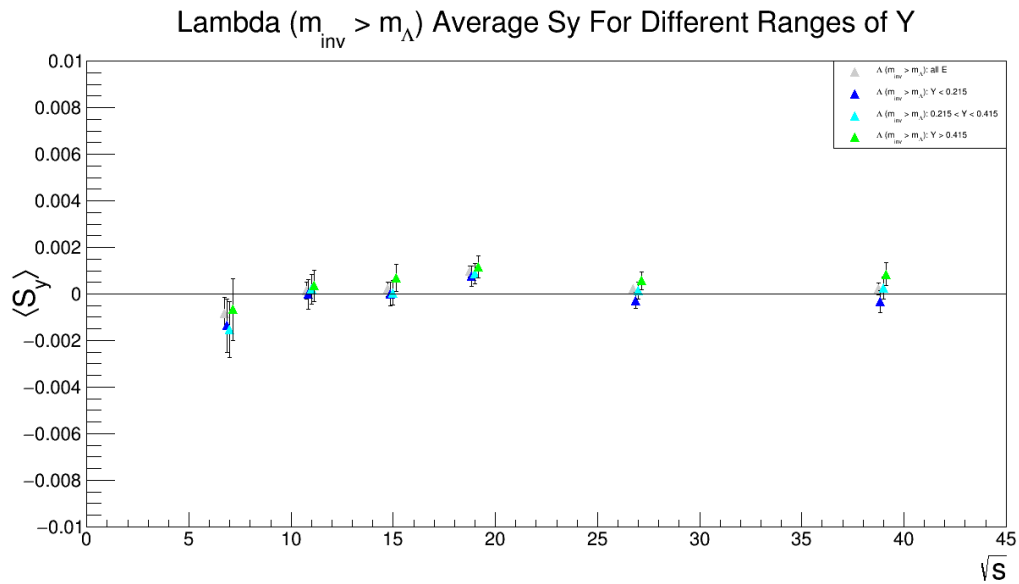


**Fig. 187:**  $\Lambda$  right of mass peak ( $m_{\text{inv}} > m_\Lambda$ ) polarization cut into three rapidity bins.

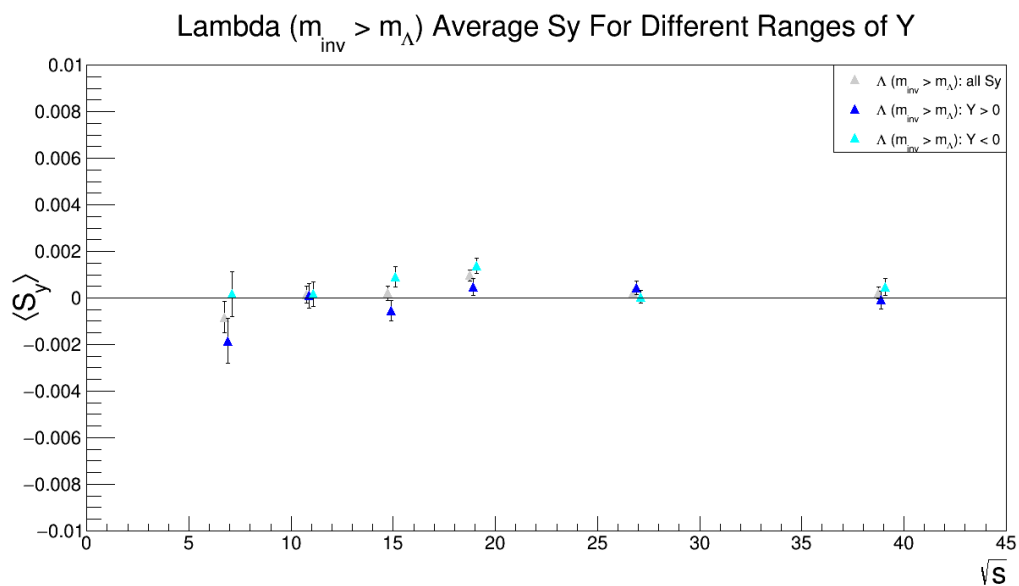


**Fig. 188:**  $\Lambda$  right of mass peak ( $m_{\text{inv}} > m_\Lambda$ ) polarization cut into positive and negative rapidity bins.

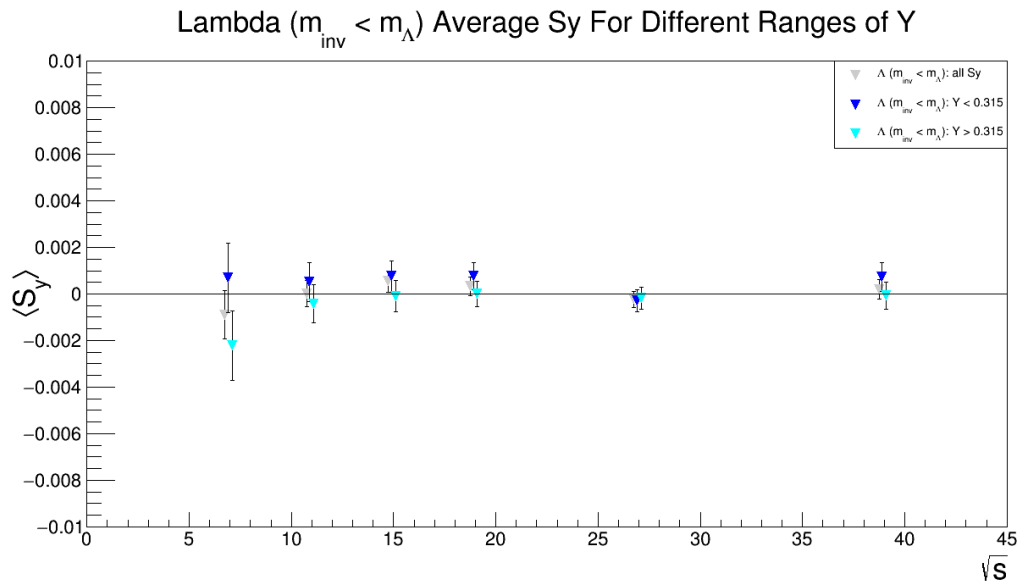


**Fig. 189:**  $\Lambda$  left of mass peak ( $m_{inv} < m_\Lambda$ ) polarization cut into two rapidity bins.

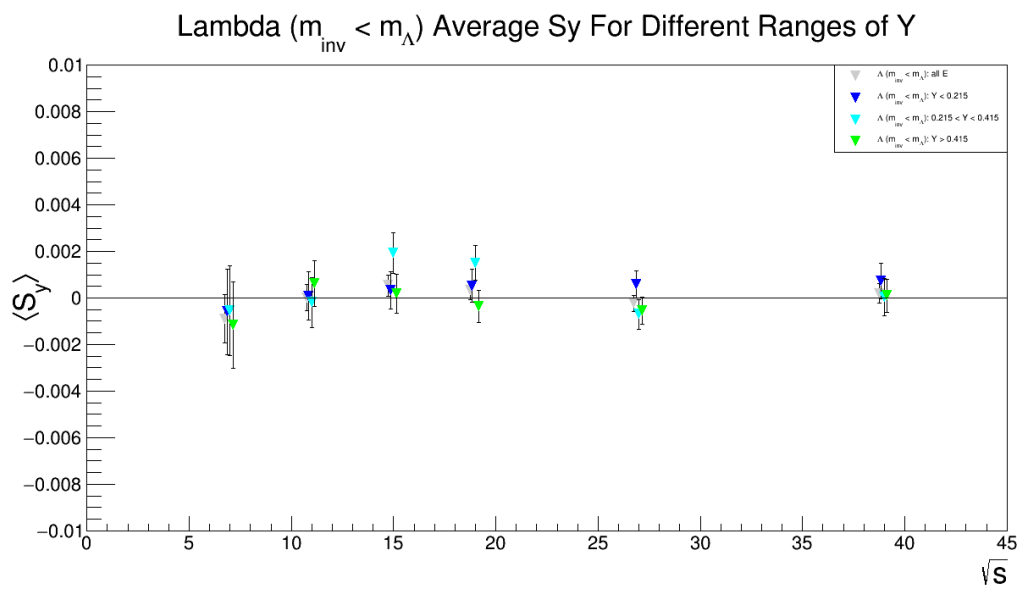


**Fig. 190:**  $\Lambda$  left of mass peak ( $m_{inv} < m_\Lambda$ ) polarization cut into three rapidity bins.

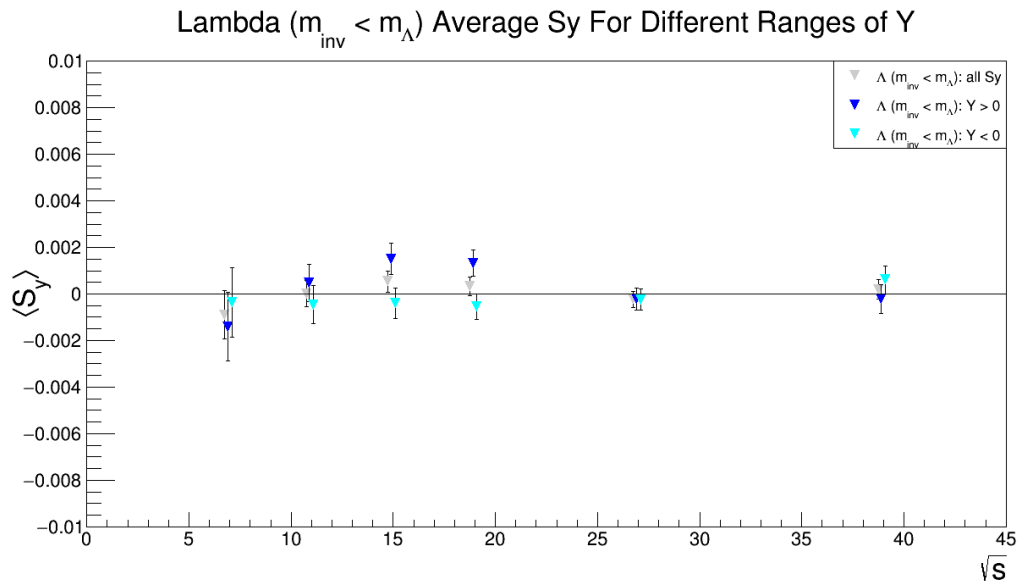


**Fig. 191:**  $\Lambda$  Left of mass peak ( $m_{inv} < m_\Lambda$ ) polarization cut into positive and negative rapidity bins.

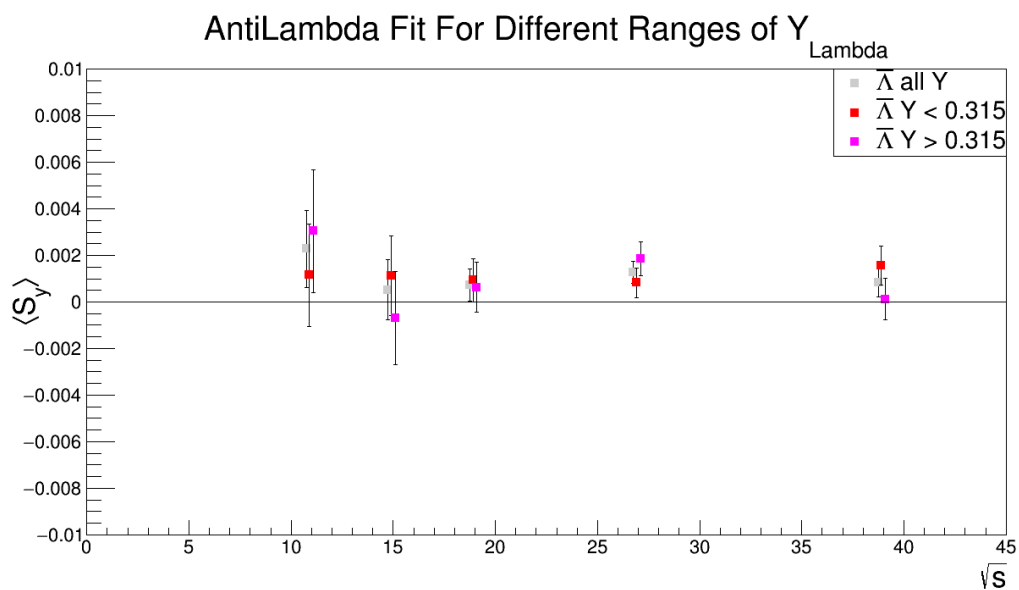


**Fig. 192:**  $\bar{\Lambda}$  polarization cut into two rapidity bins.

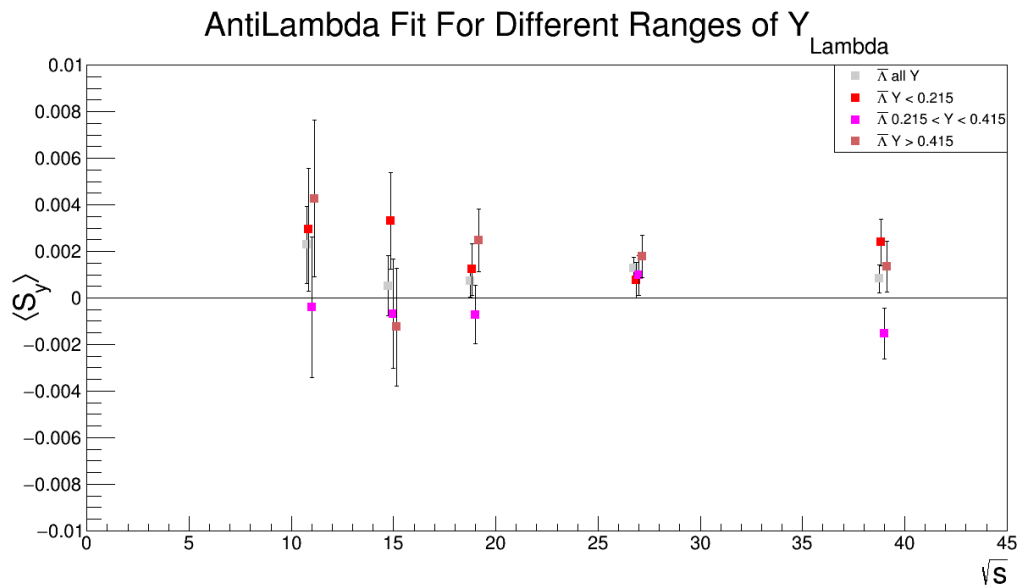


**Fig. 193:**  $\bar{\Lambda}$  polarization cut into three rapidity bins.

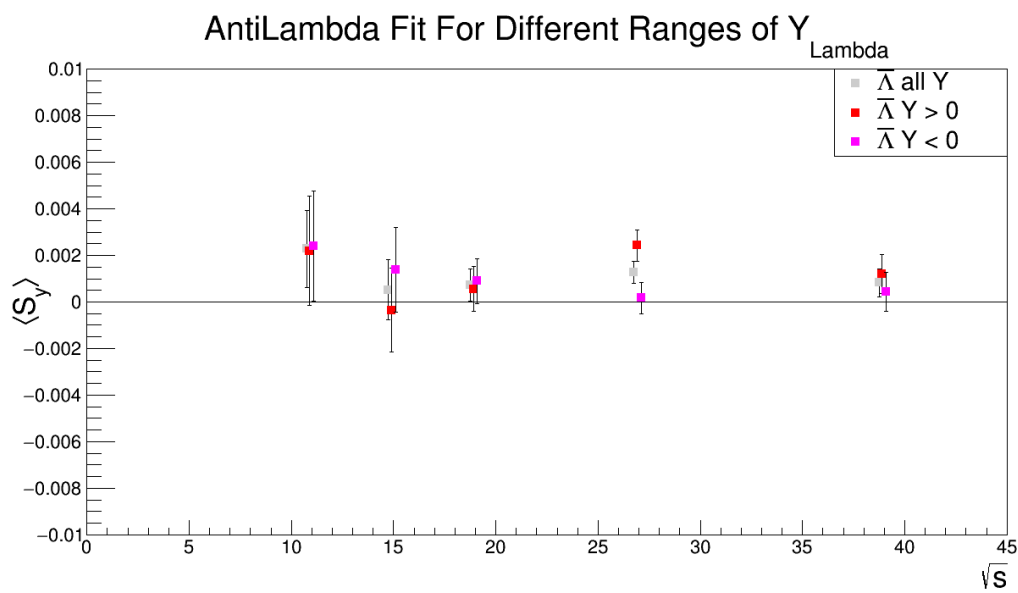


**Fig. 194:**  $\bar{\Lambda}$  polarization cut into positive and negative rapidity bins.

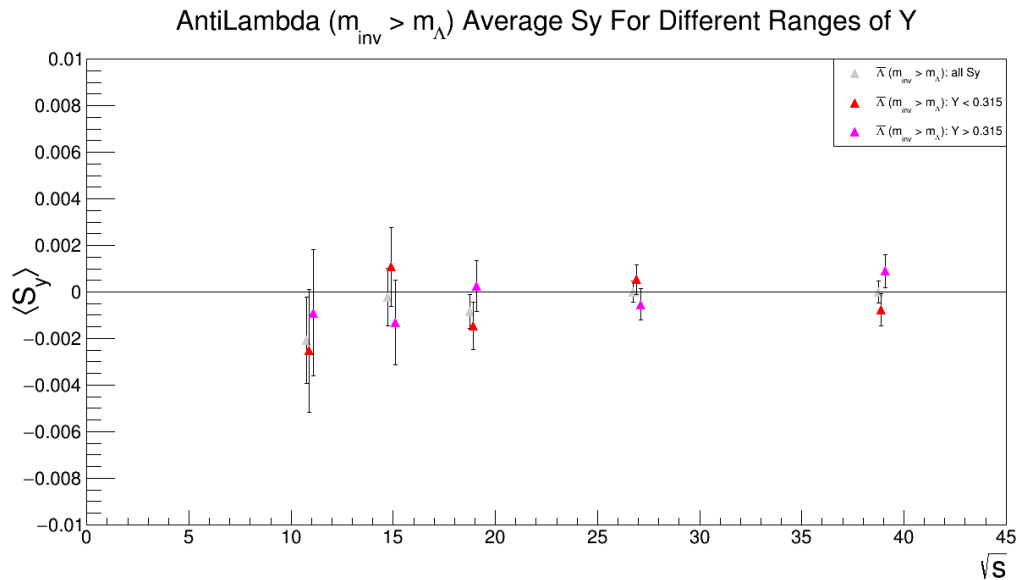


**Fig. 195:**  $\bar{\Lambda}$  right of mass peak ( $m_{inv} > m_\Lambda$ ) polarization cut into two rapidity bins.

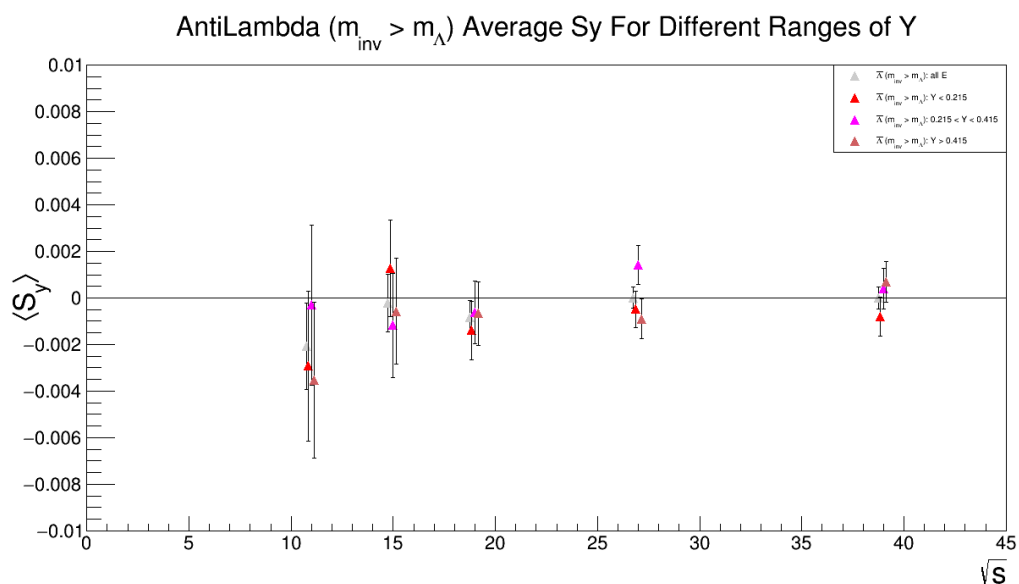


**Fig. 196:**  $\bar{\Lambda}$  right of mass peak ( $m_{inv} > m_\Lambda$ ) polarization cut into three rapidity bins.

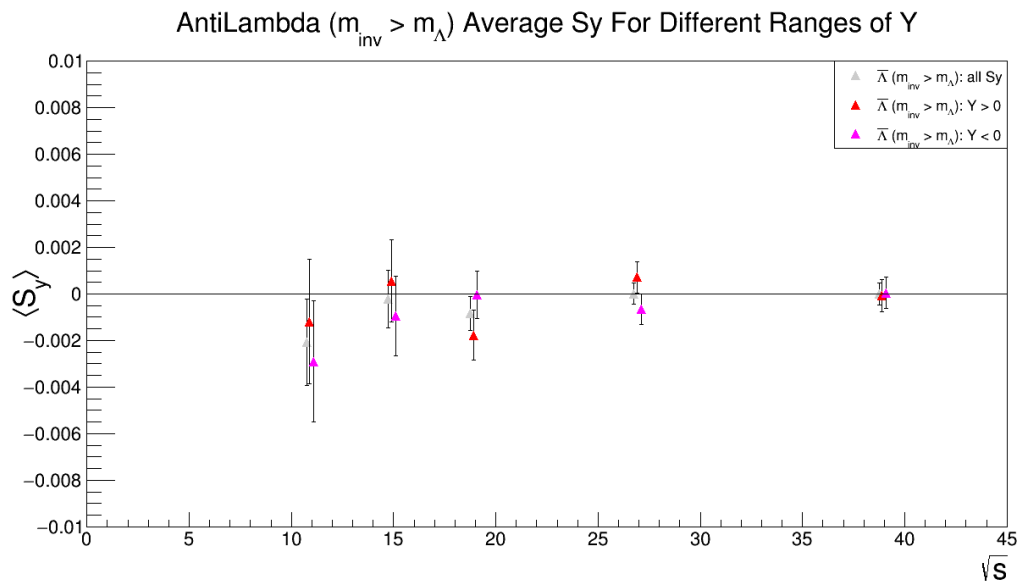


**Fig. 197:**  $\bar{\Lambda}$  right of mass peak ( $m_{inv} > m_\Lambda$ ) polarization cut into positive and negative rapidity bins.

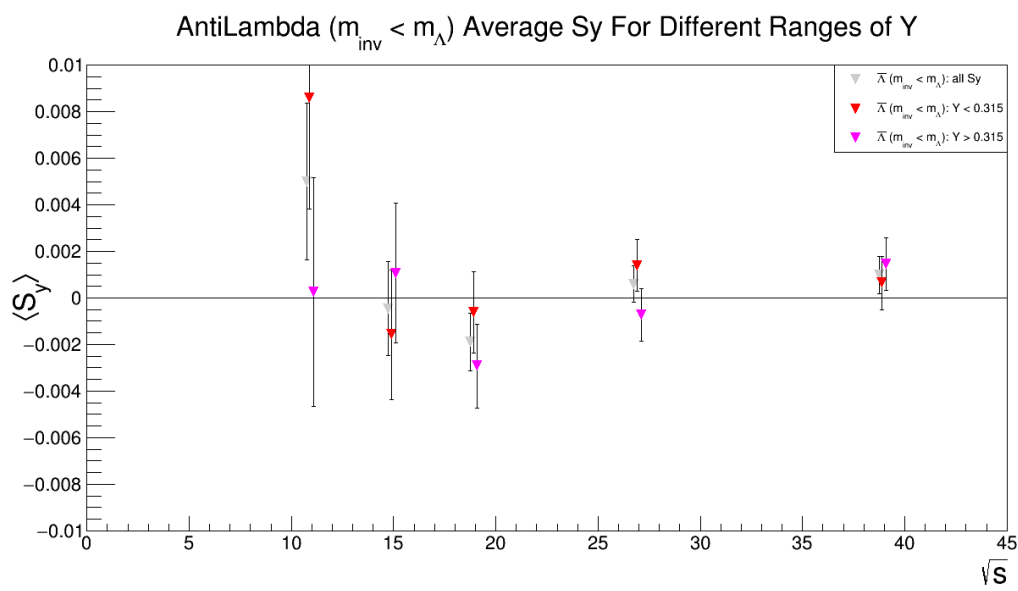


**Fig. 198:**  $\bar{\Lambda}$  left of mass peak ( $m_{inv} < m_\Lambda$ ) polarization cut into two rapidity bins.

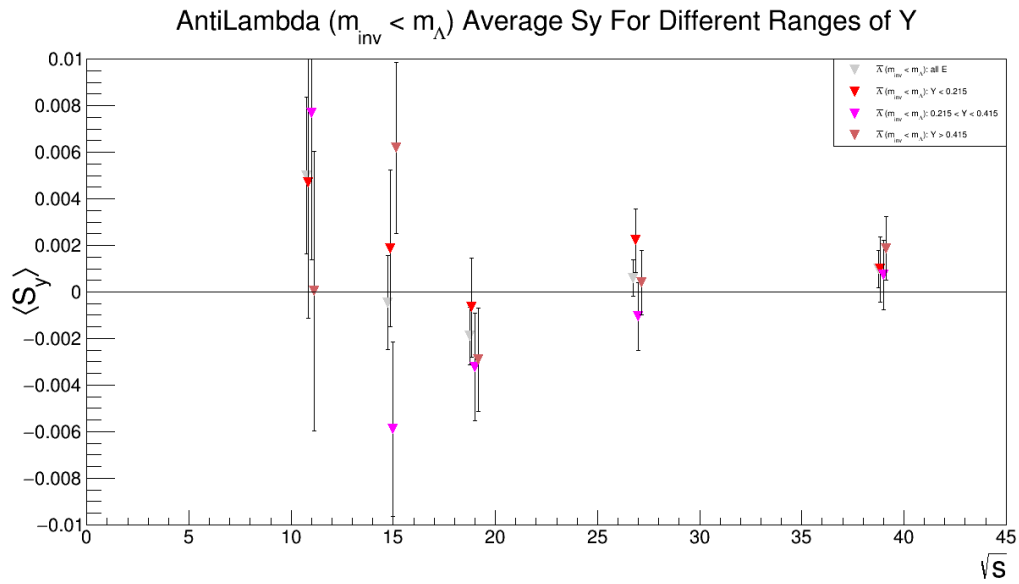


**Fig. 199:**  $\bar{\Lambda}$  left of mass peak ( $m_{inv} < m_\Lambda$ ) polarization cut into three rapidity bins.

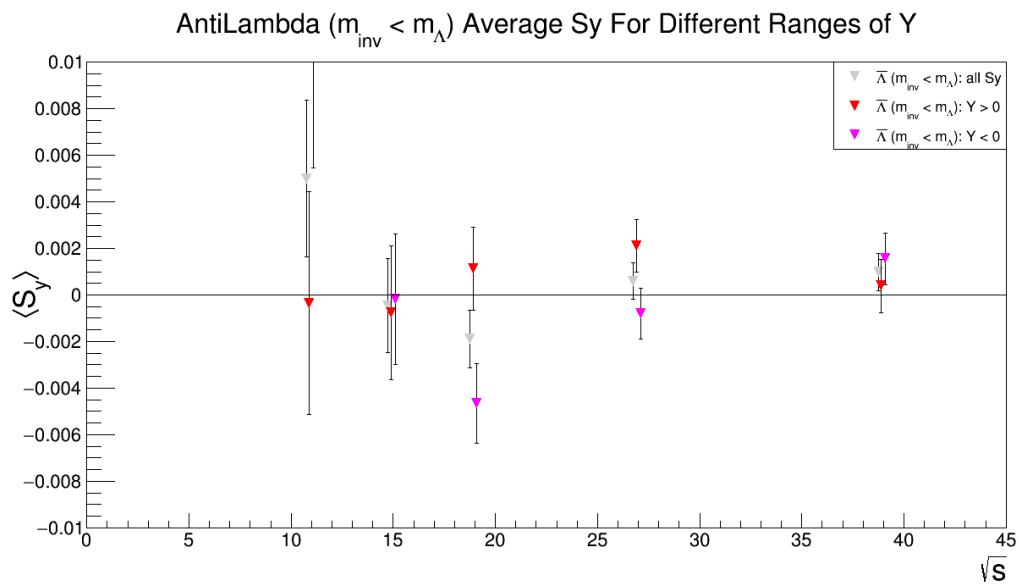


**Fig. 200:**  $\bar{\Lambda}$  Left of mass peak ( $m_{inv} < m_\Lambda$ ) polarization cut into positive and negative rapidity bins.

## 5.4 Azimuthal angle

Lambdas emitted in vs. out of plane may exhibit different polarization. One cannot look at the straight  $\phi$  dependence of the signal because it would be dominated by the helicity efficiency effect described in section 3.4. To get around this we look at Lambdas in ( $|\phi - \Psi_1| < \pi/4$  and  $|\phi - (\Psi_1 + \pi)| < \pi/4$ ) compared to Lambdas emitted out of plane ( $|\phi - \Psi_1/2| < \pi/4$  and  $|\phi - (\Psi_1/2 + \pi)| < \pi/4$ ). In the figures I quote  $\phi$  automatically with respect to  $\Psi_1$  so this is  $\cos(\phi) < 1/\sqrt{2}$  and  $\cos(\phi) > 1/\sqrt{2}$  for space.

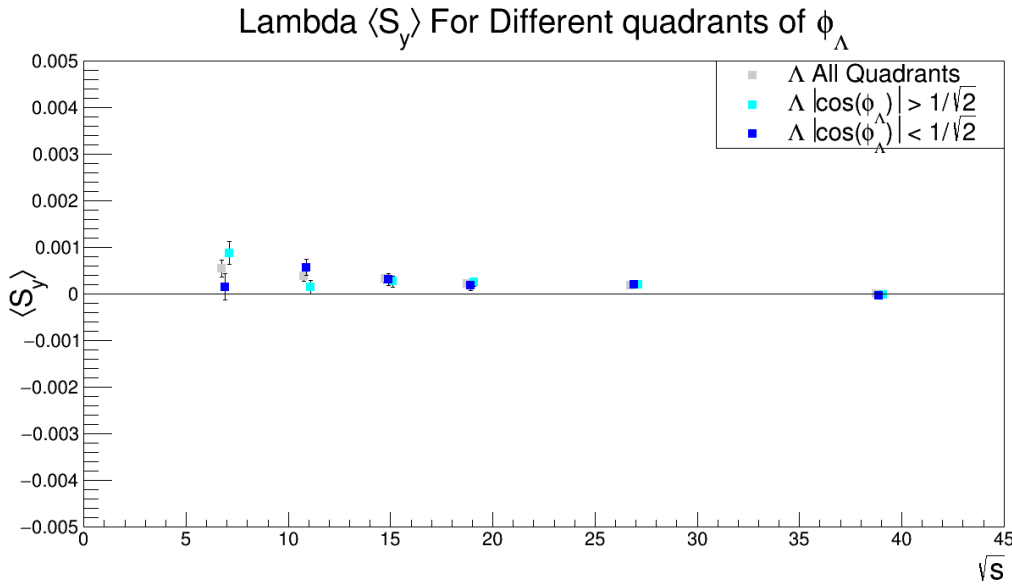


**Fig. 201:**  $\Lambda$  polarization cut into in and out of plane.

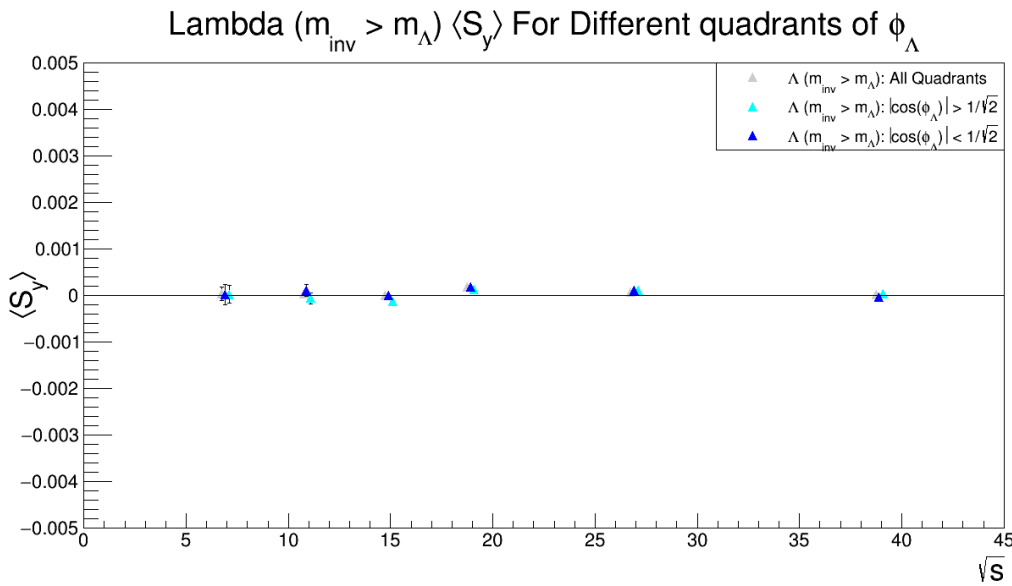


**Fig. 202:**  $\Lambda$  right of mass peak ( $m_{\text{inv}} > m_\Lambda$ ) polarization cut into in and out of plane.

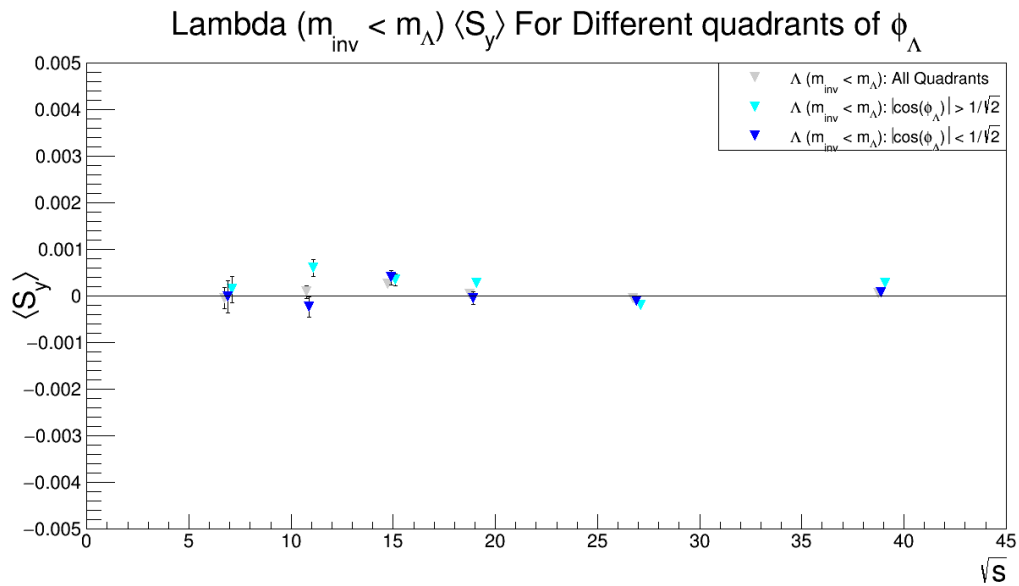


**Fig. 203:**  $\Lambda$  left of mass peak ( $m_{\text{inv}} < m_{\Lambda}$ ) polarization cut into in and out of plane.

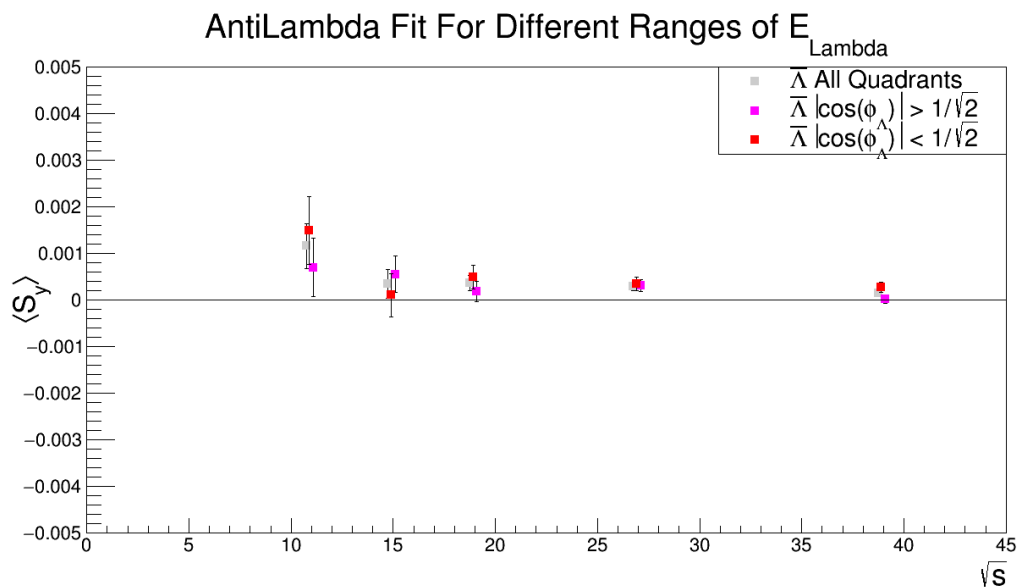


**Fig. 204:**  $\bar{\Lambda}$  polarization cut into in and out of plane.

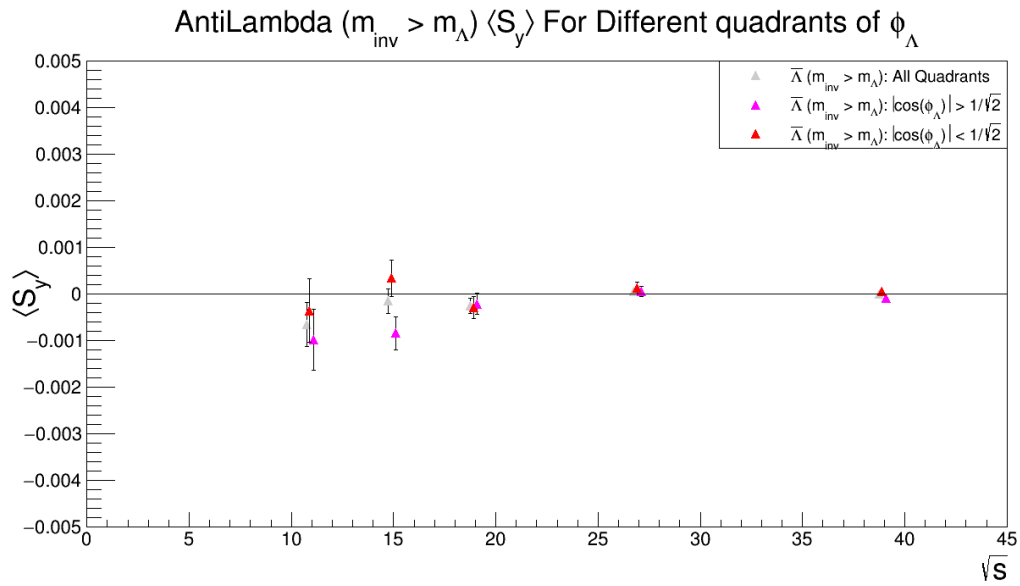


**Fig. 205:**  $\bar{\Lambda}$  right of mass peak ( $m_{inv} > m_\Lambda$ ) polarization cut into in and out of plane.

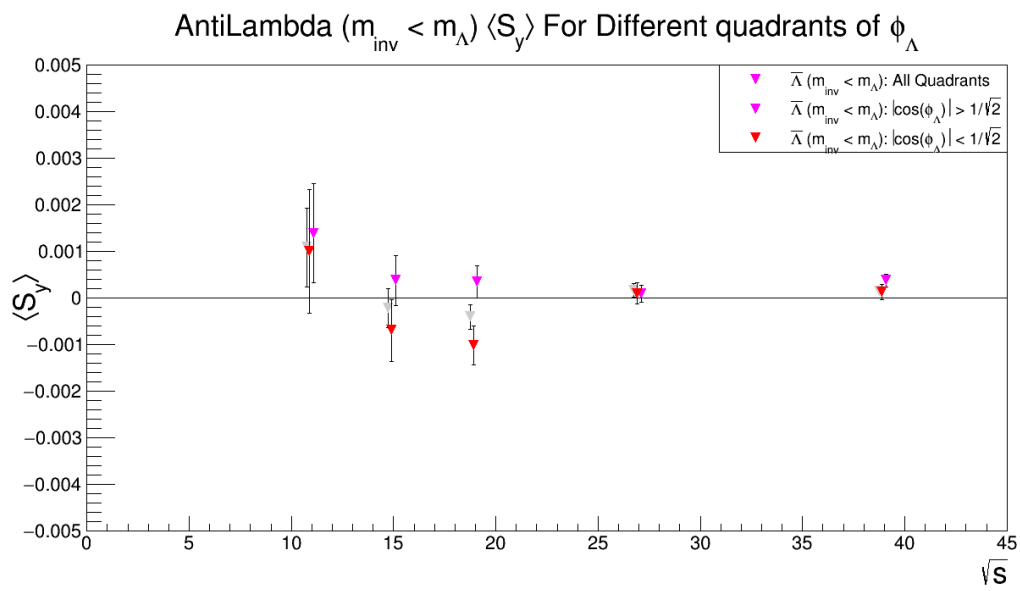


**Fig. 206:**  $\bar{\Lambda}$  left of mass peak ( $m_{inv} < m_\Lambda$ ) polarization cut into in and out of plane.

## 2075 6 Signal falsification

The purpose of this section is to provide examples of work that was done to attempt to falsify the signal. An important attempt to falsify the signal is from looking at the combinatoric background of the Lambda mass distribution. This is already discussed in section 3.2 so there is no corresponding check here.

### 6.1 Simulation comparison

2080 Typically a natural place to look to verify or falsify an experimental signal are the many models that exist. No available simulation (at least as far as I am aware) has vorticity or spin coupling so simulation can, at best, be used for falsifying the results and attempting to see if one sees the signal appear as a consequence of acceptance or kinematics. Since the analysis is so simple it is unlikely that such a falsification could occur. The tools available I have used in this analysis are HIJING, embedded Lambdas in real events, and UrQMD.

2085 Since HIJING simulations in the STAR framework have included a cut such that primary particles have  $-4.5 < \eta < 2.5$  it isn't really possible to use the BBC and thus it is not possible to make any attempt at falsifying the results, aside from assuming that  $\Psi_1$  is zero or random for every event. Because of the  $\eta$  cut many of the particles reaching the BBCs are secondary and thus there can be a large autocorrelation effect with daughters of Lambdas and the "measured"  $\Psi_1$ . Assuming that  $\Psi_1$  is zero for every event gives a result that falls right on zero.

Embedding data is very statistically challenged. Since the Lambdas in embedding aren't polarized and are not made to have any correlation with  $\Psi_1$  they can't give a number more sensitive than other simulation results.

2095 UrQMD (in which the reaction plane is known) for 19.6GeV has given  $S_y = 1.95^{-4} \pm 2.95^{-4}$  which means  $N_\sigma = 0.66$  ( $S_y$  is a variable which is qualitatively consistent with  $\sin(\Psi_1 - \phi_\Lambda^*)$ ). For UrQMD data I am given a list of Lambdas and I have to decay them myself. I give them an isotropic decay geometry so it is hardly a surprise that the results fall on zero. I do not have UrQMD tracks run through the GEANT model of STAR so I can only analyze the data as similarly to real data up to a point.

### 2100 6.2 Rotated pions

Another way to try to falsify the signal is to run the same code but rotate all of the pions in the event by  $\pi$  in the  $x - y$  plane. This should provide realistic Lambda candidates without providing any residual effects from real Lambdas leaking in. There should be a null signal in this measure. The following results are for resolution corrected polarization ( $\sin(\Psi_1 - \phi_\Lambda^*)$ ) with no scaling by  $8/(\pi\alpha)$ .

### Lambda and AntiLambda (on peak) for rotated pions

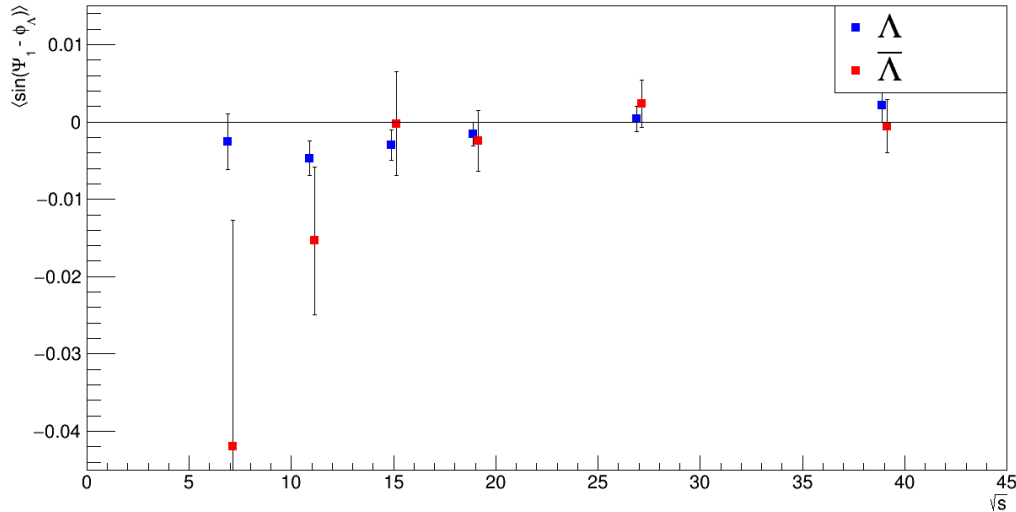


**Fig. 207:**  $\sin(\Psi_1 - \phi_\Lambda^*)$  as a function of  $\sqrt{s_{NN}}$  for  $\Lambda$  and  $\bar{\Lambda}$  where the momenta of the pions in the events have been rotated 180 degrees in azimuth.

### Lambdas for rotated pions

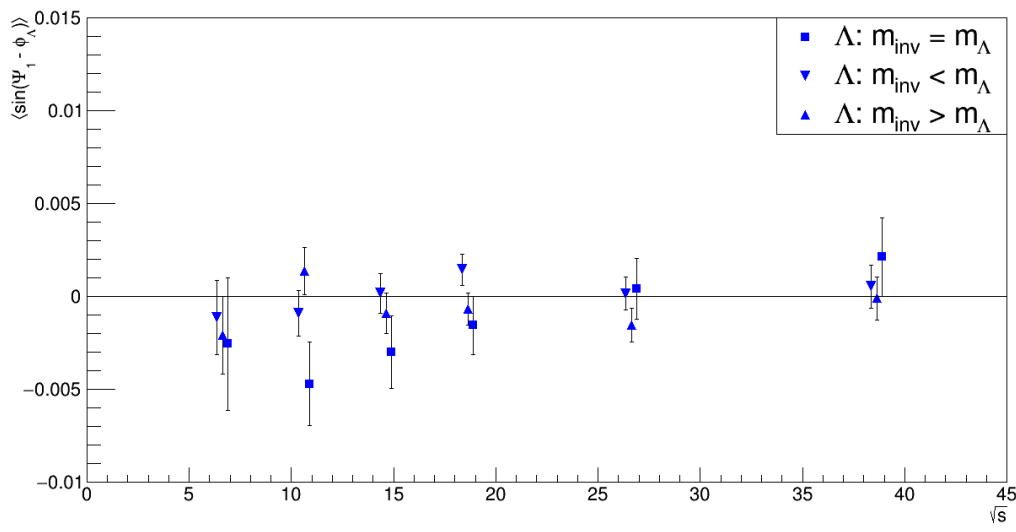


**Fig. 208:**  $\sin(\Psi_1 - \phi_\Lambda^*)$  as a function of  $\sqrt{s_{NN}}$  for  $\Lambda$  candidates that have large or small invariant mass - also referred to as off mass (both cases of  $m_{inv} > m_\Lambda$  and  $m_{inv} < m_\Lambda$ ) - where the momenta of the pions in the events have been rotated 180 degrees in azimuth.

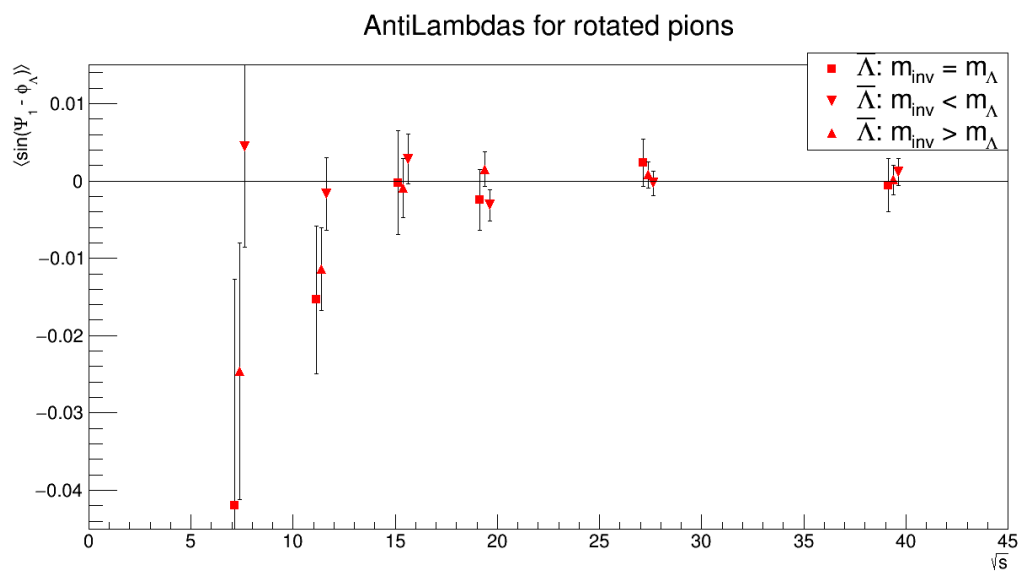


**Fig. 209:**  $\sin(\Psi_1 - \phi_{\bar{\Lambda}}^*)$  as a function of  $\sqrt{s_{NN}}$  for  $\bar{\Lambda}$  candidates that have large or small invariant mass - also referred to as off mass (both cases of  $m_{\text{inv}} > m_{\Lambda}$  and  $m_{\text{inv}} < m_{\Lambda}$ ) - where the momenta of the pions in the events have been rotated 180 degrees in azimuth.

**2105 7 STAR 2007 results**

Part of the paper is quoting the 2007 (<https://arxiv.org/abs/0705.1691>) global polarization results from STAR. The first thing to make clear is that there is a sign error in the 2007 analysis due to a mistake about the angular momentum direction, so quoted results are going to be a sign off from what you see in the paper. To compare we need results integrated over  $p_T$  in 20-50% centrality. We got these numbers  
2110 from the 2010 rows of <https://drupal.star.bnl.gov/STAR/files/starpublications/79/data.html>. To properly weight the centrality bins we assume that the number of Lambdas (AntiLambdas) in one bin centrality relative to another is the same as the ratio is for charged particles (RefMult). We get the refmult from “Centrality\_def\_refmult.txt” from StRefMultCorr averaging the two 5% centrality bins in the table.

Centrality	$62.4GeV$	$200GeV$
20-30%	167	226.5
30-40%	111.5	151.5
40-50%	71	96

**Table 17:** StRefMultCorr averaged tables for  $62.4GeV$  and  $200GeV$ 

Centrality	$P_H$	<i>error</i>	$RefMult \cdot P_H$	$(RefMult \cdot error)^2$
20-30%	-0.0001	0.0174	-0.0167	8.44367364
30-40%	0.044	0.02	4.906	4.9729
40-50%	-0.0032	0.0253	-0.2272	3.22669369

**Table 18:**  $62.4GeV$   $\Lambda$  results from 2007 paper

Centrality	$P_H$	<i>error</i>	$RefMult \cdot P_H$	$(RefMult \cdot error)^2$
20-30%	0.0096	0.024	1.6032	16.064064
30-40%	0.0282	0.027	3.1443	9.06311025
40-50%	0.0174	0.034	1.2354	5.827396

**Table 19:**  $62.4GeV$   $\bar{\Lambda}$  results from 2007 paper

Centrality	$P_H$	<i>error</i>	$RefMult \cdot P_H$	$(RefMult \cdot error)^2$
20-30%	0.000177	0.015	0.0400905	11.54300625
30-40%	-0.016	0.0178	-2.424	7.27219089
40-50%	0.031	0.0221	2.976	4.50118656

**Table 20:**  $200GeV$   $\Lambda$  results from 2007 paper

Centrality	$P_H$	<i>error</i>	$RefMult \cdot P_H$	$(RefMult \cdot error)^2$
20-30%	-0.00795	0.017	-1.800675	14.82635025
30-40%	-0.011	0.02	-1.6665	9.1809
40-50%	-0.0022	0.025	-0.2112	5.76

**Table 21:**  $200GeV$   $\bar{\Lambda}$  results from 2007 paper

Type	$P_H$	<i>error</i>
$62.4GeV$ $\Lambda$	0.0133393419	0.0116727212
$62.4GeV$ $\bar{\Lambda}$	0.0171184549	0.015918979
$200GeV$ $\Lambda$	0.0012491361	0.0101871395
$200GeV$ $\bar{\Lambda}$	-0.0077602848	0.0115104159

**Table 22:** 2007 final 20-50% centrality results tabulated from tables 18-21